Mechanisms of Aerosol Indirect Effects on Glaciated Clouds Simulated Numerically

Innocent Kudzotsa

Submitted in accordance with the requirements for the degree of
Doctor of Philosophy

University of Leeds
School of Earth and Environment
December 2013

Declaration of Authorship

The candidate confirms that the work submitted is his own and that appropriate credit has been given where reference has been made to the work of others.

This copy has been supplied on the understanding that it is copyright material and that no quotation from the thesis may be published without proper acknowledgement.

©2013 The University of Leeds and Innocent Kudzotsa

Acknowledgements

First and foremost, I would like to express my sincere gratitude to my lead supervisor Vaughan Phillips for his unwavering guidance, support and advice during the whole course of this PhD project. I would also like to thank my co-supervisor Steven Dobbie for his invaluable guidance and advice throughout my time at the University of Leeds. Furthermore, I would like to acknowledge the Department of Energy of the United States of America, USA (DoE) ASR program and the National Science Foundation of USA (NSF) for funding this research. I would also like to acknowledge the department of Meteorology at the University of Hawaii at Manoa, USA and the School of Earth and Environment at the University of Leeds, UK, mainly for providing space and computing facilities, without which, this research may have not been successful.

I would also like to acknowledge the following people whose contribution to the aerosol-cloud model development was invaluable: Marco Formenton (for developing codes for sticking efficiencies and turbulent enhancement of coagulation and debugging the ice morphology routines), Jiming Sun, John Kealy and Barry Lienert. Many thanks go to the following scientists for the various roles they played, especially on issues to do with microphysical datasets. Special mention is given to Grant Allen of the University of Manchester, UK, Aaron Bansemer of the University Corporation for Atmospheric Research (UCAR), U.S.A and Greg McFarquhar at the University of Illinois at Urbana-Champaign, USA. Additionally, the following people helped in one way or the other, for the success of this project: K. Carslaw, K. Pringle, D. Collins, L. Berg, S. A. McFarlane, Kapustin, H. Morrison and A. Fridlind and Richard Rigby and not forgetting to mention the following people, most of whom helped with proofreading: K. Tongper, B. Manzunzu, S. Munsaka, J. Mochizuki, T. Mushore, Q. Zafar, Y. Rao, A. O'Leary, I. Ahiabu and A. Babakhanyan, L. T. Saurombe. Lastly, I need to thank Alan Blyth and Jean-Pierre Pinty for their valuable advice during the review process of this thesis.

On a personal note, I would like to thank my family, friends and fellow church members for their encouragement and prayers and everyone else who has not been mentioned herein, but contributed either directly or indirectly to the success of this work. Above all, I would like to honour God the Almighty.

”Unfortunately when you most need predictability,
that’s usually when the atmosphere is
most unpredictable.” C. McElroy

”has the rain a father? or who has begotten
the drops of dew?
Out of whose womb came the ice? and the hoary
frost of heaven, who has gendered it?
Canst thou lift up thy voice to the clouds,
that abundance of waters may cover thee?
Canst thou send lightnings, that they may go
and say unto thee, here we are?
Who can number the clouds in wisdom?
or who can stay the bottles of heaven?
Job *3*8, 28-29, 34, 35, 37”

Abstract

Various improvements were made to a state-of-the-art aerosol-cloud model and it was validated against observations from field campaigns. The robustness of this aerosol-cloud model is in its ability to explicitly resolve all the known modes of heterogeneous cloud droplet activation and ice crystal nucleation. The model links cloud particle activation with the aerosol loading and chemistry of seven different aerosol species. Continental and maritime cases were simulated for the purposes of validating the aerosol-cloud model, and investigating the salient microphysical and dynamical mechanisms of aerosol indirect effects (AIE) from anthropogenic solute and solid aerosols, focusing mainly on glaciated clouds.

The results showed that increased solute aerosols reduced cloud particle sizes and inhibited warm rain processes, thus, enhancing chances of homogeneous cloud droplet and aerosol freezing. Cloud fractions and their optical thicknesses increased quite substantially in both cases. Although liquid mixing ratios were boosted, there was however a substantial reduction of ice mixing ratios in the upper troposphere owing to the increase in snow production aloft. Convective updrafts became weaker mainly in the continental case, while weak vertical velocities strengthened slightly in the upper troposphere. With an increase in solid aerosols, clouds became slightly more extensive over the continents, while the cloudiness diminished over the oceans.

The total AIE of clouds from solute aerosols was two times higher in the oceanic than in the continental case, because the sensitivity of the cloud properties to perturbation in aerosol concentrations diminishes with increasing background aerosol concentrations. Also, the AIEs of glaciated clouds were greater than those of water-only clouds by a factor of two in the continental case while both cloud types were equally important in the maritime case. The radiative importance of glaciated clouds lied in their large collective spatial extent and existence above water-only clouds. The glaciation AIE from solid aerosols had a cooling effect in continental clouds because of an increase in cloud fraction and a warming effect in maritime clouds because of a decrease in cloud fraction. In addition to the traditional AIEs (glaciation, riming and thermodynamic), sedimentation, aggregation and coalescence were new AIEs identified. Importantly, it was discovered that these individual AIEs interact, compensate and buffer each other, hence, the relative importance of contributions from responses of various processes vary during the climate change. Finally, meteorology was identified to have little effect on the mechanisms of aerosol-cloud interaction.

Contents

List of Figures

List of Tables

Acronyms

ACTIVE	Aerosol and Chemical Transport in Tropical Convection. 64, 65
AIE	Aerosol Indirect Effect. 5, 28
AP	Aerosol Particle. 9–12, 17, 43
ARM	Atmospheric Radiation Measurement. 3
ASD	Aerosol Size Distribution. 32
ASR	Absobed Solar Radiation. 25, 30
BADC	The British Atmospheric Data Centre. 65
BPC	Bulk to Particle Conversion. 8
CCN	Cloud Condensation Nuclei. 1, 10, 14, 17, 20, 32, 35
CDNC	Cloud Droplet Number Concentrations. 30
CDSD	Cloud Droplet Size Distribution. 15, 32
CEPEX	Central Equatorial Pacific Experiment. 56, 57
CHAPS	Cumulus Humilis Aerosol Processing Study. 67, 69
CLASIC	Cloud and LAnd Surface Interaction Campaign. 3, 61, 176
CSRM	Cloud System Resolving Models. 2, 39, 41, 42, 50, 70
DCC	Deep Convective Cells. 6, 35
DoE	US Department of Energy. 67
DPC	Drop to Particle Conversion. 9
DSD	Droplet Size Distribution. 40
EM	Electro-magnetic. 22
EP	Empirical Parameterisation. 46
ERFaci	effective radiative forcing from aerosol-cloud interactions. 29
FSSP	Forward Scattering Spectrometer Probe. 76

GCM	General Circulation Model. 2, 5, 27, 34, 39, 42, 87, 187
GFDL	Geophysical Fluid Dynamics Laboratory. 41
GPC	Gas to Particle Conversion. 8, 11
H-M	Hallet-Mossop. 47
IN	Ice Nuclei. 1, 18, 36
INSPECT	Ice Nuclei Spectroscopy Studies. 190
IOP	Intense Observation Periods. 3
IPCC	Intergovernmental Panel on Climate Change. 1
ISDAC	Indirect and Semi-Direct Aerosol Campaign. 187
KWAJEX	Kwajalein Experiment. 50, 59
LBA-SMOCC	Large-Scale Biosphere-Atmospheric Experiment in Amazonia-Smoke, Aerosol, Clouds, Rainfall, and Climate. 32
LCL	Lifting Condensation Level. 16
LEM	Large Eddy Model. 2
LW	Long-Wave radiation. 24
LWC	Liquid Water Content. xii, 5, 13–15, 21, 30, 76, 194
NERC	UK Natural Environment Research Council. 65
NERC-ARSF	Airborne Research and Survey Facility. 65
NWP	Numerical Weather Prediction. 15, 21, 39
OLR	Out-going Longwave Radiation. 25
PBAP	Primary Biological Aerosol Particles. 42
QPF	Qualitative Precipitation Forecasting. 40

RH	relative humidity. 12, 13, 17, 188
SGP	Southern Great Plains. 3
SW	Short-Wave radiation. 24
SWS	Strong Wind Shear. 35
TOA	top of the atmosphere. 24, 33, 86
TOGA-COARE	Tropical Ocean Global Atmosphere Coupled Ocean-Atmosphere Response Experiment. 50, 59
TWPICE	Tropical Warm Pool-International Cloud Experiment. 3, 61, 176
WRF	Weather Research and Forecasting. 40
WWS	Weak Wind Shear. 35

List of symbols

C_{CCN}	CCN number concentration m^{-3} at 1% supersaturation. 10
C_{IN}	Coeficient for IN activity spectrum. 11, 12
H	Height above cloud base (m). 32
N_{CCN}	CCN number concentration m^{-3}. 10
N_{IN}	active IN concentration (L^{-1}). 11
R_{geo}	Geometric mean radius (m). 10
R	Radius of the larger hydrometeor (m). 33, 193
T	Temperature (K). 11
b_{IN}	Constant for the IN activity power law. 12
$\bar{E}$	Mean collection efficiency for riming. 33
β	Constant for IN activity spectrum. 11
f	Total number of modes in a particle distribution. 10
i	Iterative index. 10, 189
κ	Constant for CCN power law. 10, 11
m	Mass of riming/accreting particle (Kg). 33
s_i	Supersaturation with respect to ice. 12
$u(R)$	Terminal fall speed of a particle of radius R (m s^{-1}). 33, 193
$u(R)$	Terminal fall speed of a particle of radius r (m s^{-1}). 193, 194
$\bar{A}$	Mean reflectivity of the Earth. 25, 26
D_{CW}	Cloud droplet diameter (μm). 47
D_{HM-max}	Hallet-Mossop maximum threshold (μm). 47
D_{HM-min}	Hallet-Mossop minimum threshold (μm). 47
Δz	Thickness of the cloud (m). 31
E_s	sticking efficiency. 193
E	collision efficiency. 193
M_T	Total emittance (Wm^{-2}). 23
M_λ	Monochromatic emittance (Wm^{-2}). 22
M	Solute mass (kg). 189
N_0	Intercept parameter. 15, 16, 40
$N(r)$	Particle number concentration of drops with radius, r in m^{-3}. xii, 14, 15

N	Total particle number concentration in m^{-3}. 10, 16
$\bar{F}_s$	Mean solar insolation measured at TOA (Wm^{-2}). 25
R_M	Enhancement factor/ratio. 20
R_v	Gas constant for water vapour. 188
S	Supersaturation (%). 13, 17
T_A	Effective temperature of the atmosphere (K). 25
T_B	Effective temperature of the Earth's surface(K). 25
T_d	Dew point temperature (K). 16
T_{LCL}	Temperature at LCL (K). 16, 17
T_{sat}	Air temperature at saturation (K). 16
T_w	Wet bulb temperature (K). 16
U	Up-draft velocity (m s^{-1}). 194
a	Solute effect coefficient (cm). 189
e'	Equilibrium vapour pressure over a solution droplet (Pa). 189
$e_{s,w}(\infty)$	Saturation vapour pressure over a water surface (Pa) of bulk water. 188
$e_{s,i}(\infty)$	Saturation vapour pressure (Pa) of bulk ice. 18
$e_{s,i}$	Saturation vapour pressure over an ice surface (Pa). 18
$e_{s,w}(r_c)$	Equilibrium saturation vapour pressure (Pa) of a water droplet at critical radius r_c. 188
$e_{s,w}(r)$	Equilibrium saturation vapour pressure (Pa) of a water droplet of radius r. 188
$e_{s,w}$	Saturation vapour pressure (Pa). 17, 188
$\bar{\hat{\epsilon}}$	Mean emissivity of the atmosphere. 25, 26
e	Vapour pressure (Pa). 17, 188
f_{HM}	Hallet-Mossop size dependent fraction. 47
$\hat{a}$	Absorptivity. 23
$\hat{\epsilon}$	Emissivity. 23
λ	Slope parameter. 15, 16
m_s	Molecular weight of the solute (kg). 189

μ	Shape parameter. 15, 16
q_v	Vapour mixing ratio (kg/kg). 16
r_c	Critical radius for a cloud embryo. 188
r_m	Cloud particle mass weighted radius (m). 16, 31
r^{star}	Critical radius (cm). 189
ρ_i	Bulk density of ice (kgm^{-3}). 18
ρ_w	Density of liquid water in Kgm^{-3}. 14
r	Cloud droplet radius (m). 10, 16, 188, 193
S^{star}	Critical supersaturation. 189
s_w	Supersaturation w.r.t water. 10, 17
σ_i	Surface tension of ice ($Jkg^{-1}K^{-1}$). 18
σ_w	Surface tension for water ($Jkg^{-1}K^{-1}$). 188
σ	Standard deviation. 10
τ	optical thickness. 30, 219
w_L	Liquid water content (gm^{-3}). 13, 14, 16, 31, 194
x_0	Critical impact parameter (m). 193
x	Impact parameter (m). 193

List of Constants

R_v	461.5 $\mathrm{Jkg^{-1}K^{-1}}$. 188
k	$8{\times}10^{3}s^{-1}$. 193
σ	$5.67{\times}10^{-8}\mathrm{Wm^{-2}K^{-4}}$. 23

Chapter 1

Introduction

The industrial revolution and subsequent growth in manufacturing output worldwide, has led to an increased aerosol content relative to pre-industrial times (Watson et al., 1990; Andreae et al., 2007; Takemura, 2012). Although, the upward trend of the global average of aerosol pollution continues primarily due to growing economies in Asia, particularly China and India (Streets et al., 2003; Ramanathan et al., 2007; Lei et al., 2011), most of the developed countries have already reached their peak in emitting anthropogenic aerosols (Takemura, 2012). Pollution due to biomass burning also continues to rise, particularly in the southern hemisphere (Andreae and Merlet, 2001; Takemura, 2012). These artificially induced changes in atmospheric aerosol concentrations, such as sulphate and carbonaceous aerosols, have substantially altered the chemistry and loading of the natural aerosol field (Sun et al., 2004; Salma and Maenhaut, 2006).

According to the Intergovernmental Panel on Climate Change (IPCC) reports (Solomon et al., 2007; Boucher and Randall, 2013), aerosols are one of the major climate forcing agents; they do so via two major pathways. Firstly, by their nature, aerosols can scatter and absorb shortwave radiation and also absorb and re-emit longwave radiation in different directions, thereby altering the radiation budget of the Earth (Charlson et al., 1992; Liao and Seinfeld, 1998; Myhre et al., 2009). Changes in aerosol loading and their direct interference with radiation is called the *aerosol direct effect* (Charlson et al., 1992; Haywood and Boucher, 2000). The second pathway is when aerosols act first, as Cloud Condensation Nuclei (CCN) or Ice Nuclei (IN) in the formation of cloud particles. Their changes in chemical composition and number or mass concentration may lead to modifications in clouds' microphysical and optical properties, thus, altering the Earth's radiation budget (Albrecht, 1989). This second mechanism is referred to as the *aerosol indirect effect* (Charlson et al., 1992; Haywood and Boucher, 2000; Lohmann and Feichter, 2005;

O'Donnell et al., 2011; Gettelman et al., 2012). There is also the *semi-direct* effect, which is caused by absorbing aerosols (Lohmann and Feichter, 2001; Johnson et al., 2004). These absorbing aerosols have a heating effect in the atmosphere, which may subsequently cause the evaporation of cloud particles (Johnson, 2003; Hill and Dobbie, 2008; Koch and Genio, 2010). However, this study only focuses on the indirect effects of aerosols. It is important to study the many and varied indirect influences of aerosols on clouds because initial work in this area shows that they are potentially very important, particularly in offsetting the carbon dioxide (CO_2) induced global warming (Twomey, 1974, 1977; Albrecht, 1989; Leaitch et al., 1992).

Aerosol indirect effects are affected by sub-grid scale microphysical processes, which are too small to resolve in coarse resolution General Circulation Model (GCM) (McComiskey and Feingold, 2012). In order to predict aerosol indirect effects using GCMs, cloud microphysical processes are incorporated by way of parameterizations (Menon et al., 2002a; Lohmann and Feichter, 2005; Gettelman et al., 2012). Numerical models typically focus on various scales of motion; the GCMs are the crudest (Briffa, 1999; Menon et al., 2002a), while the Cloud System Resolving Models (CSRM) (Phillips et al., 2009; Wapler et al., 2010; Morrison and Grabowski, 2011) or Large Eddy Model (LEM)s (Johnson et al., 2004; Marsham and Dobbie, 2006) are the most accurate for simulating cloud scale systems.

In this study, we focus on using an aerosol-cloud model (Phillips et al., 2007, 2008, 2009, 2013) so as to understand the detailed microphysical and dynamical processes and responses of clouds to aerosol changes before subsequent work addresses the implementation of these findings in GCMs. This deficiency in GCMs makes the accurate prediction of future climate difficult (McComiskey and Feingold, 2012), since aerosol-cloud-environment feedbacks are not allowed therein (Stevens and Boucher, 2012; Morrison and Grabowski, 2011). The computational capacity available at the moment allows subtle understanding of cloud- or meso-scale processes through the use of CSRMs (Thompson et al., 2004; Lim and Hong, 2010). This is however, not the case at the global scale where GCMs are required. Thus, until such high computational power that allows for simulation of cloud scale processes at global and long temporal scales of the order of centuries is achieved, cloud parameterization shall remain the better option for representing aerosol-cloud interactions in GCMs (Bernholdt et al., 2005; Shukla et al., 2009, 2010). Therefore, in the meantime, CSRMs ought to be utilized in order to deepen our knowledge of aerosol-cloud interactions and aerosol indirect effects so as to feed GCMs with more realistic parameterizations of cloud processes.

1.1 Aims and Objectives

Clouds control the radiation budget of the Earth (King, 1993; Liou, 2002; Lohmann and Feichter, 2005; Solomon et al., 2007), but how they will respond in future to changes in aerosol chemistry and loading, remains conjectural, and this emerges as the greatest source of uncertainty in climate prediction (Bony and Dufresne, 2005; Solomon et al., 2007; Baker and Peter, 2008; Phillips et al., 2008; Fan et al., 2012). Although, observational, modeling and laboratory studies on aerosol-cloud interactions have been carried out in the past, most of them have focused on warm clouds (Martin et al., 1994; Cui et al., 2006; Hoeve et al., 2011; Costantino and Bréon, 2013). Consequently, little is known about aerosol indirect effects of glaciated clouds (Gettelman et al., 2012). There are large uncertainties in the measurements and knowledge of ice nucleating aerosols (Cziczo et al., 2004; DeMott et al., 2011) and also, in the mechanisms of ice nucleation at different temperatures and humidity (Meyers et al., 1992; Phillips et al., 2008; Eidhammer et al., 2009). Hence, this study proposes to contribute to the knowledge of aerosol-cloud interactions (aerosol indirect effects) on glaciated clouds by way of sensitivity tests, using a state-of-the-art aerosol-cloud model (Phillips et al., 2007, 2008, 2009, 2013) that encapsulates a tested and robust heterogeneous ice nucleation scheme of Phillips et al. (2008, 2013), which treats all the four known modes of heterogeneous ice nucleation (Diehl et al., 2001, 2002; Hoppel et al., 2002; Dymarska et al., 2006).

The focus of this study is on investigating the diverse mechanisms for aerosol indirect effects via glaciated clouds from anthropogenic emissions of soluble and solid aerosols. This meso-scale modeling study is based on two simulations of Intense Observation Periods (IOP) of deep convection from the Atmospheric Radiation Measurement (ARM) sites. The first one is the Cloud and LAnd Surface Interaction Campaign (CLASIC), which was carried out over the Southern Great Plains (SGP) in Okhlahoma, U.S.A. (Miller, 2007), while the second one is the Tropical Warm Pool-International Cloud Experiment (TWPICE) campaign, which was conducted in Darwin, Australia (May et al., 2008; Fridlind et al., 2009).

1.2 The overarching aims and objectives

Below is the list of the aims and objectives set out for this study. The hypotheses that were tested are also described. The overarching aims and objectives are to:

- Explore on the meso-scale, the cloud microphysical and dynamical mechanisms

for glaciated-cloud indirect effects from anthropogenic solute aerosols. In this study, the term glaciated-cloud refers to clouds with any form of ice in them, either as mixed phase or completely glaciated clouds.

The hypothesis being tested here is that, solute aerosols modify glaciated clouds via the homogeneous freezing process of cloud droplets and of solute aerosols. Also, reduced sedimentation rates produce a lifetime effect, causing pollution by solute aerosols to modify cirrus clouds more than solid aerosols, owing to the much higher numbers of soluble aerosols relative to insoluble ones;

- Explore salient mechanisms of ice nucleation from anthropogenic increases in ice nuclei and the hypothesized intensification of precipitation production via ice crystal processes, known as the *glaciation* effect.

  The hypothesis being tested here is that, solid aerosol pollution reduces the overall numbers of ice crystals in cirrus, by reducing chances of homogeneous freezing. Also, solid aerosols increase ice crystal numbers in mixed-phase clouds by heterogeneous ice nucleation, thereby changing the phases and lifetimes of clouds in regions of weak vertical velocities;

- Explore also, the *riming effect*, which is caused by the reduction of droplet sizes due to an increase in the droplet number concentration and the freezing-related *thermodynamic or invigoration* aerosol indirect effect latent heat release during freezing of extra cloud droplets.

  The hypothesis being tested here is that, the thermodynamic and the riming indirect effects from soluble and insoluble aerosols are significant, but do not dominate the total indirect effect on all clouds (warm and cold);

- Investigate the role of wind shear in modifying the glaciated clouds aerosol indirect effects by either extending the clouds' spatial and temporal scales or, by enhancing the lateral entrainment of dry ambient air, which leads to the evaporation and the sublimation of cloud particles.

  The hypothesis being tested here is that, environmental wind shear modifies the glaciated-cloud indirect effect, by horizontally extending cirrus so as to increase its reflection of solar radiation and trapping of longwave radiation. And also by modulating the intensity of convective clouds, thereby affecting their anvil outflow and generation of cirrus;

- Examine the impact of artificially varying the amounts of upper tropospheric water vapor on the aerosol indirect effects of glaciated clouds.

  The hypothesis being tested is that, a more humid atmosphere increases the spatial extent and the lifetime of cirrus clouds, thus boosting the impacts from clouds on the radiation budget and indirect effects. It is also being hypothesized that, high upper tropospheric humidity lowers the bases of cirriform clouds aloft, boosting the aerosol indirect effects further.

1.3 Scientific Context

Lohmann and Feichter (2005) in their review paper, highlighted the incoherence of different global models' results on magnitudes of aerosol indirect effects, (both the lifetime (Albrecht, 1989) and the albedo (Twomey, 1977) indirect effects). For instance, there exist contradictions in the magnitudes of the albedo and the lifetime indirect effects. Williams et al. (2001) found an albedo indirect effect that is a factor of four greater than the lifetime indirect effect, while Lohmann et al. (2000a) and Quaas et al. (2004) concluded that, the albedo effect is smaller than the lifetime effect. The differences in the GCM parameterizations (Lohmann et al., 2000a; Williams et al., 2001; Gettelman et al., 2012) that represent aerosol-cloud interactions were cited as the major causes of these inconsistencies. Some of the key sources of these inconsistencies in the parameterizations are; whether the cloud nucleation schemes used were empirically (Lohmann et al., 2000a) or physically (Williams et al., 2001) based or, whether the auto-conversion schemes included dependencies on LWC, droplet number concentration or droplet size (Lohmann and Feichter, 2005). In order to reduce these inconsistencies, cloud-scale microphysics ought to be well understood, so as to develop more realistic cloud parameterizations for GCMs (Morrison and Grabowski, 2011; Fan et al., 2012).

Some previous researchers have carried out similar research (Khain et al., 2005; Connolly et al., 2006; Lee et al., 2009; Fan et al., 2012), however, with different tools and on different cloud systems. Morrison and Grabowski (2011) simulated the TWPICE case, focusing primarily on the overall effect of changing the aerosol loading. They had three different categories of aerosol species. Their study contrasted with ours in that, we conduct detailed sensitivity tests on different microphysical processes that lead to the overall Aerosol Indirect Effect (AIE), which is a crucial aspect underlying accurate GCM parameterizations and climate prediction. Fan et al. (2009, 2012) explored the role of aerosols and the relevance of wind shear on the dynamical and thermo-dynamical aspects of deep convective clouds. Although they

also assessed the AIE, they however, did not untangle the details of the microphysical processes underpinning the AIE. It must also be noted that their simulations were on isolated Deep Convective Cells (DCC), whereas in this study, multi-cell systems of clouds are simulated, allowing cell-to-cell interactions and feedbacks between clouds and their environment to be assessed. Many other researchers in this area, e.g., Khain et al. (2005), Lee et al. (2008b) and Cui et al. (2006), focused on individual or isolated convective systems. Although the knowledge of cloud-scale processes are important in understanding the evolution of meso-scale systems, there are however flaws associated with such analysis, particularly when global or climatic interpretations are to be derived (McComiskey and Feingold, 2012), for instance, inter-cloud and cloud-environment feedbacks may not be fully represented (Morrison and Grabowski, 2011). Other researchers on the other hand, looked at aerosol cloud interactions on warm clouds (Lee et al., 2012).

For the present thesis, the *riming, thermodynamic* and *glaciation* indirect effects are quantified. This is one of the first estimates on mesoscale cloud systems using a detailed treatment of aerosol chemistry, activation of cloud-particles and cloud microphysics. The focus was on mesoscale multi-cell cloud systems simulated over spatially large domains of the order of a few hundreds of kilometers and temporally long simulation periods of several weeks. These scales are for demonstrating the importance of feedbacks between clouds and their thermodynamic environments. The structure of this thesis is as follows. Chapter 2 provides the necessary background information that is relevant to the scope of this study and the state-of-the-art advances in the literature is also presented. In Chapter 3, the aerosol-cloud model used in this study is described along with work performed to modify and update the model. The description of the cases simulated, the aerosol-cloud model setup and comparison of the model results to observations will be given in Chapter 4. The discussion of sensitivity tests and results are given in chapters 5 and 6. Finally, conclusions and future work will be stated in the last chapter, which is Chapter 7.

Chapter 2

Background Concepts and Literature Review

2.1 Background Concepts

This chapter is presented in two sections. In the first section, the background concepts necessary for this study are described, while state-of-the-art understanding of this research area is discussed in the second section.

2.1.1 Atmospheric Aerosol Chemistry, Evolution and Dynamics

A detailed understanding of the physico-chemical and dynamical characteristics of aerosols is fundamental for the comprehension of aerosol-cloud linkage. Therefore, in this section, concepts of atmospheric aerosols that are pertinent to the scope of this study are discussed.

Aerosols are microscopic particulate matter, suspended in the atmosphere, a fraction of which forms the nuclei of cloud particles and ice crystals. Aerosols can be classified into three main size distributions according to their sizes. Those smaller than 0.1μm are called *Aitken particles* or are said to be in *nuclei mode*. Those in 0.1 - 1μm size range are called *large particles* or the *accumulation mode* and finally, those in the third category, the super-micron range, are called the *giant particles* or the *coarse mode*, they range from 1μm to a few tens of microns (Pruppacher and Klett, 1997).

Aerosols are injected into the atmosphere from both natural and anthropogenic sources. Although there are extra-terrestrial sources, the Earth dominates the sources of total atmospheric aerosol particles. Aerosol characteristics vary drastically, both spatially and temporally (Charlson et al., 1992), and depend on other factors such as meteorology and proximity to sources (Reponen et al., 2003). Concentrations are typically larger over the continents than over the oceans, as the former has several sources (Pringle et al., 2010; Takemura, 2012). The vertical pro-

files of aerosol mass and number concentrations from observations show that, these variables generally decrease with increasing altitude (Rogers and Yau, 1991; Pruppacher and Klett, 1997), although, this can vary depending on large scale advection (Shaw, 1980). It is however important to note that important exceptions are the mid troposphere in low latitudes, where upper level outflow from convection forms a source of new (soluble) aerosol particles, hence, in the tropics, the number concentrations of soluble aerosols (sulphate) usually increase with height (Clarke and Kapustin, 2002).

Aerosols are formed from various mechanisms, one of which, is the *Bulk to Particle Conversion (BPC)* (Pruppacher and Klett, 1997). This is how tiny particles dissociate from bulk sources such as plants. Plants tend to release various types of organic and biological materials such as pollen, seeds, waxes and spores, which are then transported vertically and laterally by wind and buoyancy (Shaw, 1980; Satheesh et al., 1998). Some mineral compounds are also chemically and mechanically disintegrated and the resulting fine particles can be lifted by wind. Human activities may contribute to this process. Silicate (dust) and clay particles especially from desert regions are deposited into the atmosphere by winds and can be transported over large distances, particularly when they get advected by jet streams (Shaw, 1980; Swap et al., 1992). After these particles are air-borne, they can react and be coated with other atmospheric chemical compounds to form a multicomponent aerosol particle (Fred and Seinfeld, 1980; Petters and Kreidenweis, 2007; Pringle et al., 2010). Bubble bursting from waves, ejects tiny drops of salty water solution into the atmosphere, which after evaporation, the residues can form aerosol particles that can activate cloud particles under suitable ambient conditions (Paterson and Spillane, 1969; Hoppel et al., 2002; Kapustin et al., 2012). This is the dominant mechanism for the formation of sea-salt aerosols, which are very efficient CCNs because of their high hygroscopicity (Pringle et al., 2010). Although some may sediment back onto the surface, air motions can carry a fraction.

Another source of APs e.g. soot, sulphates, carbonates and oils, is *Gas to Particle Conversion (GPC)* (Heisler and Friedlander, 1977; Fred and Seinfeld, 1980; Pruppacher and Klett, 1997). This process occurs primarily from vapour that has low boiling point, which when exhaled by industrial plants after combustion of different chemical substances, may encounter supersaturated environments, where they readily condense to form solid particles (Pruppacher and Klett, 1997). This same process can also occur in volcanic plumes and in biomass burning (Charlson et al., 1992). Some gas phase chemical reactions catalyzed by ultraviolet light can lead to homogeneous nucleation, resulting in another source of aerosol, in this case in the

solid phase. Another mechanism is the heterogeneous nucleation of an aerosol particle by deposition of gaseous particle onto a pre-existing aerosol particle (Pruppacher and Klett, 1997).

The third mechanism by which an Aerosol Particle (AP) is formed is by *Drop to Particle Conversion (DPC)*, whereby an aerosol particle may first nucleate a cloud droplet, which then grows into a large cloud droplet that can scavenge other water soluble atmospheric aerosols and gases. The dissociation of these water-soluble components into ions causes chemical reactions that may subsequently lead to the formation of other compounds. Since some of these droplets do not successfully develop into surface precipitation, they ultimately evaporate leaving a new solid aerosol particle (Pruppacher and Klett, 1997).

Solubility of aerosol particles is a key factor in determining whether an aerosol can nucleate ice or initiate cloud droplets. It has been noted that most aerosols are *multicomponent*, i.e., they contain both water-soluble and water-insoluble substances (Fred and Seinfeld, 1980; Petters and Kreidenweis, 2007; Pringle et al., 2010). This is because they are formed by coagulation of different aerosol particles and condensation or deposition of gases onto each other. On average, an AP may be approximated to be comprised of 50% water soluble inorganic matter, 30% water-insoluble inorganic material and about 20% of organic matter (Pruppacher and Klett, 1997). Maritime aerosols are found to be more soluble than continental AP (Pringle et al., 2010).

The concentration of aerosol particles over the continents is found to be in the range of 10^3 to 10^5cm^{-3} and can be in excess of 10^6cm^{-3} in urban or industrial areas (Rogers and Yau, 1991; Pruppacher and Klett, 1997; Clarke and Kapustin, 2002; Allen et al., 2008). Maritime concentrations are in the range of 100s to a few 1000s cm^{-3} as was observed over the Hawaiian region by Shaw (1980) and Clarke and Kapustin (2002) and over Darwin, Australia by Allen et al. (2008). This implies that, they decrease in number concentrations with increasing distance from their sources, which are predominantly continental (Satheesh et al., 1998; Pringle et al., 2010; Takemura, 2012). At the very extreme low concentrations, Arctic regions have been observed to have concentrations of 1 cm^{-3} and sometimes lower (McFarquhar and Coauthors, 2011; Di Pierro et al., 2013). The Aitken mode dominates the number concentrations by several orders of magnitude and the number concentrations decrease with increasing aerosol sizes (Satheesh et al., 1998). The observed aerosol size distributions fit relatively well to a tri-modal log-normal size distribution given

in Eqn. 2.1 (Pruppacher and Klett, 1997).

$$\frac{dN(r)}{d\log r} = \sum_{i=1}^{i=f} \frac{n_i}{(2\pi)^{1/2}\log\sigma_i} \exp\left[-\frac{(\log\frac{r}{R_{geo,i}})^2}{2(\log\sigma_i)^2}\right] d\log r \tag{2.1}$$

Here, n, is the total number of aerosol particles in the i^{th} mode, r, is the radius or the equivalent spherical radius for non-spherical particles of the AP and N, is the total number concentration of aerosol, while R_{geo}, is the geometric mean radii with standard deviation, σ and finally, i, is the iterative index for the number of modes represented by f. An example of this distribution is shown in Figs. 4.3 and 4.5 in the following chapter.

2.1.1.1 Cloud Condensation Nuclei (CCN)

CCN form a fraction of the whole APs budget (Junge and McLaren, 1971; Rogers and Yau, 1991; Pruppacher and Klett, 1997). It is insufficient to just mention CCN concentrations without stating the corresponding supersaturation within which they were measured (Hobbs and Radke, 1969; Fitzgerald, 1973; Gunthe et al., 2009). As explained later in Sect. 2.1.2.4, the number of CCN depends on supersaturations and it increases with increasing supersaturation and larger CCN nucleate first at low supersaturations (Kohler, 1936; Dusek et al., 2006; Gunthe et al., 2009). The geographical distribution of CCN concentrations is analogous to that of bulk aerosols with a median concentration of a few hundreds per cm^3 for maritime CCN concentration and hundreds to thousands per cm^3 for continental environments for the range of supersaturation between 0.1 and 10% (Rogers and Yau, 1991; Pruppacher and Klett, 1997; Pringle et al., 2010; Gunthe et al., 2009). CCN number concentrations, N_{CCN}, can be represented by CCN activity power law from Rogers and Yau (1991);

$$N_{CCN} = C_{CCN} s_w^{\kappa} \tag{2.2}$$

where, C_{CCN}, is the CCN concentration in an environment with 1% supersaturation with respect to a water surface, s_w, is the supersaturation (Eqn. 2.11) and κ is a constant known as the hygroscopicity parameter; both C_{CCN} and κ depend on the air-mass, whether it is continental or maritime and on other factors such as chemistry and season.

Pringle et al. (2010) provided the global distribution of κ from a numerical model. Their study showed that κ is higher over oceans (0.72±0.24) than over continents (0.27±0.21). Because of the high influence of sulphate on the κ value of aerosols, the Northern hemisphere exhibits higher values (0.3 - 0.36) than the

Southern hemisphere (0.15 - 0.17). Their study showed that, the influence of anthropogenic aerosols is to increase κ over continents and to reduce it over the oceans. For continental aerosols, the fraction of AP concentration active as CCN is between 0.01 and 0.1, whilst it is up to ≈ 0.5 for maritime aerosols due to the abundance of sea-salt aerosols (Pruppacher and Klett, 1997). CCN concentration over land tend to generally decrease with height, while those over the oceans have a tendency to remain constant or even increase with height (Clarke et al., 2006), a fact that has been attributed to in-cloud sulphate production by photochemical GPC.

Those AP that are hygroscopic are anticipated to nucleate cloud droplets (Petters and Kreidenweis, 2007; Gunthe et al., 2009). These aerosols have been found to comprise mostly sulphate compounds, ammonium, Sodium Chloride (NaCl) and soluble organic compounds (Pruppacher and Klett, 1997; Corrigan and Novakov, 1999; Svenningsson et al., 2006). Although sea-salt's water solubility (Pringle et al., 2010) and nucleation ability are significantly higher, relative to other aerosol species, it is out-numbered by other aerosol species in terms of number concentrations. The bulk of CCN are in the non-Aitken mode of aerosols, because, Aitken aerosols require higher supersaturation to activate (Kohler, 1936).

2.1.1.2 Ice Nuclei (IN)

There are four modes with which ice nuclei nucleate ice, these modes are described in Sect. 2.1.2.4.1. They are the *deposition*, *condensation*, *immersion* and *contact* ice nuclei (Meyers et al., 1992; Diehl et al., 2001, 2002; Dymarska et al., 2006; Phillips et al., 2008). Recent research by Shaw et al. (2005), confirms that, each IN particle can act in any of these modes of heterogeneous ice nucleation. The temperature of activation is quite unique for each mode of activation and it is also dependent on the chemical composition of the aerosol particle, but one particular IN may nucleate ice in one or all of the modes depending on environmental conditions (Vonnegut, 1947; Shaw et al., 2005; Phillips et al., 2008). Observations have shown that IN concentrations have much variability, especially close to their sources and also that they are strongly dependent on temperature (Hobbs and Rangno, 1985; DeMott et al., 2011). This was illustrated by Fletcher, (1962), who observed IN activity relationship with temperature of the form:

$$N_{IN} = C_{IN} e^{\beta \Delta T} \tag{2.3}$$

Here, N_{IN} is active IN concentration L^{-1} at a given ambient temperature T, while C_{IN} and β are constants which may be set at $10^{-5} L^{-1}$ and 0.6°C, respectively,

although they are not unique. ΔT represents the temperature difference between the surface of an IN and the ambient temperature.

IN have been observed to nucleate ice even at relative humidity (RH) w.r.t water that are below 100%, as long as the environment is supersaturated with respect to ice (Roberts and Hallett, 1968), and this is explained in detail in Sect. 2.1.2.5.2. Like CCN, IN concentration is also a function of supersaturation with respect to ice, and the analogous of Eqn. 2.2 is Eqn. 2.4 (Pruppacher and Klett, 1997).

$$N_{IN} = C_{IN} s_i^{b_{IN}} \tag{2.4}$$

where, s_i, is the supersaturation with respect to water, b_{IN}, and C_{IN} are constants and C_{IN} has the same meaning as in Eqn. 2.3. It is important to state that IN activation is more complex because there is dependence on both temperature and supersaturation. There are many other diverse representations of IN activity spectra in the literature e.g. Meyers et al. (1992) and Eidhammer et al. (2010), but special consideration is given to one empirical parameterization for heterogeneous ice nucleation developed by Phillips et al. (2008, 2013) because it is the one used in this thesis and is described in Chapter 3.

Apparently, the ratio of observed concentrations of heterogeneously nucleated ice particles due to primary ice nucleation (before secondary ice multiplication (Sect. 2.1.2.5)) to the bulk AP concentration can be of the order of 10^{-6} (Rogers and Yau, 1991; Pruppacher and Klett, 1997). This is a clear indication that an ice-nucleating particle is rare compared to CCN. This is inherent to the fact that, ice nucleation demands certain characteristics, which are described below that are not exhibited by most aerosols (Diehl et al., 2001; Cziczo et al., 2004; Murray et al., 2010). As described in Pruppacher and Klett (1997), IN should have some of the following characteristics for effective ice nucleation:

- *Solid*: Only when an aerosol particle is solid, can it nucleate ice (e.g. IN consisting of insoluble materials or glassy material that is partly soluble.). Also recently, Murray et al. (2010) showed that amorphous solids can also nucleate ice.

- *Size requirement*: The typical size of IN should be greater than that of Aitken sizes or at least be equal to that of an ice embryo, which is normally 0.1μm.

- *Chemical bonding*: In view of the fact that an ice lattice is held together by hydrogen bonds, IN should have a molecular lattice with surface polarity that promotes a similar bonding with water molecules.

- *Active site(s)*: Effective IN have been observed to have on their surfaces distinct active sites onto which ice nucleation can occur.

- *Crystallographic structure*: Ice nucleation on an IN is assumed to be a growth of ice on that IN, which may be promoted by the atoms or molecules of the IN being geometrically arranged in a way similar to those of ice (Vonnegut, 1947).

2.1.2 Cloud Microphysics and Dynamics

2.1.2.1 The Microstructure of Clouds

Clouds are typically classified according to their altitude in the atmosphere (i.e. low-, mid- and high level clouds) and origin (i.e. stratiform or convective clouds). On a microphysics scale, clouds are classified according to their particle concentration, particle size distribution spectra and water content (Rogers and Yau, 1991). The common feature among clouds is their RH and supersaturation (S). Most water clouds and even fog are saturated (*i.e.* their RH is typically 100%), although a value of as low as 80% is common in fog (Pruppacher and Klett, 1997). Relative humidity above and below 100% are referred to as super- and sub-saturated, respectively. RH within a liquid-cloud rarely exceeds 102% (because droplet initiation by CCN ensues quickly under these conditions and reduces the supersaturation quite quickly), although, higher values of about 107% were also observed in strong updrafts (Pruppacher and Klett, 1997), this is because ascent is the source of supersaturation in warm and mixed-phase clouds (Rogers and Yau, 1991; Korolev and Mazin, 2003). Saturated and supersaturated conditions normally exist within the interior of clouds, while subsaturation is typical at the cloud edges, owing to entrainment of dry ambient air or descent in either cloudy or cloud-free downdrafts (Blyth and Latham, 1990).

2.1.2.2 Microphysical Properties of Clouds

Clouds can be described in terms of the number concentration and the mean sizes of their particles, which are derived from the particle size distribution spectra of clouds. These two main parameters can be used to describe another bulk microphysical quantity of clouds known as the LWC, w_L, which can be expressed numerically as (Rogers and Yau, 1991):

$$w_L = \frac{4\pi {r_e}^3 \rho_w N(r)}{3} \tag{2.5}$$

where, ρ_w, and, $N(r)$, are density of water and droplet number concentration, respectively. The w_L, is typically expressed in gm^{-3} and ranges from about 0.05 to 0.25 in fog and up to $0.5\mathrm{gm}^{-3}$ in thick fog. In early-stage cumulus clouds, $w_L \approx$ 0.2 to $0.5\mathrm{gm}^{-3}$, later-stage cumulus $w_L \approx 0.5$ to $1\mathrm{gm}^{-3}$, while in thick congestus or cumulonimbus clouds $w_L \approx 0.5$ to $3\mathrm{gm}^{-3}$ and may be as high as $> 5\mathrm{gm}^{-3}$ in some of the fastest convective updrafts observed (Albrecht et al., 1990; Greenwald et al., 1993; Pruppacher and Klett, 1997). Blyth and Latham (1990) conducted aircraft observations to investigate the microstructure of clouds − LWC, $N(r)$ and r were some of the quantities observed. Fig. 2.1 is an extract from their work and it shows the horizontal cross-sections of these three quantities. It is noted that the peaks in LWC and $N(r)$ exist within the interior of the clouds and that is attributed to lack of entrainment of drier ambient air into inner cores of clouds. LWC is assumed to be invariant among clouds of the same type (Leaitch et al., 1992), although it varies strongly with height above cloud base (Rogers and Yau, 1991), but, droplet number concentrations do, since they are activated by CCN, which varies strongly in space and time, thus, the mean droplet sizes vary accordingly following Eqn. 2.5 (Twomey, 1977; Andreae et al., 2004; Rosenfeld et al., 2008).

Cloud particle concentrations primarily depend on aerosol concentration (Fitzgerald, 1974; Twomey, 1977; Andreae et al., 2004; Rosenfeld et al., 2008) and also on some other meteorological parameters such as supersaturation (Fitzgerald, 1973; Korolev and Mazin, 2003; Svenningsson et al., 2006). This is the microphysical reason underpinning the fundamental differences in cloud properties of different cloud types. Because continental aerosol loadings are higher than maritime loadings of aerosols (Allen et al., 2008; Takemura, 2012), continental clouds tend to have high droplet concentrations (Miles et al., 2000; Andreae et al., 2004) compared to their maritime counterparts (Miles et al., 2000; Phillips et al., 2009; Morrison and Grabowski, 2011). On the other hand, maritime clouds have broader size distributions and larger mean drop sizes, while continental clouds exhibit narrower size distribution spectrum with smaller mean droplet sizes at similar heights above cloud base (Miles et al., 2000; Andreae et al., 2004). This is because more cloud droplets will be competing for the same amount of available water. The typical mean droplet diameters for continental clouds is 15-20μm (Fitzgerald, 1974; Miles et al., 2000; Andreae et al., 2004), while for maritime clouds, it is about 25-30μm (Fitzgerald, 1974; Miles et al., 2000). Cloud droplet number concentrations are in the range of 100s to 1000s per cm^3 and few tens to about a hundred per cm^3 for continental and maritime clouds, respectively (Pruppacher and Klett, 1997; Rogers and Yau, 1991).

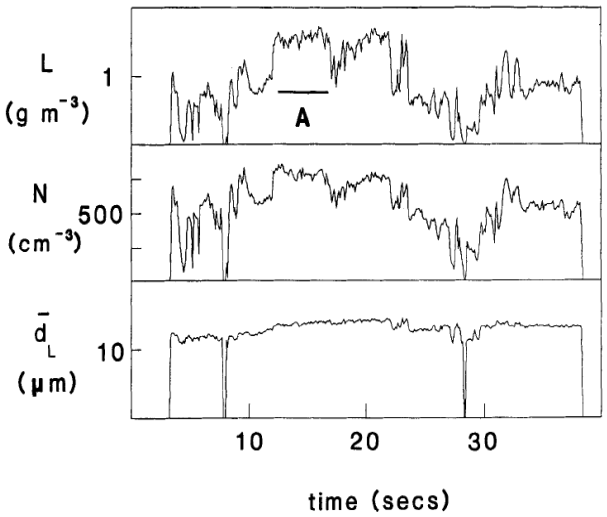

Figure 2.1: *The relationship between LWC, $N(r)$ and r measured during horizontal aircraft transect through a cloud over Montana for $r > 12\mu m$. The ten seconds on the plots correspond to a flight distance of 1km (Taken from Blyth and Latham (1990))*

2.1.2.3 Size Distributions of Cloud Particles

Several observations of cloud droplet size distributions e.g. by Miles et al. (2000) and Andreae et al. (2004) have been obtained in different cloud types and under different meteorological conditions, but they all seemed to exhibit some characteristic shape (Pruppacher and Klett, 1997). The size distribution spectrum of cloud droplets depends primarily on aerosols. For Numerical Weather Prediction (NWP) purposes, some statistical distributions have to be assumed for Cloud Droplet Size Distribution (CDSD)s. Typical CDSDs available in the literature and used in most bulk microphysics schemes are the exponential size distribution (Eqn. 2.6) as explained by Kessler (1969)

$$N(r) = N_0 \exp^{-\lambda r} \tag{2.6}$$

or the γ-distribution, Eqn. 2.7 (Clark, 1974; Walko et al., 1995; Mitchell and Arnott, 1994; Pruppacher and Klett, 1997);

$$N(r) = N_0 r^{\mu} \exp^{-\lambda r} \tag{2.7}$$

In equations 2.6 and 2.7, N_0, μ and λ are respectively, the intercept, shape and slope parameters of the distribution. However, most of the microphysics schemes that apply the γ-distributions usually set the shape parameter μ to zero, literally retaining the exponential distribution (Thompson et al., 2008). Some bulk microphysics schemes, however, deviate from the norm by employing complex distribu-

tions such as the log-normal distribution for the size distributions of their hydrometeors, Eqn. 2.1 (Clark and Hall, 1983). Integrating Eqn. 2.7 with respect to r from zero to ∞ yields Eqn. 2.8, which is the total number of cloud droplets in the whole size distribution spectra per cubic meter.

$$N = \int_0^\infty N(r)dr = \frac{N_0\Gamma(\mu+1)}{\lambda^{(\mu+1)}} \tag{2.8}$$

In order to estimate the mean droplet radius from the above γ-distribution, an integration from zero to ∞, of the product of r and $N(r)$ is performed and then divided by the total number, N, of cloud droplets given in Eqn. 2.8 to get r_m, (Eqn. 2.10):

$$r_m = \frac{1}{N}\int_0^\infty rN(r)dr = \frac{\Gamma(\mu+2)}{\Gamma(\mu+1)\lambda} \tag{2.9}$$

Here, r_m, is the mass weighted mean radius of the droplets. Now revisiting expression 2.5 for w_L, using equations 2.8 and 2.10, w_L can then be expressed as:

$$w_L = \frac{4\pi\rho_w N_0}{3}\int_0^\infty r^3N(r)dr = \frac{4\pi\rho_w N_0}{3}\frac{\Gamma(\mu+4)}{\lambda^{(\mu+4)}} \tag{2.10}$$

The above expressions are quite critical in numerical modeling in order to accurately characterize the distribution spectra for cloud particles. The distribution parameters (N_0, μ and λ) characterize such cloud properties but do not have universally constant values. Aircraft observations, e.g. Heymsfield et al. (2007a,b) showed that these parameters are statistically related to each other in any cloud system.

2.1.2.4 Liquid Phase Microphysics

If a moist air parcel of vapor mixing ratio, q_v, is cooled, it reaches a temperature T_{sat}, where it becomes saturated (Rogers and Yau, 1991; Pruppacher and Klett, 1997). There are several pathways by which a parcel of moist air can reach saturation; (a) by cooling it isobarically and adiabatically, it reaches saturation at the dew point temperature, T_d, (b) isobaric evaporative cooling causes saturation at the wet bulb temperature, T_w, and (c) lifting an air parcel adiabatically causes expansion and cooling that leads to saturation at a level called the Lifting Condensation Level (LCL) and temperature, T_{LCL}. The third pathway is the most crucial in cloud microphysics, thus, it is more often referred to herein (Rogers and Yau, 1991; Pruppacher and Klett, 1997).

When a rising moist air parcel reaches the LCL, it is said to be at saturation and its corresponding saturation vapor pressure, $e_{s,w}(T_{LCL})$ is given by the Clausius-Clapeyron equation and is a function of temperature only (Kołaczkiewicz and Bauer, 1985). At this level, condensation may take place, however, in the absence of proper CCN, condensation will not ensue. When this parcel continues rising due to its buoyancy or external forces, a new temperature T' can be reached with new saturation vapour pressure $e_{s,w}(T')$ and supersaturation, s_w:

$$s_w = \frac{e}{e_{s,w}(T')} - 1. \tag{2.11}$$

The ratio of the parcel's vapour pressure, e, to its vapour pressure at saturation, $e_{s,w}$, gives the saturation ratio, S, as shown in Eqn. 2.12 (Rogers and Yau, 1991);

$$S = \frac{e}{e_{s,w}} \tag{2.12}$$

2.1.2.4.1 Heterogeneous Activation of Cloud Droplets Homogeneous activation of cloud droplets requires some very high supersaturation, which are unrealistic in the real atmosphere (Rogers and Yau, 1991), thus, only heterogeneous nucleation of cloud droplets is covered under this section. Heterogeneous cloud droplet activation is done by a CCN (Kohler, 1936; Junge and McLaren, 1971; Ming et al., 2006). Only water soluble, or hygroscopic, or wettable CCN are known to nucleate cloud droplets, as their presence in water solution tends to reduce the solution's equilibrium vapour pressure quite substantially, while neutral or hydrophobic aerosols require unrealistic supersaturations for activation as in homogeneous nucleation (Kohler, 1936; Petters and Kreidenweis, 2007). Most aerosol particles are multicomponent, i.e., they comprise of substances of different chemical compositions (Fred and Seinfeld, 1980; Petters and Kreidenweis, 2007; Pringle et al., 2010), hence, the mass and chemistry of the water soluble component determines the nucleating efficiency of the AP. Therefore, as the RH rises, the water soluble component of the CCN deliquesces and undergoes diffusional growth (Pruppacher and Klett, 1997).

When smaller than a critical radius, the solution droplet's size is maintained at a stable equilibrium, such that the vapor pressure (saturated) at the surface always equals the ambient vapor pressure (Kohler, 1936; Rogers and Yau, 1991; Petters and Kreidenweis, 2007). But when larger than this critical radius, no stable equilibrium is possible and there is activation, namely uncontrollable growth to form a cloud droplet (Kohler, 1936; Rogers and Yau, 1991). This critical radius is reached at the corresponding critical supersaturation. This description of the CCN activity

was developed originally by Kohler (1936) and it is widely known as the *Kohler theory*. A detailed analytical development of this process is given in Appendix A or in Rogers and Yau (1991); Pruppacher and Klett (1997).

The Kohler theory is however, somehow complex, because of the high number of degrees of freedom; to compute the critical supersaturation over an aqueous solution droplet, the solute mass, molecular weight, bulk density, dissociable ions and activity coefficient are required a priori (Pringle et al., 2010), and this is quite cumbersome, especially for multicomponent aerosol species. However, recent work by Petters and Kreidenweis (2007) provided a more convenient way of determining the CCN activity of hygroscopic aerosols by prescribing only the hygroscopicity parameter of the aerosol and obviating the need to determine the aforementioned physico-chemical properties of the solution droplet. The equilibrium supersaturation in the interior of a cloud, well above cloud-base, depends on vertical velocity and liquid-water content (Rogers and Yau, 1991; Korolev and Mazin, 2003; Ming et al., 2006). For a uniformly ascending air parcel, the supersaturation reaches a maximum at the cloud-base and subsequently diminishes monotonically to assume a quasi-steady state supersaturation when droplet size distribution becomes mono-disperse (Rogers and Yau, 1991).

2.1.2.5 Ice-Phase Microphysics

A unique characteristic of water in clouds is that it can exist in liquid form even in temperatures down to as low as -40°C (Vonnegut, 1947; Anderson et al., 1980; Hirst et al., 2001). Sub-zero temperatures are necessary for the development of ice. There are two major pathways by which ice can nucleate within a cloud. As in water clouds, heterogeneous nucleation can occur (Roberts and Hallett, 1968; Murray et al., 2010; Crawford et al., 2011), this is whereby vapour or condensate deposit onto a foreign substrate called IN. Unlike in water clouds where homogeneous freezing is not feasible under real atmospheric conditions, ice crystals can form homogeneously from super-cooled cloud droplets at temperatures between -36 and -40°C (Anderson et al., 1980; Phillips et al., 2007).

The equilibrium saturation vapour pressure over a small ice embryo (e.g. less than about a micron) during or just after nucleation $e_{s,i}$ can be expressed similarly as for water with the Kelvin equation (La Mer and Gruen, 1952) as presented in Eqn. A.1 by replacing the water parameters with the ice parameters, σ_i, $e_{s,i}(\infty)$ and ρ_i being surface tension, saturation vapour pressure over an ice surface and bulk

density for ice, respectively (Rogers and Yau, 1991).

$$e_{s,i}(r) = e_{s,i}(\infty)e^{(\frac{2\sigma_i}{R_v\rho_i T_r})} \tag{2.13}$$

Always, the saturation vapour pressure is less over an ice than over a water surface (List, 1951; Buck, 1981; Murphy and Koop, 2005), whether for a flat surface or a small particle. For cloud-ice and ice precipitation, this surface tension/curvature effect is minimal and the exponential factor is practically unity (Rogers and Yau, 1991).

2.1.2.5.1 Homogeneous Freezing of Ice Crystals Homogeneous freezing of ice crystals is strongly dependent on the occurrence of statistical fluctuations of stable ice-like structures/embryos and the sizes of the water droplet. Both of these properties intrinsically depend on the surface tension of ice-liquid interface (Rogers and Yau, 1991). Observations and laboratory experiments have shown that homogeneous freezing occurs at around (-36 to -40)°C depending on the droplet sizes (Vonnegut, 1947; Anderson et al., 1980; Hirst et al., 2001), with larger supercooled drops freezing first (Phillips et al., 2007). This subsequently leads to *preferential evaporation* as discovered by Heymsfield et al. (2005) and studied by Phillips et al. (2007) with a numerical model. Preferential evaporation occurs owing to the co-existence of ice crystals and water droplets in an environment where the ambient maybe sub-saturated with respect to water, thus, the growth of ice crystals is favored, while water droplets evaporate (Hallett and Mossop, 1974; Korolev, 2007), therefore, not all droplets will freeze homogeneously at -40°C, but a fraction of them evaporates (Heymsfield et al., 2005; Phillips et al., 2007). The conditions required for homogeneous deposition of vapour to nucleate ice are too stringent in the atmosphere, hence, it may not occur (Rogers and Yau, 1991; Pruppacher and Klett, 1997).

2.1.2.5.2 Heterogeneous Nucleation of Ice Crystals Some clouds at sub-zero temperatures, but warmer than the homogeneous freezing temperature of supercooled droplets have been found to be *glaciated* − i.e. comprising ice crystals (Heymsfield, 1977). This indicates the existence of another mode of ice nucleation, which is *heterogeneous nucleation*. There are four major pathways by which this occurs depending on the availability of the rare deposition or freezing nuclei;

- **Deposition**; Vapour can deposit onto a *deposition nuclei* with the same principle that governs heterogeneous nucleation of cloud droplets (Sect. 2.1.2.4.1)

for ice saturated ambient conditions (Diehl et al., 2001; Hoppel et al., 2002; Dymarska et al., 2006).

- **Condensational freezing**; Occurs when the *freezing nuclei* act first, as a CCN, then under suitable temperatures, freezing ensues (Diehl et al., 2001).
- **Contact freezing**; This happens when appropriate freezing nuclei get into contact with the surface of a super-cooled cloud droplet either from outside, (*out-side-in*) or from in-side (*in-side-out*) of the super-cooled cloud droplet and cause freezing (Fukuta, 1975; Diehl et al., 2002).
- **Immersion freezing**; In this case, an IN is already immersed into a super-cooled cloud droplet and can effect freezing (Diehl et al., 2002; Marcolli et al., 2007).

There are several factors that determine which particle nucleate ice with what mode of nucleation. These include environmental conditions, and the history of the evolution of the particle in the cloud. It is not known yet, which mode is more important than the other simply because the knowledge of homogeneous and heterogeneous ice nucleation is still low (Pruppacher and Klett, 1997). The first stage of growth of an ice crystal is basically diffusional before growth by particle interaction ensues. There are several advances in numerical weather modeling to develop parameterizations of ice nucleation (Meyers et al., 1992; Eidhammer et al., 2009). The one by Phillips et al. (2008, 2013) that treats all the four modes of heterogeneous ice nucleation is discussed in Sect. 3.1.3.

2.1.2.5.3 Ice Multiplication Surprisingly, observations of ice number concentrations have shown that the number concentrations of ice crystals can be several orders of magnitude higher than IN number concentrations (Gardiner and Hallett, 1985; Gultepe et al., 2001; McFarquhar et al., 2007; DeMott et al., 2011). This leads to another mechanism of ice production called *secondary ice multiplication* (Hallett and Mossop, 1974; Gardiner and Hallett, 1985). The *enhancement factor/ratio*, R_M, (Eqn. 2.14) is the ratio of IN number concentration to ice crystal number concentration and it has been found to be temperature dependant.

$$R_M = \frac{N_{IN}}{N_i} \tag{2.14}$$

Several hypotheses have been used to explain this discrepancy; the Hallett-Mossop process is an ice multiplication process by the formation of splinters during riming, most effectively within the -3 to -8°C temperature range (Hallett and

Mossop, 1974). The other mechanisms are by mechanical fracturing of fragile ice crystals during impact and fragmentation of relatively large individual cloud or rain drops during freezing (Pruppacher and Klett, 1997; Rogers and Yau, 1991). Finally, the ice multiplication factor may have contributions from an instrument artifact affecting aircraft probes. This instrument artifact is due to ice shattering, which is the mechanical fracturing of large ice crystals at the housing (or entrance) of the ice particle measuring probes, which can result in spurious ice number concentrations being recorded (Field et al., 2006; McFarquhar et al., 2007; Nousiainen et al., 2011). However, Hobbs (1969) observed such a large ice multiplication factor using hand-held instruments without any such bias.

2.1.2.6 Particle-Particle Interaction and Precipitation Formation

In the real atmosphere, cloud droplets or ice crystals do not grow indefinitely by diffusion (Rogers and Yau, 1991). This is because the water budget is constrained mostly by the thermodynamics of the cloud parcels and their environment. Hence, competition for water by cloud droplets depletes the water vapour (Korolev, 2007), thus, abating the free growth of cloud droplets by diffusion. Thus, cloud droplets can only grow to a few tens of microns by diffusion (Rogers and Yau, 1991), however, precipitation reaching the ground is seen to have droplets with typical sizes of the order of a few millimeters (Marshall and Palmer, 1948; Sheppard and Joe, 1994). There are primarily two processes of precipitation formation, which are the *warm-rain* (Beard and Ochs III, 1993) and *ice crystal* processes (Young, 1974b). This is because, when the cloud particle sizes exceed about 20μm, they begin to have substantial fall velocities with large drops falling much faster than smaller ones, otherwise they can be assumed to be stationary (Mitchell, 1996; Orr and Kropfli, 1999; Yamamoto et al., 2008) [1].

Cloud particle interaction happens among the same or different hydrometeor species, for instance, in a cloud with all five species of hydrometeors that are commonly treated in NWP, (*i.e. cloud droplets, cloud ice, rain, snow and graupel*) a myriad of interactions are found. The interaction of a solid hydrometer such as graupel, snow or ice with a liquid particle such rain or cloud droplets is called *riming* (Borys et al., 2003). If this interaction takes place between snow (or ice) and cloud (or rain), then, the result may lead to the formation of a graupel particle or snow especially in low LWC. *Aggregation* is the term used to describe the interaction between solid particles (Hobbs et al., 1974). This process produces Snow

[1] NB, the reader is referred to Appendix C for the mathematical illustration of hydrometeor particles interactions.

precipitation. In general terms, *accretion* is a term used to describe the growth of hydrometeors through interaction with each other, but may also be used in place of riming (Rogers and Yau, 1991). *Coalescence* is used for cloud droplet−cloud droplet interaction but is sometimes extended also to rain droplet−cloud droplet interaction. Snow is produced in weak vertical velocities but not so much in deep convection. In deep convection with warm bases, warm rain processes are more prevalent (Phillips et al., 2001, 2002, 2005)

2.1.3 Radiation, Clouds and Climate

Radiation is one of the mechanisms of energy transfer; other common mechanisms are *convection* and *conduction* (Siegel and Howell, 1992). Unlike other forms of energy transfer, radiation does not require a medium for energy propagation; hence, radiant energy can propagate through a vacuum. This is the primary mechanism by which solar energy reaches the Earth.

Radiation from the sun propagates in the form of electromagnetic (EM) waves and is not a single or narrow band of wavelengths, but a wide range of continuously varying wavelengths comprising the *electromagnentic spectrum*. What the retina of our eyes is sensitive to, is just a narrow band of the Electro-magnetic (EM) spectrum called the *visible* region of wavelengths (0.4 - 0.7)μm (Liou, 2002). EM waves of wavelengths shorter than 0.4μm are called the ultra-violet, x-rays and γ-rays while those longer than 0.7μm are the infrared, microwaves and radiowaves (Liou, 2002).

2.1.3.1 Black Body and its Laws

The sun can be assumed to be a *black body*. A black body is a conceptualized body that absorbs all radiation incident on it at a given temperature and it is also a perfect emitter. Every body is constituted of atoms and molecules, which radiate energy, E, in the form of packets called *quanta* or *photons* given by,

$$E = (n + 1/2)h\nu \tag{2.15}$$

as postulated by Planck, where, n, is the quantum number, h is known as the Planck's constant (6.63×10^{-34} Jsec) and, ν, is the frequency of the oscillator. The Planck's law postulated that the monochromatic emittance, M_λ, emitted by a black body is a function of the wavelength, λ, and the temperature, T, of the body, i.e.

$$M_\lambda(T) = \frac{2hc^2}{\lambda^5(e^{hc/K\lambda T} - 1)} \tag{2.16}$$

where, c, is the speed of light and, K, is the Boltzmann constant (1.38×10^{-23} JK^{-1}).

The spectral emittance of a black body as described by *Plank's-law* is a function only of temperature of the body and wavelength and its total emittance, M_T, can be described by the *Stephan-Boltzmann law* (Eqn. 2.17), which is an integral of Eqn. 2.16 over the whole range of wavelengths from 0 to ∞.

$$M_T(T) = \sigma T^4 \tag{2.17}$$

where, σ is a constant (5.67×10^{-8} $\mathrm{Jm}^{-2}\mathrm{sec}^{-1}\mathrm{K}^{-4}$) known as the *Stefan-Boltzmann* constant. By partially differentiating Eqn. 2.16 with respect to λ, the *Wein's Displacement Law* is achieved, which states that the wavelength of the maximum emittance, λ_m, is inversely proportional to the temperature of the body, i.e.

$$\lambda_m = 2.9 \times 10^{-3}/T \tag{2.18}$$

This relationship (Eqn. 2.18) enables the determination of the temperature of the black body (e.g. the sun) from the wavelength of its maximum monochromatic emittance.

When two bodies (one of which is a black body) are placed parallel to each other, they exchange radiation until a thermodynamic equilibrium is reached. Because the other body is not a black body, it does not absorb all the energy incident on it, hence, it is called a *grey* body. The ratio of the absorbed irradiance to the total emitted by a black body is called the absorptivity, $\hat{a}$. Therefore, at thermodynamic equilibrium, the grey body absorbs $\hat{a}M_T$ and this should be equal to the emitted energy $\hat{\epsilon}M_T$. i.e. $\hat{a}M_T = \hat{\epsilon}M_T$ where, $\hat{\epsilon}$, is the emissivity of the grey body, i.e. the ratio of the emitted energy by the grey body to the black body incident energy. Consequently, the *Kirchhoff's law* states that:

$$\hat{a} = \hat{\epsilon} \tag{2.19}$$

For a grey body, $\hat{a} = \hat{\epsilon} < 1.$, while for a black body both $\hat{a}$ and $\hat{\epsilon}$ are equal to 1 (Liou, 2002).

2.1.3.2 Absorption, Reflection and Scattering

When a photon of light encounters an obstacle, it can either be *absorbed, scattered* or *reflected*. Absorption occurs when matter extracts all or part of the incident energy and converts it to other forms of energy, while reflection is the re-direction of photons at a discontinuity without changing the wavelength of the photon. Scattering occurs

when matter extracts all or part of the incident energy and reradiates all of it in several other directions, however, without changing its wavelength (King, 1993; Liou, 2002). Scattering is dependent on the size of the particle (e.g. aerosols, air molecules, cloud particles) interacting with the photon.

The scattering behavior of a particle is described by its size parameter, x, which is the ratio of its circumference to the wavelength, λ, of the incident radiation for a spherical particle.

$$x = 2\pi a/\lambda \tag{2.20}$$

where, a, is the radius of the particle. Particles with radii, a, much smaller than the wavelength of the incident photon (with $x \ll 1$) act like a dipole, i.e. they tend to scatter the radiation as much in the forward as in the backward directions. The scattering by these types of particles is called the *Rayleigh scattering* and the intensity of the scattered radiation is inversely proportional to the fourth power of the wavelength of the incident radiation, i.e.

$$I_\lambda \approx \frac{1}{\lambda^4} \tag{2.21}$$

The fact that in the visible region of the EM spectrum, blue light has shorter wavelengths than other colors e.g. red and orange makes it scattered more than other colors, hence, the sky appears blue when viewed away from the sun. The sky appears red-orange when the sun is towards the horizon due to the back-scattering of shorter wavelengths by air molecules as sun's rays travel longer distances (Shaw, 1982; Rozenberg, 1960). In *Mie-scattering*, particles of comparable dimensions (e.g. aerosols and cloud or rain droplets) to the wavelength of the incident light have a size parameter, $x \geq 1$, and tend to scatter photons predominantly in the forward direction and are responsible for phenomena such as rainbows and halows (Rozenberg, 1960; Liou, 2002).

2.1.4 Clouds and Climate

For the insolation reaching the Earth system through the top of the atmosphere (TOA), a portion ($\approx 30\%$) of it, is reflected back to outer space by clouds, aerosols and the Earth's surface. Some ($\approx 20\%$) of it, is absorbed by atmospheric constituents, such as, water vapour and dust particles, therefore, only a fraction ($\approx 50\%$) of it, is absorbed by the Earth's surface (Hobbs, 1993). The radiation at the Sun's wavelengths are typically called the Short-Wave radiation (SW), while that radiated by the Earth back to space is called Long-Wave radiation (LW) (King, 1993).

SW and LW are roughly distinct since the emission temperatures of the Sun and the Earth are so different. About 12% of the LW escapes into space through the atmospheric window (Dall'Oglio et al., 1976; Liou, 2002) and clouds are the main particles that affect the window.

For a balanced climate system, radiative equilibrium is assumed; therefore, the radiative fluxes entering and leaving the climate system measured at the TOA would balance, thus,

$$\bar{F}_s(1-\bar{A}) = \bar{\hat{\epsilon}}\sigma_{Pl}T_A^4 + (1-\bar{\hat{\epsilon}})\sigma_{Pl}T_B^4 \tag{2.22}$$

where, $\bar{F}_s$, is the mean solar insolation measured at TOA, $\bar{A}$, is the mean reflectivity of the Earth, $\bar{\hat{\epsilon}}$, is the mean emissivity of the atmosphere while, T_A, and, T_B, are respectively, the Earth's atmosphere and surface effective temperatures (Liou, 2002). The term on the left side of Eqn. 2.22 represents the average insolation absorbed by the climate system, Absobed Solar Radiation (ASR). The first term on the right represents the mean longwave radiation emitted by the Earth's atmosphere, while the last term represents the radiation emitted by the Earth that escapes into space without being attenuated. In summary, the terms on the right represent the Outgoing Longwave Radiation (OLR). The distribution of the annually averaged ASR and OLR is shown in Fig. 2.2, the region of surplus ASR is between ±45°N and elsewhere OLR is in surplus. The imbalance in the distribution of ASR and OLR drives the general circulation.

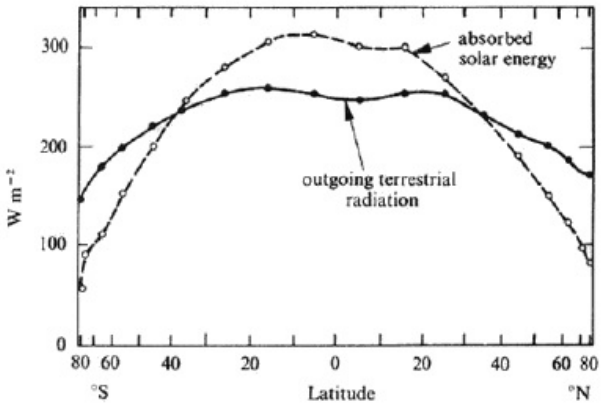

Figure 2.2: *Absorbed Solar Radiation (ASR) and Outgoing Long-wave Radiation (OLR) latitudinal distribution (Taken from Houghton (1986))*

For a climate system at equilibrium, the global net radiative flux, F_{net}, measured at the TOA, which is given by Eqn. 2.23,

$$F_{net} = A\bar{S}R - O\bar{L}R \tag{2.23}$$

should be equal to zero. Here, $A\bar{S}R$ and $O\bar{L}R$ are the global means of incoming and outgoing radiative fluxes. Any constraint offsetting the balance in Eqn. 2.23 causes climate change and is called a *climate forcing* (Charlson et al., 1992; Liou, 2002). This can either be CO_2 altering the emissivity, $\bar{\epsilon}$, of the atmosphere (Mercer, 1978) or aerosols, or clouds, altering $\bar{A}$, the reflectivity of the Earth (Charlson et al., 1992; Haywood and Boucher, 2000; Lohmann and Feichter, 2005; Johnson, 2003). Surfaces properties e.g. Siegel and Howell (1992) and King (1993), solar input, etc., all are parameters whose changes may cause a climate forcing. Fig. 2.3 is an extract from the fifth IPCC report (Boucher and Randall, 2013) showing different atmospheric components and their respective radiative forcings due to their changes from the pre-industrial era (year 1750).

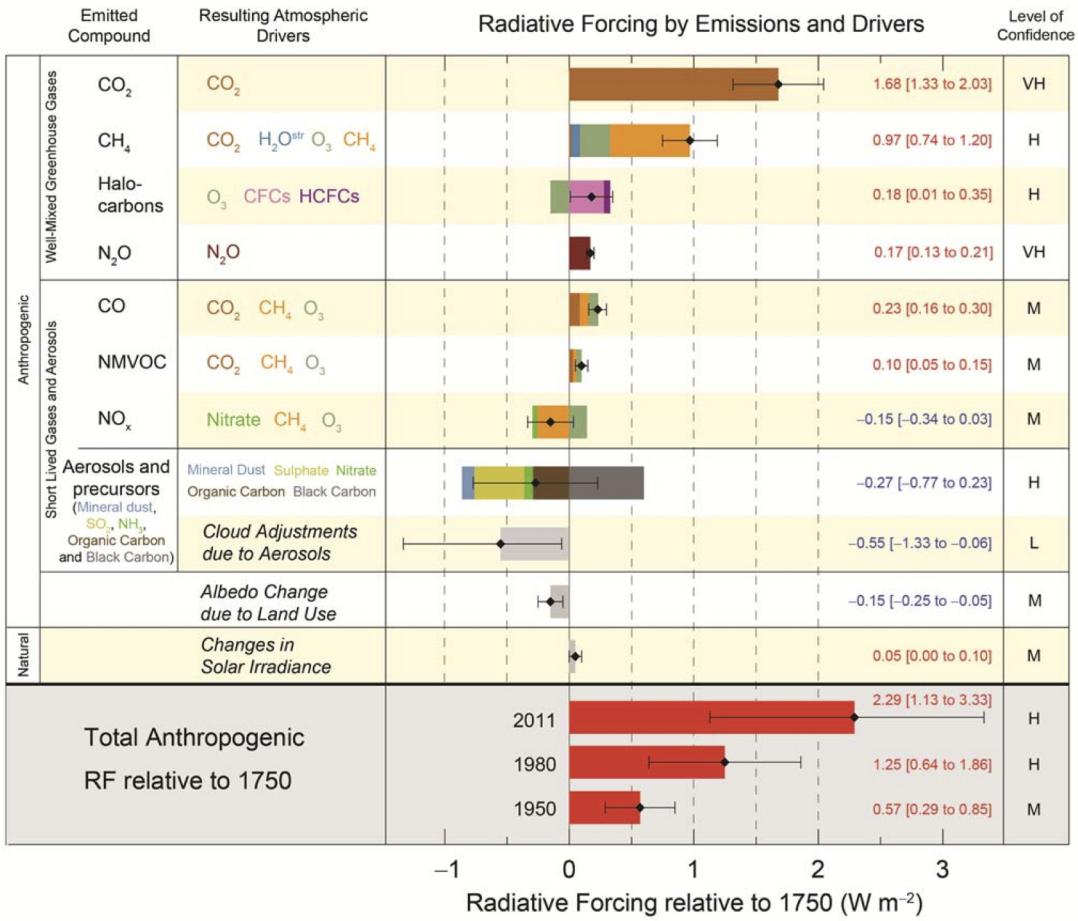

Figure 2.3: *Radiative forcings from various radiative forcing agents from the pre-industrial era to the present-day (Taken from Boucher and Randall (2013))*

On average, clouds cover about half of the Earth at any given time (Liou, 2002), this makes them a very important component of the Earth's radiation budget. Clouds control radiation in opposing ways depending on their micro- and macrophys-

ical properties. They reflect shortwave radiation back to space, hence, cooling the Earth, on the other hand (Charlson et al., 1992; King, 1993), they have a *green-house effect* when they trap OLR. It is generally understood (e.g. Harrison et al. (1990) and Gettelman et al. (2012)) that high and optically thick clouds have a green-house effect because of their low emitting temperatures, while low-clouds mainly because of their high LWC and small radii become highly reflective in the shortwave (Brient and Bony, 2012). On average, clouds cool the Earth (Ramanathan et al., 1989; Lohmann and Feichter, 2005). In GCM, clouds need to be well represented in order to accurately predict climate, hence, several of their properties need to be well represented as explained by Yang et al. (2012.). They used observed vertical structures of crystal habits and roughness to highlight the importance of these ice features in radiative forcing of clouds and how their complex structures can be represented simplistically in cloud models.

2.2 Literature Review

2.2.1 Aerosol-Cloud Interaction with Radiation: Indirect Effects

It is essential to note that clouds regulate the radiation and precipitation budgets of the Earth. Hence, perturbations to the stable state of the aerosol field (loading and chemistry) modify the net radiative forcing from clouds, thus, affecting the Earth's climate system. This effect of aerosols on the Earth's climate system through their interaction with clouds is called the Aerosol Indirect Effect AIE (Haywood and Boucher, 2000; Lohmann and Feichter, 2005). The review paper by Lohmann and Feichter (2005), states different hypotheses for aerosol indirect effects, most of which are not yet fully understood. These hypotheses can be divided into two primary categories, which are:

- The *cloud albedo effect*, (Lohmann and Feichter, 2005) also known as the *first indirect effect* from Ramaswamy et al. (2001) or the *Twomey effect* by Twomey (1977). In this study it is referred to as the *cloud albedo-emissivity effect*, because the emissivity of the cloud is also affected by changing the aerosol field in a similar way as the albedo (e.g. Freidenreich and Ramaswamy (1999)).

- The second primary category is the *cloud life-time effect*, (Lohmann and Feichter, 2005) also called the *second indirect effect* (Ramaswamy et al., 2001) or the *Albrecht effect* by Albrecht (1989).

Briefly, the cloud albedo-emissivity effect is the change in the TOA radiative fluxes, resulting from the change of the cloud's reflectance, caused by a reduction in mean sizes of cloud particles, while on the other hand, the lifetime indirect effect results from the redistribution of the cloud mass. These changes are caused by changes in the aerosol field and detailed explanation on each of these effects is presented in the following sections.

There are multiple contributions to the lifetime effect, mainly from microphysical processes that are dependent on the aerosol field, e.g. riming, which gives rise to the *riming indirect effect*, latent heating change (e.g. from freezing of cloud droplets), which gives rise to the *thermodynamic indirect effect* and heterogeneous ice nucleation by extra ice nuclei yields the *glaciation indirect effect*. Other aerosol indirect effects are the *semi-direct effect* (Johnson et al., 2004) as investigated by Hill and Dobbie (2008), who used bin-resolved cloud microphysics with a homogeneously mixed layer of black carbon (BC) as the absorbing aerosol in the boundary layer. They noted that the semi-direct effect reduces the daytime liquid water path (LWP)

and effective droplet radius, (r_e), and also increases the optical thickness, (τ), of the cloud. Their results showed a negative radiative forcing for the semi-direct effect. Finally, aerosols also alter the surface energy budget, hence, they modify meteorological processes such as evaporation, precipitation and convection and this effect is referred to as *surface energy budget indirect effect*. However, for the purposes and objectives of the present thesis, the semi-direct and surface energy budget effects are not considered.

A detailed explanation of the aforementioned indirect effects is provided in the following subsections. The cloud albedo indirect effect is usually distinguishable from the other indirect effects because it has a purely quantifiable radiative forcing in the global climate simulations, whereas the other indirect effects are not classified as forcings because they involve complex feedbacks in the climate system (Solomon et al., 2007). This study attempts to analyze these feedbacks. However, the fifth IPCC report refined definition by considering both albedo-emissivity and lifetime indirect effects as the effective radiative forcing from aerosol-cloud interactions (ERFaci).

2.2.1.1 Cloud Albedo-Emissivity Effect

When aerosol concentrations surge in a cloud whose water-content (mass concentration and condensate) is fixed, the cloud droplet or ice crystal concentration of such a cloud rises subsequently (Andreae et al., 2004). This is a consequence of higher CCN concentrations nucleating numerous cloud droplets. However, there will be competition for water vapour from these numerous cloud droplets or ice crystals, and their mean radius diminishes. In a cloud, mass concentration and condensate may stay fixed. This is because the thermodynamical state of the atmosphere (humidity, temperature) determines the cloud-base temperature, the adiabatic liquid water content and entrainment of air that dilutes air parcels. So it is the atmospheric thermodynamics and dynamics that determines the liquid water content initially, not aerosols.

However, anthropogenic increases in aerosols may increase the mean global droplet numbers and induce flux changes through the albedo-emissivity effect (Charlson et al., 1992). This albedo effect was explained well by Twomey (1974) who used data collected from a monitoring station near the south-eastern coast of Australia to quantitatively explain the effect of urban/industrial pollution on the cloud droplets' concentration and their effective radius. He concluded that anthropogenic aerosol pollution may at that time had induced an increase in the global cloud droplet concentration of approximately 3%. Leaitch et al. (1992) collated in-situ measurements

of sulphate and nitrate aerosols from multiple cloud samples observed during different field campaigns on clean and polluted clouds over eastern North America. They compared these with their respective coincident measurements of Cloud Droplet Number Concentrations (CDNC) and observed that polluted clouds had over 50 % more CDNC compared to their clean counterparts. Andronache et al. (1999) also carried out a modelling study using a high resolution non-hydrostatic model to investigate the effect of sulphate aerosols on deep convective clouds, his simulations showed a reduction of up to 2μm in mean radius of cloud droplets and an increase of 5-20cm^{-3}m of cloud droplet concentration.

There is an intricate relationship between cloud micro- and macrophysical properties and the cloud's optical properties, which moderate the Earth's radiation budget. Different cloud types register different radiative signatures on the Earth's climate system. Thick low-level clouds have higher optical thickness compared to higher altitude cirrus clouds. Therefore, low clouds tend to be highly reflective causing a cooling effect in the climate system as less insolation would reach the ground. On the other hand, cirrus clouds tend to be less reflective to shortwave radiation (insolation/incoming solar radiation (ASR) because of their low water contents and they cause a stronger warming by absorbing longwave radiation and emitting at low temperatures. They then re-emit this LW radiation back to the Earth's surface thereby warming the climate system in a similar manner as the greenhouse gases - a warming effect.

The main radiative property of a cloud is its cloud albedo. It is essentially a measure of the cloud's reflectivity. A higher albedo implies a highly reflective cloud. Cloud albedo depends on a myriad of the cloud's bulk microphysical properties, but it is primarily dependent on the LWC and effective droplet size (Han et al., 1998). The albedo of a cloud can be expressed mathematically in terms of its optical thickness. Twomey (1974) described a cloud with optical thickness, τ, as one that transmits the fraction $e^{-\tau}$ of radiation through it, hence, the albedo, A, can be expressed as in Eqn. 2.24.

$$A = 1 - exp^{-\tau} \tag{2.24}$$

Lohmann et al. (2000b) reviewing the work of (Han et al., 1998) explained the contrasting mathematical relationships between cloud optical thickness and effective radii. For optically thick clouds, with optical thickness, $\tau > 15$, the optical thickness, τ_{thick}, is given by:

$$\tau_{thick} = \frac{3}{2}\frac{w_L \Delta z}{r_m} \tag{2.25}$$

where, w_L is the liquid water content in gm^{-3}, Δz is the cloud's geometrical thickness and r_m, is the mass weighted mean radius of the cloud droplets. This expression shows that for optically thick clouds, the optical thickness is inversely proportional to the effective radius; hence, the cloud albedo increases with decreasing effective radius, under the assumption that LWC remains constant. If expression 2.5 is substituted into expression 2.25 then τ_{thick}, for optically thin clouds with $\tau < 15$ would be expressed as:

$$\tau_{thin} = 2r_e N(r)\rho_w \Delta z \tag{2.26}$$

in which case, τ, for optically thin clouds is directly proportional to the effective radius, r_e, of a cloud particle and increases with increasing effective radius. Equation 2.26 was valid under the assumption that, $N(r)$, was constant, which was expected of a cloud in the droplet growth state.

Equation 2.25 expresses the most prevalent and conventional scenario, and Han et al. (1998) found it to be the dominant situation in continental and all thick clouds, but the second expression, Eqn. 2.26 was found to be predominant in thinner maritime clouds and in thinner clouds over tropical rain forest. Hence, they concluded that in regions where aerosol concentrations are already high for instance over the continents, clouds will follow the τ-r_e in Eqn. 2.25, while in clean aerosol conditions, for example in marine conditions, clouds will follow the τ-r_e in Eqn. 2.26.

The industrial era caused air pollution from combustion of fossil fuels. Sulphate aerosols are the dominant product of this industrialisation while black carbon (soot) is also another major anthropogenic aerosol component whose burden in the atmosphere rose significantly since the pre-industrial era. These changes in aerosol loading have caused an increase in the cloud albedo and observations also confirmed this. Feingold (2003) showed an increase in reflectance with increasing aerosol concentration. This cloud albedo-emissivity effect is the only indirect effect that so far has a quantifiable radiative forcing. Accordingly, it is defined by Menon et al. (2002a) as the net change in the cloud radiative forcing at the top of the atmosphere, while Rotstayn and Liu (2003) defined it as, the net change in short wave radiation at the top of the atmosphere. Both definitions are almost similar since the component of the longwave radiation in the cloud albedo effect is insignificant (Rotstayn and Penner, 2001). The fourth IPCC report (Solomon et al., 2007) estimated the cloud albedo effect to have a generally negative radiative forcing, which is between -0.22 and -1.85Wm^{-2} for warm clouds.

2.2.1.2 Cloud Lifetime Effect

The lifetime effect can be defined as the change in mass distribution of condensate in a cloud that leads to a change in net radiative flux entering the top of the atmosphere. This happens chiefly due to alterations in the processes of precipitation production (accretion and auto-conversion), and sedimentation rates of cloud particles. An increase in the CCN loading results in an increase in the concentration of cloud droplets initiated. This causes a reduction of the mean effective radii of cloud droplets as explained in Sect. 2.2.1.1, the same principle is also true even for ice-only clouds in which the ice crystal number concentration increases, either from CCN changes (homogeneous freezing) or from IN changes (heterogeneous nucleation). Smaller cloud particles are less effective in microphysical processes that form precipitation within a cloud such as riming, accretion, aggregation, sedimentation, collision and coalescence processes because their small size lowers their collision efficiency. Consequently, precipitation processing is suppressed therein, thereby prolonging the life span of a cloud in the atmosphere. This obviously alters the water cycle and the radiation energy entering the climate system.

Microphysically, the aerosol concentration, chemistry and of course the Aerosol Size Distribution (ASD) determines the CCN activity spectrum. It is this CCN activity spectrum, coupled with the updraft velocity at the cloud base that determines the cloud-base CDSD. The evolution of the CDSD with height is a function of the CDSD at the cloud base, hence, apart from other dynamical factors, the cloud base CDSD has the first order importance in determining the height, H, above cloud base at which precipitation should form (Andreae et al., 2004; Rosenfeld et al., 2008). When the cloud base CDSD has a mean value towards smaller sizes, H would possibly be larger, leading to a delay in precipitation onset. This is the fundamental microphysics process that underpins the cloud lifetime effect.

Due to the presence of tiny and numerous cloud droplets in relatively shallow clouds, the probability of collision and coalescence is reduced in a cloud. This leads to precipitation suppression, as such, cloud lifetime increases. Most observations have shown suppression of precipitation or absence of drizzle in polluted clouds. Andreae et al. (2004) analyzed data from the 2002, Large-Scale Biosphere-Atmospheric Experiment in Amazonia-Smoke, Aerosol, Clouds, Rainfall, and Climate (LBA-SMOCC) campaign. The campaign covered the period ranging between the smoky dry season (September) and ended during the wet season (November) when the aerosol concentration approached the background concentrations due to effective aerosol washout by precipitation. In order to eliminate the dynamical and

thermodynamic effects on clouds, they analysed only data from cases taken during the campaign that were dynamically and thermodynamically similar, in which case, only the aerosol fields were perturbed. They found out that heavy smoke from wild fires in this region delays the onset of precipitation to $H = 5000$ m in the smoky dry season, compared to $H = 1500$ m during the wet season. In the wet season, cloud droplets coalesce and grow faster to precipitate, as is the case with maritime clouds. Their findings corroborated those of Ferek et al. (2002) who analysed satellite cloud data of ship induced tracks, off the west coast of Washington. Ferek et al. (2002) found out that drizzle production was suppressed within these ship tracks compared to their ambient clouds. Mahowald and Kiehl (2003) made a similar observation with dust over the Sahara desert where precipitation was suppressed by mineral aerosols during desert dust outbreaks in low-level clouds and they also noted a net increase in ice phase clouds. In all these three cases discussed above, droplet sizes were also found to have dropped significantly. Studies such as these provide evidence for, and improved understanding of the effects of anthropogenic pollution on the radiative and bulk microphysical properties of clouds.

Accordingly, models also show reduced or delayed precipitation formation especially in water- or mixed-phase clouds with increased loadings of soluble aerosols (Menon and Del Genio, 2007). However, Lee et al. (2008b) noted an increase in area-averaged precipitation with increasing aerosol loadings. Although autoconversion was markedly reduced in their simulations, a compensatory effect of increased accretion of cloud liquid led to higher precipitation efficiency. Also, evaporative cooling simulated, enhanced low-level convergence, which contributed to this increase in precipitation for convective cases. Different model runs predict different magnitudes for the cloud albedo and cloud lifetime effects; Solomon et al. (2007) reports that the Twomey effect (albedo effect) at the TOA is four times greater than the cloud lifetime effect, conversely, Quaas et al. (2004) the opposite.

2.2.2 Riming Indirect Effect

The rate of growth of a solid hydrometeor of radius, R, by riming can be derived from the geometric sweep-out concept and be represented in the final form as:

$$\frac{dm}{dt} = \bar{E}\omega_l \pi R^2 u(R) \tag{2.27}$$

where, m, is the mass of the solid hydrometeor, $\bar{E}$, is the mean collection efficiency and, ω_l, is the liquid water content while, $u(R)$, is the terminal fall speed of the particle (Rogers and Yau, 1991). Smaller droplet sizes tend to reduce the riming rate

because collision efficiency for droplet-ice collisions is strongly sensitive to droplet sizes. In the wake of the discussion given in sections 2.2.1.1 and 2.2.1.2 it is logical to conclude that the rate of growth of graupel by riming $\frac{dm}{dt}$ decreases with increasing aerosol loading. This effect is referred to as the riming effect (Lohmann and Feichter, 2005).

This riming effect was investigated by Borys et al. (2003) using mountain-top in-situ and remote sensing measurements over the northern Rocky Mountains of Colorado, USA during the winter of 2001. The campaign was carried out to investigate the second aerosol indirect effect on precipitation formation. They found that, the higher concentrations of anthropogenic aerosols altered the microphysical processes by inhibiting or even shutting off completely, the growth of snow by riming and consequently, reducing the snow fall rates. The fact that snowfall rates were found to be higher when snow growth included riming, and also that riming occurred when supercooled droplets had a diameter greater than a certain minimum threshold of $10\mu m$ confirmed that more aerosols reduce the riming efficiency. Also, riming did not take place when aerosol concentrations were higher, a scenario likely to be caused by anthropogenic aerosol pollution.

Lohmann (2004) carried out a GCM simulation to investigate whether anthropogenic aerosol pollution would decrease snowfall rates. Size-dependent riming efficiency was used in these simulations and the results showed that snowfall rates actually increase with less efficient riming conditions. Although this result contrasted with observations, Lohmann attributed this disagreement to cloud feedbacks in the climate system. They added that, the lifetime indirect effect (Sect. 2.2.1.2), reduces surface insolation and builds up climatic conditions that favour snow production through other processes such as aggregation rather than riming. This contradiction between observations and model results is expected because, there are only few observational and modelling studies that have been carried out so far to assess the riming effect, which is why modeling studies as this one are of higher importance.

2.2.3 Thermodynamic Indirect Effect

The thermodynamic effect, also known as the invigoration effect (Morrison and Grabowski, 2011; Gettelman et al., 2012) is an aerosol indirect effect resulting from a change in cloud dynamics, due to (changes in the burden of condensate or) latent heating patterns. Because an increase in aerosol loading gives rise to numerous but tiny cloud droplets (sections 2.2.1.1 and 2.2.1.2), warm rain precipitation production is delayed or completely inhibited through reduced chances of collision and coalescence of cloud droplets. Consequently, these numerous but tiny cloud droplets may

be pushed aloft beyond the freezing level by an updraft. The subsequent freezing of these droplets can release vast amounts of latent heat, which strengthen updrafts. Rosenfeld et al. (2008) developed a conceptual model using satellite retrievals of cloud-top temperatures, T, and cloud particle effective radius relationships. He noted that, updraft strength in deep-convective clouds was stronger when the effective radius of cloud droplets at cloud-base was smaller, which is also the microphysical process underpinning the development of severe storms and tornadoes.

Khain et al. (2005), using a two dimensional bin-resolving cloud model, investigated the effects of aerosols on cloud dynamics and precipitation efficiency. They noted that the strength of updrafts increases with aerosol loading as a result of increased buoyancy arising from latent heat release upon freezing of small cloud droplets. An increase of cloud top height and the overall cloud lifetime were also noted in his simulations. In addition to the invigoration of the updrafts, Khain et al. (2005) also discovered that wind shear detrains precipitating particles from convective cores into subsaturated regions of the clouds and the subsequent thawing, evaporation and sublimation of hydrometeors led to adiabatic cooling. If this is augmented by condensate loading, it results in the strengthening of downdrafts ahead of the cumulonimbus cells thereby promoting the formation of secondary cells and squall line development. The effect of aerosol loading on precipitation was seen to be a reduction in the precipitation efficiency under continental conditions, the opposite was however true for maritime cases.

Fan et al. (2009) in a modeling study, simulated isolated DCCs and found that the effects of wind shear on the overall effect of aerosols should not be downplayed. Under Strong Wind Shear (SWS), they noted a suppression of convection with increase in aerosol loading, which was stronger in humid than in drier conditions. On the other hand, in Weak Wind Shear (WWS), an increase in CCN concentrations was seen to invigorate convection but a saturation point existed beyond which suppression of convection emerged again. This phenomenon was attributed to the imbalance between condensational heating and evaporative cooling. In WWS, condensational heating is dominantly higher than evaporative cooling but they cancel each other out with CCN loading. These results corroborate those of Lee et al. (2008a) who noted that SWS reduces the interaction between microphysics and dynamics.

In contrast to Khain et al. (2005)'s findings, Storer and van den Heever (2013) did not see the invigoration effect for mature updrafts in their series of two-dimensional large-scale simulations of DCC. They discovered that, although, extreme values of vertical velocities occurred more frequently in polluted DCCs, the average updraft velocities in fact decreased. This was linked to the building up of the drag force due

to condensate loading, although, latent heating strengthened early stage updrafts of the storms. Cui et al. (2006) echoed similar findings of aerosol loading suppressing convection, in a modelling study where they also noted a reduction in precipitation production. But Cui agreed with Khain et al. (2005) in downdraft invigoration. Hill et al. (2008) simulated a non precipitating marine cloud and noted that increasing the CCN promoted cloud-top evaporative cooling that enhanced entrainment and strengthened the boundary layer dynamics.

Although, the invigoration effect is widely conceived as an effect involving only the ice-phase, (Lohmann and Feichter, 2005; Khain et al., 2005; Cui et al., 2006), another researcher, Lee et al. (2009) carried out sensitivity tests to investigate the impacts of aerosol chemistry on microphysics and precipitation in mesoscale cloud systems of warm-based convection. This was done by artificially prohibiting all ice processes in their simulation. They noted that the convective invigoration still occurred when aerosol loading was boosted. They also found that increasing solute aerosol (CCN) loading, increases CDNC, which then increases cloud water content and reduces auto-conversion quite significantly. This series of microphysical processes promoted evaporative cooling and strengthened downdrafts, which subsequently promoted low-level convergence, which then fuelled the updrafts. The invigoration effect in the full simulations was found to have little dependence on the ice phase. These tests of Lee et al. (2009) suggested that invigoration of cloud thermodynamics does not predominantly occur as a result of freezing. This importance of evaporation and condensation is commonly understood to be a consequence of differences in latent heats of freezing and evaporation, which differ by about an order of magnitude. Contrary to these microphysicists, Seifert and Beheng (2006) argued that cloud microphysics does not play a critical role in cloud dynamics but, other meteorological conditions such as convective available potential energy and vertical wind shear do.

2.2.4 Glaciation Indirect Effect

Active IN nucleate ice crystals at sub-zero temperatures and at sufficiently positive supersaturations with respect to ice. In mixed-phase clouds, the cloud remains relatively saturated with respect to the water. This happens because as soon as the environment becomes sub-saturated, water droplets evaporate, maintaining the cloud in water-saturated conditions. It is understood that the saturation ratio with respect to water is always greater than that with respect to ice. Hence, a mixed-phase cloud is mostly, continually supersaturated with respect to ice. Thus, IN may activate and diffusional growth of ice crystals is promoted. Thus, if ascent is weak

enough, then evaporation of cloud-droplets accompanies the vapour growth of ice (Korolev and Mazin, 2003; Korolev, 2007). Therefore, if IN loading increases, more ice crystals may be nucleated, giving rise to a more glaciated cloud. This may improve the precipitation efficiency of a cloud through the ice phase and consequently change the radiative properties of the cloud, thus, causing a glaciation indirect effect.

This indirect effect was first hypothesised by Lohmann (2002a) who suggested that, in addition to dust particles (which are dominant sources of ice crystals), if a fraction of soot are anthropogenically injected into the atmosphere then frequent glaciation of supercooled clouds may occur. This frequent glaciation enhances precipitation production through the ice-phase and may consequently reduce the lifetime and optical depth of clouds to cause increased absorption of insolation into the climate system. However, recent laboratory studies have changed the traditional perspective of black carbon having high IN activity regardless of its origin. Koehler et al. (2009) observed little or no heterogeneous ice nucleation from soot that was produced by various types of fossil-fuel combustion at temperatures greater than -40 degrees C. Crawford et al. (2011), in a laboratory experiment to determine the efficiency of soot as IN, found higher IN activity for soot with low carbon content (about 5%) than for high carbon soot ($\approx$ 30%) or more. The low carbon soot originates primarily from biomass burning where higher rates of oxidation occur due to the availability of adequate oxygen. On the other hand, high carbon soot is produced chiefly from industrial fuel combustion, which is mostly incomplete due to limited oxygen inside the combustion chambers. Thus, it is important to know the sources of soot particles especially in model developments for accurate prediction of climate and especially the glaciation effect.

This *glaciation effect* is hypothesised to improve the precipitation efficiency, consequently, it has the potential to alter the lifetime/extent of mixed-phase clouds and create a type of cold-cloud lifetime effect. The extent to which the former outweighs the latter depends on the aerosol chemistry (Lohmann, 2002a). The increase in loading of aerosols such as dust and soot, which act as IN in mixed-phase clouds is thought to cause the glaciation effect (Solomon et al., 2007). Connolly et al. (2006) studied the glaciation indirect effect in a Hector cloud over the Darwin, Australia. They noted that increasing IN resulted in enhancement of aggregation and accretion rather than the Bergeron-Findeisen process. The importance of the glaciation effect in this simulation of a Hector thunderstorm was however found to be minimal. Zeng et al. (2009) investigated the influence of wind shear on aerosol indirect effect. They noted that, upper tropospheric cloud ice content decreases slightly with increasing wind shear. This was primarily because strong vertical wind shear extended the

cloud horizontally, thus, increasing its reflectance of shortwave fluxes and reducing the upward infrared fluxes at the top of the atmosphere.

Chapter 3

Model Description

3.1 Introduction

Since the advent of NWP in the middle of the twentieth century, there has been a rapid advancement in the development of numerical weather and climate models. Since then, computational power and speed has grown by more than a hundred times (Shukla et al., 2010), enabling the development of relatively high resolution CSRMs. High resolution CSRMs permit process-scale or cloud-scale microphysical and dynamical processes to be understood and also facilitate the development of parameterizations, which can be incorporated into GCMs, where temporal and spatial resolutions are still low. CSRMs encapsulate microphysics schemes, which resolve the cloud and precipitation processes.

Microphysics schemes come in two different forms. Those that explicitly predict the size distribution of cloud-particles, aerosols or precipitation and multiple prognostic microphysical parameters at each size-bin are referred to as *emulated bin-resolving* or *detailed* or *explicit* microphysics schemes (Young, 1974a; Feingold et al., 1994; Geresdi, 1998:; Rasmussen et al., 2002). *Bulk* microphysics schemes predict a few bulk characteristics of hydro-meteors and prescribe some of the microphysical parameters of the size distribution. Emulated schemes are quite detailed and normally prognose and write out plenty of bulk characteristic parameters, thus, requiring more computational power and memory. Due to these technical limitations, explicit schemes are not yet operationally applicable for timely weather forecasting purposes. On the other hand, most of the microphysical parameters that are predicted by explicit integration in bin-microphysics models are simply parameterized in bulk schemes. Therefore, limited prognostic variables are predicted in bulk-microphysics schemes and limited explicit integration is also performed rendering them applicable for real-time weather forecasting and climate prediction.

The typical Droplet Size Distribution (DSD) being used in most bulk schemes is the exponential size distribution (Eqn. 2.6) as explained in Kessler (1969) or the gamma distribution of the form shown in Eqn. 2.7 (Clark, 1974; Walko et al., 1995; Mitchell and Arnott, 1994). Some of the bulk microphysics parameters have fixed intercept parameters, N_0, for all hydro-meteor species as it was in the original work of Lin et al. (1983). Flaws in this approach have however been discovered for instance in Reisner et al. (1998), were that approach promoted excessive depletion of cloud water. Accordingly, more robust techniques for determining N_0, have since been introduced (Reisner et al., 1998; Thompson et al., 2004), which depend on either temperature or mass mixing ratios. Some bulk microphysics schemes, however, deviate from the norm by employing complex distributions such as the log-normal distribution for the size distributions of hydrometeors (Clark and Hall, 1983).

Microphysics schemes can further be sub-divided into either single or multi-moment microphysics schemes. Single moment schemes e.g. Lin et al. (1983); Kessler (1969); Cotton et al. (1986) usually calculate the mass mixing ratios only. Alternatively, both the number concentrations and mass mixing ratios have lately been increasingly prognosed simultaneously in double moment schemes (Morrison and Pinto, 2005; Seifert and Beheng, 2006). Double-moment schemes have proved to be superior over single moment schemes in terms of accuracy, especially in simulating precipitation in deep convective cells (Lim and Hong, 2010). Due to the prediction of extra terms in double-moment schemes, their computational expense is amplified, hence, curtailing their use in real time weather forecasting and climate prediction models. As a consequence, limited double-moment microphysics schemes have been favored (Thompson et al., 2008; Phillips et al., 2007, 2009; Lim and Hong, 2010) because they improve Qualitative Precipitation Forecasting (QPF) at the same time being fast enough to meet numerical weather prediction (NWP) requirements (Thompson et al., 2008). This is the scope within which the limited double-moment bulk microphysics scheme presented here was developed. In this section, the model used for this research is described and the improvements undertaken thereto are elaborated.

3.1.1 Dynamical Framework of the Model

The numerical model utilised here was an aerosol-cloud model developed under the general framework of the Weather Research and Forecasting (WRF) model, with a hybrid bulk microphysics package described in Phillips et al. (2007, 2008, 2009). Improvements to the heterogeneous ice nucleation scheme described in Phillips et al. (2013) were also incorporated into this microphysics scheme. The bulk mi-

crophysics scheme has recently been partially transformed into a hybrid bin/bulk cloud-resolving model (Sect. 3.2.2). It is a CSRM, which has prognostic variables of a two-moment bulk microphysics for cloud liquid, cloud ice and the sulphate aerosol specie and a one-moment treatment of precipitation. The CSRM is a non-hydrostatic and an an-elastic fluid flow model with periodic boundary conditions and forty vertical levels. The vertical resolution is approximately 500m, with the model-top set at 20km. The model grids are 2km wide, with the whole domain size being 170km. The integration time steps of 10 seconds are being used. Prognostic microphysical variables are written out at an interval of five minutes for analysis.

The dynamic solver of the model solves the fully compressible non-hydrostatic equations using the Eulerian approach. The vertical coordinates of the model are terrain following σ-coordinates prescribed by the model-top pressure. The model time split integration is based on the 3^{rd} order Runge-Kutta integration scheme with an integration time step of 10 seconds, while the high frequency acoustic wave integration time step is set at 6s. Periodic boundary conditions are applied in the dynamic solver. The heat and moisture fluxes are prescribed at the model surface, while a sponge layer with a thickness of 5km is applied at the model top in order to damp the reflection of the gravity and sound waves at the model top.

Turbulence in the model is treated using the Medium Range Forecast (MRF) model Planetary Boundary Layer (PBL) scheme (Hong and Pan, 1996). This scheme resolves the vertical sub-grid scale fluxes caused by eddy transports. It also treats horizontal and vertical mixing of fluxes provided by the surface layer and the land surface schemes. For the radiative transfer, the Geophysical Fluid Dynamics Laboratory (GFDL) radiation scheme (Freidenreich and Ramaswamy, 1999) is incorporated into the aerosol-cloud model. The scheme treats LW and SW scattering properties of both cloud liquid and cloud ice. These treatments depend on the predicted mean sizes of cloud ice, both of which are predicted in the model following the double moment treatment of cloud ice and cloud droplets in the microphysics scheme.

In tropical maritime (TWPICE) and mid-latitude continental (CLASIC) cases simulated in this project, a two-dimensional domain was applied. Several authors in the literature for different types of studies have used two-dimensional schemes. Tompkins (2000) studied the effect of dimensionality on the model performance and concluded that 2-D CSRMs are more powerful in simulating organized structures such as squall lines relative to scattered convection. In both cases simulated in this study, convection was quite organized, hence, a two-dimensional simulation is a good option for both computational efficiency and model accuracy, although loosing the third dimension implies missing the actual three dimensional effects of aerosol

on clouds, especially the spatial coverage of clouds and also the 3 dimensional turbulence lost which can affect the transport and mixing of aerosol. Convection is maintained in a standard way for CSRM by including additional tendencies of heat and moisture. The tendencies are derived from the derived large scale forcing, observed from a network of soundings used in the case being simulated. These tendencies are added as extra sources to the evolution equations for potential temperature and vapour mixing ratio. Random perturbations of humidity in the boundary layer initiate convection.

3.1.2 Aerosol Treatment

The aerosol-cloud model has a semi-prognostic aerosol component, in the earlier version of the aerosol-cloud model (Phillips et al., 2009), six aerosol species were treated. In this thesis, the insoluble organic aerosol group was split into Primary Biological Aerosol Particles (PBAP) and non-biological insoluble organics (Phillips et al., 2013). In addition, the larger and smaller modes of the sulphate aerosol group are now prognosed independently and treated as if they were two different aerosol species. Furthermore, a fraction of soluble organic aerosols now acts as IN at relevant temperatures and supersaturations. This gives a complement of nine species, each with its own independent prognostic variables such as mass or number mixing ratios.

These aerosols are classified into two main categories, namely, the soluble and the solid aerosols. The classification of the chemical composition of aerosols follows that commonly found in some of the most modern GCM.

- The soluble aerosol species are ammonium sulphate (its bi-modal distribution is separated into two independent modes as $SO4_1$ and $SO4_2$), sea-salt (SS) and soluble organic carbonaceous material (SO).

- The insoluble aerosol group comprises mineral dust/metallic (DM), soot/black carbon (BC), insoluble non-biological organic (O), primary biological aerosol particles (BIO) and finally, there is a fraction of the soluble organic group (SO) that becomes glassy at very cold temperatures (SOLO).

All species can nucleate liquid droplets, however, in the previous version of the hybrid bulk/bin microphysics scheme, solute aerosols could not nucleate ice, but, an exception has now been applied to soluble organics in line with recent laboratory observations of Murray et al. (2010). In this version, the non-biological insoluble organics group no longer nucleates ice heterogeneously.

Aerosol particles are either assumed to be internally or externally mixed with each other depending on how their different components are mixed together. Lesins et al. (2002) describes an externally mixed sample of aerosols as one in which, each aerosol component is physically separated from each other creating an external mixture of chemically pure modes. On the other hand, they define an internally mixed aerosol as one whose homogeneous structure reflects the chemical and physical average of different contributing aerosol components. Petters and Kreidenweis (2007) referred to internally mixed aerosol particles as multicomponent particles. Two chemically and physically different aerosol particles can be externally mixed with each other, although, they may be internally mixed with other components. These definitions are visually demonstrated in Fig. 3.1b

External mixing is assumed for all solute aerosol species as schematically illustrated in Fig. 3.1a. Insoluble aerosols (dust, soot, insoluble ogranics) are assumed to be externally mixed with each other, but, also internally mixed with some components of soluble aerosols (Fig. 3.1b), therefore, they are able to initiate cloud droplets. The soluble fractions of the respective IN groups are shown in Table 3.1, following Clarke et al. (2004). A log-normal distribution described by Pruppacher and Klett (1997) is assumed for all aerosol size distributions with distribution parameters of each mode (geometric mean size, spectral width, ratio of total numbers between multiple modes) being constrained by observations. These parameters are shown in Table 3.1 for the cases simulated in this study. Insoluble aerosols particles are assumed aged and hence, they are coated with soluble components such as sulphate on their surfaces enabling them to activate both cloud droplets and cloud ice.

The semi-prognostic aerosol component treats all processes that alter aerosol loadings inside clouds (wet processes). The scheme is semi-prognostic in the sense that aerosol profiles are artificially reset to their initial profiles at regular time intervals. All dry processes are neglected since they are assumed to act only on time-scales longer than those of the mean flow advecting through the meso-scale domain. 'Below-cloud' scavenging of aerosols is neglected (but may be included in future work). Depletion of aerosols occurs by in-cloud nucleation/precipitation scavenging (activation of cloud particles that are then accreted onto precipitation). The aerosol mass and number mixing ratios are predicted, hence, the model is double moment in this regard. The model tracks mass and number mixing ratios of aerosols in the environment (i.e. those which are not activated), in clouds and in precipitation. This makes it possible for the model to account for all the sources and sinks of every AP. It is not within the scope of this study to explicitly represent

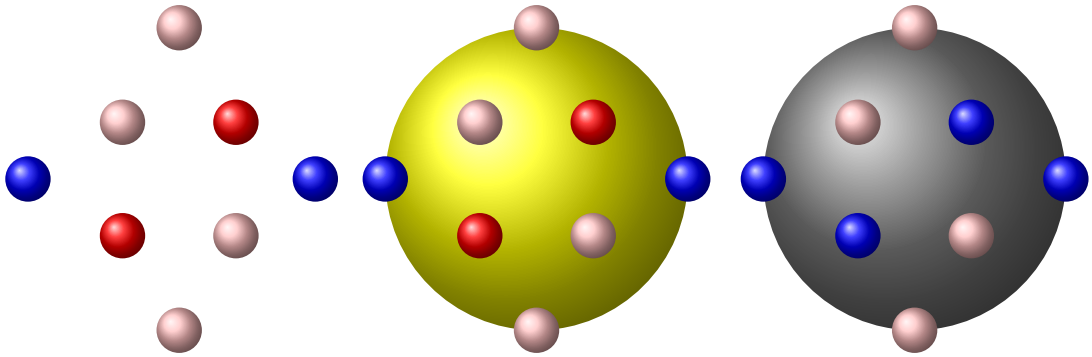

(a) (b)

Figure 3.1: *(a) External mixing of various aerosol particles. (b) Two large spheres represent two aerosol particles that are externally mixed, however the externally mixed large aerosol particles are also internally mixed with other aerosol species seen as small spheres on their surfaces (right). NB. The spheres in (b) have been enlarged for clarity, not for change in the size distributions of the aerosols.*

changes in aerosol loading due to lateral advection of aerosols into and out of the domain, hence, the population of interstitial aerosols in the air is reset to their respective initialization profiles at specific intervals, which at present is every 3 hours. This interval is justifiable as it lies with the range of the average life span of most precipitating convective cells in the real atmosphere.

3.1.3 Cloud Microphysics

The microphysics scheme outlined herein is chiefly a bulk microphysics scheme, although, some processes are treated explicitly. These processes include most of the coagulation processes (such as aggregation and riming). The scheme is double moment with regard to cloud ice and cloud droplets. A γ-distribution (Eqn. 2.7) is prescribed for cloud droplets and cloud ice size distributions. This technique of bulk-microphysics schemes allows mean sizes of cloud particles to be determined through the slope parameter λ_x (Eqn. 3.1).

$$\lambda_x = \left[\frac{\Gamma(4+p_x)\rho_x \frac{\pi}{6} n_x}{\Gamma(1+p_x)q_x}\right]^{\frac{1}{3}} \tag{3.1}$$

where subscript, x, represents either cloud droplets (c) or cloud ice (i), Γ, is the Γ-function. Here, p_c and p_i are the distribution's shape parameters, which were set in this aerosol-cloud model at 3.5 and unity Phillips et al. (2007), respectively. Bulk densities ρ_c and ρ_i are respectively set to 1000 and 800 kgm^{-3}, while n_x, is the number mixing ratio with q_x being the mass mixing ratio. Once the mean size has

Aerosol group	Number of Modes	$\log_{10}$ of Standard deviation $\log_{10}(\sigma_x)$	Geometric mean, Rm_x (μm)	Solubility parameter
Sulphate (SO4)	2	0.30, 0.27; 0.049, 0.161	0.04, 0.08; 0.03, 0.18	
Sea-Salt (SS)	2;3	0.30, 0.33; 0.05, 0.16, 0.26	0.01, 0.50; 0.03, 0.18, 4.4	
Soluble Organics (SO)	2	0.30, 0.27; 0.049, 0.161	0.04, 0.08; 0.03, 0.18	
Dust/Metalic (DM)	2	0.28, 0.20	0.8, 3.0	0.15
Black Cardon (BC)	1	0.20	0.2	0.80
Insoluble Organics (O)	1	0.20	0.2	0.80
Biological Aerosols (BIO)	2	0.40, 0.60	0.17, 0.47	0.80

Table 3.1: *Aerosol properties; the comma separates the modes, where different aerosol specifications were applied for mid-latitude continental and tropical maritime cases, a semi-colon is used with the former representing CLASIC and the latter representing TWPICE.*

been predicted, the average concentration of cloud particles can then respectively be derived from prognosed mass-mixing ratios. Hence, the scheme is double moment with respect to cloud particles. Also, the scheme comprises a semi-prognostic aerosol component that currently accommodates seven different aerosol species, making it ideal for aerosol-cloud interactions studies. This microphysics scheme can however, be applied in a wide range of studies (e.g., weather forecasting and cloud electrification research purposes).

3.1.3.1 Supersaturation and Species of Condensate

The bulk-microphysics scheme predicts the supersaturation and the diffusional growth of all the five species of hydro-meteors being treated in the model, which are: *cloud droplets, cloud ice, rain, snow* and *graupel*. This is done by a linearized supersaturation scheme of Phillips et al. (2007). Primarily, nucleation of cloud droplets takes place at the cloud base at positive supersaturation. In addition, in-cloud nucleation is also allowed when the predicted in-cloud supersaturation is high enough (relative to the critical saturation of droplet activation at the cut-off size of the aerosol size distribution). The prognostic variables that are advected, diffused and modified by microphysical conversions are: mass and number mixing ratios of cloud-liquid (Q_w, n_w) and of cloud-ice (Q_i, n_i), mass mixing ratio of snow (Q_s), graupel (Q_g) and rain (Q_r).

3.1.3.2 Initiation and Nucleation Processes

3.1.3.2.1 Initiation of Cloud Droplets The initiation and nucleation of cloud droplets and cloud ice respectively, is treated explicitly in the model. All seven aerosol species described in Sect. 3.1.2 can initiate cloud droplets. The activation of cloud particles takes place both at the cloud-base and in-cloud as long as the superasaturation is high enough to activate new cloud particles. At the cloud-base, droplet nucleation from solute aerosols is treated using the Ming et al. (2006) scheme. The Ming et al. (2006) scheme is a parameterization scheme that is formulated from the first principles of droplet activation and it explicitly links the droplet number concentration with the aerosol size distribution and updraft velocity. In-cloud droplet nucleation by solute aerosols follows the κ-Kohler theory of Petters and Kreidenweis (2007). The same theory is applied for droplet-nucleation by multicomponent solid aerosols, both at cloud-base and in-cloud. An algorithm to detect a new cloud base was developed by Phillips et al. (2007) and is also used in this study.

The prognostic variables of aerosols that are diffused and advected are the mass mixing ratio, Q_x, of aerosols available in the atmosphere, and the number mixing ratio, $n_{x,a}$, of aerosols that have been lost due to activation of cloud droplets. At every time-step and every nucleation event inside a cloud, $n_{x,a}$, is incremented by the number of new CCNs that have been activated in that time step. In cloud-free environments, $n_{x,a}$, is set to zero. The symbol, x, represents the aerosol specie.

The sources of aerosols in the model are: large-scale advection into the domain, which is represented by the initial profiles of aerosols prescribed at the initialization of the model and by the resetting of aerosol profiles at 3-hourly intervals. This resetting of aerosols is an abrupt process in which the aerosol profiles are instantaneously reset to their initial profiles after every three hours. Total evaporation of cloud droplets and sublimation of cloud ice are the other sources of aerosols. The sinks of aerosols in the model include, the nucleation and activation of cloud ice and the washout of aerosol by precipitating hydrometeors.

3.1.3.2.2 Heterogeneous Nucleation of Cloud Ice As for ice nucleation, an Empirical Parameterisation (EP) of heterogeneous ice nucleation developed by Phillips et al. (2008, 2013) was used. In this EP, nucleation from all known modes of heterogeneous ice nucleation (*deposition, condensation, immersion* and *contact freezing*) is treated. Most importantly, the scarcity of ice nucleation at sub-saturated conditions and the dependence of IN on the total surface area of each aerosol species are treated with the EP. The principal property of the empirical parameterization

scheme for heterogeneous ice-nucleation is the baseline total surface area of all IN, whose sizes are greater than a minimum threshold of 0.1μm. The development of the EP was based on the Continuous Flow Diffusion Chamber (CFDC) measurements of IN taken during the Ice Nuclei Spectroscopy Studies one and two (INSPECT-1 and -2). The original EP described for the first time by Phillips et al. (2008), has since been modified to conform to new advances in cloud microphysics (Phillips et al., 2013) and is described in more details in Appendix. B.

3.1.3.2.3 Homogeneous Freezing of Cloud Droplets and Aerosols Homogeneous freezing of cloud droplets takes place at -36°C. Preferential freezing is assumed, i.e., larger droplets freeze first depending on supersaturation and ascent velocity according to the parameterization by Phillips et al. (2007). Consequently, rapid condensational growth of ice crystals ensues with subsequent reduction of supersaturation. Smaller cloud droplets, start evaporating to keep the cloud close to water saturation, thus, total evaporation occurs for some of the small cloud droplets without freezing. The parameterization also predicts the fraction of cloud droplets that do not freeze. Also, homogeneous freezing of interstitial aerosols is applied at cold temperatures and higher humidifies near water saturation, taking into account the curvature and surface tension effects at temperatures below -40°C.

3.1.3.2.4 Ice Multiplication Secondary multiplication of cloud ice by the Hallet-Mossop process is also applied in the model between -3°C and -8°C by assuming that, for every milligram of liquid being accreted onto snow or graupel, a total 350 small ice crystals with initial diameters of 5μm are ejected at -5.5°C. A linearly increasing droplet-size dependent parameterization to determine the fraction, f_{HM}, of Hallet-Mossop (H-M) splinters produced per every event is treated in this scheme (equations 3.2 - 3.4). It requires that no splinters be ejected by droplets of sizes less than 16μm.

$$f_{HM} = \frac{D_{CW} - D_{HM-min}}{D_{HM-max} - D_{HM-min}}, \quad for \;\; 16\mu m < D_{CW} < 24\mu m, \tag{3.2}$$

$$f_{HM} = 0., \quad for \;\; D_{CW} < 16\mu m, \tag{3.3}$$

$$f_{HM} = 1., \quad for \;\; D_{CW} > 24\mu m \tag{3.4}$$

where, D_{CW} is the cloud droplet diameter, while D_{HM-min} and D_{HM-max} are the minimum and maximum droplet size thresholds for the parameterization.

3.1.3.3 Autoconversion Processes

3.1.3.3.1 The Autoconversion of Cloud Droplets to Rain The rate of autoconversion of rain from cloud particles ($\partial q_r/\partial t$) is treated using the scheme of Khairoutdinov and Kogan (2000) (Eqn. 3.5).

$$\left(\frac{\partial q_r}{\partial t}\right) = 1350 q_c^{2.47} n_c^{-1.79} \tag{3.5}$$

This is a robust bulk parameterization based on the results of a bin-resolving model. It depends primarily on predicted cloud droplet number and mass mixing ratios n_c and q_c, respectively.

3.1.3.3.2 The Autoconversion of Cloud Ice to Snow The rate of conversion of cloud ice to snow follows a modified version of Ferrier (1994)'s parameterization when the slope parameter, λ_i, of the ice crystal size distribution exceeds a certain minimum threshold, λ_{i0} (Eqn. 3.6).

$$\left(\frac{\partial q_s}{\partial t}\right) = \frac{\partial q_i}{\partial t}\left(1 - \left(\frac{\lambda_i}{\lambda_{i0}}\right)^3\right) \tag{3.6}$$

where, $\lambda_{i0} = \Gamma(2+\mu_i)/(150e^{-6}\Gamma(1+\mu_i))$ for the shape parameter, μ_i.

3.1.3.3.3 The Autoconversion of Snow to Graupel The autoconversion of snow to graupel is dependent on the riming rate of cloud liquid onto snow. It is determined by deducting the sum of mass mixing ratios of snow gained through depositional growth and accretion of cloud ice from the total mass gained by snow through accretion of super-cooled cloud droplets. Half of this difference becomes the mass of graupel gained through autoconversion. This treatment follows the semi-empirical treatment developed by Swann (1998) and requires the snow content to exceed a critical threshold of 500μg.

3.1.3.4 Growth Processes

The principal mechanism by which precipitating hydrometeors grow in the model is via particle-particle interactions (i.e. accretion, riming and aggregation). The diverse combinations of these interactions being treated presently in the model are shown in Table D.1 (Appendix D). All the collection processes i.e. the riming process of cloud liquid by solid precipitating hydrometeors, the aggregation process between solid precipitating hydrometeors and cloud ice, the aggregation of snow and ice and

also the accretion of ice by rain are all treated explicitly in the model using the emulated bin-microphysics approach, detailed in Sect. 3.2.2. On the other hand, the rate of accretion of cloud liquid onto rain, PRACW, is treated using the bulk scheme of Khairoutdinov and Kogan (2000) as:

$$PRACW = 67.(Q_L Q_R)^{1.15} \tag{3.7}$$

where, Q_L and Q_R are respectively the liquid cloud and rain mixing ratios. This treatment is applied for the liquid water contents which are less than $1gm^{-3}$, as these were the conditions within which their scheme was tested, while on the other hand, when the liquid water content is greater than $2gm^{-3}$, the bulk scheme of Phillips et al. (2007) is applied as:

$$PRACW = cQ_L Q_R^{0.95} \sqrt{\frac{\rho_s}{\rho_a}} \tag{3.8}$$

where, ρ_s and ρ_a are respectively the air densities at the surface and at the model level, while c is a constant derived from Lin et al. (1983). Elsewhere, a linear interpolation is applied to predict the accretion rate.

The accretion of cloud liquid onto precipitation is treated using the power law bulk parameterization of Khairoutdinov and Kogan (2000), when the cloud liquid water content is less than 1gm^{-3}. This is because that was the range of cloud liquid content within which this parameterization was developed and validated. On the other hand, when the cloud liquid water content is greater than 2gm^{-3}, the treatment of Phillips et al. (2007) is applied. Elsewhere, a linear interpolation is applied using these two parameterizations. All the other coagulation processes shown in Table D.1 are treated using the bin-resolving microphysics approach as detailed in Sect. 3.2.2.

3.1.3.5 Sedimentation of Hydrometeors

The sedimentation (fall speed) of cloud particles, U_x (i.e. subscript x = cloud ice (i) and cloud droplets (l)) is treated as shown in Eqn. 3.9.

$$U_x = a_x \frac{\Gamma(4 + p_x + b_x)}{\Gamma(4 + p_x)\lambda_x{}^{b_x}} \sqrt{\frac{1.2}{\rho_a}} \tag{3.9}$$

where $a_w = 2.97{\times}10^7$, $b_w = 2$, $b_i = 0.813$ and,

$$a_i = 2.53 \left(\frac{1.e^6 \rho_i \pi}{6} \right)^{0.271} \sqrt{\frac{1.112}{\rho_{as}}} \tag{3.10}$$

are constants. Symbols, p_x, are shape parameters, while, ρ_{as}, and, ρ_a, are surface-air density and air density, respectively. Finally, ρ_i is the ice bulk density. A similar approach of Lin et al. (1983) is applied for the treatment of rain and graupel's terminal fall speeds. The only exception is that an intercept parameter for rain $N_{0,r}$ of Thompson et al. (2004) that is dependent on the mass mixing ratio is being applied instead. As for snow, the treatment of snow fall speeds described by Heymsfield et al. (2007a) is used to determine the terminal fall speeds. Following the introduction of bin-microphysics treatment for coagulation processes in the model; the mass-weighted fall speeds from hydrometeor's mass spectra are used for prediction of sedimentation rates. A detailed numerical description of the terminal velocities and mass weighted fall speeds of these hydrometeors is elaborated in Appendix F.

3.2 Model Improvements

One of the primary goals of this PhD project was to modify and validate the bulk-microphysics scheme using two ARM cases (the tropical maritime − TWPICE and the mid-latitude continental − CLASIC cases). Some of the model development was performed in the early stages of the project before the core ARM's cases were simulated. Two contrasting maritime cases of deep convection, which were previously simulated by the earlier version of the CSRM (Phillips et al., 2009) were therefore used to assess its robustness and accuracy. The two campaigns are the Tropical Ocean Global Atmosphere Coupled Ocean-Atmosphere Response Experiment (TOGA-COARE) (Webster and Lukas, 1992) and the Kwajalein Experiment (KWAJEX) (Kaneyasu et al., 2001), which are both maritime cases. The campaigns took place in December 1992 over the North Pacific Ocean and August 1999 over Kwajalein Atoll, Marshall Islands respectively. Below, are the modifications applied to the model, with detailed descriptions being demonstrated in subsequent sub-sections.

- The sulphate aerosol group has now been dualised, giving rise to two separate sulphate ASDs, the fine and the accumulation modes, which are now being treated as two independent aerosol species.

- Not only the mass mixing ratios of the sulphate aerosol group are being predicted, but, also their number concentrations. This enables their mean sizes to be predicted rather than being prescribed a priori. This special treatment was coded only for sulphate aerosols because their dominance in the atmosphere

in terms of number concentrations and their superior influence as CCN over other aerosol species.

- Emulated bin-microphysics treatment has also been implemented to all coagulation processes (e.g., riming, aggregation and accretion).
- Furthermore, a gamma distribution for all precipitation hydro-meteors has replaced the old exponential one.
- Most importantly, ice morphology has also been incorporated to allow accurate treatment of the collision and sticking efficiencies, taking into account their dependence on temperature and sizes.
- A novel treatment for the empirical parameterization of heterogeneous nucleation of cloud ice introduced by Phillips et al. (2013) has been incorporated into this version of the model.

3.2.1 Sulphate Aerosol Treatment

A bi-modal, log-normal distribution is applied for sulphate aerosols as for most other aerosol groups. The earlier version of the scheme treated sulphate aerosols as a sum of these two modes. However, in the current version of the aerosol-cloud model, the two modes (the Aitken and accumulation) of sulphate aerosols have been separated into two independent modes. Each mode is now represented by independent prognostic variables of number and mass mixing ratios. This treatment transformed the scheme into two-moment for the sulphate group. In summary, the two modes of the sulphate group are being treated as two different aerosol species. This special treatment was applied because ammonium sulphate is perhaps the dominant aerosol specie in terms of number concentrations in the atmosphere and its influence on the microphysics, especially of water clouds is high. Since sulphate has now been dualised, five new prognostic variables have been introduced.

- $Q_{SO4_{x,id}}$, which is equal to the total mass mixing ratio of sulphate, here, $x =$ 1 or 2, represents the first and second modes, respectively (the subscript 'id' means that this mixing ratio is 'ideal', i.e, the variable represents the background aerosol budget.)
- $n_{SO4_{x,id}}$, are the corresponding number mixing ratios.
- In addition to these variables, similar variables are also defined for sulphate mass mixing ratios; in air, in cloud and in precipitation as $Q_{SO4_{x,air}}, Q_{SO4_{x,cld}}$

and $Q_{SO4_{x,prec}}$, respectively. The same variables are also introduced for their corresponding number mixing ratios.

Furthermore, the mean sizes of sulphate aerosols are no longer being prescribed but predicted instead, because of the double moment treatment applied to them. The initialization of the model is done using the observed aerosol profiles. These profiles are in the form of mass mixing ratios $Q_{SO4_{x,id}}$, while the number mixing ratios $n_{SO4_{x,id}}$ are inferred from observed mass mixing ratios by prescribing a constant density for sulphate, $\rho_{SO4} = 1.7418 \times 10^3 \mathrm{Kgm}^{-3}$ and assuming a spherical shape for sulphate aerosols. The total number mixing ratio, $n_{SO4_{x,id}}$, is advected and diffused in a similar way as with all other prognostic variables for aerosols (e.g. $Q_{SO4_{x,id}}$) and its sources and sinks are similarly treated. The size distribution of each sulphate mode is diagnosed for temporary grids of size-bins from the bulk diagnostic variables ($Q_{SO4_{x,id}}; n_{SO4_{x,id}}$) by assuming a log-normal size distribution from Pruppacher and Klett (1997), shown in Eqn. 3.11.

$$dn_{SO4_x}(r) = \sum_{x=1}^{2} \frac{n_{SO4_x}}{(2\pi)^{1/2} log\sigma_x} \exp\left[-\frac{(log\frac{r}{R_x})^2}{2(log\sigma_x)^2}\right] dlogr \tag{3.11}$$

Here, $dn_{SO4_x}(r)$ is the number mixing ratio of sulphate within the size bin. Twenty size bins are prescribed for all aerosol species; the resolution however depends on the aerosol size spectrum. $n_{SO4_{x,id}}$ is the ideal total aerosol number mixing ratio, while, r, and, R_x, are the mean and geometric mean radii, respectively, with standard deviation, σ_x. These two prognostic variables, $Q_{SO4_{x,id}}$, and, $n_{SO4_{x,id}}$, have similar sources and sinks (e.g. nucleation and advection).

3.2.2 Emulated Bin-microphysics Treatment for Coagulation Processes

An emulated bin microphysics has been incorporated into the model for most coagulation processes shown below and in Table D.1:

- graupel (g) accreting snow (s),
- graupel (g) accreting ice (i),
- graupel (g) accreting supercooled cloud droplets (l) (riming),
- snow (s) accreting ice (i),
- snow (s) accreting cloud droplets (l) (riming),
- freezing of rain (r) upon accreting cloud ice (i).

A γ-distribution has now replaced the exponential-distribution for precipitating particles (g, s and r) following Mitchell and Arnott (1994). The intercept and shape parameters for snow are now treated using equations F.7 and F.8 in Appendix F. The size distribution spectrum is discretized into a total of thirty-three size bins for each of the aforementioned hydrometeors. A mass grid $m_x(D_x)(j)$ is prescribed using Eqn. 3.12 by prescribing a minimum diameter $D_{min,x}(j)$ at $j = 1$ for each $x = g, i, s, r, l$ and incrementing the mass from one size bin to the next by a prescribed factor (of 1.5 for all x except for $x = i$ where the factor is 2.) to fill up all the size bins.

$$m_x(D_x)(1) = \frac{\pi \rho_x(D_x) D_{min,x}^3}{6} \tag{3.12}$$

$D_x(j)$ is calculated from Eqn. 3.12 for, $x = r, i, l, g$, and for index, $j = 1, 2, 3.., N_t$, where, $N_t = 33$, is the total number of size bins for each hydro-meteor, and ρ_x is the bulk density of the xth species. As for, $x = s$, a power law of the form of Eqn. F.2 is used.

The collision kernels, χ_{xy}, for the interacting particles, $x = g; y = i, l, s$, $x = s; y = i, l$ and $x = r; y = i$ are predicted for each model level during initialization, using thermodynamic variables of basic state for Eqn. 3.13. In the following expressions, x and y are used to denote microphysical species of the interacting particles with the former representing the larger of the two.

$$\chi_{xy}(j,k) = E_{c,xy}(j,k) E_{s,xy} A_{xy}(j,k) |V_{tx,sfc}(j) - V_{ty,sfc}(k)| \sqrt{\frac{\rho_{sfc}}{\rho_a}} \tag{3.13}$$

where, $E_{c,xy}$, is the collision efficiency between x and y, values of which are interpolated from the Explicit Microphysics Model (EMM) results of Phillips et al. (2005) for $x = g; y = i, l$ and $x = s; y = i$ whereas for the other collision efficiencies, look up tables are used. $E_{s,xy}$ are the sticking efficiencies between collision of particles x and y as given above. The geometric cross section, A_{xy}, is calculated from Eqn. 3.14.

$$A_{xy}(j,k) = \pi (D_x(j)/2 - D_y(k)/2)^2 \tag{3.14}$$

$V_{tx,sfc}$, is the terminal velocity of the hydrometeor of maximum diameter, $D_{x,y}$, calculated at the surface using an expression of the form of Eqn. F.1 in Appendix F, where the coefficients are as given in Table E.1. The last term on the right in Eqn. 3.13, with surface air density, ρ_{sfc}, and air density, ρ_a, at a given model level is the altitude correction factor for the terminal velocity.

These collision kernels enable the numerical prediction of the increment of mass, $Ac_{x,y}$, by accretion, aggregation and riming as:

$$Ac_{x,y} = \sum_{j=1}^{N_t} \sum_{k=1}^{N_t} \chi_{xy}(j,k) N_x(j) N_y(k) M_y(k) \rho_a \tag{3.15}$$

where, $N_{x,y}$ and $M_{x,y}$ are the numbers and masses in each size bin for each corresponding hydrometeor.

3.2.3 Ice Morphology

Table 3.2 shows the ice morphologies (dentrites, sectors and stellars) being treated in the model, which depend on size, temperature, bulk density and shape (axial ratio). A habit dependent sticking efficiency is prescribed. Its dependence on temperature and on whether supersaturation is positive or negative is also treated. The sticking efficiencies in Table 3.2 are for collisions between snow and ice crystals, while for graupel and ice collisions, the sticking efficiency is assumed to be a hundredth of those in the table. A sticking efficiency of unity is assumed for the collisions between ice and rain.

3.2.4 Empirical Parameterizations for Heterogeneous Ice Nucleation

Following the development of a novel treatment for the empirical parameterization of heterogeneous nucleation of cloud ice introduced by Phillips et al. (2008), improvements to specifications of some the parameterizations have since been made (Phillips et al., 2013). These improvements have been incorporated into this version of the model. Briefly, the major modifications to the parameterization are:

- The group that represented all insoluble organics as IN has been replaced by a group of Primary Biological Aerosol Particles (PBAPs). This treatment removed non-biological aerosols from acting as IN. This is consistent with field observations of PBAPs nucleating ice e.g. Prenni et al. (2009); Pratt et al. (2009); Garcia et al. (2012). There is little evidence of insoluble organic aerosols acting as IN (Cziczo et al., 2004).

- The nucleation of ice by soluble organics that become glassy at very low temperatures (approximately less than -65°C) following laboratory studies of Murray et al. (2010).

- The black carbon aerosols that nucleate ice are now required to have an intrinsically hydrophilic surface with less organic coating on their surfaces.

Temperature $T°C$	Ice morphology	Sticking efficiency when supersaturation is positive	Sticking efficiency when supersaturation is negative
0.0 to -4.0	plates	0.1	0.1
-4.0 to -6.0	columns	0.6	0.1
-6.0 to -9.4	columns	0.1	0.1
-9.4 to -12.0	plates	0.4	0.1
-12.0 to -17.4	dentrites, sectors, stellars	1.	0.1
-17.4 to -22.0	plates	0.4	0.1
$<$ -22.0	columns	0.25	0.1

Table 3.2: *Ice morphology and their respective sticking efficiencies*

- Transition from a fixed onset temperature for initiation of ice nucleation by all aerosol groups to species' specific onset temperatures for heterogeneous ice nucleation.
- Specifications of the baseline surface areas of black carbon and dust are now being prescribed more accurately following observations of Clarke et al. (2004) and Eidhammer et al. (2010), respectively.

3.3 Assessment of the Model Improvements

The original version of the microphysics module was developed in C++ programming language, hence, before these new improvements to the model were applied, the source code had to be translated to Fortran 90, and was also ported from a different computing system with a different architecture to another. Hence, inoder to test the functionality and performance of the model after these operations, two cases which were previously simulated and published by Phillips et al. (2009) with the unmodified version of the model were re-simulated and treated as the standard reference point for assessing the model performance.

3.3.1 Simulated Cases

3.3.1.1 Kwajalein Experiment (KWAJEX)

The Kwajalein Experiment (KWAJEX) took place from 25 July to 31 August 1999 over the Pacific Ocean close to the Kwajalein Atoll of the Marshal islands. The

KWAJEX mission was basically aimed at taking cloud and precipitation measurements that would then be used for the calibration of the Tropical Rainfall Measuring Mission (TRMM). The convair-580 aircraft of the University of Washington had a wide range of instrumentation onboard. Clouds and aerosol microphysical properties were measured during this campaign. Aerosol measurements were done using the PMS, PCASP and an FSSP for the dry sizes of aerosols.

Convection during KWAJEX was relatively weak and was characterized by isolated cumulonimbus clouds that were observed during the first week of the experiment. During the second week of the campaign, small and shallow precipitating cumulus congestus clouds characterized the weather conditions in the experiment domain. During the later stages of the experiment, isolated cumulonimbus clouds as in the first week of the experiment were experienced. The cloud-tops in KWAJEX were generally below the 10km altitude.

3.3.1.2 The Coupled Ocean Atmosphere Response Experiment (TOGA-COARE)

The Coupled Ocean Atmosphere Response Experiment (TOGA-COARE) experiment took place over the western Pacific Ocean. The intensive observation period (IOP) took place between November 1992 and February 1993. The core objective of the experiment was to understand the role of the western warm pool on the global ocean atmosphere system (Lin, 1996).

In Phillips et al. (2009), the TOGA-COARE case was simulated from the 20-25 December 1992. This period was selected because it is the period during the whole IOP of TOGA-COARE that was characterized by several episodes of intense deep convection (Krueger and Lazarus, 1999), with maximum cloud-top heights of 12-14km above the mean sea level.

The instrumentation used during TOGA-COARE included rawinsonds to measure the temperature and water profiles of the atmosphere. The International Satellite Cloud Climatological Program (ISCCP) data was used to estimate the cloud fraction, cloud-top temperature, IWC and IWP. However, there were no measurements of ice crystal microphysical properties that were made during TOGA-COARE. Hence, for the comparison of our model predictions of crystal number concentrations in the upper troposphere with observations, data from a different field campaign (Central Equatorial Pacific Experiment (CEPEX)) that had taken place in the same region, although, a year later were used. This was the most appropriate available data to conduct the comparison, and we acknowledge the assumption made regarding the cloud properties in these two campaigns being assumed to be similar or

representative.

3.3.2 Model Specifications

The model was initialized using domain averages of observed thermodynamic (vapour and temperature) profiles. Their corresponding thermodynamic tendencies, together with profiles of horizontal wind and pressure were used as large-scale forcing. Convection was initiated using random perturbations of moisture in the lower troposphere. It was maintained by including additional tendencies of heat and moisture due to the observed large-scale advection from a network of soundings in the simulated cases. Aerosol profiles were prescribed from aircraft observations for the simulated cases. In the instances of lack of observations, data from other similar campaigns in similar regions were used. Model specifications described in Sect. 3.1.1 were used for both simulations.

3.3.3 Results From Model Simulations

The results of the simulations are shown in Figs. 3.2 - 3.4. For the TOGA-COARE simulations (Figs. 3.2), the results were compared to the aircraft observations from CEPEX (Heymsfield and McFarquhar, 1996) due to the absence of aircraft observations in TOGA-COARE above the freezing level. CEPEX was conducted over the same region and month but a year later. The simulation shows two peaks; one in the Hallett-Mossop region (5 - 6 km altitude), the second peak above the 8km altitude is attributed to homogeneous freezing of super-cooled cloud droplets and of aerosols at around -36°C.

Data for observed profiles were corrected for mechanical shattering of ice crystals (Sect. 2.1.2.5.2). Only crystals greater than 100μm are shown. Hence, the model results were averaged accordingly. These model profiles were conditionally averaged over visible and highly visible cloud regions for TOGA-COARE. Visible cloud was defined for clouds with optical depth, $\tau > 0.2$, while highly visible was for optical depths, $\tau > 3$, over a layer of at least 500m. This was done in order to conform to the flight patterns used during the campaigns. Figures 3.3 and 3.4 compare the observed and predicted profiles of cloud droplets.

Although a 'near-perfect' agreement is found in the upper troposphere for our model comparison with CEPEX data (Fig. 3.2), the situation is not known in the lower troposphere. Furthermore, it should be noted that these observations are from CEPEX and not TOGA, therefore, caution should be taken when interpreting these results. However, in light of the above-mentioned theoretical and technical

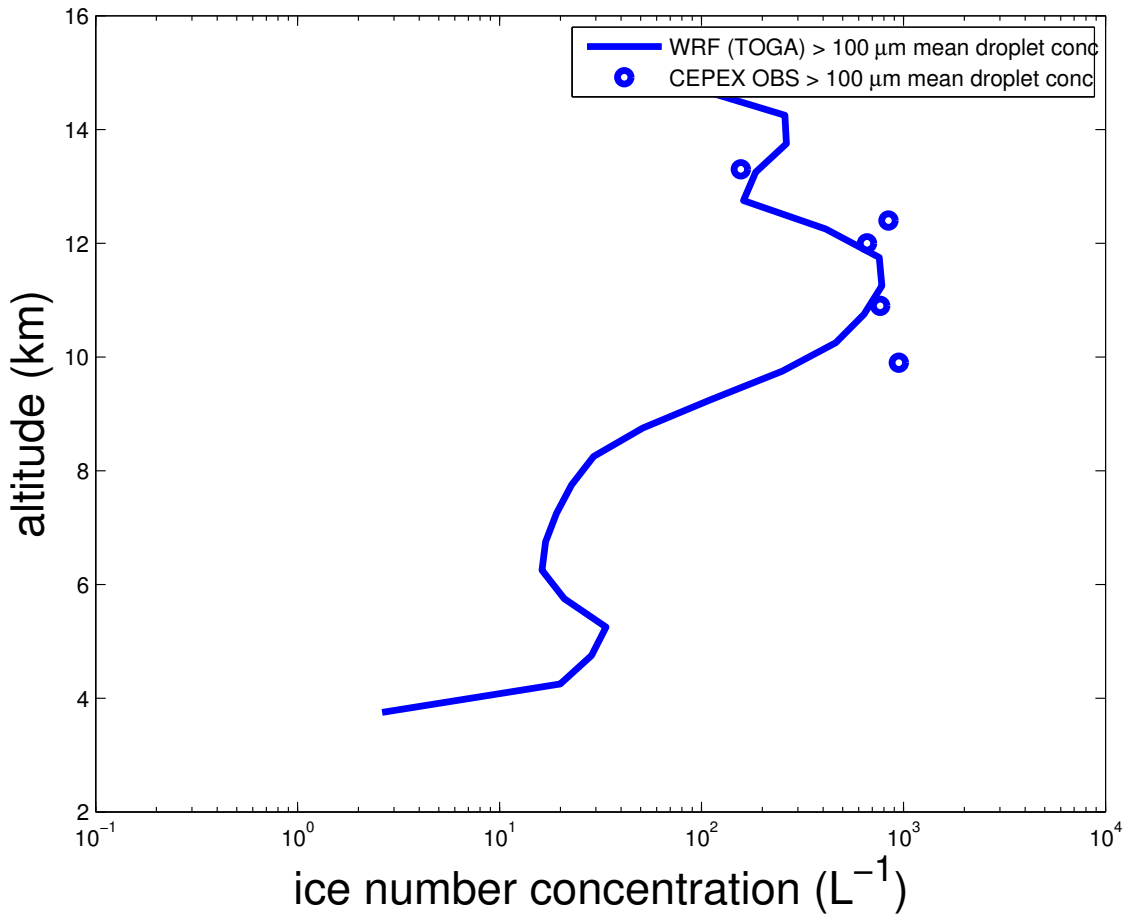

Figure 3.2: *Ice number concentrations predicted in TOGA-COARE (Webster and Lukas, 1992). The predictions are compared with CEPEX 2-DC probe measurements due to unavailability of aircraft data in sub-zero temperatures in TOGA-COARE. These observed concentrations shown here have been corrected for shattering bias. Hence, only sizes greater than 100µm have been used for the comparison of model results with observations.*

deficiencies, it can thus be concluded that the model performance is satisfactory in the prediction of ice crystals especially for the TOGA-COARE simulation. The same conclusion can also be drawn from the model's performance in predicting cloud droplets. The better theoretical understanding and parameterization of warm rain microphysical processes explains the good agreements in model results and observations of cloud droplets (Figs. 3.3 and 3.4).

The transition from prescribing to predicting the mean sizes, coupled with the dualisation of sulphate aerosol particles yielded significant improvement, particularly in the number concentrations of ice crystals aloft. This is because, by accurately predicting the sizes of sulphate aerosols, the prediction of the number concentrations if cloud droplets could be improved, hence, the number homogeneously frozen

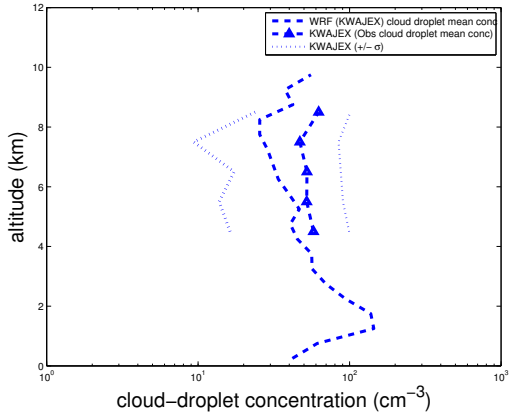

Figure 3.3: *Predicted mean cloud droplet concentration in KWAJEX compared with aircraft observations. Conditional averaging has been performed over highly visible (definitions given in text) cloud regions following the flight patterns during the campaign.*

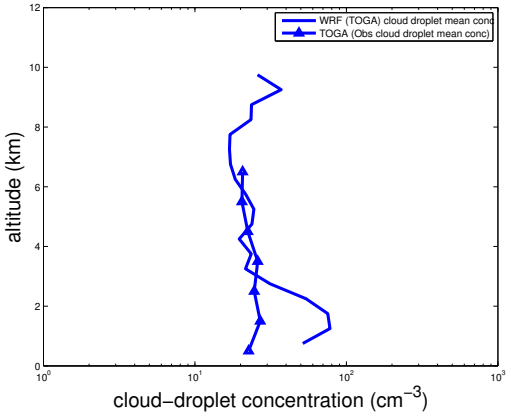

Figure 3.4: *Predicted mean cloud droplet concentration in TOGA-COARE compared with aircraft observations. Conditional averaging has been performed for over visible and highly visible (definitions given in text) cloud regions following the flight patterns during the campaign.*

cloud particles are accurately predicted as well. In the published results of Phillips et al. (2007, 2009), not shown here, the model predicted ice concentrations, which were about an order of magnitude higher than observations for the TOGA-COARE case. However, agreement with observations in mixed-phase clouds where the Hallet-Mossop ice multiplication process produces a broad peak in ice concentration in the aircraft data has worsened relative to Phillips et al. (2009) especially for KWAJEX. This model deficiency could be due to the nature of the size distribution, which we assumed for the hydrometeors, the single moment of precipitation being applied in the model.

3.4 Summary

This section dealt with one of the primary objectives of the project, which is modifying and validating the hybrid bulk/bin microphysics aerosol-cloud model. Core campaigns for this project (the tropical maritime and mid-latitude continental) were not simulated yet at this stage. However, two other cases (KWAJEX and TOGA-COARE), which were previously simulated by Phillips et al. (2007, 2009) were utilised for comparison instead. Rigorous and extensive comparison (for multiple diagnostic fields) of the aerosol-cloud model using core ARM cases is outlined in the following chapter. More focus at this stage was given to a few microphysical properties, namely cloud droplets and ice crystals number concentrations.

The main modifications performed to the model included the dualised treatment of the sulphate aerosol group. A double moment approach was also treated for the two sulphate groups where their mass mixing ratios and number concentrations were now predicted. This enabled the prediction of their mean sizes instead of prescribing them a priori. Their dominance in terms of number concentrations in the atmosphere and their effectiveness in nucleation especially of water clouds was considered for this special treatment. Detailed microphysics is now being applied to most accretion processes. This improvement allows accretion processes to be predicted more accurately by resolving them explicitly in-lieu of the traditional technique of parameterizing. Despite the superiority of the bin-microphysics over the bulk parameterizations, the bin-microphysics may not be applied to all microphysics processes in the model, as it would demand more computational power and time. Additionally, a γ-distribution is now being assumed for all precipitating hydrometeors in place of the simple exponential one. Other changes have involved encapsulating different ice morphologies so as to accurately resolve collision and sticking efficiencies. Finally, recent improvements in the empirical parameterization of heterogeneous ice nucleation described in Phillips et al. (2013) have been incorporated.

As noted in Fig. 3.2 - 3.4, the aerosol-cloud model performance is satisfactory. A good reproduction of observed profiles for the number concentrations of cloud droplets is notable in Figs. 3.2 - 3.4. A protruding peak at around -2°C is primarily due to nucleation of cloud droplets at cloud-base. CCN activity is higher at cloud-base than in-cloud due to the requirement for higher in-cloud supersaturations for the initiation of new cloud droplets. Preferential sedimentation of cloud particles is however another contributing factor to that peak. The steep drop in cloud concentration may be due to the evaporation of cloud droplets as they sediment out of the clouds through the cloud-base into sub-saturated ambient conditions.

Chapter 4

Comparison of Model Results With Observations from Simulated Case Studies

One of the primary objectives for this study was to use the ARM data from aircraft, satellite and ground-based observing platforms for both CLASIC and TWPICE to compare with results from the aerosol-cloud model. These cases were simulated using the updated version of the aerosol-cloud model (Sect. 3). Close collaboration with the aircraft scientists who were involved in the respective campaigns was maintained during the assessment of the model performance by comparing its predictions with observations so as to interpret the observational data properly.

4.1 Description of Cases

Two campaigns were chosen for this study as the core simulations − one is a tropical maritime case and the other is a mid-latitude continental case. We chose to use contrasting continental and marine cases to study two contrasting cases with very different aerosol amounts and types. Both experiments are recent and took advantage of latest technologies and probes in the measurement of clouds' and aerosols' micro- and macrophysical parameters, thus, increasing the reliability of the datasets.

4.1.1 Tropical Warm Pool-International Cloud Experiment (TWPICE)

The Tropical Warm Pool International Cloud Experiment (TWPICE) (May et al., 2008) was a three-and-a-half weeks long maritime case of deep convection. It was carried out from the 17^{th} of January to the 12^{th} of February in 2006 over Darwin, north west of Australia (lat = -12.425° and lon = 130.891°). The campaign comprised both a dense network of ground-based and air-borne observation platforms including a research ship. Fig. 4.1 shows the TWPICE domain and the dense net-

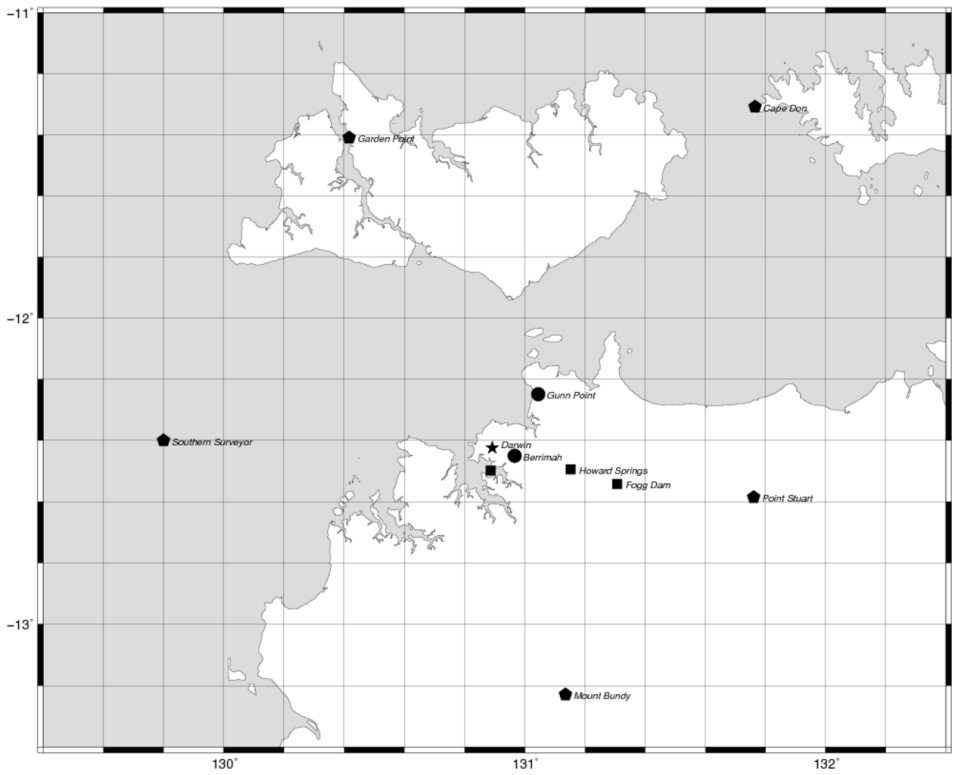

Figure 4.1: *The domain of the Tropical Warm Pool-International Cloud Experiment (TWPICE), Darwin (lat, lon = 12.47° N, 130.83° W) in early 2006, with both ground and sea-based observation stations used for the campaign being shown in figure.*

work of observing platforms deployed therein. A fleet of three aircraft at low and high altitude participated in the campaign, sampling the whole column of the atmosphere up to the lower stratosphere. The campaign domain covered a radius of about 150km. This makes the case ideal for validating our aerosol-cloud model because of the availability of spatially extensive and temporally continuous microphysics and thermodynamic dataset.

The campaign was generally aimed at improving the understanding of the microphysics of deep convection. It focused on the understanding of how factors affecting formation, evolution and dissipation of convective cells influence the properties of particles found in convective anvils. Also, the dataset thereof was essential for calibrating remote-sensing tools, initializing, forcing and validating atmospheric numerical models such as Cloud Resolving Models (CSRMs) and Global Climate Models (GCMs). The other key objective of the campaign was to comprehend and enable the modelling of the linkage between atmospheric microphysical properties and the strength and organization of deep convection and the characteristics of its remnants, which are typically the cirrus clouds and anvil outflows (May et al., 2008).

4.1.1.1 Ground Based Observations

In the TWPICE domain, two long term observing platform were already in operation. These were the meteorological observing station that are operated by the Bureau of Meteorology (BoM), Australia and the ARM Climate Research Facility (ACRF) site belonging to the Department of Energy (DoF) Atmospheric Radiation Measurement (ARM) program. The instrumentation at the BoM station comprised the 5.6GHz Scanning Polarimetric data to measure three-dimensional hydrometeor distribution, the operational Scanning Doppler weather radar, that measured the spatial distribution of convection and precipitation, the 50MHz wind profiler for the vertical profiles of wind, the 920MHz wind profiler providing the vertical profiles of wind and precipitation. Also, ten automated weather stations that were planted at different sites within the domain provided the continuous measurements of pressure, temperature, humidity, wind speed and direction at the 10m levels. In addition to these, a dense network of traditional rain gauges was also employed for in-situ precipitation measurements.

As for the DoE research facility, more sophisticated instruments to probe the microphysical and optical properties of clouds were used. Both a millimeter cloud radar and a micro-pulse lidar, provided measurements for cloud boundaries as well as microphysical and optical properties of clouds, respectively. The Vaisala celiometer measured the cloud-base height, while the total sky imager provided cloud cover. The vapor and water contents of the atmosphere were measured using microwave radiometers, while the raindrop size distribution was provided by the disdrometer. The broadband radiometers were available for measurements of the upward and downward components of solar and terrestrial radiation fluxes.

In addition to these instruments at the permanent stations, several other instruments were deployed specifically for the TWPICE campaign. These included the lightning sensors and radiosondes that were launched at every three-hour intervals to measure the vertical profiles of temperature, humidity and pressure (May et al., 2008). To complement the land-based measurements, the Australian national research vessel, the Southern Surveyor, operated by the Common-Wealth Scientific and Industrial Research Organization (CSIRS) was used for ocean-based measurements and carried similar instrumentation as those on land-based stations in addition to those instruments that were specified for marine measurements.

4.1.1.2 Aircraft Measurements

A total of four aircraft were specifically used for TWPICE, while another aircraft for the Aerosol and Chemical Transport in Tropical Convection (ACTIVE) campaign (4.1.1.4) raised the fleet to five aircraft. There were two high altitude aircraft, the Egret, from the Airborne Research Australia (ARA) and the Proteus from the ARM program, which respectively sampled 8 - 15 and 8 - 16km. They had the instrumentation to measure upper tropospheric RH, cloud particle sizes distribution, crystal habits, aerosol size distribution, water contents and radiation measurements. The other two flights, the Demona, for ARA and the Twin Otter of the University of Washington, USA, were both low altitude aircraft, flying within the 10m to 2km altitude and 1km to 3km altitudes, respectively. The Demona had instrumentation to measure turbulence, SW and LW radiation fluxes, while the Twin Otter had vertically pointing cloud radar and a 530nm polarization lidar to support higher altitude measurements. All the aircraft also had the instrumentation to measure state parameters.

The Egret aircraft carried the DMT Cloud, Aerosol and Precipitation Spectrometer (CAPS) probe to sample the cloud particle number concentrations. It measured the droplet and ice crystal spectrum with diameters ranging from 0.3 to 2000 μm. The DMT Cloud Droplet Probe (CDP) was also onboard and it measured the size distribution of cloud particles with sizes ranging from 2 - 62 μm, while the Cloud Imaging Probe (CIP) measured ice crystal concentrations with diameter ranges of 10 - 2300 μm.

The flight patterns for the high altitudes flights were aimed at sampling the microphysical and aerosol properties of cirrus clouds; hence, the flight patterns were designed to sample both the fresh anvil outflow and also the aged cirrus. As for the low level flights, the flight patterns were designed to sample the boundary structure in both the rear and the front of the storms.

4.1.1.3 Meteorological Conditions

The Intensive Observation Period (IOP) of TWPICE was characterized by three distinct periods with different meteorological conditions, the active monsoon, the suppressed monsoon and the monsoon break periods. A monsoon period was defined in TWPICE as an instant where 700hPa airflow was averagely a westerly airflow for at least four consecutive days (May et al., 2008).

4.1.1.3.1 The Active Monsoon Period During the active monsoon period, there was a persistence of cirrus overcast over the whole domain and a prevalence of organized deep convection with cloud-tops reaching as high as the tropopause, hence the fresh anvil outflow with aged cirrus (May et al., 2008). The airflow during this period was westerly from the surface up to 300mb (Allen et al., 2008). This weather pattern persisted from the 17th to the 22nd of January.

4.1.1.3.2 The Suppressed Monsoon Period This period started from the 23rd and persisted up to the 2nd of February, it was characterized by a deep inland low that drove stable westerly airflow into the domain. Although a quasi-static Mesoscale Convective System (MCS) developed during this period, convection was suppressed and the cloud-tops during this period rarely exceeded the 10km altitude (May et al., 2008; Allen et al., 2008).

4.1.1.3.3 The Monsoon Break Period The low-pressure system of the suppressed monsoon period disappeared on the 3rd of February, causing easterly airflow at 700mb followed by three days of clear skies. In the days following these clear skies, scattered convection prevailed, which developed into more organized multi-cellular system during the later stages of the monsoon break period (May et al., 2008).

4.1.1.4 Aerosol Data

Aerosol data for TWPICE was obtained from ACTIVE campaign (Vaughan et al., 2008; Allen et al., 2008). ACTIVE was a sister campaign of TWPICE and was funded by the UK Natural Environment Research Council (NERC). The campaign was conducted between November of 2005 and February of 2006 over Darwin, Australia (lat = -12.425° and lon = 130.891°). There was one aircraft deployed during the ACTIVE campaign, the Dornier 228-101 aircraft, which was owned by Airborne Research and Survey Facility (NERC-ARSF). Dornier profiled the lower troposphere for aerosol physico-chemical properties.

This field campaign had two phases, the second one ran concurrently and also in the same domain with TWPICE. The raw data from the ACTIVE campaign is freely available for download on The British Atmospheric Data Centre (BADC) website (`http://badc.nerc.ac.uk/home/index.html`). The objective of ACTIVE was to characterize how the monsoon-induced and localized land-based convection influence the chemical composition and number concentration of tropospheric constituents.

The payloads for the Dornier aircraft that measure the number and size distribution of aerosols included the Ultra High Sensitivity Aerosol Spectrometer (UH-

SAS), which measured the dry diameters of aerosols ranging from 55 to 800nm. The Aerosol Spectrometer Probe (ASP) also measured the dry diameters of aerosols ranging from 0.21 to 4.2 μm. The Grim Aerosol Technik (GmbH) is another optical probe that was used to measure the dry sizes of aerosol ranging from 0.3 to 25 μm. The FSSP probe measured particle sizes in the supermicron mode ranging from 0.5 to 32 μm (May et al., 2008). The Donier aircraft mainly sampled the cloud free atmospheres.

4.1.2 Cloud and LAnd Surface Interaction Campaign (CLASIC)

The Cloud and LAnd-Surface Interaction Campaign (CLASIC) (Miller, 2007) was a three-weeks long continental case of deep convection. It was carried out from the 10^{th} to the 30^{th} of June in 2007 over the research facility of the U.S Department of Energy (DOE) called the Atmospheric Radiation Measurement-Climate Research Facility - Southern Great Plains (ARM-SGP). The site is in Oklahoma, U.S (lat = 36.61° and lon = 97.49°). Fig. 4.2 shows a cartoon of the experiment domain for CLASIC and the network of observing platforms deployed for the campaign.

The campaign was aimed at investigating the interaction between the land surface, sub-surface, biosphere and atmosphere. It also focused on investigating how the changes in land surface properties affect the formation and the properties of convection especially of shallow cumulus clouds. This was to be done by taking advantage of the winter wheat harvest that would normally take place during the intense observation period. The experiment period was, however, characterized by a record-high rainfall (wettest June in 87 years), hence, no winter wheat harvest occurred because of the prevalence of deep convection that also affected many flights (Miller M., personal communication). This does not however, affect the assessment of our model performance, because the data available are sufficient for the purposes of this study. A combination of surface-based and airborne platforms was deployed for both in-situ and remote measurements in CLASIC.

4.1.2.1 Ground Based Observations

The surface sites were used for the campaign and provided detailed large scale forcing through enhanced three-hour radiosonde observations which were launched from these stations.

4.1.2.2 Aircraft Measurements

A fleet of five aircraft was used for this field campaign. The NASA ER-2 aircraft, the Twin Otter of the Center for Interdisciplinary Remotely Piloted Aircraft Studies (CIRPAS), the Twin Otter international, the Duke Bell Helicopter and the ARM Cesna 206. The ER-2 sampled the cloud macro and microphysical structures using the onboard cloud radar, lidar and precipitation radar and the MAS solar and infrared spectrometers.

4.1.2.3 Meteorological Conditions

The campaign period for CLASIC was characterized by the wettest summer in record for the city of Oklahoma. This was caused by the existence of a quasi-permanent high-pressure cell that set over the south east of the USA for much of the campaign period. This high-pressure system drove low-level southeasterly airflow into Oklahoma, advecting moisture from the Gulf of Mexico. At the upper levels, a couple of slow moving upper level troughs, coupled with this low-level pattern caused these incessant large amounts of rainfall during the CLASIC campaign. Shallow convection was the dominant cloud type in CLASIC.

These wet conditions experienced during the campaign period did not help to meet the research objectives of the campaign, which was to characterize the effects of the change in land surface properties on cumulus convection. It was expected that the harvesting of the winter wheat during this period would help to address the research question; however, no winter wheat was harvested because of the wet conditions that were experienced. As a result, very little post campaign funding was availed for the CLASIC campaign; hence, little information is available in the literature for the details and analysis of this campaign.

4.1.2.4 Aerosol Data

The aerosol data were acquired from the Cumulus Humilis Aerosol Processing Study (CHAPS) (Berg et al., 2009), a sister campaign of CLASIC that was funded by the US Department of Energy (DoE) that was conducted concurrently with CLASIC. The focus of CHAPS was to obtain detailed physical, chemical and radiative properties of CCN and aerosols in general from urban pollution and contrast them with their natural fields. Aircraft profiling of below-cloud, in-cloud and above-cloud regions of the lower troposphere were conducted. Two aircraft were deployed in CHAPS; the DoE G-1 aircraft conducted in-situ measurements of microphysical and chemical properties of aerosols in the lower troposphere. The National Aero-

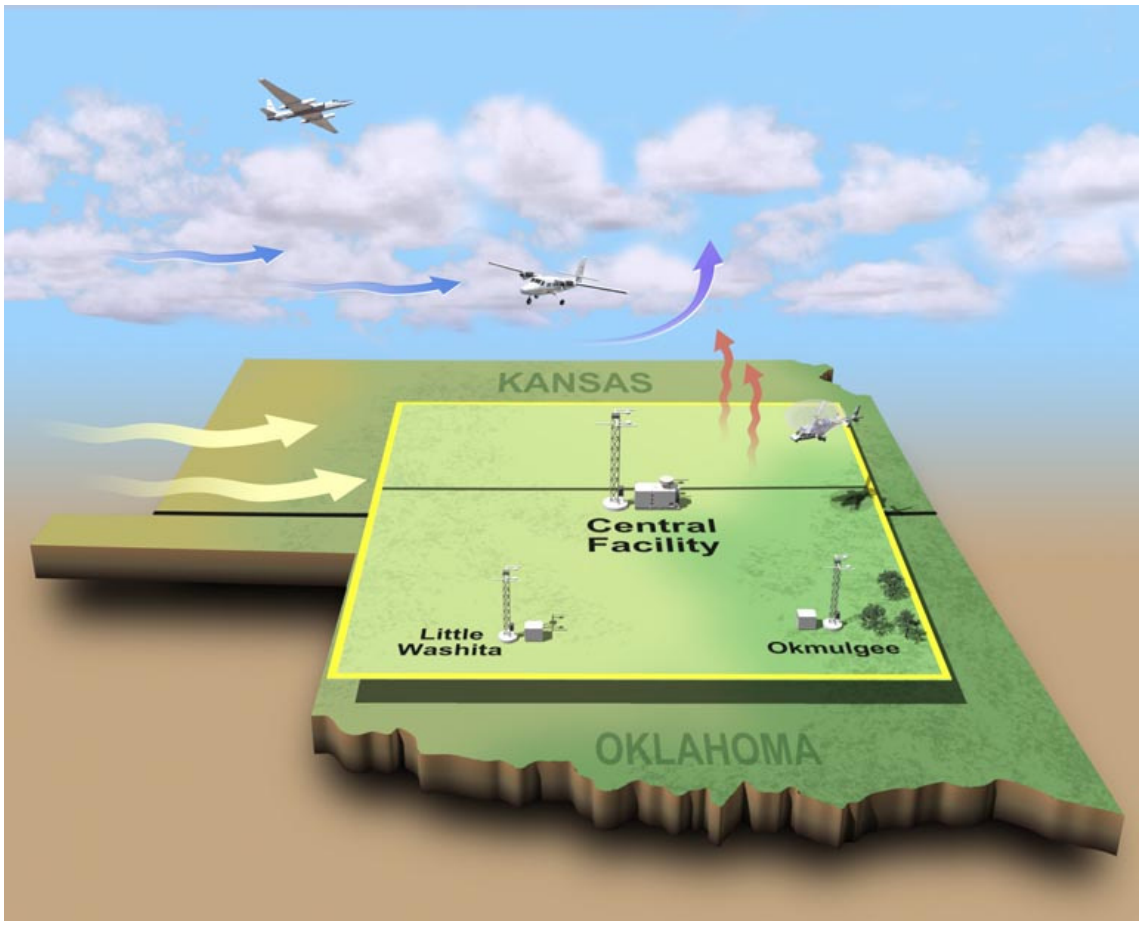

Figure 4.2: *A cortoon of the Cloud and Land Surface Interaction Campaign (CLASIC) domain, highlighting some of the observation strategies that were employed in the campaign and some of the processes that were explored. It took place in Oklahoma, USA (lat, lon = 35.56° N, 96.85° W) in June 2007.*

nautics and Space Administration (NASA) B200 aircraft mainly conducted remote measurements of aerosol and cloud optical properties such as back scattering and extinction properties, the details of which are not quite relevant to this study.

The G-1 aircraft payload comprised of the TSI 310 condensation particle counter that was used to measure aerosol particle number concentrations. The aerosol size distributions were measured using a couple of probes such as the Scanning Mobility Particle Sizer (SMPS) and the Fast Integrated Mobility Spectrometer (FIMS). The CAPS which consist of both the CAS and the CIP provided the number of cloud droplets (0.5 - 50μm) and precipitation with sizes ranging from 25 - 1550 μm. Other instruments such as the Maycomm TDL hygrometer, and the Geber PVM - 100A probe made measurements of RH and LWC, respectively.

The flight patterns that were employed during CHAPS involved level-legged flights, flying below cloud-bases, through the clouds and also above the cloud-top.

But since the cloud-tops were not at the same height, there were a few instances where the flights intersected through some clouds. In order to explore the effects of the urban plume from the Oklahoma City on the microphysical and optical properties of the aerosols and clouds, the flight patterns were also designed to sample the downwind and upwind regions of the city. The aerosol species that were measured in CHAPS included sulphates, dust, soot, organics (Figure 4.5). The scientists involved in this campaign recommend the use of the aerosol data from CHAPS especially for model studies (such as ours) that are related to aerosol activation.

4.2 Simulations and Results

4.2.1 Specifications of the Campaign Simulations

In addition to general specifications of the model given in Sect. 3.1.1, further impositions were applied to the model depending on the nature of the case being simulated.

4.2.2 The Tropical Maritime Case - TWPICE

A quasi-maritime and a quasi-land specification was applied for TWPICE, since the campaign domain was approximately 50% land and 50% ocean. A fixed sea-surface temperature of 29°C was applied following Fridlind et al. (2009); Fridlind and Co-authers (2012); Morrison and Grabowski (2011).

The aerosol data in Fig. 4.3 was derived from Allen et al. (2008). These aerosol data were measured during the ACTIVE campaign (Sect. 4.1.1.4) and the species that were measured during the campaign were sulphate, sea-salt and organic aerosols (both soluble and insoluble aerosols). Primary Biological Aerosol Particles (PBAPS) were assumed to be 50% of the measured insoluble organics (Pruppacher and Klett, 1997). Black carbon (soot) and dust were not measured during the campaign; hence, the model outputs of these species from the Global Model of Aerosol Processes (GLOMAP) model were applied (by courtesy of Ken Carslaw and Kirsty Pringle). For the aerosol profiles above the altitudes were aircraft measurements were made, constant mass mixing ratios which were equal to the mass mixing ratios at the highest flight level were assumed for species that were measured during the campaign. This is similar to how other researchers (Fridlind et al., 2009; Morrison and Grabowski, 2011) have treated the problem. A lognormal distribution with distribution parameters similar to those prescribed by Fridlind et al. (2009) in their model inter-comparison study and from Matthias-Maser and Jaenicke (1995) for carbona-

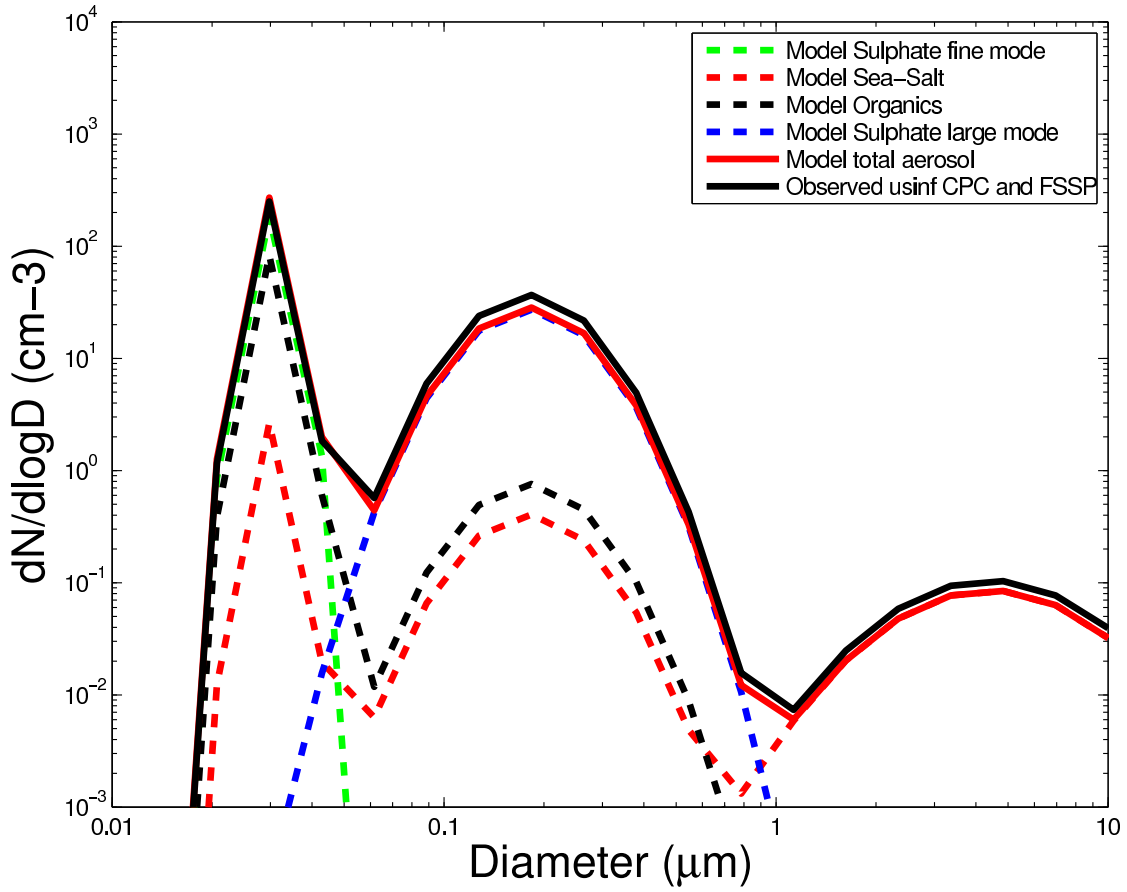

Figure 4.3: *A tri-modal aerosol size distribution applied to the model for TWPICE case. Distribution parameters given by Fridlind et al. (2009), taken from Allen et al. (2008) have been applied. The species are explained in the legend.*

ceous and PBAPs was adapted. The simulation was started from 17 January 2006 at 0300Z and ended at midnight of the 12^{th} of February 2006. The vertical profiles of the aerosols used to initialize the model are shown in Fig. 4.4.

4.2.3 The Mid-Latitude Continental Case - CLASIC

As for the CLASIC case, purely continental specifications were imposed. The aerosol data applied in the CSRM is shown in Fig. 4.5. No distribution parameters were prescribed by the campaign scientists, hence, those from Phillips et al. (2009) were assumed for corresponding aerosol species as shown in Table. 3.1. This is because Phillips et al. (2009) simulated an ARM's case that took place over the same domain as in CLASIC. For aerosol profiles at altitudes above the flight ceilings, the same extrapolation technique applied for TWPICE above was also used here.

The simulation was commenced at 0000Z of 10 June 2007 and ran to the midnight of 30 June 2007. For both cases, the model output was written out at 5-minute

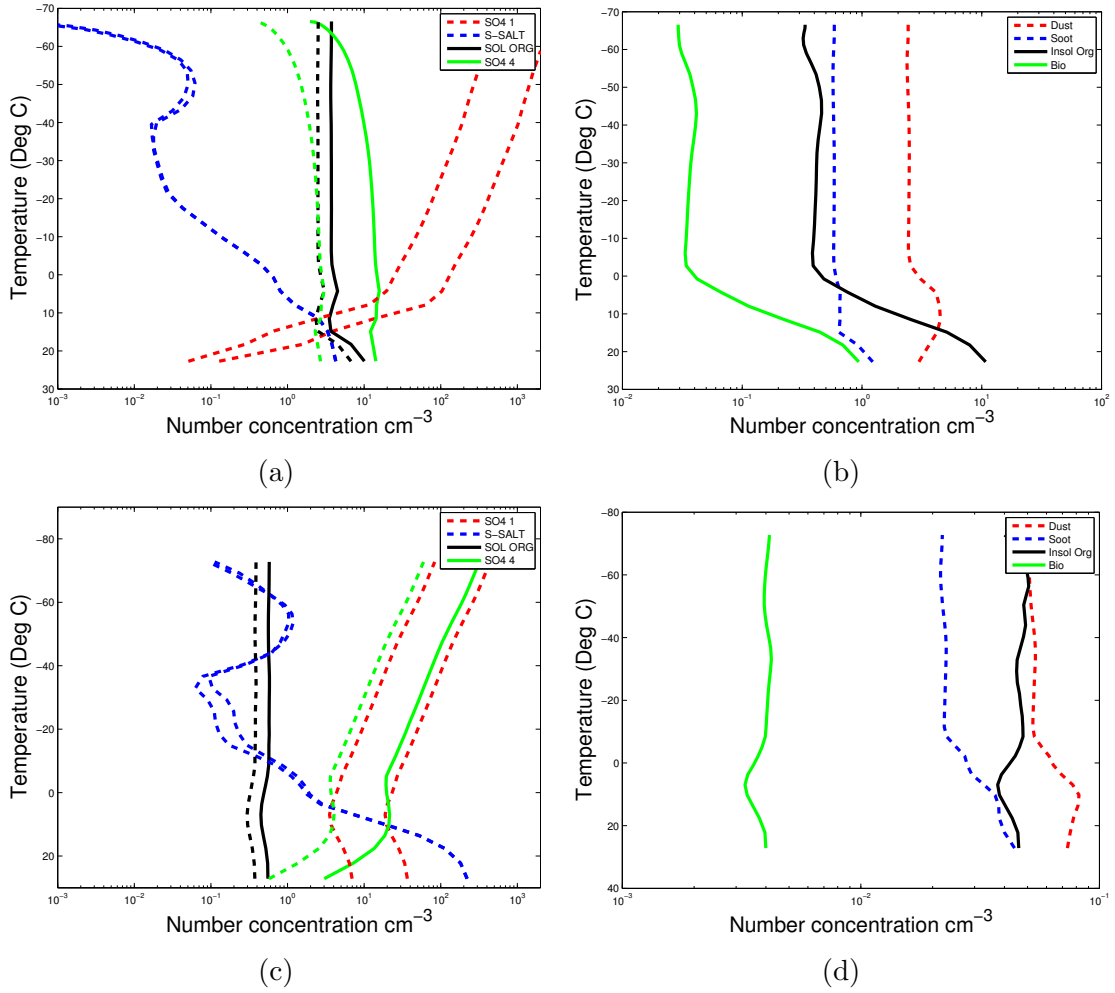

Figure 4.4: *Vertical profiles of aerosol mass mixing ratios in* kg^{-1}. *The solid lines represent present-day scenarios while the broken lines represent pre-industrial scenarios. Solute aerosols are shown in (a) for CLASIC and (c) for TWPICE, while solid aerosols are shown in (b) for CLASIC and (d) for TWPICE. These profiles were used to initialize the simulations. NB: the pre-industrial profiles are not relevant in this chapter, but in the following chapters.*

intervals of the simulation time and 36 hours of the model spin-up were allowed during the analysis of the model results. Where the mean profiles or the time-series are provided in the following discussions, they represent the averages of the entire simulation domain (168km wide) and of the entire simulation periods, which are 26 days and 21 days for TWPICE and CLASIC, respectively. This technique of domain and simulation averages is a standard technique that at the present is widely used by several researchers in the literature e.g. Fridlind et al. (2009); Morrison and Grabowski (2011) and Fan et al. (2013) when analyzing model results and also when comparing the model results to observations.

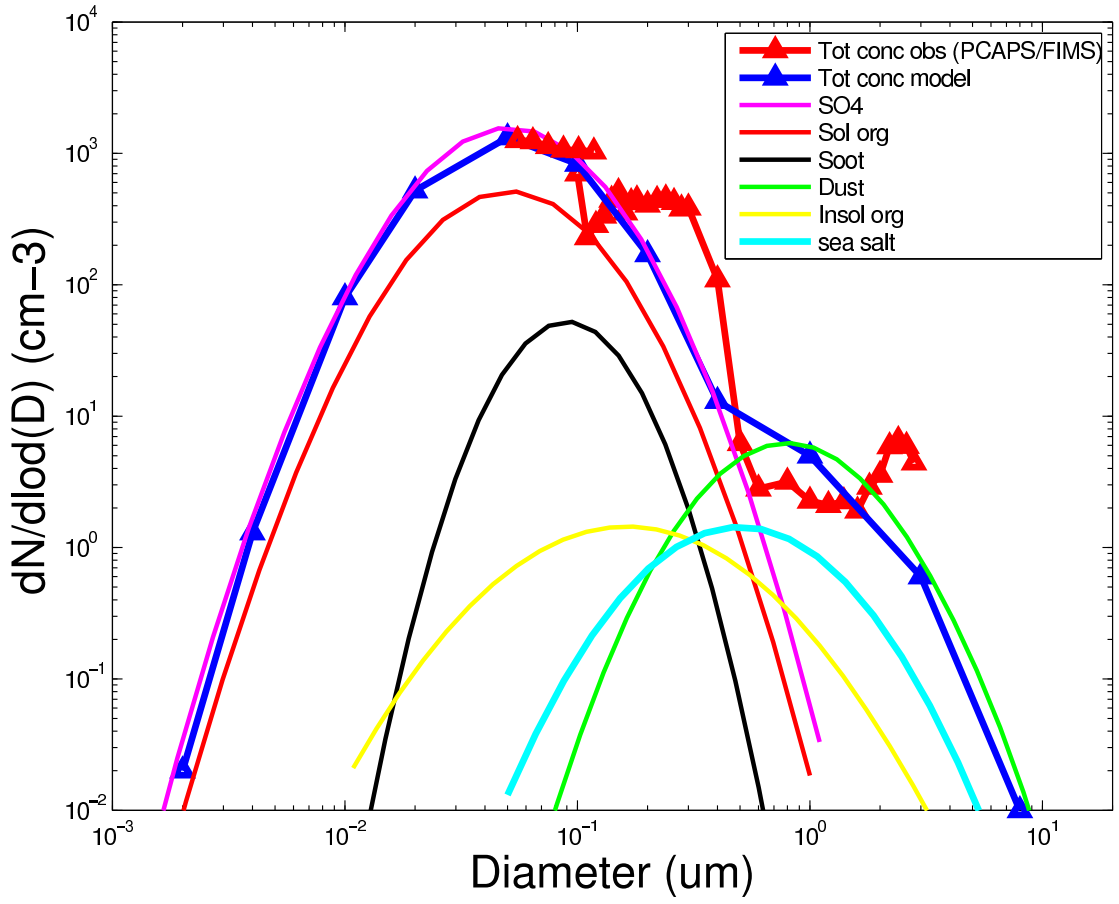

Figure 4.5: *A tri-modal aerosol log-normal size distribution applied to the model for CLASIC case. Distribution parameters prescribed by Phillips et al. (2009) have been applied. The respective species are as explained in the legend.*

4.2.4 Microphysical Properties

4.2.4.1 Ice Crystal Number Concentrations

Figures 4.6 and 4.7 show the mean mass-mixing ratios of clouds, unconditionally averaged over the whole domain and simulation period for TWPICE and CLASIC, respectively. This is to show on average, the type of clouds that were simulated by the model in the two cases. It is apparent that the clouds in TWPICE were more stratified than they were in the CLASIC case. Also, it can be seen that the model captured a wide range of clouds, ranging from low-level fog to upper-level cirrus. As expected, the high mass-mixing ratios of clouds appeared in the regions where liquid clouds are expected. In Fig. 4.8 and 4.9, the vertical profiles of ice number concentration for the predicted and observed values are shown. It is noticeable that for TWPICE, the model prediction lied within the 90% confidence interval of the population mean. This was true at least in the regions where comparison with

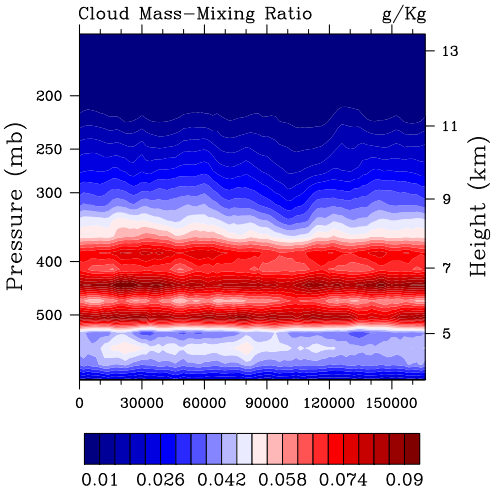

Figure 4.6: *Mean mass-mixing ratios of clouds that are averaged unconditionally over the entire simulation period for both TWPICE. The x-axis is the domain width in meters.*

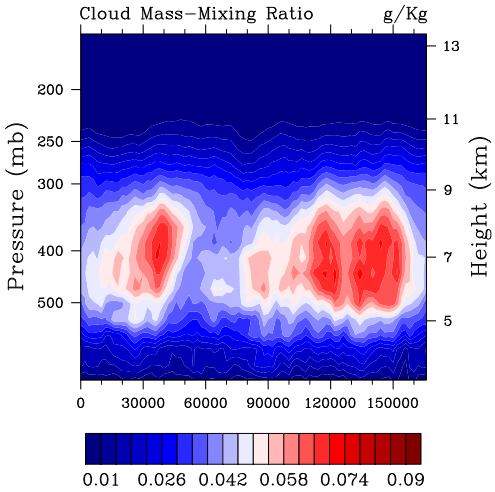

Figure 4.7: *Mean mass-mixing ratios of clouds, averaged unconditionally over the entire simulation period for CLASIC. The x-axis is the domain width in meters.*

observations was allowed. The red curve in the figure (Fig. 4.8) represents the observations. It is an average of flight measurements from nine different days taken during the campaign using the Cloud Imaging Probe (CIP).

Unfortunately, the other two probes (the CDP and the CAPS) that were deployed during the campaign in the Egrett aircraft developed technical faults during much of the campaign period, hence, the data from these two instruments were not used here for comparison with our model results. The CIP probe (as explained above) counted all particles with diameters of 10 to 2300 μm. These size rages include giant aerosols, cloud droplets and cloud ice. However, at altitudes above the 10km fight level, negligible amounts of giant aerosols (diameters > 10 μm) exist, owing to gravitational effects and due to the onset of homogeneous freezing of cloud droplets at around the 9km altitude in TWPICE, no cloud droplets would be expected from these CIP data. But still there is an issue of ice shattering that tends to inflate crystal number concentrations (Sect. 2.1.2.5.2), to evade this problem, the CIP data was corrected for ice shattering at cut-off sizes of 100μm by Aaron Bansemmer of UCAR Boulder, Colorado. Hence, both the predicted and observed concentrations in Fig. 4.8 are for ice crystals of sizes greater than 100μm.

The ice number budget profiles of sources of ice crystals in the model shown in Figs. 4.10a and 4.10b show that dust is the dominant source of heterogeneously nucleated ice crystals in the model for both TWPICE and CLASIC. However, soot and biological aerosols still have substantial contribution to the total number con-

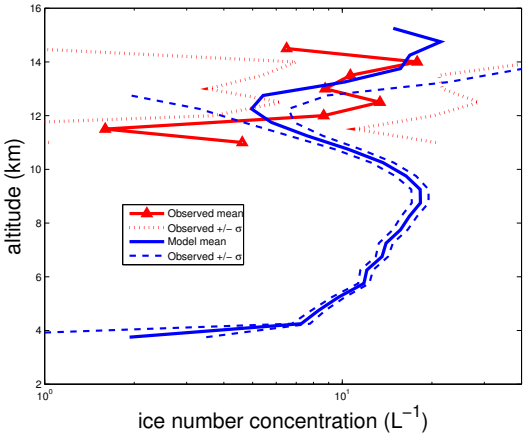

Figure 4.8: *Mean number concentrations of crystals with effective diameters greater than 100 μm for TWPICE. The solid lines represent the average values, while the broken lines represent standard deviations from the mean. The blue lines represent the model results, while the red ones are for observations. Conditionally averaged over regions of weak vertical velocities (vertical velocity less than 1. m s^{-1}) and cloudy regions with IWC greater than 0.001 gm^{-3}.*

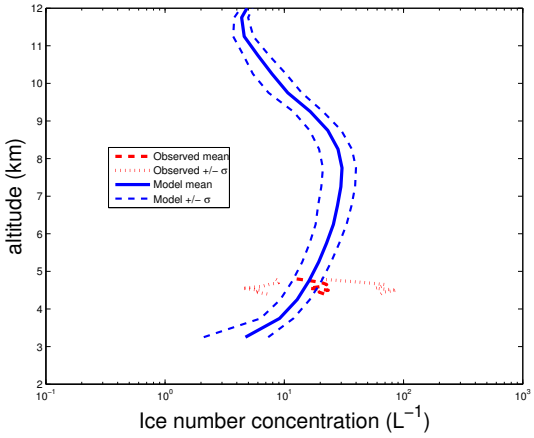

Figure 4.9: *Mean number concentrations of crystals with effective diameters greater than 100 μm for CLASIC. The solid lines represent the average values, while the broken lines represent standard deviations from the mean. The blue lines represent the model results, while the red ones are for observations. Conditionally averaged over regions of weak vertical velocities (vertical velocity less than 1. m s^{-1}) and cloudy regions with IWC greater than 0.001 gm^{-3}.*

centration of heterogeneously nucleated ice crystals. It should however be noted that homogeneous aerosol and cloud droplet freezing are by far the most dominant sources of ice crystals as shown in the following chapter (Figs. 5.2 and 5.21). The Halett-Mossop process 3.1.3.2.4, which is an ice multiplication process is the second dominant source of ice crystals in the model.

Observational data for ice crystal number concentrations are limited for CLASIC (Fig. 4.9). This is because most of the flights during the campaign traversed only the lower troposphere, where water clouds were prevalent. Also, the orders of magnitude of the predicted ice number concentrations are in good agreement with those found by other researchers (Mitchell, 1994; Kajikawa and Heymsfield, 1989) in their modeling and observational studies.

The higher ice number concentrations in CLASIC relative to TWPICE are expected and explicable in terms of the ocean-land contrast for aerosol fields as explained in Sect. 2.1.1. There were higher aerosol number concentrations in the continental CLASIC than in the maritime TWPICE. The CLASIC aerosol scenario was even more polluted as it was conducted near urban areas in Oklahoma (Fig. 4.4). Also, the incessant deep convection during the campaign period (Sect. 4.1.2)

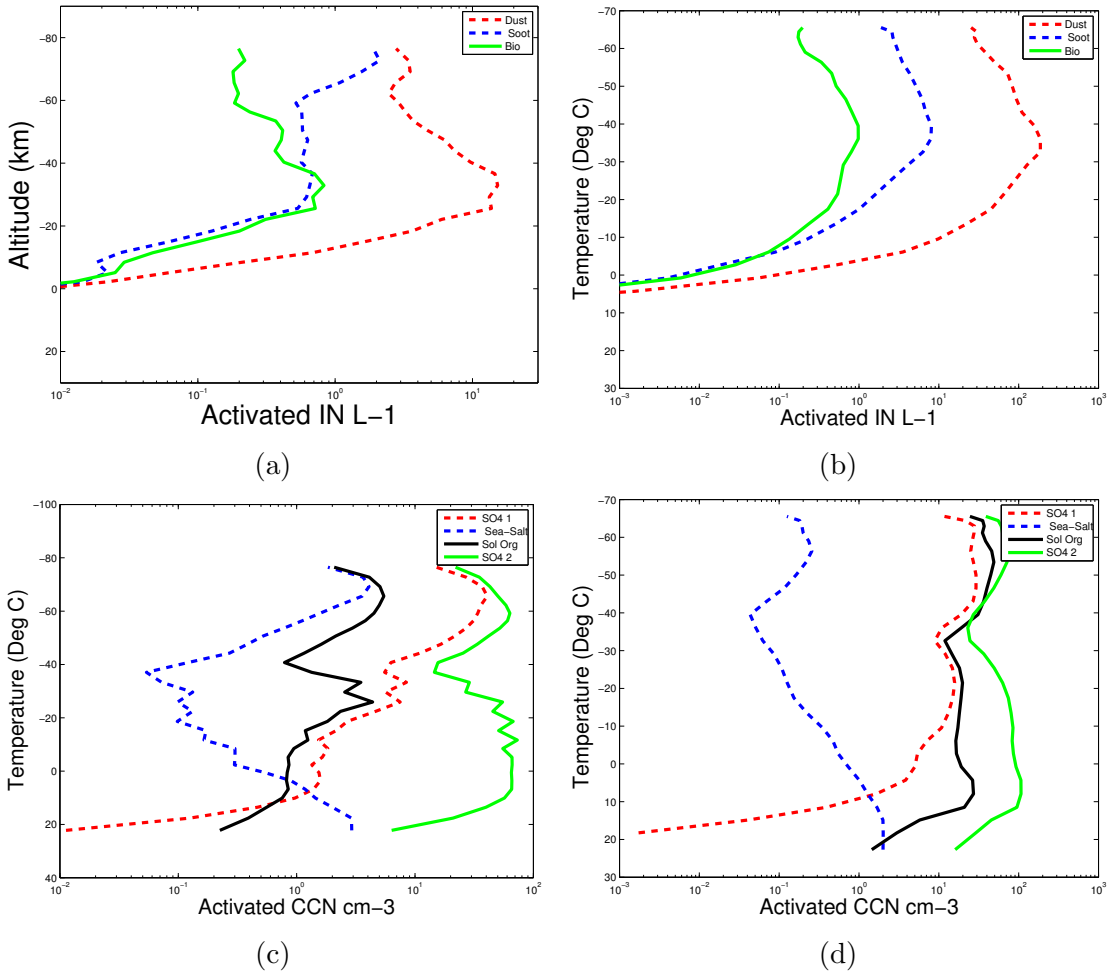

Figure 4.10: *The number budgets of activated aerosol particles (a) activated IN in TWPICE, (b) activated IN in CLASIC, (c) activated CCN in TWPICE and (d) activated CCN in CLASIC control runs. The different lines represent activation from different aerosol species.*

entails high number concentrations of crystals, primarily because deep convection is characterised by faster updrafts and higher supersaturations, which favour the activation of more CCN and IN.

A peak within the Hallett-Mossop region (5 - 6 km altitude) is more prominent in TWPICE than it is in CLASIC particularly because in nature, the H-M process is dependent on several factors (such as temperature and LWC) and the size of the accreting particles is also one of the important factors. The parameterization for the H-M process used in this study depends on the amount of supper-cooled liquid water collected either by graupel or snow particles and this collection processes is a function of the sizes of the interacting hydrometeors. This finding was noted as well by Aleksic et al. (1989) in a modelling study to investigate the H-M processes. In their simulations, glaciation from the H-M process was more predominant in maritime

than in continental clouds. This was primarily because of reduced liquid water collected through riming and suppressed graupel formation in continental clouds. The mean sizes of cloud droplets in the this study (Figs. 5.1 and 5.22) are smaller in CLASIC than in TWPICE especially within the temperature range were the H-M process is active (-3 to -8 °C), primarily due to their contrasting aerosol fields (Fig. 4.4). A second peak in ice number concentration (due to homogeneous freezing of cloud droplets and aerosols) is seen in both simulations, although it is more distinct in CLASIC than in TWPICE. This is mainly because homogeneous freezing is more favourable in continental than in maritime clouds because of the smaller sizes of cloud particles that characterise continental clouds relative to maritime clouds. Smaller sizes of cloud particles delay the onset of rain; hence, clouds have a higher chance of growing deeper to reach the homogeneous freezing levels.

4.2.4.2 Cloud Droplet Number Concentrations

Figures 4.11 and 4.12 show the average vertical profiles of droplet number concentrations for TWPICE and CLASIC, respectively. By referring to both Figs. 4.10c and 4.10d which are showing the number budgets of the sources of cloud droplets from all the different aerosol species being treated in the model, it can be seen that the accumulation mode of sulphate aerosols is the dominant source of cloud droplets, especially in TWPICE. In CLASIC however, soluble organics are equally important because of the relatively high soluble organics to sulphur ratio in CLASIC compared to TWPICE. Another budget of cloud droplets from solid aerosol shows that droplets from solid aerosols contribute less than 10% of the total cloud droplets.

A Forward Scattering Spectrometer Probe (FSSP) mounted on the wing of the Dornier aircraft during the ACTIVE campaign measured droplet number concentration. The Forward Scattering Spectrometer Probe (FSSP) probe measures particles with sizes ranging from 0.5 - 32 μm and has the potential to include supermicron aerosols in its measurements of cloud droplet concentrations, hence, a minimum threshold for LWC of 0.001 gm^{-3} was imposed for cloud-screening from FSSP data. We applied this thresholding technique following the advice of Grant Allen of Manchester University, who was a flight scientist during the TWPICE field campaign. The observations curve in Fig. 4.11 is an average of flight measurements taken from fourteen different days of the campaign. The model results were conditionally averaged over regions of weak vertical velocities, where the magnitudes vertical velocities were less than 0.5m s^{-1}. This was done to match the flight pattern of the campaign; the Dornier aircraft always avoided cores of convection due to severe turbulence. Also, all the ACTIVE and TWPICE aircraft did not specifically target and sample liquid

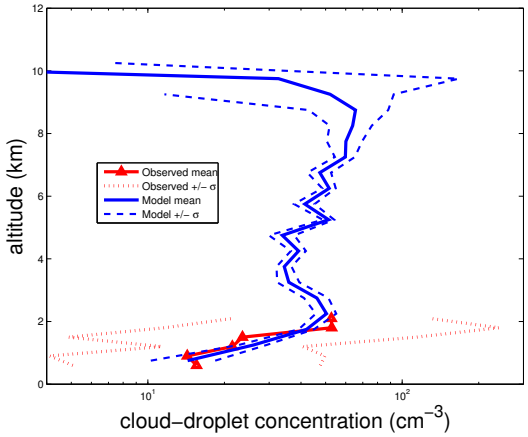

Figure 4.11: *Mean number concentrations of cloud droplets for the TWPICE campaign. Conditionally averaged over regions of weak vertical velocities (vertical velocity less than 0.5 m s^{-1}) and cloudy regions with ice water content greater than 0.001 gm^{-3}. The solid lines represent the average values, while the broken lines represent standard deviations from the mean. The blue lines represent the model results, while the red ones are for observations.*

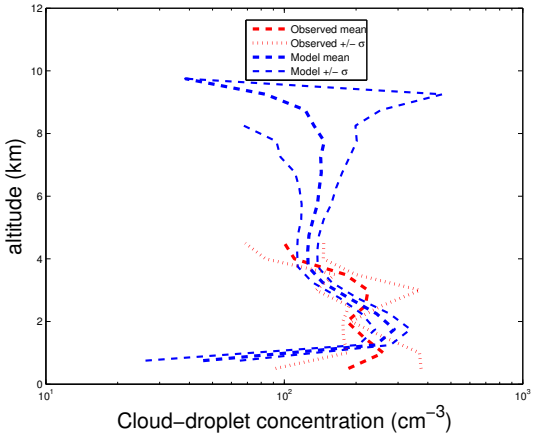

Figure 4.12: *Mean number concentrations of cloud droplets for the CLASIC campaign. Conditionally averaged over regions of strong vertical velocities (vertical velocity greater than 0.5 m s^{-1}) and cloudy regions with ice water content greater than 0.001 gm^{-3}. The solid lines represent the average values, while the broken lines represent standard deviations from the mean. The blue lines represent the model results, while the red ones are for observations.*

phase clouds but there were occasional passages through shallow cumulus cloud (G. Allen of Manchester University, personal communication).

For CLASIC, the Cloud, Aerosol and Precipitation Spectrometer (CAPS) probe measured the droplet number concentrations. The CAPS comprises the Cloud Aerosol Probe (CAS) and the Cloud Imaging Probe (CIP) for measurements within the 0.5 to 50 and the 25 to 1550 μm size ranges. The observations curve shown is an average of flight measurements using the CAPS probe for size bins between 5 and 50 μm (our thresholds for cloud particle sizes) taken from thirteen different days of the campaign. Cloud screening was done by selecting instances where LWC was greater than 0.013gm^{-3} to eliminate instances were only aerosols were detected by the CAS at its lowest sizes of the measured spectrum. CLASIC was characterized by shallow convection producing heavy precipitation (Sect. 4.1.2), so the comparison to observations is done by conditionally averaging the predicted number concentrations of cloud droplets over clouds with vertical velocities greater than 0.5m s^{-1}.

Satisfactory agreement between observations and model results is seen in Figures 4.11 and 4.12, showing the strength of the model in resolving these microphysical processes. Also, the higher cloud droplet number concentrations in CLASIC rela-

tive to TWPICE are explicable in terms of their contrasting aerosol scenarios (as explained for ice crystal concentrations). The strong peaks in cloud droplet concentrations being shown at 2km altitude are reminiscent of the one expected at cloud bases. Since, supersaturations attain their maximum values within a few meters above cloud-base and decrease gently to a steady value beyond that level, so does the droplet number concentration (Rogers and Yau, 1991). The other explanation is the onset of collision and coalescence aloft, which depletes cloud number through rain production. Finally, because of preferential sedimentation of larger cloud droplets that peak can also not be averted.

4.2.4.3 Mean Radius of Ice Crystals

The mean sizes of cloud ice are important in assessing the radiative properties of clouds, for instance in the determination of the extinction coefficient (Mitchell, 1994), which is a measure of how strongly a substance attenuates the radiative fluxes. Therefore, the model predicts the mean sizes of cloud-ice and results are shown in Figs. 4.13 and 4.14. A good agreement between observations and model predictions is noted for TWPICE (Fig. 4.13). The decrease of mean crystal sizes with height is primarily due to an increase with height of total number concentrations of ice particles (Figs. 4.8 and 4.9), which increases the competition for the same amount of available vapour. Sedimentation of ice crystals out of cirrus clouds and the growth of crystals by vapour diffusion promotes riming and aggregation during descent. Other mechanisms of crystal growth such as aggregation are also effective in higher temperatures. No comparison with observations is shown for CLASIC due to the unavailability of ice-phase data; however, predictions are quite realistic with reference to TWPICE.

4.2.5 Radiation Statistics and Macrophysical Properties

Table 4.1 shows the radiation statistics for the upward and downward components of radiation measured at the top of the atmosphere (TOA) and at the surface for both TWPICE and CLASIC. The observations statistics were downloaded from the ARM's website (`www.arm.com`), where they are available freely for both cases.

The highest percentage bias of 33.75% for the upward component of SW radiation at the top of the atmosphere for TWPICE was attributed to the fact that the model predicted higher middle level cloudiness than observations (Fig. 4.15), this would imply a higher optical depth and, hence, higher reflectivity in the SW ranges by clouds. Still on the same campaign, the negative bias of -5.56% resulting from a

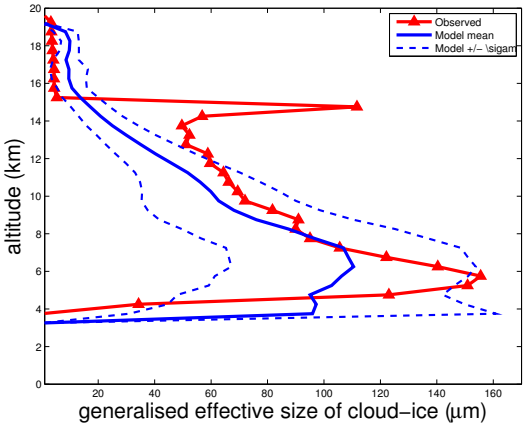

Figure 4.13: *Vertical profiles of mean effective diameter of ice crystals for TWPICE. Conditionally averaged over cloudy regions where effective crystal diameter was greater zero. The solid lines represent the average values, while the broken lines represent standard deviations from the mean. The blue lines represent the model results, while the red ones are for observations.*

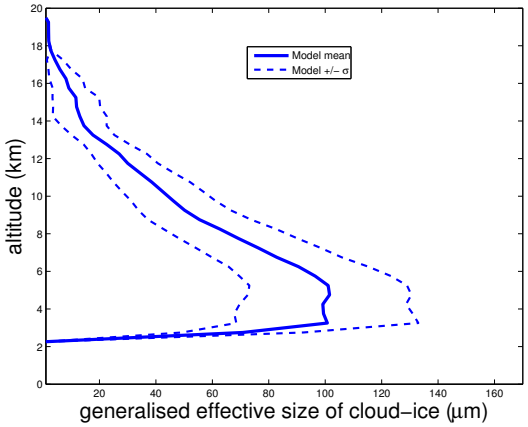

Figure 4.14: *Vertical profiles of mean effective diameter of ice crystals for CLASIC. Conditionally averaged over cloudy regions where effective crystal diameter was greater zero. The solid lines represent the average values, while the broken lines represent standard deviations from the mean from the model. The were no observations to compare with the model results.*

higher absolute value in the downward component of the long-wave radiation at the surface was explained in terms of the strong temperature dependence of the emitted radiative flux (Stefan-Boltzmann law, Eqn. 2.17). Fig. 4.17 and 4.18 show that the model is generally colder than observations; hence, long-wave radiation emitted to space would be lower.

For CLASIC, it is not immediately explainable from the available analysis why a higher positive bias of 16% is available for the downward component of short-wave radiation at the surface, but, parsimonious evidence available in Fig. 4.16 suggests that on average, the model predicted slightly less cloudiness than observations, and thus, more insolation was transmitted to the surface and also, the model systematically predicts less LWC than observations, hence, the optical thicknesses of clouds predicted in the model are less than those of observed clouds. All other biases are within reasonable ranges of less than $\pm 10\%$. This satisfactory model performance for the radiation statistics is crucial for the core objective of this study. Accurate assessment and quantification of optical properties of clouds require high confidence in prediction of TOA radiative fluxes.

Figures 4.19 and 4.20 show area averaged cumulative precipitation that is unconditionally averaged over the whole domain of the study and over the whole simulation period for both TWPICE and CLASIC, respectively. A 'near-perfect' agree-

ment between model predictions and observations is predicted in both simulations particularly for TWPICE.

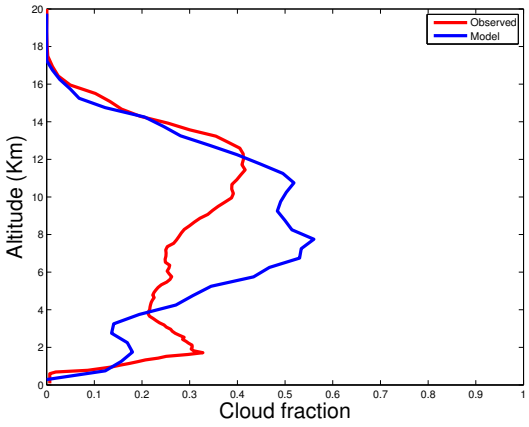

Figure 4.15: *Vertical profile of cloud fraction for TWPICE averaged over the whole simulation domain for cloud mixing ratios greater than 0.01 gkg^{-3}. The blue line represents the model mean, while the red line represents the observed mean.*

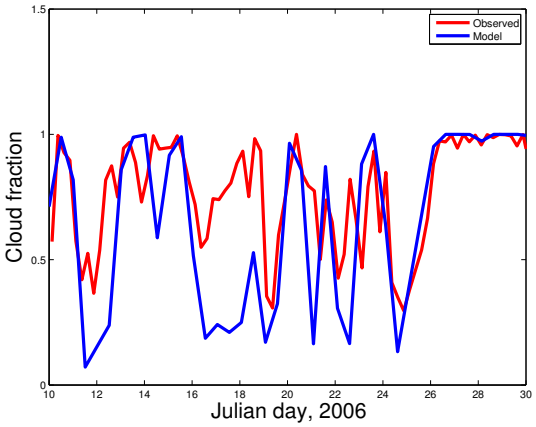

Figure 4.16: *Time series of cloud fraction for CLASIC averaged over the whole simulation domain for cloud mixing ratios greater than 0.01 gkg^{-3}. The blue line represents the model mean, while the red line represents the observed mean.*

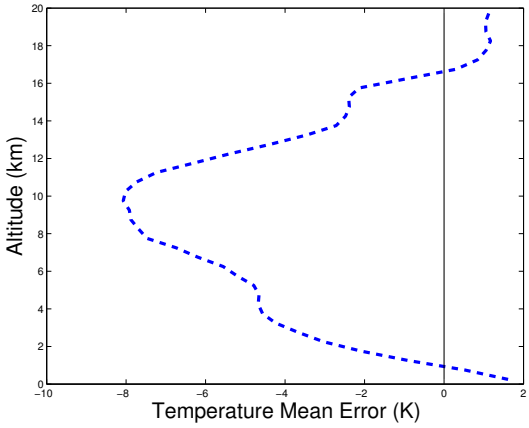

Figure 4.17: *Unconditionally averaged vertical profile of temperature bias (model mean minus observations mean) for TWPICE.*

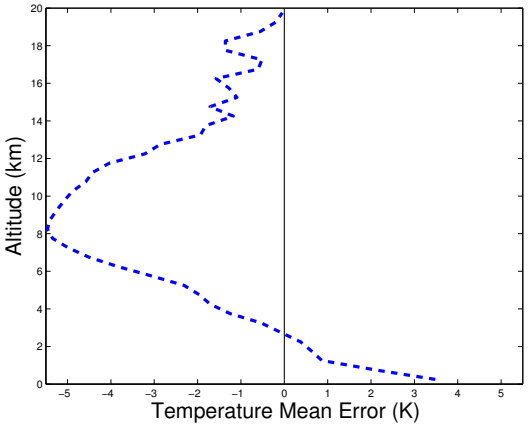

Figure 4.18: *Unconditionally averaged vertical profile of temperature bias (model mean minus observations mean) for CLASIC.*

Precipitable water in a column of the atmosphere is defined as the total amount of liquid water that would be obtained if all the vapour in that column would condense and precipitate out. Although it does not have a direct relationship with surface precipitation, it however is a good measure of the moisture budget of the atmosphere. The model predictions and observations for this parameter are shown in Figs. 4.21

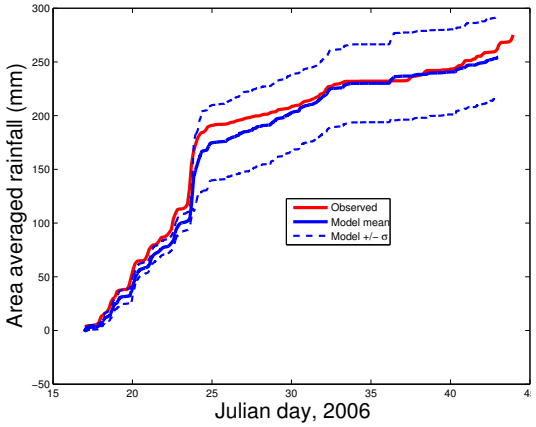

Figure 4.19: *Cumulative precipitation in mm unconditionally averaged for the whole four-week simulation period of TWPICE. The solid lines represent the average values, while the broken lines represent standard deviations from the mean. The blue lines represent the model results, while the red ones are for observations.*

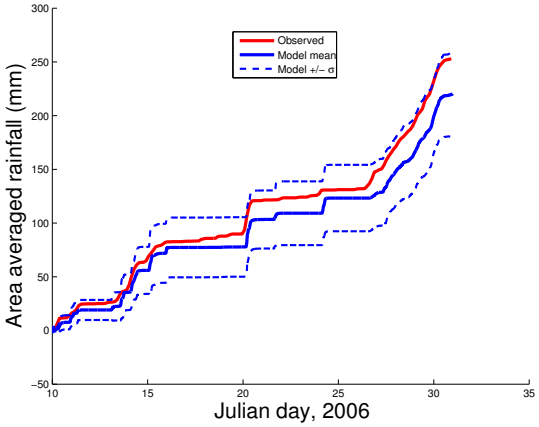

Figure 4.20: *Cumulative precipitation in mm unconditionally averaged for the whole three-week simulation period of CLASIC. The solid lines represent the average values, while the broken lines represent standard deviations from the mean. The blue lines represent the model results, while the red ones are for observations.*

and 4.22 for TWPICE and CLASIC, respectively. A tendency of underestimating this quantity both at the beginning and towards the end of the simulation for both cases by the model is exhibited. It is not immediately clear why this tendency is obtained.

4.3 Summary

A series of model developments were carried out in this study as clearly elaborated in Sect. 3.2. Subsequently, the comparison of the model results with observations were performed by simulating two contrasting tropical scenarios of deep convection, the Tropical Warm Pool-International Cloud experiments (TWPICE) and Cloud and LAnd Surface Interactions Campaign (CLASIC), which are respectively maritime and continental. Some of the fields compared with observations have been presented in the results sections (sections 4.2.4 and 4.2.5). The comparison of the model results to observations has shown (where comparison was possible) satisfactory agreement between model simulations and observations and the model standard deviations being within a reasonable range of less than 40% of the model mean values. The available observation dataset was obtained from a dense network of ground-based observation platforms, aircraft, ships and satellites.

Predictions of both crystal and droplet number concentrations have lied within

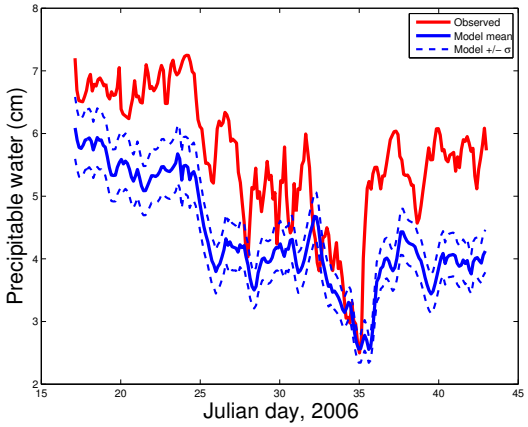

Figure 4.21: *Time series of precipitable water in cm for the whole three-week campaign period of TWPICE averaged over the whole simulation domain and over cloudy regions. The solid lines represent the average values, while the broken lines represent standard deviations from the model mean. The blue lines represent the model results, while the red ones are for observations.*

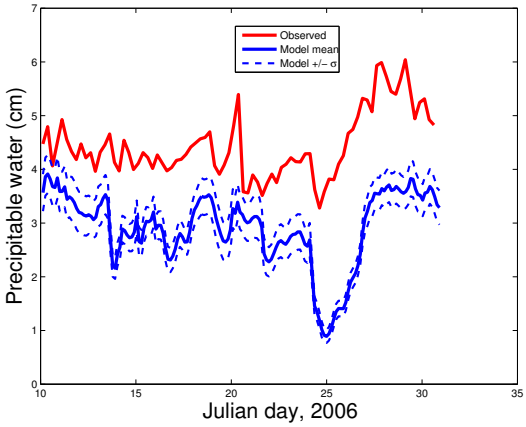

Figure 4.22: *Time series of precipitable water in cm for the whole three campaign period of CLASIC averaged over the whole simulation domain and over cloudy regions. The solid lines represent the average values, while the broken lines represent standard deviations from the model mean. The blue lines represent the model results, while the red ones are for observations.*

90% confidence intervals of observations. Similar proximity of predictions to observed scenarios was also noted for mean sizes of ice crystals. These microphysical properties are of great importance in radiation and aerosol-cloud interactions for determining the optical properties of clouds. Precipitation has also been predicted more accurately by the scheme for both cases especially for CLASIC. This further affirms the robustness of the model. Moreover, the radiation statistics were also simulated decently, with a model bias of less than ±25% for both top of the atmosphere and surface radiative fluxes. Downward and upward components of long- and short-wave radiations were predicted for both cases.

This scheme has been improved and upgraded, making it adaptable to a wide range of atmospheric science studies particularly investigations of aerosol-cloud interactions. This updated and rigorously validated aerosol-cloud model allows research of aerosol indirect effects and was used to investigate the different mechanisms of aerosol indirect effects particularly on glaciated clouds. This study was the first of its kind using such a robust, state-of-the-art microphysics scheme comprising a semi-prognostic aerosol component, encapsulating diverse aerosol species and explicitly treating their loadings and chemical compositions. The focus of the next chapter is to investigate different and salient mechanisms by which changes in aerosols field, both in their number concentration and chemical composition affect

Radiation fluxes (Wm^{-2})	SW TOA upwards	SW SFC downwards	LW TOA upwards	LW SFC downwards
Model TWPICE	174.16	213.36	210.12	404.23
Observed TWPICE	130.22	216.06	201.88	428.16
Percentage bias (%)	33.75	-1.25	4.08	-5.56
Model CLASIC	196.69	240.36	199.89	371.10
Observed CLASIC	184.26	206.32	225.04	403.82
Percentage bias (%)	6.74	16.50	-11.17	-8.10

Table 4.1: *Unconditionally averaged statistics for upwards and downwards components of radiation for TWPICE and CLASIC. The abbreviations are as follows: SW = Short-Wave, LW = Long-Wave, TOA = Top Of the Atmosphere, SFC = SurFaCe.*

the optical properties of clouds. The main objectives of the study was to explore the cloud microphysical and dynamical mechanisms for glaciated cloud indirect effects on the mesoscale, focusing mainly on glaciation, thermodynamic and riming indirect effects (Lohmann and Feichter, 2005) from anthropogenic soluble and solid aerosols. Important feedbacks associated with these indirect effects are investigated as well as quantifying their respective radiative forcings. This was done by way of sensitivity tests as described in the following chapter (Chapter 5).

Chapter 5

Influence of Solute Aerosols on Indirect Effects via Glaciated Clouds

The core objective of this study was to perform numerical modelling sensitivity tests in order to identify salient microphysical and dynamical pathways of aerosol indirect effects on glaciated clouds from anthropogenic aerosol pollution. The numerical modelling has been based on observed cases, each lasting three to four weeks, and covering a wide mesoscale domain. Each simulation resolved entire cloud systems including a wide range of cloud-types, i.e. convective, stratiform and cirriform clouds. In each scenario, different meteorological conditions were expected to prevail, giving rise to different types of organization of cloud-types. Therefore, cloud-cloud interactions are also accounted for in this study. Thus, multiple techniques were applied to isolate various types of indirect effects on glaciated clouds from this conundrum of aerosol indirect effects. The chief tools used were sensitivity tests of various microphysical processes, by altering only aerosol conditions between pre-industrial and present-day. Such tests were performed for various configurations of the model, to deduce the mechanisms by which aerosols influence clouds.

5.1 Hypotheses

Several hypotheses of how increased aerosol modifies the microphysical and radiative properties of clouds were tested in this study. The list of the aims and objectives and the hypotheses tested in this PhD thesis is given in Sect. 1.2.

5.2 Methodology

The approach for verifying or disproving these scientific hypotheses is to perform sensitivity tests using the validated simulations of two cases of cloud systems shown

in Chapter 4. The first part of this analysis examines results from the sensitivity tests of CLASIC, which is a mid-latitude continental case (Chapter4), while the second part examines results from TWPICE. Furthermore, in order to compare and contrast, if any noticeable microphysical differences arising from these contrasting cases, the final level of the analysis is dedicated to highlighting these.

The first hypothesis outlined in Sect. 5.1 that anthropogenic solute aerosols from soluble materials modify glaciated clouds through homogeneous aerosol and cloud droplet freezing was tested first. By this hypothesis, it is stated that, homogeneous freezing produces a cold-cloud albedo/emissivity effect by boosting crystal numbers aloft. Soluble aerosols are traditionally known to initiate cloud droplets, although recent laboratory studies have discovered that some soluble organic CCN become glassy at very low temperatures and activate ice too (Murray et al., 2010). Murray et al. (2010) introduced to the cloud microphysics community that, an aerosol must be solid in order to act as an IN and does not necessarily need to be insoluble. Although, this effect of glassy aerosols has been incorporated in the microphysics model (Sect. 3.2.4), it is worthwhile to mention that, for the purposes and objectives of this part of the study, this treatment (of soluble organics becoming glassy at very low temperatures) was switched off in order to study in isolation, the effects from solute aerosols initiating cloud droplets.

As described above (Sect. 3.1.2), the model classifies aerosols into two major categories; the soluble and the insoluble species. Although solid aerosols are assumed externally mixed with each other, they are coated (or internally mixed) with some of the components of solute aerosols such as sulphate and soluble organics. Thus, solid aerosols can initiate both cloud droplets (Petters and Kreidenweis, 2007) and cloud ice, while solute aerosols do not heterogeneously nucleate ice. In sensitivity tests described in this chapter, the addition of solute aerosol material only perturbs the number concentrations of liquid cloud droplets by increased CCN activity and of cloud-ice by homogeneous freezing of aerosols and cloud droplets. The solute aerosol species altered are: sulphate, soluble organic aerosols (their IN activity is not treated in this Chapter) and sea-salt.

The microphysics mechanisms of activation of cloud particles that are affected by increased solute aerosols are as follows.

- Cloud-base droplet activation by solute aerosols (sulphate, sea-salt and soluble organic aerosols).

- In-cloud droplet activation by solute aerosols (sulphate, sea-salt and soluble organic aerosols).

- Homogeneous aerosol freezing of solute aerosols (sulphate, sea-salt and soluble organic aerosols) at the homogeneous aerosol freezing level.
- Homogeneous cloud droplet freezing near -36 °C level.

Although droplet activation by solid aerosol (dust/metallic, soot, insoluble organics-non biological aerosols, and primary biological particles) is still treated in these sensitivity tests, their number and mass concentrations are not perturbed when present-day and pre-industrial aerosol conditions are contrasted. Accordingly, it is assumed that the number and mass concentrations of cloud droplets from these solid aerosols remain unchanged. The tests exploring this hypothesis are described below.

5.2.1 Test A: The Total and Albedo-Emissivity Aerosol Indirect Effects

The total aerosol indirect effects

The principal objective here is to assess the role that anthropogenic solute aerosols have played in modifying the properties of all clouds from pre-industrial times to present-day, by their initiation of cloud droplets via either condensation or homogeneous freezing. This is done by conducting a pair of model simulations − one for the present-day aerosol scenario (PDCTRL, which is the control simulation), while the other is with a pre-industrial solute aerosol burden (PINSOL, i.e., without anthropogenic solute aerosols). These simulations are performed using present-day thermodynamic conditions for the model forcing. The difference between the control simulation, F_{PDCTRL}, and pre-industrial simulation, F_{PINSOL}, net radiative fluxes at TOA (evaluated at the model top, which is roughly at 20 km altitude) becomes the total *aerosol indirect effect* or simply the *net change in the radiative fluxes at the TOA*, F_{net}, in Eqn. 5.1.

The radiative flux is defined as the total amount of radiative power (or radiative energy per second) passing through normal to a unit area, hence it has the units of Wm^{-2}. The flux can be evaluated at any altitude within the model propagating upwards or downwards. In this study, the flux is evaluated at the top of the model atmosphere (TOA) and we will evaluate net changes to the radiative fluxes. For our model, we use 20km as the top of the atmosphere. In our calculations we include both shortwave and longwave radiation.

$$F_{net} = F_{PDCTRL} - F_{PINSOL} \tag{5.1}$$

This is a standard technique that has been applied by several other researchers in previous studies (e.g. Gettelman et al. (2012); Lohmann et al. (2010); Haywood

et al. (2009)) albeit in global studies of aerosol indirect effects using GCM. The control run for simulated cases was specified as described in Sect. 3. In other words, the same aerosol fields and thermodynamic conditions described in Sect. 3 above were utilised.

In order to specify the pre-industrial aerosol fields, the work of Takemura (2012) on the global distribution of atmospheric aerosols from the pre-industrial era (1850) to future projections (2100) (using global models) was used. An adjustment factor for each particular aerosol species being treated in the model (Table 5.1) was inferred from Takemura (2012). Sulphate is the most affected aerosol specie and increased by a factor of five from pre-industrial times. All organics (soluble and insoluble species) have gone up by approximately 50%, while the number and mass concentrations of soot were boosted by a factor of over three. Dust and sea-salt have the least changes among all the aerosol species. These adjustment factors were used to estimate the corresponding pre-industrial aerosol number and mass distributions.

There is however uncertainties with our assumptions of the adjustment factors when estimating our preindustrial aerosol scenarios, mainly because these are derived from model simulations, which may not be perfect. Other researchers (e.g. Morrison and Grabowski (2011); Fan et al. (2013)) have applied a single arbitrary factor (e.g. 6 in the case of Fan et al. (2013)) to all aerosol species when estimating their pre-industrial aerosol concentrations and this shows that there is no unique way of prescribing the pre-industrial aerosol concentrations.

The albedo-emissivity aerosol indirect effects of glaciated clouds

The radiation scheme used herein is the GFDL radiation scheme (Freidenreich and Ramaswamy, 1999). Cloud particle mean diameters and net radiative fluxes are respectively the inputs and outputs for this scheme. Thus, in order to determine the albedo-emissivity aerosol indirect effect of a targeted cloud type, two calls to the radiation scheme are performed. The first call is a routine radiation call made by the model using the cloud properties determined by the model. This will include both first and second indirect effects so in order to isolate the second indirect effect we perform a second call to the radiation scheme that is not coupled to the model (off-line) at each radiation time-step and we fix the mean size of the cloud as a function of temperature (in the form of lookup tables) in this calculation. The temperature dependent mean size is determined from the CNTR simulation and so by subtracting the first and second radiation calls we are able to isolate the second indirect effect. By using lookup tables for liquid and/or ice in the calculations this enables us to isolate the indirect effects for each cloud type.

Soluble Aerosol material	Adjustment Factor
Ammonium Sulphate (SO4)	0.19
Sea-Salt (SS)	1.
Soluble Organics (SO)	0.67

Table 5.1: *Fractional changes of soluble aerosol scenarios from pre-industrial (1850) to present-day (2000) number and mass distributions (inferred from Takemura (2012)).*

By using equation 5.1 with F_{PDCTRL} and F_{PINSOL} from the first calls of the radiation scheme, we get the total aerosol indirect effect from aerosol which encapsulates both the lifetime and the albedo-emissivity effects (we can call this, F_{eff}, the effective aerosol indirect effect). By using equation 5.1 again, but now with F_{PDCTRL} and F_{PINSOL} from the second calls of the radiation scheme, we get a hypothetical aerosol indirect effect, F_{hyp}, which is the total aerosol indirect effect without the cloud sizes responding to aerosol changes (the albedo-emissivity effect). Subtracting F_{hyp}, from F_{eff}, gives us the estimate of the cloud albedo-emissivity effect. If this technique is applied to a given cloud type, then their corresponding cloud albedo-emissivity effects can be estimated. In order to determine the albedo-emissivity effects for glaciated clouds, the droplet and crystal sizes are fixed only in glaciated clouds and the technique described above is repeated.

Albedo-emissivity of Ice-only and Mixed-Phase Clouds

The albedo-emissivity effect of ice-only clouds is inferred by fixing the mean sizes of ice crystal via the use of look-up tables in completely glaciated clouds only. This is performed in the second call to the radiation scheme as described in Test A. For mixed-phase clouds, the mean sizes of ice crystals are fixed only in mixed-phase clouds during the second call to the radiation scheme. This analysis of the output was designed to investigate the proportional contributions of the ice and liquid components of mixed-phase clouds to the albedo emissivity effect of mixed-phase clouds.

5.2.2 Test B: Isolating 'Lifetime' Indirect Effects for Glaciated Clouds

In this test, indirect effects from aerosols on liquid-only clouds are eliminated first. This is done by using look-up tables of droplet numbers or, of droplet mean sizes to eliminate the sensitivity of certain microphysical processes to changes in aerosol loading. These microphysical processes are the *auto-conversion, collision-coalescence,*

sedimentation and the radiative properties of clouds, because in nature, all these processes depend on the mean size of cloud particles. Therefore, by simultaneously fixing the number concentrations or mean sizes of cloud-droplets in all these processes, the response of the lifetime of water clouds to solute aerosol pollution could be eliminated from the meteorology of the simulation.

These look-up tables are temperature and vertical velocity dependent and are created from the control simulation. The same look-up tables are used for both the present-day and the preindustrial runs. The aerosol indirect effect of glaciated clouds is then estimated by using Eqn. 5.1.

Test B.1: Aerosol Indirect Effects of Ice-only Clouds
In order to isolate aerosol indirect effects on ice-only clouds from the total indirect effects of glaciated clouds, the responses of the microphysical processes of ice-only clouds to aerosol are eliminated from the simulation to only allow responses from processes of mixed-phase and liquid-only clouds to control the aerosol indirect effects. In this test, the mean sizes of ice crystals in ice-only clouds are fixed again by using look up tables similar to the ones used above, but only in microphysical processes of ice-only clouds, such as autoconversion of cloud ice to snow, aggregation of snow and cloud ice, aggregation of graupel and cloud ice, sedimentation of cloud ice and their optical processes.

This eliminates the contribution of ice-only clouds to the total indirect effect of aerosols from all clouds. When Eqn. 5.1 is used, a hypothetical total aerosol indirect effect without the ice-only clouds aerosol indirect effect is determined. If this hypothetical aerosol indirect effect is subtracted from the total aerosol indirect effect, F_{net}, estimated in Test A, then the ice-only clouds aerosol indirect effect is estimated.

Test B.2: Aerosol Indirect Effects of Ice in Mixed-phase Clouds
Since we now have the aerosol indirect effects of glaciated clouds from Test B and the ice-only clouds indirect effect from Test B.1, the mixed-phase clouds aerosol indirect effect can be determined by subtracting the aerosol indirect effect of ice-only clouds from that of mixed-phase clouds.

5.2.3 Test C: Investigating the Riming Indirect Effect

Here, we test the hypothesis that soluble anthropogenic aerosols induce a riming effect by reducing the mean sizes of cloud droplets and reducing the efficiency with which supercooled cloud droplets are collected by solid hydrometeors. In order to evaluate this phenomenon, the temperature and vertical velocity dependent look-up

tables are utilised to fix droplet sizes in the riming routines of the microphysics scheme. In other words, the whole of Test B is repeated, but with the look-up tables of the cloud droplet sizes being used in the riming routine of the microphysics scheme in order to eliminate the sensitivity of this scheme to changes in aerosol loading. What we get here after applying Eqn. 5.1 is a hypothetical TOA glaciated clouds flux change without the riming effect. By subtracting this hypothetical TOA glaciated clouds flux change from the actual glaciated clouds flux change in Test B. we get the riming indirect effect.

5.2.4 Test D: Investigating the Freezing-Related Thermodynamic Indirect Effect

The hypothesis being tested here is that, the thermodynamic, riming and glaciation indirect effects from soluble and solid aerosol are significant but do not dominate the total AIE on all clouds. This is executed by repeating Test A, but with all temperature adjustments that arise from the latent heating released during all phase changes that involve ice (e.g. freezing and melting) being switched off. By using Eqn. 5.1 we get a hypothetical total aerosol indirect effect but without the thermodynamic indirect effect. Hence, if we subtract this hypothetical indirect effect from the true total cloud indirect effect estimated from Test A, the thermodynamic aerosol indirect effect is determined.

5.2.5 Test E: Role of Wind Shear on Glaciated Clouds AIE

Meteorology modifies aerosol indirect effects in different ways. Here we test the hypothesis that environmental wind shear modifies glaciated cloud indirect effects by horizontally extending cirrus. In order to examine this effect, Tests A. and B. are repeated, but with reduced horizontal wind shear. The horizontal wind shear is reduced following the method of Zeng et al. (2009), where the large-scale horizontal wind is reduced by a predefined factor. This factor is determined by dividing air pressure (at a given model level) by its surface pressure.

5.2.6 Test F: Upper Tropospheric Humidity on Glaciated Clouds

The hypothesis being tested is that relative humidity modifies glaciated cloud indirect effects by lowering the bases of cirriform clouds and increasing its horizontal extent. Also, it is being hypothesized that the rates of sublimation as solid precipitation falls out of the cloud are reduced because of the humid ambient air. This is explored by rerunning Test A. and B., but with the vapour mixing ratios above the

7km altitude incremented by one standard deviation. A summary of all these sensitivity tests is presented in Table 5.2, the abbreviations in the table are described in full in the table caption.

Simulation	Radiation Scheme	Rain Autoconversion	Snow Autoconversion	Collision and Coalescence	Particle Aggregation	Riming of droplets	Fall Velocity	Latent Heat	Low Wind Shear	Relative Humidity
Test A	-	-	-	-	-	-	-	-	-	-
Test B	FDS-WOC	FDN-WOC	-	FDN-WOC	-	-	FDS-WOC	-	-	-
Test B.1	FCS-IOC	-	FCS-IOC	-	FCS-IOC	-	FCS-IOC	-	-	-
Test B.2	FCS-MPC	-	FCS-MPC	-	FCS-MPC	FCS-MPC	FCS-MPC	-	-	-
Test C	FDS-WOC	FDN-WOC	-	FDN-WOC	-	FDS-MPC	FDS-WOC	-	-	-
Test D	-	-	-	-	-	-	-	No TA-F/M	-	-
Test E	-	-	-	-	-	-	-	-	WWS	
Test F	-	-	-	-	-	-	-	-	-	HUT-RH

Table 5.2: *A summary of the core sensitivity tests performed in this study, look-up tables were used to fix the droplet/crystal sizes/number concentrations in the relevant routines. These tests comprise a pair of simulations, one is with present-day and the other is with pre-industrial number and mass concentrations of aerosols. Meaning of abbreviations: FDS = Fixed droplet size, FCS = Fixed crystal size, FDN = Fixed number concentration, GC = Glaciated clouds, IOC = Ice-only clouds, MPC = Mixed-phase clouds, WOC = Water = Water only clouds, TA-F/M Temperature adjustments from freezing and melting, WWS = Weak wind shear, HUT-RH = Higher upper tropospheric relative humidity. A dash (-) means no change from the control run.*

5.3 Results From the Mid-latitude Continental Case (CLASIC)

5.3.1 Response of Cloud Microphysical Properties to Increased Solute Aerosols

Two model runs described in Test A were conducted, the results of which are analyzed in order to understand the aerosol indirect effect caused by solute aerosols from pre-industrial to present-day. In most of the analysis plots presented in the following sections, two curves are used; the red curve represents the present-day aerosol conditions (PDCTRL), while the blue curve represents the pre-industrial aerosol conditions (PINSOL), unless it is specified in the text.

5.3.1.1 Initiation of Cloud Droplets

Cloud Droplet Concentrations

Figure 5.1a compares the droplet number concentration between the pre-industrial and present-day simulations. These prognostic variables are conditionally averaged over all cloudy regions and entire simulation period and in this analysis, a cloudy grid-box is defined as a grid-box with the mass mixing ratio of either cloud ice or cloud liquid greater than zero. It is noticeable that, the continental control run reported significantly more cloud droplets than the corresponding pre-industrial continental run by nearly a factor of two. This outcome brings into focus the aspect of the non-linearity of the CCN activity of aerosols when compared to the net aerosol perturbation, because, sulphate aerosols increased by approximately a factor of five from pre-industrial to present-day (Fig. 4.4 and Table 5.1).

An explanation for why the droplet concentration only doubled is the inability of other anthropogenic solute aerosols to act as CCN under the prevailing meteorological conditions, and also, cloud droplets initiated at the cloud-base are higher in the present-day, hence, supersaturations are decreased more quickly. Thus, in-cloud nucleation of cloud droplets may subsequently be less prolific. In-cloud nucleation occurs inside a cloud when the local conditions such as supersaturations are high enough to cause initiation of new cloud droplets. Some of the questions that emerge from this finding, however, are whether these un-traced aerosols have any radiative feedbacks on clouds.

Cloud Droplet Sizes

It is the thermodynamical state of the atmosphere (which is the same in these simu-

lations) that determines the water content of a cloud, not the aerosol loading (Sect. 2.2.1.1), therefore, aerosol pollution triggers competition for water vapour by extra cloud particles, leading to smaller mean sizes of cloud droplets. This concept is reviewed from the data in Fig. 5.1b, which compares the mean droplet sizes from the two runs. Apparently, the mean sizes of droplets have become smaller (by about 4 microns $\approx 20\%$) due to anthropogenic pollution. These current results corroborate the findings of a great deal of previous observational and modeling workers, for instance, Twomey (1974); Albrecht (1989); Phillips et al. (2003) who noted reductions of mean sizes of cloud droplets with increasing aerosol number concentrations, such as the anthropogenic increase of aerosol from preindustrial times to present-day in our case. More recently, Pandithurai et al. (2009) noted similar trends when they performed a series of local scale observational campaigns, using surface-based remote sensing systems during episodic events of increased CCN concentrations. Moreover, with the advent of satellite technology (satellites are able to provide continuous measurements of aerosol properties over large domains) and data, Breon et al. (2002) reviewed that this phenomenon is not only significant locally, but occurs on global scales as well.

5.3.1.2 Initiation of Cloud-Ice

Ice Crystal Concentrations

The core hypothesis of this part of the investigation is that anthropogenic solute aerosols modify ice clouds through homogeneous freezing. This phenomenon is explicable through Fig. 5.1c, which presents the ice crystal number concentrations per liter. There is a substantial increase of upper tropospheric ice crystal concentrations above -40°C (the 9 km altitude) of almost a factor of 2. This increase is independent of the fact that in the aerosol-cloud model used in this study, solute aerosols are not primary sources of ice crystals in terms of heterogeneous nucleation, and thus, homogeneous freezing is responsible for the increase of ice crystal concentrations aloft.

It is apparent that no cloud droplets exist beyond the -40°C temperature level (Fig. 5.1a), indicating the homogeneous freezing level. There is an increase of approximately a factor of two in cloud droplet number concentrations compared to a factor of about 1.5 for ice crystal concentrations from pre-industrial to present-day (Figs. 5.1a and 5.1c). This discrepancy in fractional increases of cloud droplet and ice crystal concentrations is due to the fact that, inasmuch as homogeneous droplet freezing increased with increasing aerosols, the number of droplets that evaporated

during homogeneous freezing increased also, thus, not all extra cloud droplets froze, as noted from the ice crystal number budget (Fig. 5.2).

Figure 5.2 shows the ice number budget of the various sources of ice crystals treated in the model. Details of each bar in the bar chart are given in the caption. The bar chart shows that the droplet and aerosol freezing are the major sources of cloud ice. And in terms of aerosols freezing, sulphate aerosols dominate the sources because of their large number concentrations relative to other aerosols in the atmosphere. As for heterogeneous ice nucleation, dust dominates the sources followed by soot, while biological aerosols nucleate very little ice. The treatment of homogeneous freezing in the microphysics scheme follows the treatment of the process by Phillips et al. (2007) in which, homogeneous freezing of large cloud droplets ensues first, allowing for evaporation of smaller cloud droplets and vapour growth of new crystals depending on ice supersaturation.

It is noted that extra ice crystals (which are assumed to have been nucleated by homogeneous freezing of extra cloud droplets) are greater than the extra cloud droplets by a factor of over 100. This incoherence is primarily because homogeneous freezing of cloud droplets is actually not the only primary source of ice crystals aloft, but equally important, are homogeneous aerosol (CCN) and rain droplet freezing and other ice multiplication processes (Fig. 5.2). Rain can freeze homogeneous at very cold temperatures, and also when in contact with solid hydrometeors, and hence producing extra ice crystals. While the collection of liquid mass by either graupel or snow promotes the H-M process of ice multiplication.

Ice Effective Radius

A slight reduction of the effective sizes of ice crystals (of about 5 microns $\approx 15\%$) is noticeable in the upper troposphere commencing from the level of homogeneous freezing (Fig. 5.1d). The dominant mechanism for this reduction is the competition for available water vapour by extra ice crystals from homogeneous freezing. The second mechanism is the low deposition coefficient (which is a measure how efficiently excess vapor is taken up by growing ice particles) that characterizes some of the ice crystals, hence, the amount of vapour transfer to the ice phase is reduced (Gao et al., 2004). Also, faster sedimentation of larger ice crystals due to the influence of gravity on larger particles compared to smaller particles can explain why small sizes are predicted aloft.

The other finding emerging here is the increase of mean sizes of ice crystals in the lower troposphere (typically, mixed-phase clouds). This finding is interesting

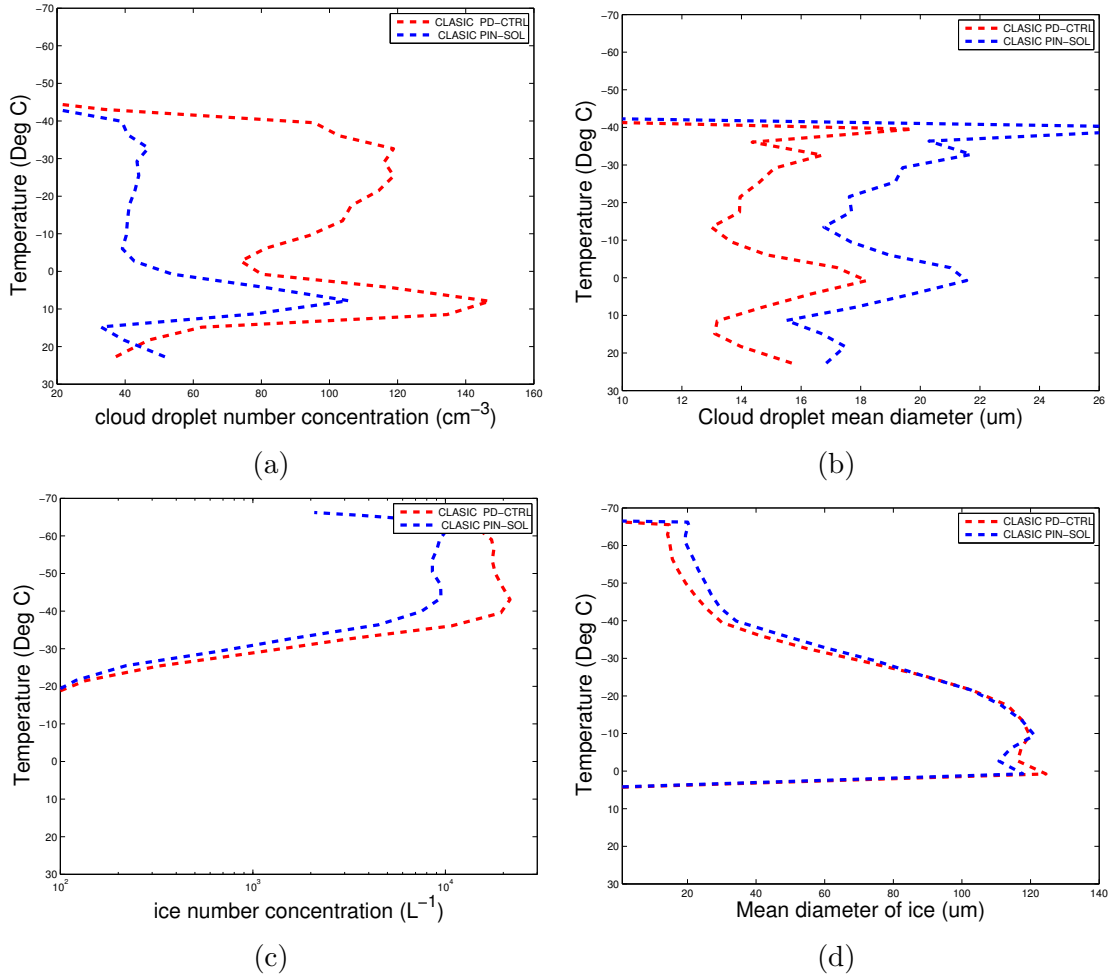

Figure 5.1: *(a) Cloud droplet number concentrations (cm^{-3}), (b) cloud droplet mean diameter in μm, (c) ice Crystal number concentration (L^{-1}) and (d) ice crystal effective radius (μm), all conditionally averaged over cloudy region (right) for CLASIC*

because it contradicts with the generally accepted concept that pollution of a cloud by aerosols should reduce the sizes of cloud droplets. The predicted increase in the mean sizes of ice crystals can be explained by a conceptual model (schematically presented in Fig. 5.3) of ice crystals in anvil outflow subsiding into the lower troposphere (mixed-phase clouds) and growing mainly by the Bergeron-Findeisen process.

As clouds in the mixed-phase region become more glaciated; under suitable supersaturations and updraft speeds, intense vapour growth of ice crystals is bound to occur, through the 'Bergeron-Findeisen' processes at the expense of the liquid components of the cloud. This model is consistent with the concept of repartitioning of cloud mass from a more liquid-based cloud to a more glaciated cloud with increasing solute aerosol loading as discussed later in Sect. 5.3.3.2. This finding

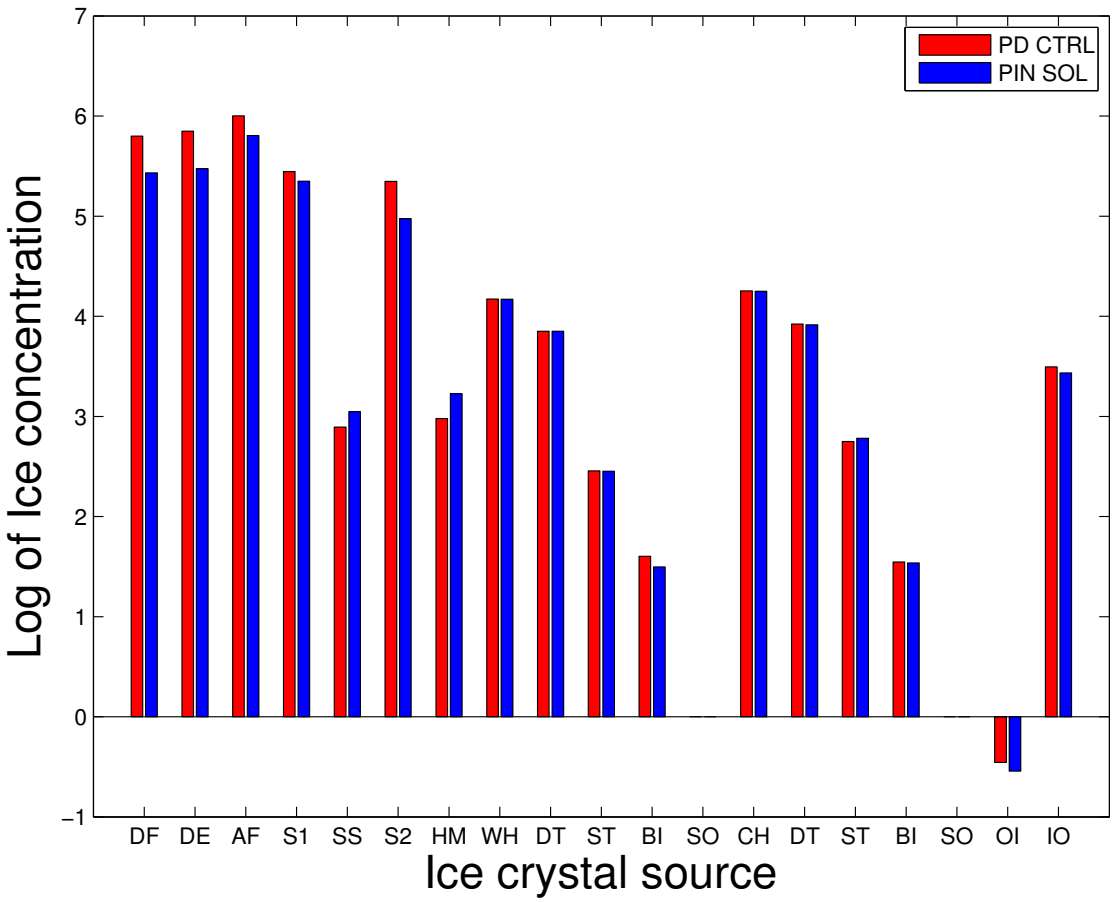

Figure 5.2: *The budget of ice number from the effect of solute aerosols for the mid-latitude continental case (CLASIC). Meanings of abbreviations in (d) DF = droplets frozen homogeneously, DE = droplets evaporating during homogeneous freezing, AF = aerosols frozen homogeneous, (S1, SS, S2) droplets in 1st mode of SO4, sea-salt, 2nd mode of SO4 aerosols, respectively, that froze homogeneously. HM = H-M splinters, WH = total crystals from Warm Heterogeneous nucleation (Condensational, Depositional, and Immersion at temperatures > -30 °), (DT, ST, BO, SO) crystals by Warm Heterogeneous nucleation of dust, soot, biological organics and soluble organics, respectively. CH = total crystals from Cold Heterogeneous nucleation (Condensational, Depositional, and Immersion at temperatures < -30 °), (DT, ST, BO, SO) crystals by dry deposition from dust, soot, and biological organics and soluble Organics, respectively. Finally, OI and IO stand for total ice crystals from Outside-In and Inside-Out Contact freezing.*

is also supported by the fact that, present-day clouds have become more glaciated than pre-industrial clouds (Sect. 5.3.2).

5.3.1.3 Water Contents

The water content of a cloud is a powerful diagnostic variable of a cloud because it helps to determine the type of cloud, the rate of growth of cloud droplets and also the rate at which hydrometeors interact together as they grow into precipitation.

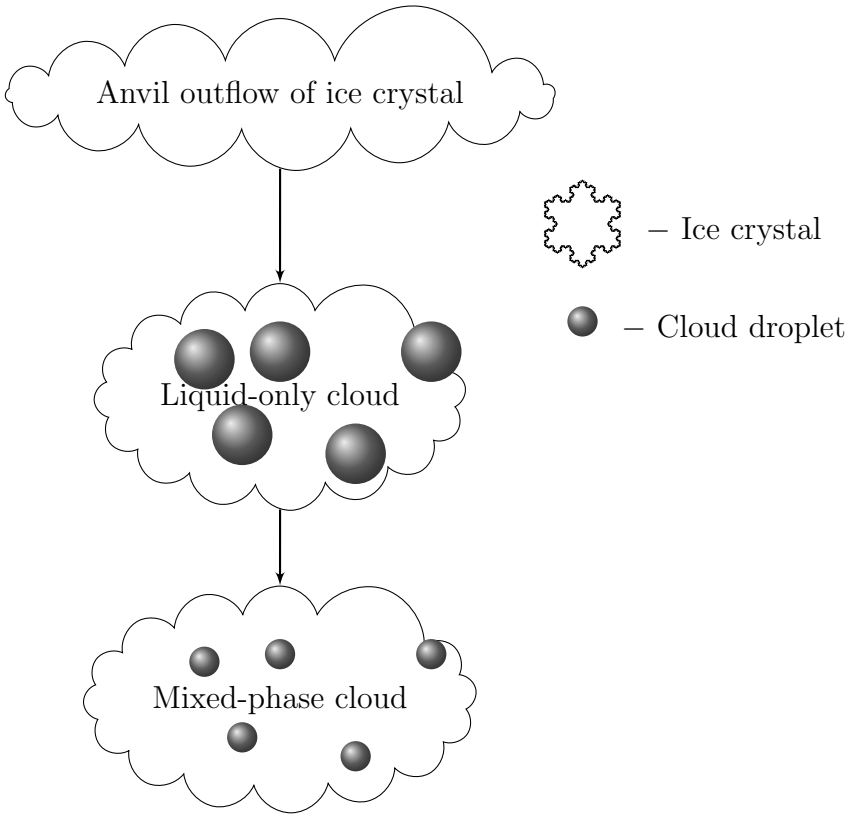

Figure 5.3: *A conceptual model, demonstrating how ice crystals from anvil outflow can subside into mixed-phase clouds, where they grow into larger ice crystals by the 'Bergeron-Findeisen process'.*

Chen et al. (2011) analyzed satellite data of ice water contents and noted that, the vertically resolved ice water contents in clouds with ice crystals that are smaller than 100 μm contribute up to 60% of the global mean of ice water contents, especially in the mid-latitudes. Thus, since the mean sizes of the upper tropospheric ice crystals in this case study are less than this cut-off size, it therefore implies that their response to aerosol changes is of significant radiative importance. The data from Figs. 5.4a and 5.4b highlight the mass mixing ratios of clouds. The liquid and ice mixing ratios are less sensitive to changes in aerosol loading especially in the lower troposphere. This is expected, since, the atmospheric thermodynamics and not the aerosol loading, control the water contents of the cloud.

In the free troposphere (but in the mixed-phase region of clouds), both liquid and ice water mass are however, significantly higher in the present-day than in the pre-industrial era, while the ice mixing ratios of cirrus clouds is lower in the present-day. The increase in both liquid and ice water contents is dominantly linked to the increase in mixed-phase cloudiness (Sect. 5.3.3) and a reduction in rain production (Fig. 5.5a), while, the reduction in ice water content is attributed to the surge in

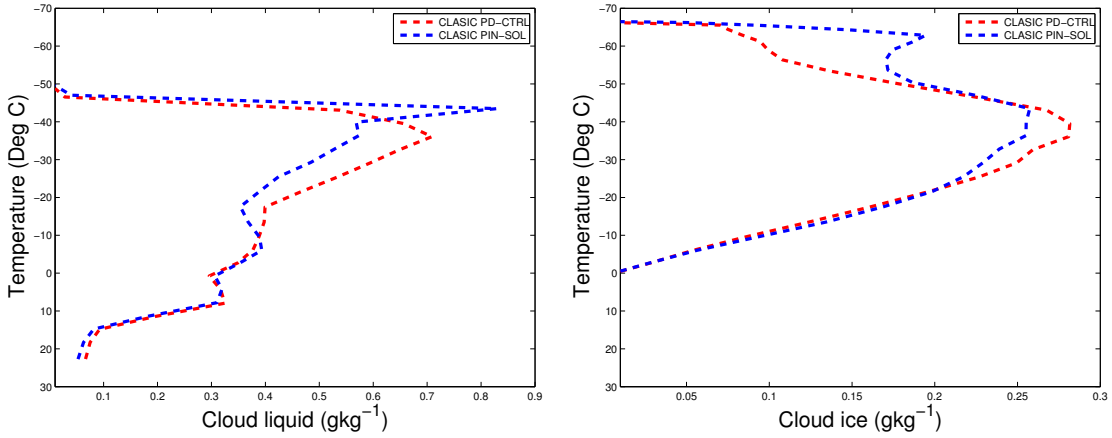

(a) (b)

Figure 5.4: *Cloud mass-mixing ratios, (a) liquid-cloud mass mixing ratio unconditionally averaged in all clouds and (b) ice-cloud mass mixing ratio unconditionally averaged in all clouds for the CLASIC case.*

the unconditionally averaged snow mass mixing ratio aloft (Fig. 5.6c). Another discovery from the two figures is the tendency of increasing sensitivity to changes in aerosol loading with increasing height. This is explicable in terms of in-cloud activation of droplets by small aerosols in deep convective updrafts, which accelerate aloft. Continental air has many such small aerosols that can activate aloft (warm rain process would tend to cause a reduction of sensitivity with height).

5.3.1.4 Precipitation from the Warm Rain Process

In the aerosol-cloud model used here, warm rain is produced mainly by autoconversion and collision-coalescence processes. These processes largely control the rain mass mixing ratio in mixed-phase and water-only clouds. Rain mass-mixing ratio is a powerful parameter to diagnose the precipitation efficiency of a cloud unlike surface precipitation, which is only a measure of the mass of precipitating hydrometeors that survived evaporation and sublimation to reach the ground. The mild sensitivity of surface precipitation to aerosol perturbation is attributed to the prescribed large-scale forcing, which dominantly controls the water and static energy budgets of the cloud (Morrison and Grabowski, 2011). A significant reduction in rain mixing ratio in the present-day simulations is apparent especially in mixed-phase clouds, because of the increase in the glaciation of clouds with increasing aerosol concentrations (Figs. 5.5a and 5.5b). Although the dominant mechanism for the suppressed rain production in the present-day is less effective collision-coalescence process due to the reduction in mean sizes of cloud droplets (Fig. 5.1b), there are,

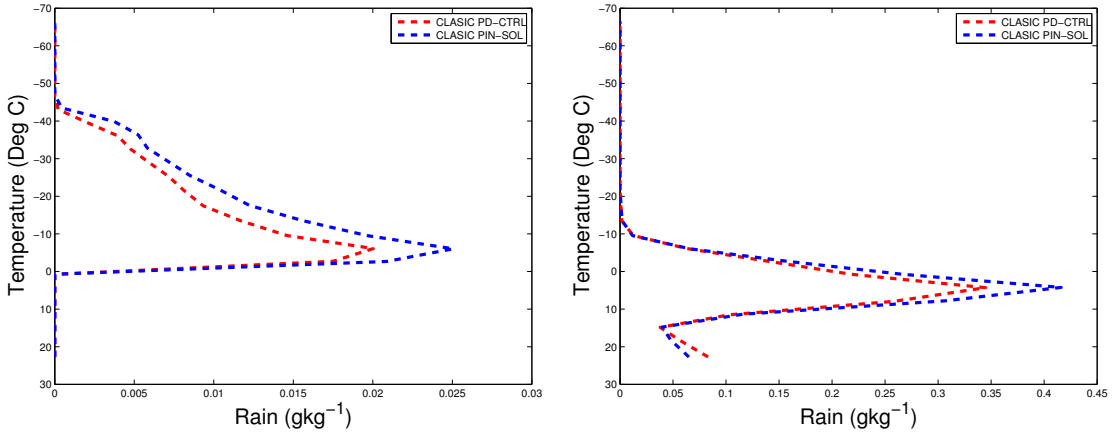

(a) (b)

Figure 5.5: *(a) Rain mass-mixing ratios in mixed-phase and (b) in liquid-only clouds, unconditionally averaged over the whole domain and simulation period for the CLASIC case.*

however, other secondary mechanisms for this reduction in rain mixing ratios. The first secondary mechanism is the repartitioning of condensate from rain to snow, because in the present-day, more ice crystal are being produced owing to homogeneous freezing of cloud droplets and aerosols. Hence, more snow is being produced leading to the depletion of the liquid phase by the ice-phase (Fig. 5.6). The distributions of the mass mixing-ratios of precipitation species shown in Fig. 5.6 of snow maxima appearing above the graupel maxima while the rain maxima appears below all other precipitating hydrometeors is consistent with the distributions found by Dudhia and Lim (2008) in their modelling study. This redistribution of condensate is due to changes in atmospheric conditions that tend to favour the formation of snow over rain as explained by Lohmann and Feichter (2005) and also noted by Zeng et al. (2009). Another mechanism for this finding is the proliferation of ice crystals aloft - ice crystals, snow pellets or graupel particles subside from anvil outflow, into mixed-phase clouds, and exhaust the liquid mass, via the 'Bergeron-Findeisen' process (Fig. 5.3), especially when ambient supersaturation ratio lies between the critical supersaturations over a water surface and that over an ice surface (Korolev, 2007), this explanation is supported by the increased glaciation that in the present-day that has been predicted.

5.3.1.5 Precipitation from the Ice-Crystal Process

Precipitation production in the ice phase has increased in the present-day via snow production aloft, although the intrinsic mass mixing ratio of snow in all clouds was

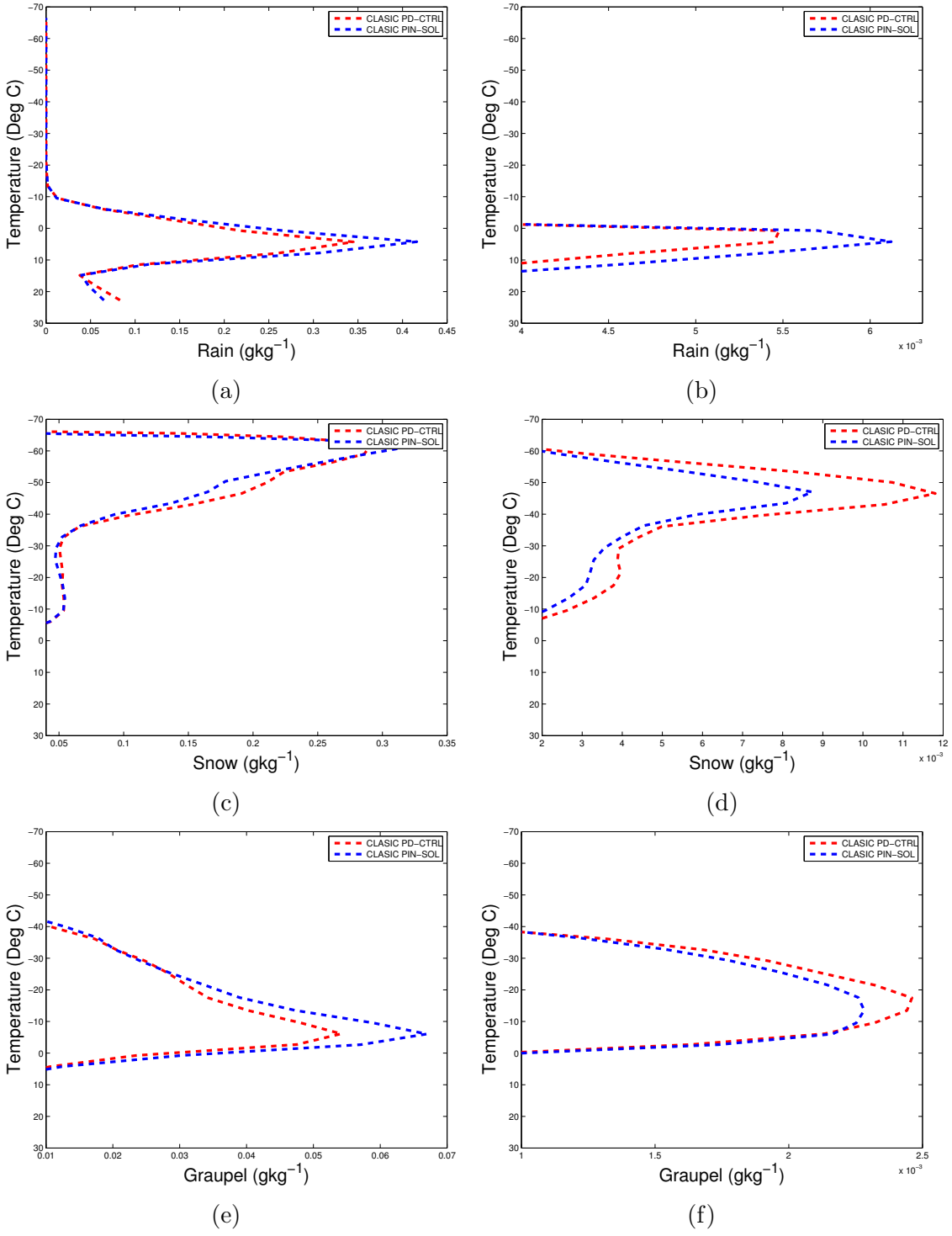

Figure 5.6: *(a and b) Rain mass-mixing ratios, (c and d) Snow mass-mixing ratios and (e and f) Graupel mass-mixing ratios. Figures on the left represent profiles of conditional averages over cloudy regions, while those on the right represent profiles of unconditional averages over the whole domain and simulation period for the CLASIC case.*

somehow insensitive to increased aerosols (Fig. 5.6c), unconditional average of snow

mixing ratio over the whole simulation shows a significant increase in snow production when solute aerosol concentrations were raised (Fig. 5.6d). These contrasting responses suggest that, intrinsically, the average snow production by clouds was unchanged, although the snow-producing clouds became more extensive. This discovery is supported by the cloud fraction statistics shown Sect. 5.3.3. This increase in domain-wide snow production is responsible for the reduction in ice mixing ratio aloft. The average graupel production by clouds diminished in the present-day (Fig. 5.6e), primarily because of the reduction of mean sizes of cloud droplets, however, the increase in cloud extent with increasing aerosol burden caused an increase in domain-wide graupel production (Fig. 5.6f). Precipitation increase through snow production is predominant in regions of weak vertical velocities.

5.3.2 Response of Cloud Dynamical Properties to Increased Solute Aerosols

Unexpectedly, there is weakening of updrafts with vertical velocities greater than 1m s^{-1} in the free troposphere with increased aerosol loading (Fig. 5.7a). This outcome is attributed to increased gravitational burden due to increased condensate loading particularly in mixed-phase clouds (Figs. 5.4 and 5.10), which is caused by a rise in droplet and crystal number concentrations in the control simulation. Previous researchers e.g. Storer and van den Heever (2013) and Cui et al. (2006) also detected similar trends and attributed them to gravitational loading, especially for deep-convective clouds. As for weak vertical velocities, a strengthening of vertical velocities is evident especially in the upper troposphere (Fig. 5.7c), which can be attributed to latent heat release during homogeneous freezing of extra cloud droplets. Downdrafts have shown weak sensitivities to increased aerosols, although a significant strengthening of weak downdrafts was predicted (Figs. 5.7b and 5.7d). Surging gravitational burden as well as evaporative cooling from falling hydrometeors can cause strengthening of downdrafts.

Evidence of the thermodynamic effect (Test D) is quite significant (Fig. 5.8a). This figure demonstrates the change in predicted mean atmospheric temperature from pre-industrial to present-day aerosol scenario. It is apparent that, the mean atmospheric temperature increased by as much as 0.5°C in the upper troposphere. This finding is principally attributed to the release of latent heat during homogeneous freezing. The fact that the temperature change is maximum at the homogeneous freezing level is consistent with the fact that homogeneous freezing of aerosols and cloud droplets is the cause. The cooling near the 0°C level is attributed to evaporative cooling caused by precipitating hydrometeors as supported by the increase

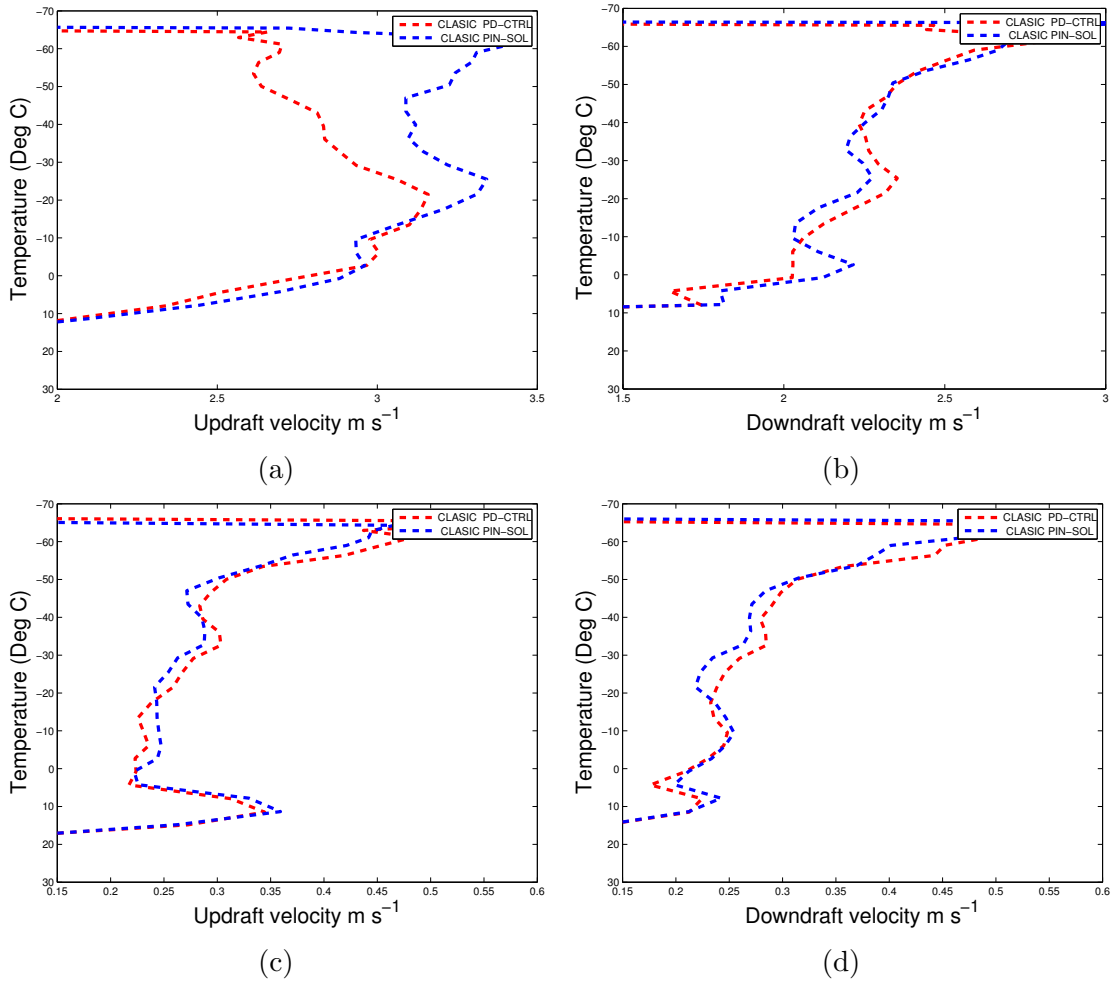

Figure 5.7: *Vertical profiles of positive (updrafts) and negative (downdrafts) ascent conditionally averaged over deep-convective clouds ($\omega > 1ms^{-1}$) and clouds with weak vertical velocities ($\omega < 1ms^{-1}$): (a) updrafts in strong vertical velocities, (b) downdrafts in strong vertical velocities, (c) updrafts in weak vertical velocities, (d) downdrafts in weak vertical velocities for CLASIC.*

in relative humidity at about the same altitude (Fig. 5.8b).

The predicted reduction of relative humidity in the upper troposphere (Fig. 5.8b) arises mainly from increased competition for vapour by extra ice crystals, increased snow production and subsequent decrease of ice-only cloud mass.

5.3.3 Response of Cloud Extent to Increased Solute Aerosols

5.3.3.1 Horizontal Cloud Fraction

Looking at the broader properties of the clouds across the domain, described as the macrophysical features, Fig. 5.9a presents changes in domain-averaged cloud fractions. This is the fraction of the horizontal area of the domain covered by grid-

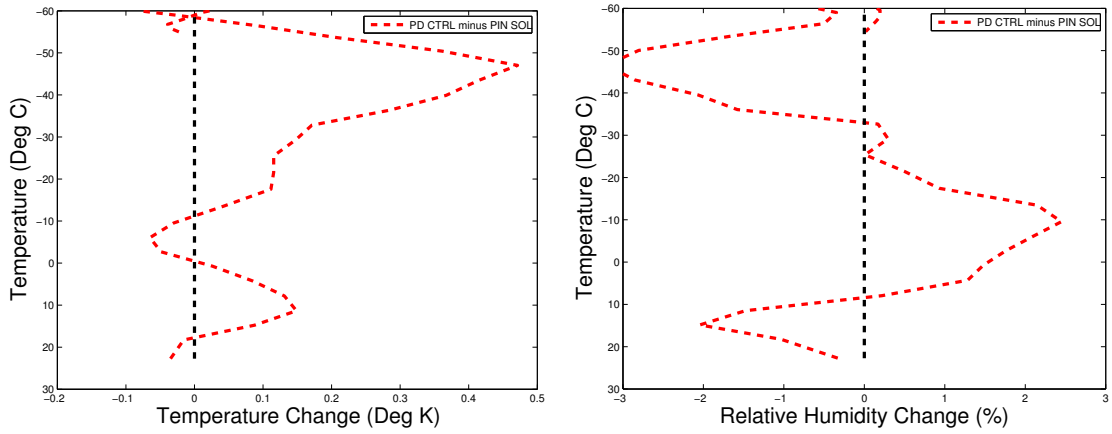

(a) (b)

Figure 5.8: *Unconditionally averaged mean change in (a) temperature and (b) relative humidity for CLASIC.*

columns that have cloud in them. The meaning of this cloud fraction is similar to the cloud fraction measured by satellites or other ground-based cloud fraction measuring instruments such as total sky imagers, or as estimated by an observer on the ground. On the other hand, Fig. 5.9b shows the change in volumetric cloud fraction. The volumetric cloud fraction is the fraction of the volume of the whole domain and entire simulation period that is occupied by clouds. To put it in another way, Fig. 5.9a illustrates the degree of changes in the horizontal extent of the clouds, whereas Fig. 5.9b encapsulates the lifetime component and mass budget of the clouds by including changes in vertical, as well as horizontal, extent.

A distinct increase in the fractions of all cloud regimes was simulated by the present-day run relative to the pre-industrial simulation. The largest changes in horizontal coverage are in mixed-phase clouds followed by ice-only clouds (Fig. 5.9a), while the volumetric cloud fraction also shows increases in the extent of mixed-phase and ice-only clouds, the largest increase is in ice-only clouds followed by mixed-phase clouds (Fig. 5.9b). This means that the fractional increase in the horizontal extension of mixed-phase clouds is higher than that of ice-only clouds when aerosol pollution is included, but ice-only clouds have spread into more volume.

In other words, ice-only clouds are now deeper than mixed-phase clouds. This indicates that some of the mixed-phase clouds in the present-day have been repartitioned to ice-only clouds. This happens because vapour growth of more numerous ice crystal from extra homogeneous freezing act to boost water subsaturation and evaporation of cloud-liquid (e.g. Korolev (2007)), especially in widespread regions of weak vertical velocities (stratiform clouds).

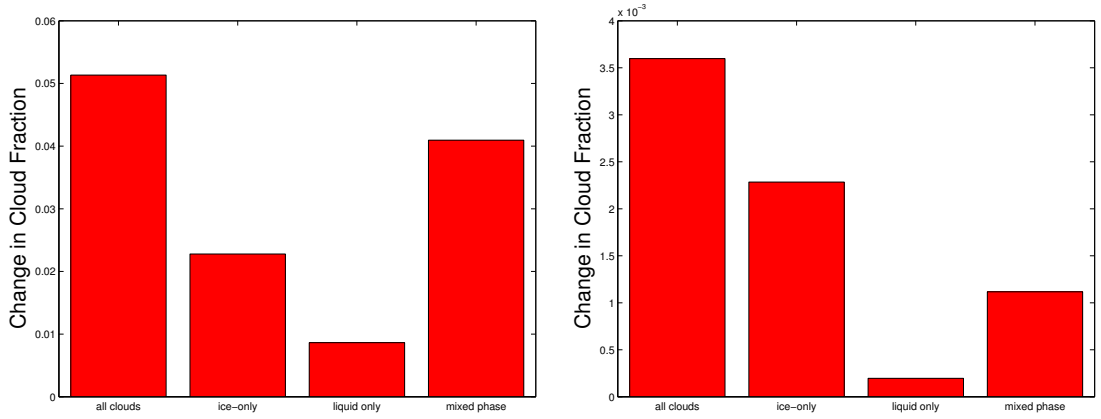

(a) (b)

Figure 5.9: *(a) Change in cloud fraction for all types of cloud species and (b) change in volumetric cloud fraction for all types of cloud species, in the present-day simulation relative to 1800. A grid-column (a) or grid-box (b) is defined as cloudy when the mass mixing ratio of either ice or liquid is greater than zero for CLASIC.*

5.3.3.2 Ascent dependent Vertical Profiles of Cloud Fraction

Figure 5.10 shows the vertical profiles of vertical cloud fractions for different cloud phases as a function of vertical velocity (conditionally averaged over regions of strong vertical velocities, where vertical velocity, $\omega >= 1ms^{-1}$, and weak vertical velocities, where vertical velocity, $\omega < 1ms^{-1}$). Expectedly, stratiform (weak vertical velocities) clouds are clearly more extensive than deep convective (strong vertical velocities) clouds. From this data, it can be seen that ice-only clouds are predominantly more horizontally extensive relative to other cloud types, because large shear has a tendency of creating more storm-relative flow aloft, so anvils from convective plumes are spread out over large distance. On the other hand, liquid-only (also referred to as warm- or water-) clouds are surprisingly the least extensive of all cloud types. Again, (with reference to Figs. 5.9a and 5.9b) mixed-phase clouds exhibit the highest absolute change in horizontal cloud fraction.

Present-day clouds are more horizontally extensive, chiefly through the mixed-phase category, because, it has been demonstrated that warm rain processes became less effective, because of a reduction in mean sizes of cloud droplets (Fig. 5.5a), accordingly, the lifetime of clouds is prolonged. The increasing sensitivity with increasing altitude is also supported by the insensitivity to the increase of solute aerosols of the fraction of water-only clouds.

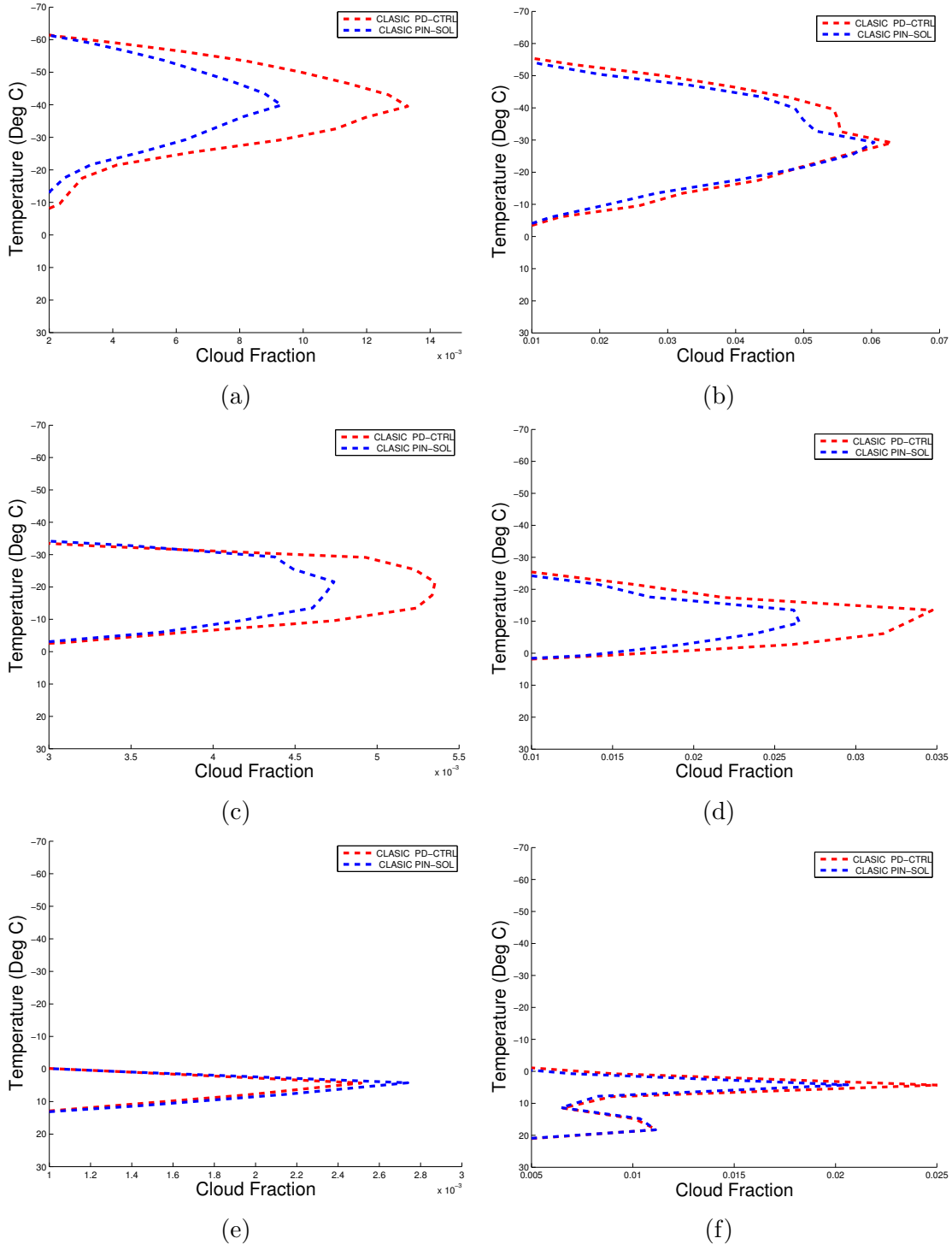

Figure 5.10: *Vertical profile of cloud fraction for all three types of phase of clouds, conditionally averaged over regions of strong vertical velocities (vertical velocity* $\omega >= 1ms^{-1}$*) (left) and weak vertical velocities (vertical velocity* $\omega < 1ms^{-1}$*) (right). (a) and (b) are for ice-only clouds, (c) and (d) are for mixed-phase clouds, (e) and (f) are for liquid-only clouds for CLASIC.*

5.3.4 Other Cloud Property Responses to Increased Solute Aerosols

Examining some of the cloud properties as a function of vertical velocity in each grid-box, Figs. 5.11a and 5.11b, show responses of cloud mass for a given velocity grid to changes in aerosol loading. On one hand, LWC is increased by aerosol pollution at all velocities, while on the other hand; IWC per each vertical velocity grid shows no sensitivity to changes in aerosol loading. The increase in LWC is reminiscent of the suppression of coalescence, which allows more liquid mass aloft to persist as indicated by the increase in cloud droplet number concentration.

Supersaturations

Another interesting phenomenon drawn from these results is the weakening of supersaturations due to increases in aerosol loading (Fig. 5.11c). This finding was attributed to the proliferation of cloud droplets, which compete more for excess vapour, since supersaturation is simply the balance between production and loss of excess vapour. This is why higher supersaturations were detected in maritime clouds than in continental clouds (Lamb and Verlinde, 2011). Another factor contributing to the reduction in present-day supersaturations is the weakening of present-day strong updrafts.

5.3.5 Response of Cloud Optical Properties to Increased Solute Aerosols

One of the main goals of this study was to investigate how microphysical processes described above impact on the radiative properties of clouds. Before paying special attention to the rigorous radiative statistics presented in the following section, the response of clouds' optical properties to aerosol loading is examined first. Different phase-types of clouds responded differently to changes in aerosol number concentrations (Fig. 5.12). These results show that, the optical thickness of clouds dilated in the present-day. Mixed-phase clouds exhibited the highest increases in optical thickness. The relationship between cloud properties and its optical thickness per every grid-point is presented in Eqn. 2.25.

The optical thickness is directly and inversely proportional to the water content and effective radius of cloud droplets, respectively. The increase in the water content of liquid clouds in the mixed-phase region of clouds (Fig. 5.4a) and the reduction of the effective radius of cloud droplets (Fig. 5.1b) causes the enhancement of the optical thickness of liquid-only and mixed-phase clouds. As for ice clouds, although, the effective radius diminished in the upper troposphere (Fig. 5.1d), the ice mixing ratio decreased quite substantially; hence, optically thinner cirrus clouds are pre-

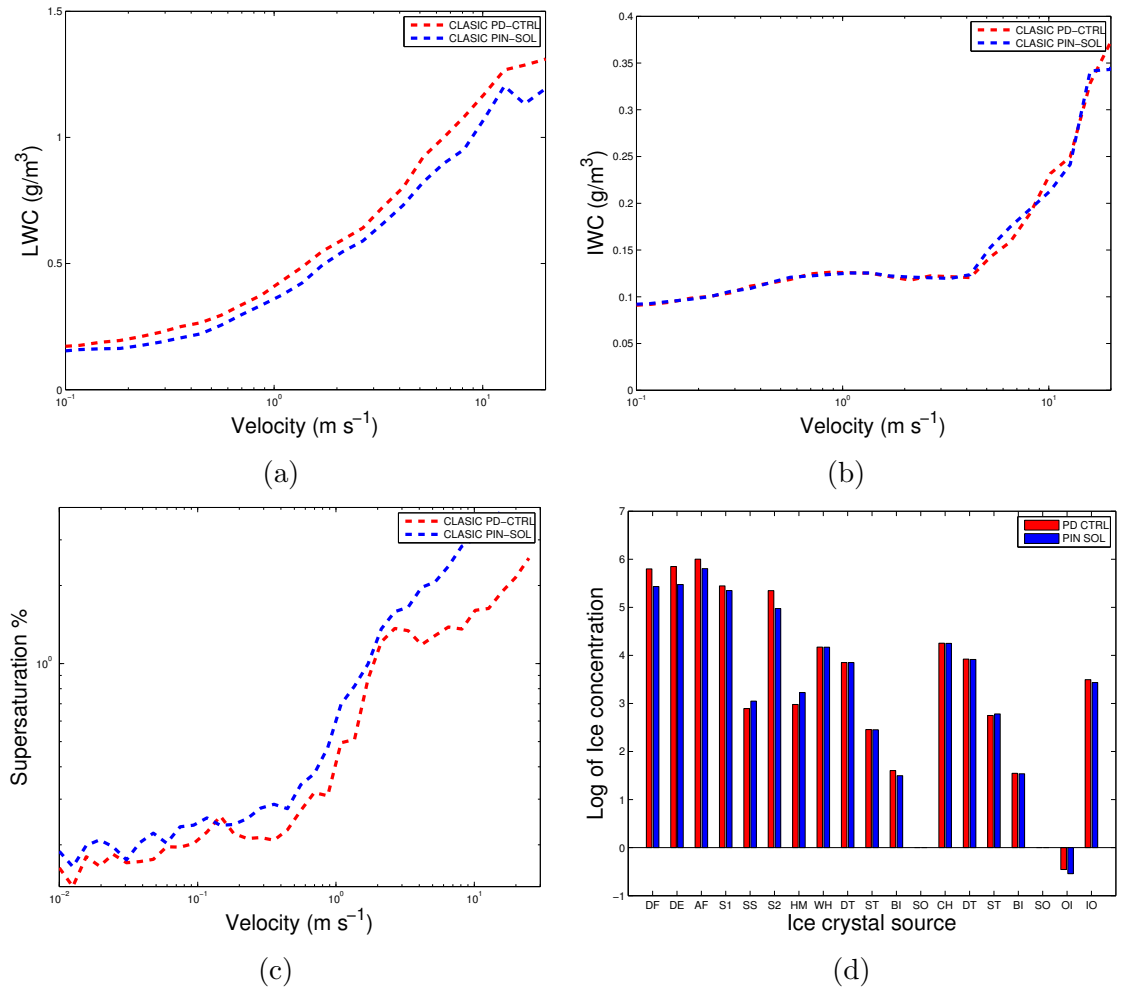

Figure 5.11: *Cloud properties as a function of vertical velocity conditionally averaged over cloudy regions. (a) Liquid Water Content, (b) Ice Water Content (c) Water Supersaturation, (d) Ice Number Budget for CLASIC. Meanings of abbreviations in (d) DF = droplets frozen homogeneously, DE = droplets evaporating during homogeneous freezing, AF = aerosols frozen homogeneous, (S1, SS, S2) droplets in 1^{st} mode of SO4, sea-salt, 2^{nd} mode of SO4 aerosols, respectively, that froze homogeneously. HM = H-M splinters, WH = total crystals from Warm Heterogeneous nucleation (Condensational, Depositional, and Immersion at temperatures > -30 °), (DT, ST, BO, SO) crystals by Warm Heterogeneous nucleation of dust, soot, biological organics and soluble organics, respectively. CH = total crystals from Cold Heterogeneous nucleation (Condensational, Depositional, and Immersion at temperatures < -30 °), (DT, ST, BO, SO) crystals by dry deposition from dust, soot, and biological organics and soluble Organics, respectively. Finally, OI and IO stand for total ice crystals from Outside-In and Inside-Out Contact freezing.*

dicted in the present-day. The complex response of mean sizes of ice crystals to aerosol loading gave rise to a complex response of the grid-point optical thickness of clouds. The optical depth of a cloud is a powerful parameter for assessing the overall influence of clouds on radiation. Three pathways by which the optical thickness of a cloud can change are identified as, either;

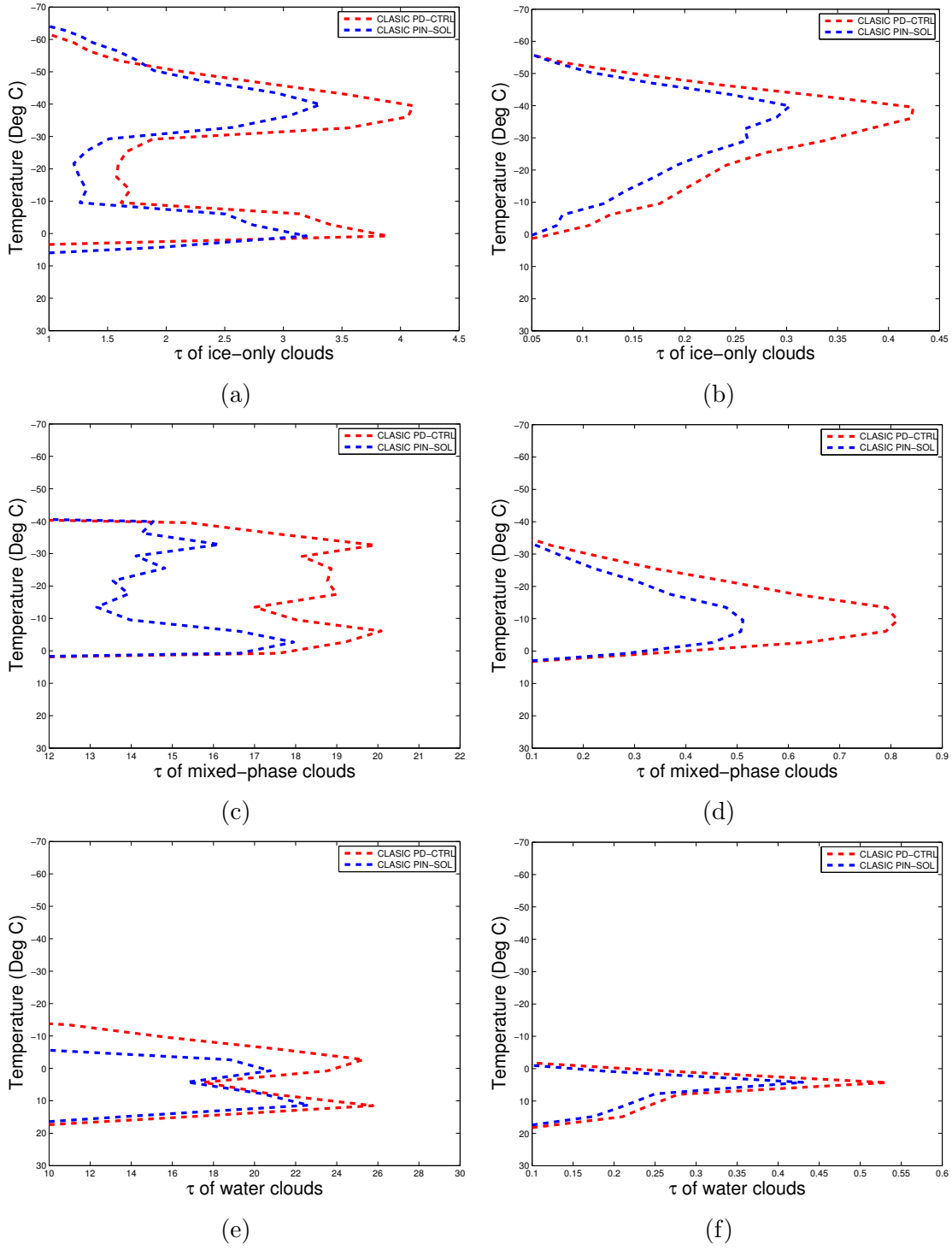

Figure 5.12: *Cloud optical thickness, τ, per 0.5 kilometer for different cloud phases in CLASIC, conditionally averaged over cloudy regions (left) and unconditionally averaged (right). (a) and (b) and for ice-only clouds, (c) and (d) are for mixed-phase clouds, (e) and (f) are for liquid-only clouds.*

- The water content per grid box rises (i.e., clouds become denser). In other words, τ, in Eqn. 2.25 should increase, through either, a surge in water content,

or a reduction in effective radius, or.

- The lifetime of clouds should generally be prolonged, or.
- Clouds should become vertically deeper.

These three pathways were explored. The first one is presented in Fig. 5.12 (on the left column). It clearly shows that clouds indeed became denser in the present-day, because of the suppression of precipitation by tiny cloud droplets. On the other hand, the right column of Fig. 5.12 was used to explain the other two pathways by performing unconditional averaging over the whole domain and simulation duration. Remarkably, τ, increased in all cloud types; the distinct increase in the domain averaged τ, is also attributed to the predicted increase in the cloud fractions of all cloud types. Although it is true that this second pathway is powerful in assessing aerosol indirect effects on the lifetime and spatial extent of clouds, it is however not intuitive to disentangle their respective proportions. Overall, all cloud phases were optically thicker in the present-day runs (Fig. 5.13). Fig. 5.13 shows that:

- Liquid-only clouds are optically denser (conditionally averaged) with increased aerosols but the response of domain-averaged optical thickness is minimal because, their horizontal cloud cover increased slightly.
- Mixed-phase clouds are more horizontally extensive and have higher water contents in the present-day (because of more detrainment of vapour and liquid from convective plumes), so their optical thickness both conditionally and unconditionally averaged is greater.
- Ice-only clouds have similar optical properties per cloud, but are more horizontally extensive, so their optical thickness throughout the domain increased.

5.3.6 Response of Radiative Fluxes and Cloud Radiative Properties to Increased Solute Aerosols

Figure 5.14 presents results of aerosol indirect effects via glaciated clouds from solute aerosols (PDCTRL - PINSOL), which were derived using the methods described in Sect. 5.2. The full meanings of abbreviations used in the plot labels (of clusters of three bars) are given in the figure's caption. The total aerosol indirect effect is equal to -9.46 $\pm$1.4 Wm^{-2}. The total AIE, represented by the cyan bar in the bar chart, is the total change of net radiative fluxes at the TOA. The TOA radiative fluxes are unconditionally averaged over the whole domain and the indirect effects

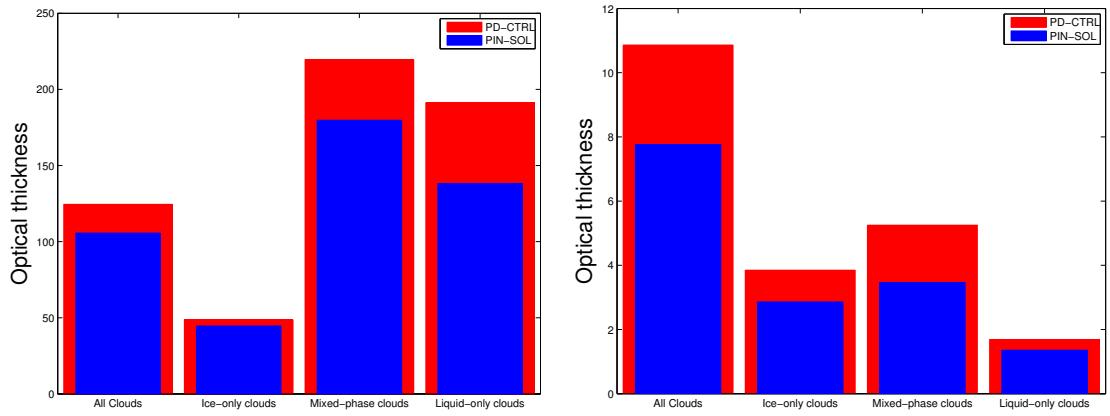

Figure 5.13: *Superimposed optical thicknesses predicted in the CLASIC simulation of mid-latitude continental clouds; (a) conditionally averaged over grid-boxes in which the mass mixing ratio of a targeted cloud type is greater than zero and (b) unconditionally averaged of the entire domain and duration of the simulation. Optical depth from each cloud-type is plotted by assuming that no other cloud-types are present.*

(or the TOA radiative flux changes) are estimated by differencing the present-day and the pre-industrial TOA net radiative fluxes in test A.

The corresponding green bar represents the indirect effects of glaciated (mixed-phase plus ice-only) clouds (-6.33 $\pm$0.95 Wm^{-2}), while the red bar represents the aerosol indirect effects of water-only clouds (-3.13 $\pm$0.47 Wm^{-2}). The same glaciated cloud indirect effect bar appears again in the second cluster (glaciated cloud aerosol indirect effect (GC-AIE)) with its corresponding ice-only (-4.14 $\pm$0.62 Wm^{-2}) and mixed-phase (-2.49 $\pm$0.37 Wm^{-2}) cloud components of the indirect effects of aerosols on glaciated clouds. The third cluster (the glaciated clouds lifetime (GCL-AIE)) provides the lifetime indirect effects for glaciated (-4.08 $\pm$0.61 Wm^{-2}), ice-only (-2.96 $\pm$0.44 Wm^{-2}) and mixed-phase (-1.42 $\pm$0.21 Wm^{-2}) clouds. These lifetime effects are derived by subtracting the corresponding albedo-emissivity effects of glaciated clouds (GCAE-AIE), which are given in the last cluster (derived from test A) from their corresponding counter-parts in the second cluster.

For our mesoscale area over Oklahoma, in which cloud cover is dominated by glaciated clouds aloft (Fig. 5.9), the aerosol indirect effect of glaciated clouds is stronger than that of water-only clouds. Globally, by contrast, the generally accepted hypothesis from previous studies states that, warm clouds make the largest contribution to the net radiative properties of all clouds, hence, to the indirect effects of aerosols as well (e.g. Charlson et al. (1992); King (1993); Gettelman et al. (2012)). This striking outcome is a consequence of the fact that glaciated clouds in this study were more extensive and affected most by changes in aerosol loadings in

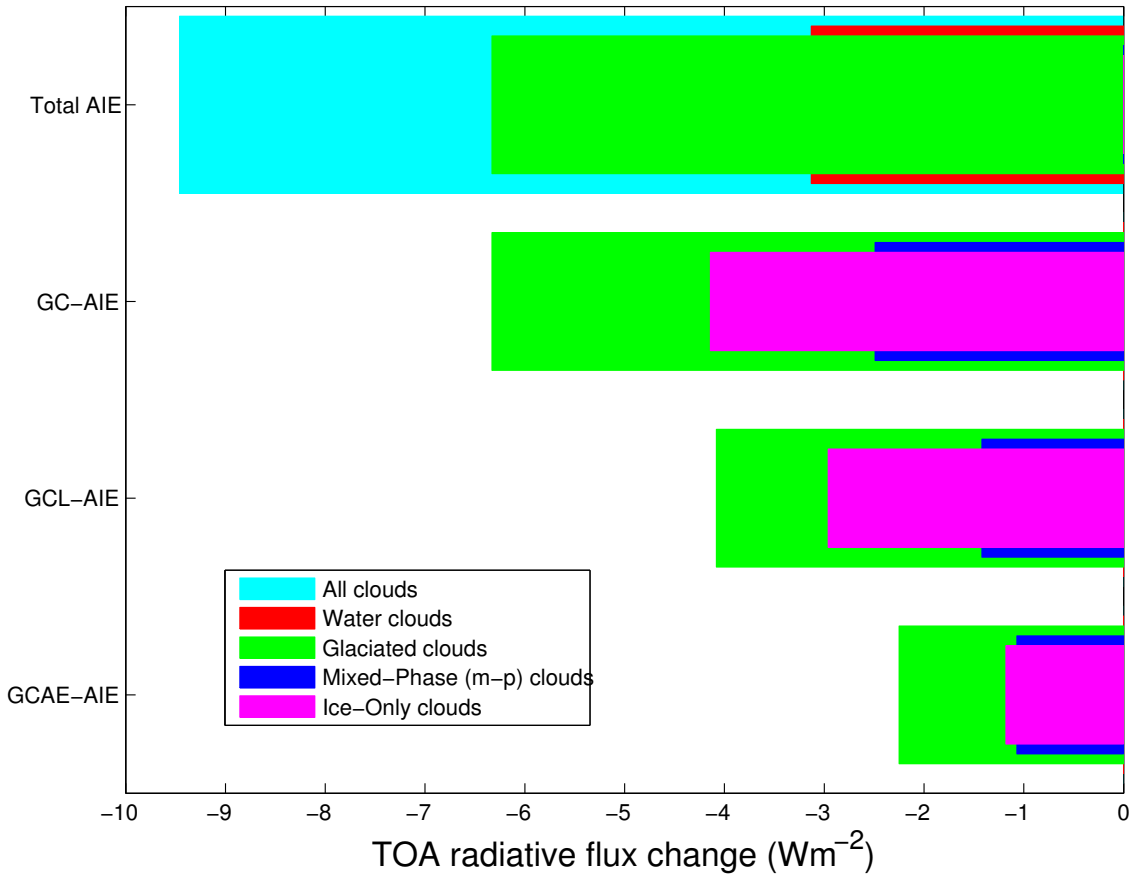

Figure 5.14: *Glaciated clouds aerosol indirect effects from solute aerosols (PDCTRL - PINSOL), results are derived mainly from tests A and B through identifying salient microphysical processes that are responsible for modifying cloud radiative properties in CLASIC. Meaning of abbreviations: GC-AIE = Glaciated Clouds AIE, GCL-AIE = Glaciated Clouds Lifetime AIE, GCAE-AIE = Glaciated Clouds Albedo-Emissivity AIE.*

terms of horizontal coverage and domain-wide optical properties (Figs. 5.9a, 5.9b and 5.12), while liquid-only clouds were much less extensive and less sensitive.

Concerning the glaciated clouds indirect effects, surprisingly, it is noticeable that ice-only clouds exhibit a higher aerosol indirect effect than mixed-phase clouds, despite the domain-averaged optical depth of ice-only clouds increasing less than that of mixed-phase clouds. As noted below, the reason is the sunlight being reflected first by ice-only clouds and dominance of short-wave effects over long-wave ones. The lifetime effect of ice-only clouds also dominates the glaciated clouds aerosol indirect effect. Several research questions emerged from these bar charts and most of them are addressed in the following section.

5.3.6.1 All Clouds

Negative net aerosol indirect effect from all clouds

The net negative radiative flux change at the TOA (Fig. 5.14) clearly shows that the effect of anthropogenic aerosols is to cool the climate of our Earth. Thus, aerosol effects on clouds have the potential to offset the global warming exerted by greenhouse gases. Several complementary factors gave rise to this outcome. Most importantly, an increase in solute aerosols boosts the CCN loading and consequently, the number concentration of droplet embryos rises (Fig. 5.1a). Since the number concentration of aerosols has minimal effect on the mean water content of a cloud, it is therefore apparent that the mean droplet size diminishes, as extra cloud droplets compete for the available water vapour (Fig. 5.1b). Tiny but numerous cloud droplets reflect more shortwave fluxes back to space (the evidence is the negative radiative flux change at the TOA from the albedo-emissivity effect of glaciated clouds (GCAE-AIE) shown in the bar chart). This is called the 'Twomey' or cloud-albedo indirect effect. The same albedo-emissivity also occurs in ice-only clouds (Lohmann and Feichter, 2005), as evidenced by the reduction in crystal sizes aloft (Fig 5.1d). The ice-only cloud albedo-emissivity effect also had a cooling effect primarily due to increased reflection of shortwave fluxes by smaller and numerous ice crystals.

In addition, the precipitation efficiency of liquid-only clouds is reduced, leading to a prolonged lifetime of the cloud. This prolonged lifetime is caused by reduced warm rain production (Fig. 5.6). This delay in the onset of warm rain production also subsequently enhances the chances of homogeneous freezing of cloud droplets, which boosts ice crystal concentrations aloft (Fig. 5.1c). These complementary factors lead to increased cloud coverage (Fig. 5.9a and 5.9b) causing a reduction of solar radiation transmitted into the climate system. Fig. 5.10 underlined that this escalation of the cloud fraction is predominantly via stratiform type clouds, particularly mixed-phase clouds. Also, the optical thickness of the clouds in the present-day deepened (Fig. 5.12). Finally, an indication that the reflectivity of clouds was strengthened is the predicted negative change of radiative fluxes at the TOA (Fig. 5.14).

In summary, the dominant pathway for the negative net AIE of clouds is the increase in cloud droplet number concentration, which resulted in the reduction of cloud droplet mean sizes. Subsequently, the warm rain processes were inhibited leading to the proliferation of homogeneous freezing of cloud droplets. Consequently, more ice crystals were detrained from convective cores especially in the mixed-phase regions of the clouds, hence clouds; especially glaciated clouds became more exten-

sive and optically thicker.

5.3.6.2 Glaciated Clouds

GC-AIE greater than WC-AIE

The term glaciated clouds in this study refers to clouds comprised of ice crystals, either in their mixed- or ice-only cloud phases. The glaciated clouds aerosol indirect effect (GC-AIE = -6.33) is apparently stronger than the indirect effect for water-only clouds (WC-AIE = -3.13 $\pm$0.5 Wm^{-2}). From Eqn. 2.25 and also from Figs. 5.1b, 5.1d, 5.4 and 5.13, it is noticeable that water clouds exhibit a larger conditionally averaged optical thickness than glaciated clouds, because of higher water contents and relatively small droplet radii compared to glaciated clouds (Brient and Bony, 2012); however, liquid-only clouds have a small horizontal coverage.

In this case study, liquid-only clouds contributed a small proportion to the whole cloud mass. Thus, their contribution to the total optical properties of clouds was small. This is expected for a tropical case where forced glaciation due to the prevalence of strong convective updrafts and generation of a glaciated layer-cloud by detrainment of ice is likely. Another factor is that glaciated clouds were more responsive to aerosol changes than liquid-only clouds. Additionally, glaciated clouds exist above water-only clouds; hence, they have the first interaction with solar radiation before it reaches the water-only clouds below them. Again, since water only clouds have not shown substantial changes, of their horizontal coverage due to aerosol changes compared to the massive increases in cloud fractions of glaciated clouds (Figs. 5.9a, 5.9b and 5.10), it can thus be concluded from results in this study that glaciated clouds in the present-day climate have become more extensive than water only clouds.

The dominant mechanism giving rise to this result is the strong modification of glaciated clouds by homogeneous freezing of cloud droplets and solute aerosols and the subsequent detrainment of cloud ice from convective cores into stratiform/cirrus clouds.

IOC-AIE greater than MPC-AIE

In the second cluster of the bar charts, the presented aerosol indirect effects of glaciated clouds show a negative flux change (solar cooling, -6.33 $\pm$0.95 Wm^{-2}) due to aerosol pollution. These include both the lifetime and albedo-emissivity effects. Ice-only clouds dominate the flux change (-4.14 $\pm$0.61 Wm^{-2}) more than mixed-phase clouds (-2.49 $\pm$0.41 Wm^{-2}). This remarkable finding brings into focus, novel insights into the higher importance of ice-only clouds in determining the net indirect

effects of clouds.

This occurs because ice-only clouds exist above mixed-phase clouds, and have the first interaction with downward solar radiation. The ice-only cloud and mixed-phase clouds are produced by outflow from convective clouds, so they tend to overlap in the vertical. Also, the absolute increase of the volumetric cloud fraction of ice-only clouds is actually higher than that of mixed-phase clouds (Fig. 5.9b) so that as well as being more extensive, ice-only clouds have also become deeper. Furthermore, the changes in cloud fractions (Fig. 5.10) and optical thickness per grid-depth (Fig. 5.12) and microphysical properties (e.g. Fig. 5.4) are higher for ice-only clouds than for other cloud types, owing to the massive detrainment of cloud ice into stratiform clouds.

Lifetime effect

The lifetime aerosol indirect effects for glaciated clouds (GCL-AIE, -4.08 $\pm$0.57 Wm^{-2}) presented in the third cluster of the bar-charts show that the lifetime effect of mixed-phase clouds (-1.42 $\pm$0.18 Wm^{-2}) is about half that of ice-only clouds (-2.96 $\pm$0.41 Wm^{-2}). Despite the predicted greatest increase of cloud fractions for mixed-phase clouds (Fig. 5.9a). The same arguments explained above, also explain this result.

The Albedo Effect

A negative flux change (solar cooling) for the albedo-emissivity effect due to aerosol pollution of glaciated clouds was predicted here (-2.25 $\pm$0.3 Wm^{-2}). This is mostly controlled by an increase in both droplet and ice crystal number concentrations followed by a reduction in mean sizes of cloud particles (Figs. 5.1d and 5.1b). Despite the fact that mean sizes of ice crystals are greater than those of water droplets by over a factor of four, ice-only clouds exhibit a slightly stronger albedo-emissivity effect (-1.18 $\pm$0.18 Wm^{-2}) compared to mixed-phase clouds (-1.07 $\pm$0.16 Wm^{-2}), primarily because of the massive increase in number concentrations of ice crystals and also the extent of ice-only clouds, which enhanced their reflectivity. Also, their first interaction with solar radiation makes them more important.

5.3.6.2.1 Mixed-Phase Clouds The net flux change of the aerosol indirect effect of mixed-phase clouds is negative (-2.49 $\pm$0.41 Wm^{-2}), implying a cooling effect on the climate system. Now, in order to have a subtle understanding of the microphysical processes that control aerosol indirect effects in mixed-phase clouds, further sensitivity tests were carried out.

Coalescence Effect

Since a mixed-phase cloud comprises both ice and liquid components, it was discovered that the liquid component exhibits a smaller indirect effect (-0.83 ±0.12 Wm^{-2}) compared to the ice component (-1.66 ±0.27 Wm^{-2}). This smaller contribution from the liquid relative to the ice component is attributed to the reduction in the effectiveness of collision-coalescence of cloud droplets, and it yields a new indirect effect called coalescence indirect effect caused chiefly by the reduction of the mean sizes of cloud droplets, which inhibits coalescence and boosts the cloud lifetime (Fig. 5.1b).

Secondly, rain production in the mixed-phase regime has dwindled quite significantly (Fig. 5.5a). The third evidence for this outcome is the conspicuous increase of the cloud fraction and optical thickness of mixed-phase clouds due to aerosol pollution (Figs. 5.9a, 5.9b and 5.11). Furthermore, a reduction in graupel production (Fig. 5.16a) implies the inefficiency of the riming process (which is the dominant growth mechanism for graupel), which depends on the mean sizes of cloud droplets. All these processes compliment each other in prolonging the lifetime and/or extent of the liquid component of mixed-phase clouds when solute aerosol pollution is included.

But the dominant mechanism for the coalescence indirect effect is the reduction of the mean sizes of cloud droplets, which makes the collision-coalescence process less effective. Consequently the lifetime and spatial extent of the cloud increases.

Aggregation Effect

The aggregation indirect effect is an aerosol indirect effect that arises from the response of the aggregation process of clouds to changes in aerosol loadings. It was assessed by the use of look-up table of the mean sizes of ice crystals in completely mixed-phase clouds.

The dominant mechanism for the exhibited negative sign (-1.66 ±0.25 Wm^{-2}) for the aggregation indirect effect is the aggregation process in mixed-phase clouds which became less effective in the present-day primarily due to the reduction of the mean sizes of ice crystals, causing an increase in lifetime and extent of glaciated clouds.

The Riming Aerosol Indirect Effect

From Test C, the riming indirect effect, which is an aerosol indirect effect that arises

from the response of the riming process of clouds to changes in aerosol loadings, was assessed. The TOA flux change of the riming indirect effect in Fig. 5.15a is strongly negative (-3.97 $\pm$0.61 Wm^{-2}), implying a cooling of the climate system.

This is because the riming indirect effect arises from the inhibition of the growth of solid hydrometeors through less efficient accretion of supercooled cloud droplets by graupel or snow particles (this mechanism has been noted through the reduction of the rain mass mixing ratios in mixed-phase clouds (Fig. 5.5a)). This phenomenon, thus, prolongs the lifetime of mixed-phase clouds and a negative flux change of the aerosol indirect effect is therefore produced. In this study, a great reduction in cloud droplet sizes was produced by the aerosol pollution, and it led to significant reduction in graupel production and this emerged to be the dominant microphysics mechanism for the riming aerosol indirect effect.

The Freezing-Related Thermodynamic Aerosol Indirect Effect

Figure 5.15a shows a negative flux change at the TOA from the freezing-related thermodynamic aerosol indirect effect, which was inferred from Test D. With this effect, more aerosols delay the onset of precipitation owing to the small particle sizes; hence, the cloud grows deeper until it reaches freezing levels.

The numerous cloud droplets freeze at this level prompting the release of vast amounts of latent heat that tend to invigorate the dynamics of clouds. There is weak evidence for this release of latent heat during freezing of cloud droplets, in the strengthening of both weak updraft and weak downdraft (Figs. 5.7c and 5.7d). This invigoration effect then intensifies the ice crystal processes as seen by the intensification of snow production aloft and may shorten the cloud lifetime.

In the sensitivity tests, the other type of thermodynamic indirect effect not involving ice was not tested (Sect. 2.2.3). Although Khain et al. (2005) agrees with the aforementioned idea, they further hypothesized that due to the wind shear that tilts convective cores, the condensate would precipitate from outside supersaturated cores of deep convection, hence, evaporative cooling ensues. This environmental cooling leads to the development of strong downdrafts and the subsequent creation of cold pools and new secondary cells. Their explanation is similar to what we found as the dominant mechanism for the freezing-ralated thermodynamic aerosol indirect effect (-4.31 $\pm$0.64 Wm^{-2}); a higher cloud fraction, particularly for clouds with strong updrafts (Figs. 5.10a and 5.10c), implying more reflection of solar radiation. This phenomenon was also echoed by Lee et al. (2008b), when they found a compensatory effect of precipitation production during the formation of cold pools and the subsequent secondary cells, however, from the thermodynamic

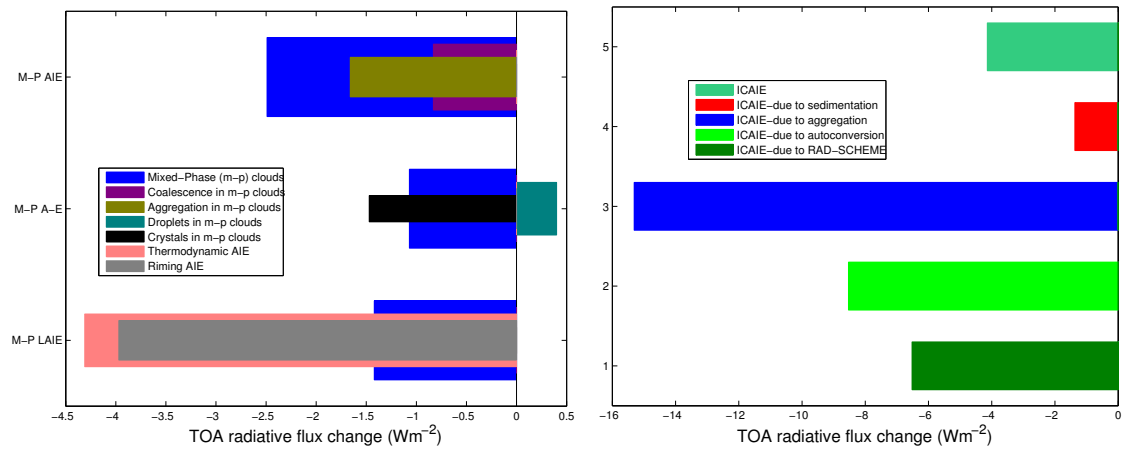

(a) (b)

Figure 5.15: *Radiation statistics for (a), mixed-phase clouds and (b), ice-only clouds for CLASIC. The meanings of the abbreviations: M-P AIE = mixed-phase aerosol indirect effects (including both lifetime and albedo/emissivity effects), M-P A-E = Mixed-phase albedo emissivity effects, M-P LAIE = Mixed-phase lifetime aerosol indirect effects, ICAIE = Ice clouds aerosol indirect effects.*

effect that did not involve ice.

Both the thermodynamic and riming indirect effects are individually much stronger than the net indirect effect of glaciated clouds. This is not the first time that such a response has been noted, the latest report of the IPCC (the fifth assessment report Boucher and Randall (2013)) compiled evidence from several modelling studies and concluded that individual indirect effects interact and compensate each other, hence the resultant aerosol indirect effect from clouds may not be reflective of what the individual effects show. Also, Lohmann and Feichter (2005) suggested that the individual aerosol indirect effects may not be necessarily additive.

Albedo Effect

Remarkably, the reflectivity of ice crystals within mixed-phase clouds dominated the albedo-emissivity effect therein, exhibiting a negative radiative flux change (-1.47 $\pm$0.22 Wm^{-2}) at the TOA, which was attributed to the massive increase in number concentrations of ice crystals and the reduction in mean sizes of ice crystals in mixed-phase clouds. Also, smaller particles interact with more radiation than the same water in bigger particles. On the other hand, the albedo-emissivity effect of water droplets within mixed-phase clouds surprisingly had a slight warming effect (0.4 $\pm$0.12 Wm^{-2}).

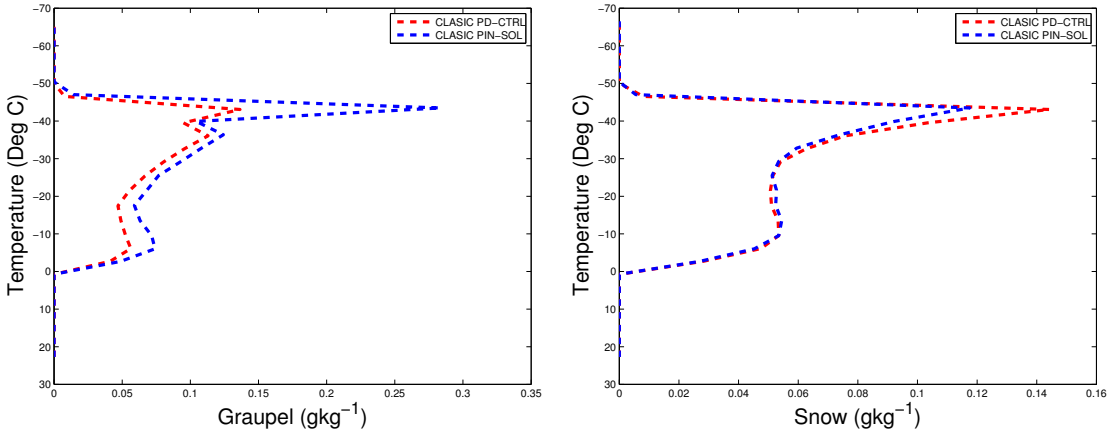

(a) (b)

Figure 5.16: *(a) Mean mixing ratios of graupel and (b) Mean mixing ratios of snow, conditionally averaged over mixed-phase clouds in CLASIC.*

5.3.6.2.2 Ice-Only Clouds Due to the higher importance of ice-only clouds (-4.14 $\pm$0.67 Wm^{-2}) compared to mixed-phase clouds (-2.49 $\pm$0.41 Wm^{-2}) in controlling the aerosol indirect effects in glaciated clouds, further sensitivity test were carried out to disentangle the individual contributions of each microphysical process involved. This was done by performing separate pairs of runs, with mean sizes of ice crystals in targeted microphysical processes of ice-only clouds being fixed. The identified processes were aggregation (-15.31 $\pm$2.29 Wm^{-2}), sedimentation (-1.37 $\pm$0.21 Wm^{-2}), and auto-conversion (-8.53 $\pm$1.28 Wm^{-2}). All these processes become less efficient with an increase in aerosol pollution, hence, increasing the lifetime of ice-clouds.

Surprisingly, the results show that the sum of the indirect effects of each of these individual microphysical processes is not comparable to the net aerosol indirect effect of ice-only clouds − the individual indirect effects are much larger (Fig. 5.15b). This discrepancy arises because of the limitation of sensitivity tests as a way of determining relative contributions from different processes to the overall flux change. Sensitivity tests cause perturbation of many processes, with compensating responses beyond the impact on the target process being perturbed. Fig. 5.15b shows that aggregation of ice particles becoming less prolific when ice particles are smaller due to aerosol pollution, reducing precipitation and increasing cloud extent, is the most important mechanism for the aerosol pollution to affect the flux change at TOA.

Albedo/emissivity

Due to the increase in ice crystal number concentrations in the present-day sce-

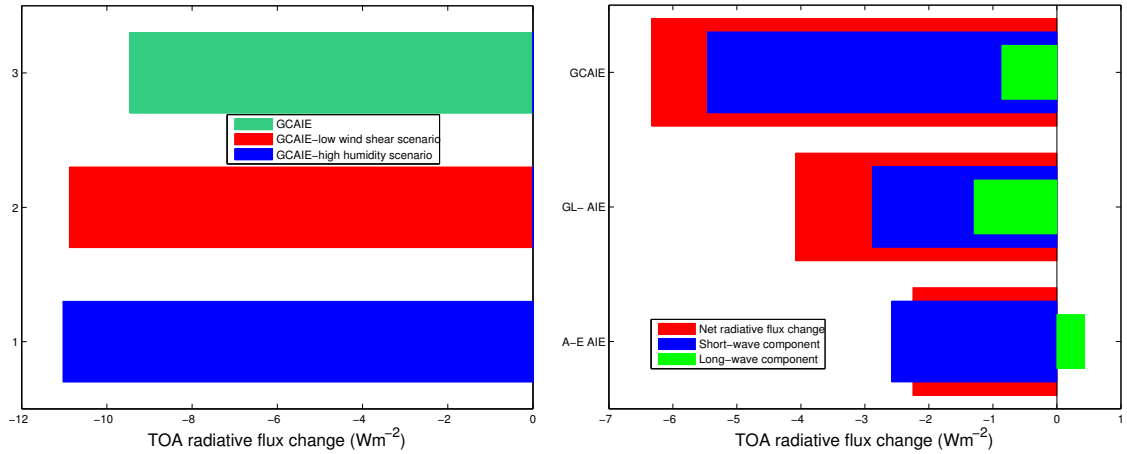

(a) Different meteorology scenarios (b) Long- and short-wave components

Figure 5.17: *(a) The role of meteorology on glaciated cloud aerosol indirect effects and (b) the respective contributions of short- and long- wave components to the net AIE in CLASIC. Meanings of abbreviations: GCAIE = Glaciated clouds aerosol indirect effects, GL-AIE = Glaciated cloud lifetime indirect effects, A-E AIE = Albedo-emissivity indirect effects.*

nario and the consequent reduction in the effective sizes of ice crystals, the albedo-emissivity effect of ice-only clouds caused a negative radiative flux change at the TOA (-1.18 ±0.18 Wm^{-2}), causing a cooling in the present-day climate (Fig. 5.14).

5.3.7 Meteorological Factors Affecting AIEs

Further, sensitivity tests were carried out to investigate how meteorological conditions control the aerosol indirect effect of glaciated clouds. This sub-section analyses the impacts of wind shear and relative humidity on indirect effects of glaciated clouds.

5.3.7.1 Effects of Wind Shear on AIEs

There was a slight net increase in the cloudiness of a weak wind shear scenario in this continental case, despite the fact that the cloud fraction of other cloud types diminished under the weak wind shear scenario relative to the control run (Fig. 5.18a). This finding was contrary to the microphysical principles upon which the investigated hypothesis was based. The expectation was that strong wind shear spreads clouds more in the horizontal, hence, reflecting more radiation back to space. However, this increase in cloudiness was attributed to weak precipitation production especially of snow (Fig. 5.18b), despite the conspicuous increase in the number

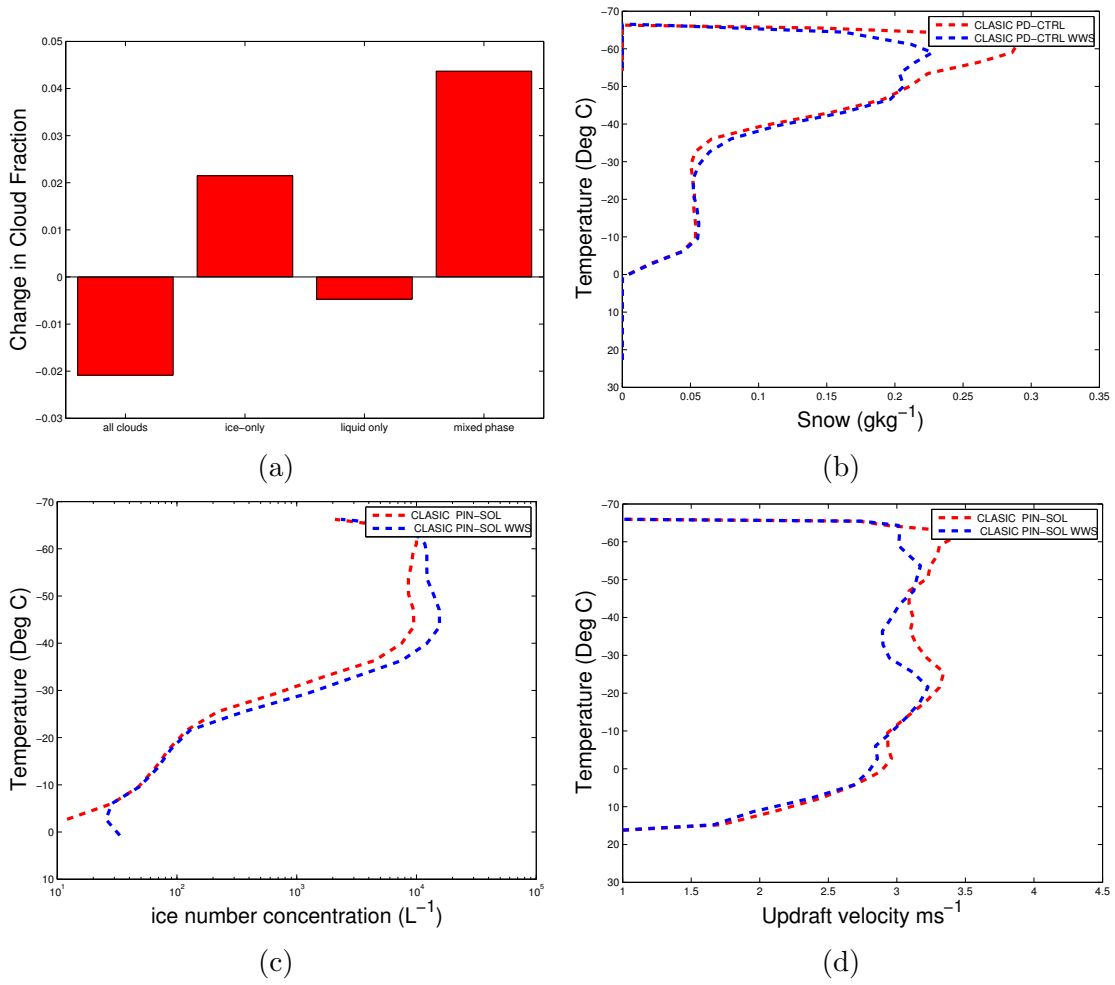

Figure 5.18: *Response of different cloud properties to horizontal wind shear in CLASIC. N.B. The blue curve represents present-day weak wind shear scenario while the red represents present-day strong wind shear scenario. (a) Cloud fraction, (b) Snow mixing ratios, (c) Ice crystal number concentrations and (d) Snow mixing ratios.*

concentrations of ice crystals aloft (Fig. 5.18c) in ice-only clouds under the weak wind shear scenario. As a result of the poor scavenging of the mass of cloud ice, the mass mixing ratio of cloud ice proliferated (Fig. 5.18b).

Consequently, more radiation was reflected back to space by clouds under the weak wind shear scenario. About 3 $\pm$0.45 Wm^{-2} of solar radiation was reflected back to space due to the reduction in wind shear, hence, for the mid-latitude continental scenario, weak wind shear surprisingly caused a cooling of the climate system. This finding resulted from the invigoration of cloud dynamics (Fig. 5.18d), which enhanced the detrainment of cloud ice aloft. But due to the weakening of snow production, the loading of IWC aloft was enhanced, causing clouds to become optically thicker and more extensive under the weak wind shear scenario.

Focusing on the aerosol-cloud interactions, it was noted that the mechanisms of

aerosol indirect effects on clouds under weak wind shear conditions were microphysically similar to those in strong wind shear conditions. Hence, the net aerosol indirect effects from clouds between these two different wind shear scenarios were relatively comparable. A net indirect effect of -10 ±1.5 Wm^{-2} due to aerosol pollution was predicted for a weak wind shear scenario.

5.3.7.2 Effects Upper Tropospheric Relative Humidity on AIEs

Under a scenario of higher upper tropospheric relative humidity, both present-day and pre-industrial clouds became more reflective, thereby reflecting as much as 15 ±2.25 Wm^{-2} of radiation energy back to space compared to a low relative humidity scenario. This higher reflectivity occurred despite the fact that the cloud fraction of a higher relative humidity case was about 7% less than that of a lower humidity scenario (Fig. 5.19a), owing to increased precipitation production. The increased reflectivity therefore arose from the increased volumetric cloud fraction (Fig. 5.19b) and optical thickness (Fig. 5.19c) of the clouds.

The primary mechanisms for the increased optical thickness of the clouds under a higher relative humidity scenario are the increased ice crystal number concentration (Fig. 5.19d) and cloud water contents (Fig. 5.19e). The high crystal number concentration of ice clouds was facilitated mainly by enhanced homogeneous freezing of sulphate aerosols. Invigoration of cloud dynamics was also noted under a high humidity scenario (Fig. 5.19f).

The influence of aerosols under these artificially perturbed meteorological conditions have; however, not been very different microphysically, from those under the original meteorological conditions. The total aerosol indirect effect (-11.03 ±1.65 Wm^{-2}) due to aerosol pollution was predicted under the high humidity scenario and was slightly higher than that of the normal meteorological conditions.

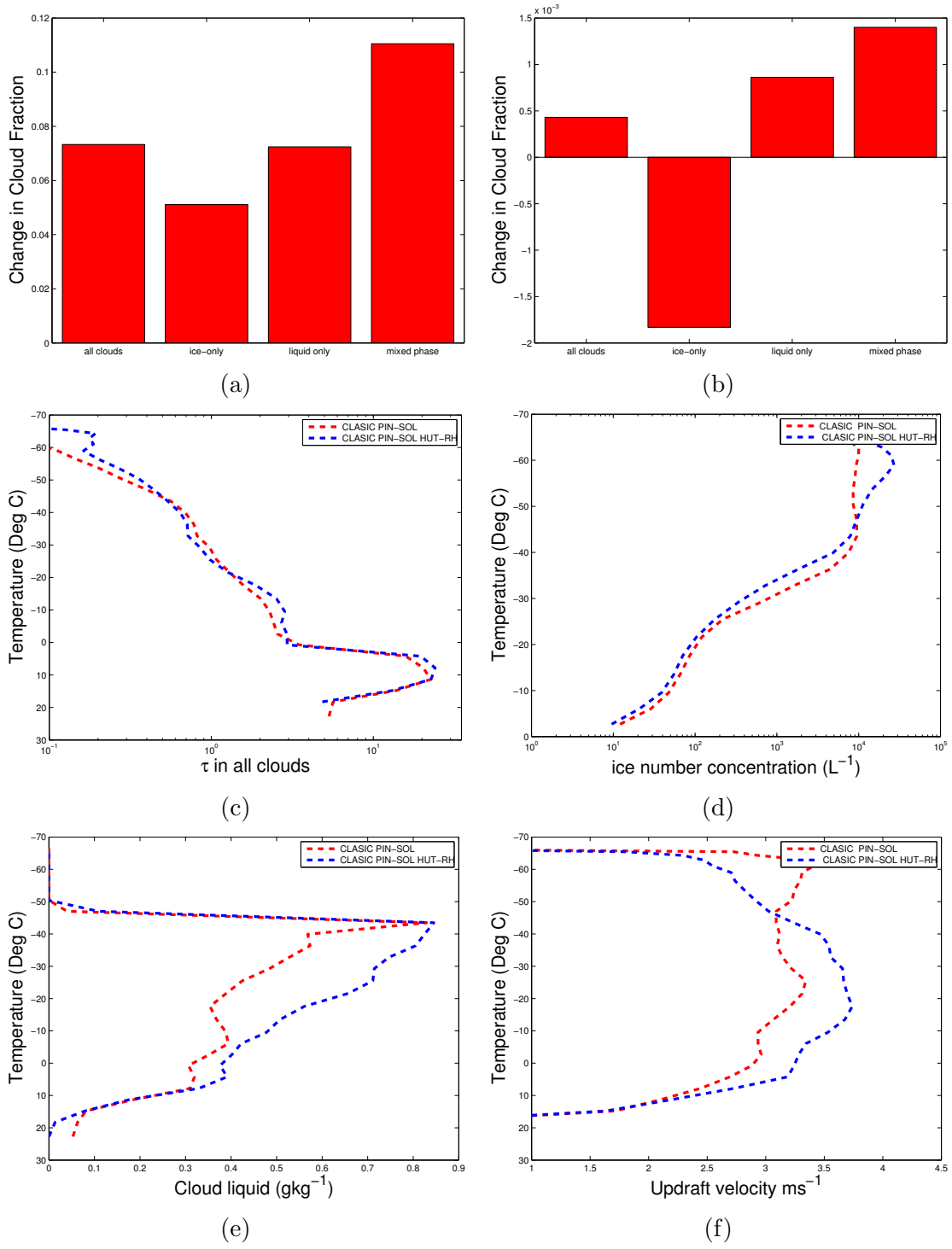

Figure 5.19: *Response of different cloud properties to upper tropospheric humidity in CLASIC. The blue curve represents the pre-industrial higher humidity scenario while the red represents the pre-industrial low upper tropospheric humidity scenario. (a) Cloud fraction, (b) Volumetric cloud fraction, (c) Optical thickness, (d), Ice crystal concentration (e), Liquid water content and (f) Strong updrafts* $\omega > 1ms^{-1}$.

5.4 Results from a Tropical Maritime Case (TWPICE)

This section presents results from the second case study of this research. There are three major differences between the first and second cases. First and foremost, CLASIC is a continental case, while TWPICE is a maritime one. Secondly, not only are the geographical locations of TWPICE and CLASIC different, but also their climatic regions and latitudinal locations differ; CLASIC is a mid-latitude case while TWPICE is a tropical one. Finally, since TWPICE is located in a remote maritime location near Darwin, Australia, it is inherently characterized by low aerosol concentrations. The same methodology used in CLASIC (Sect. 5.2) is also used to isolate aerosol indirect effect on glaciated clouds in TWPICE. Furthermore, similarities in microphysical processes were noted between the two cases; hence, only significant differences are highlighted in this section, thus, few graphical illustrations are presented.

5.4.1 Response of Cloud Microphysical Properties to Increased Solute Aerosols

Despite having applied equal percentage increases of aerosol number and mass concentrations in both CLASIC and TWPICE, there are still several differences between TWPICE and CLASIC simulations. The major differences emerging especially in cloud properties are premised on the contrast in aerosol loading between CLASIC and TWPICE (Fig. 4.4). The same scaling factor applied to CLASIC to determine the pre-industrial aerosol scenarios was also applied here in TWPICE since it was derived from a global model as a global factor (Takemura, 2012).

5.4.1.1 Initiation of Cloud Droplets

Figure 5.20a shows the number concentrations of cloud droplets for both the present-day and the pre-industrial aerosol conditions, the number concentrations are much lower than those predicted in CLASIC, owing to the low number concentrations of aerosols in TWPICE relative to CLASIC. The number concentration of cloud droplets (Fig. 5.20a) was increased by a factor of four in the maritime control simulation (present-day) relative to the pre-industrial simulation in TWPICE. This sensitivity to changes in aerosol loading was greater than for the continental case, as expected from greater sensitivity of CCN activity and of the supersaturation to aerosol loading (Twomey's formula) for maritime clouds relative to continental clouds. Among solute aerosols, sulphate is by far the dominant source of cloud droplets followed by soluble organics for both the pre-industrial and present-day

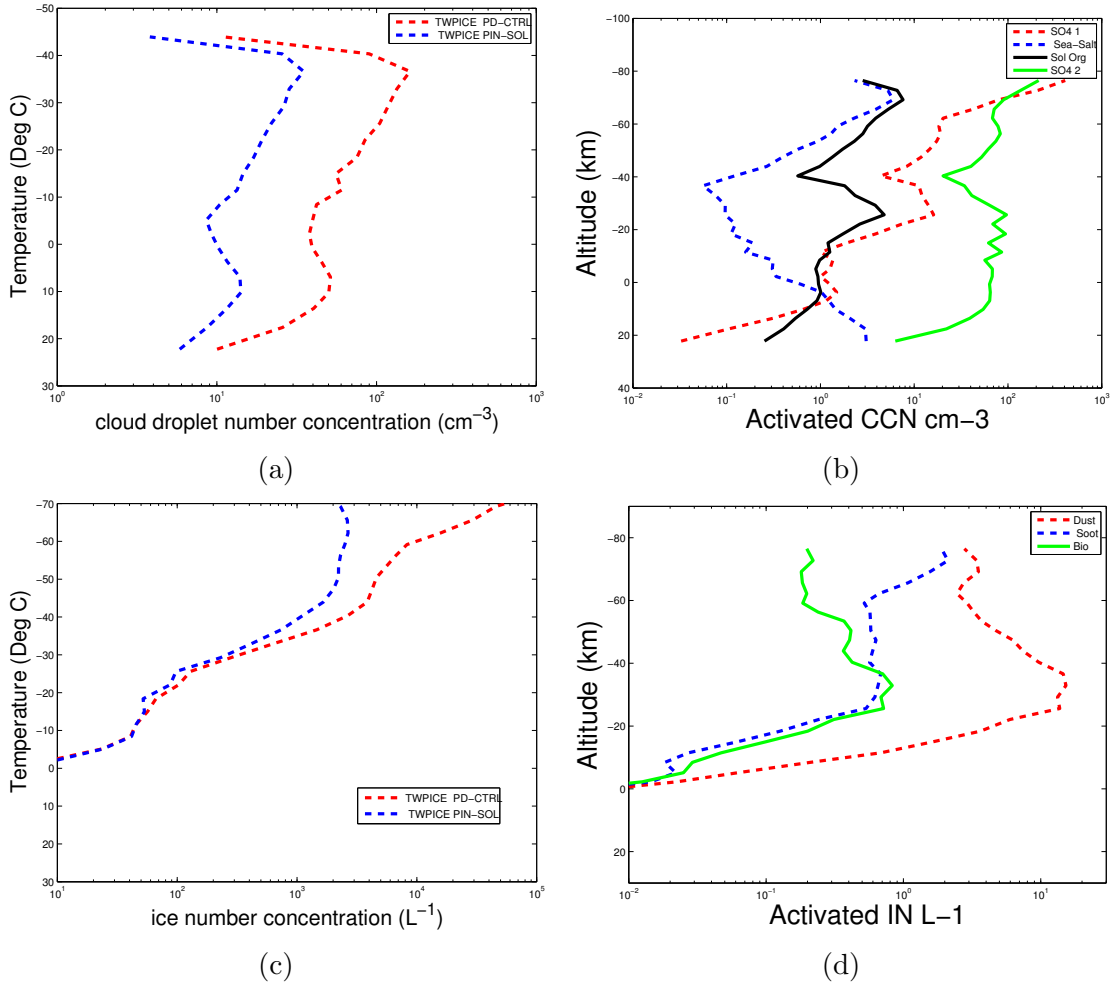

Figure 5.20: *Conditionally averaged (a) cloud droplet and (c) ice crystal number concentrations from TWPICE and their corresponding nucleation sources ((b) and (d), respectively) from the various species of aerosols being treated in the model.*

aerosol scenarios. The accumulation mode of sulphate aerosol is dominant in the lower troposphere; however, in the upper troposphere, the Aitken mode is an equally important source of cloud droplets. It can therefore be concluded that the accumulation mode of sulphate aerosols controls the number concentrations of cloud droplets (Fig. 5.20b).

It is important to note that a perfect agreement between cloud droplet loading and activated CCN concentration is not immediate - number concentration of activated CCN is slightly higher than that of cloud droplets. This discrepancy is expected because; some cloud droplets grow into precipitation (rain drop) by collision-coalescence. In addition to all these aforementioned cloud droplet sinks, evaporation and homogeneous freezing of cloud droplets may account for this discrepancy.

5.4.1.2 Initiation of Cloud Ice

Figure 5.20d shows the number budget of primary sources of ice crystals. As clearly indicated, dust is the dominant source of ice crystals from heterogeneous nucleation for the control simulation. Also, IN activity is found to be more effective above the homogeneous freezing level. As for the total crystal concentrations (Fig. 5.20c), the fractional response is two times more for the maritime case than for the continental one. This finding is explained by the higher IN activity exhibited by the clean maritime atmosphere than by the continental one. This is because in maritime atmospheres IN concentrations are low relative to the continental atmospheres, hence, the ice supersaturations are not depleted quickly in maritime clouds. Therefore, a higher fraction of solid aerosols is nucleated in maritime compared to continental clouds.

It is remarkable to note that the average number of ice crystals is about three orders of magnitude greater than the average number of activated IN. This brings into focus the concept of extra sources of ice crystals such as homogeneous droplet and aerosol freezing and ice multiplication processes, such as the H-M process. Similar findings for tropical cases of deep convection were shown by Phillips et al. (2007). The ice number budget (Fig. 5.21) shows that homogeneous aerosol freezing, particularly of sulphate aerosols outnumbers other sources of ice crystals. Homogeneous freezing of cloud droplets is about 20% less than that of aerosols. Other equally important sources of ice crystals are: homogeneous droplet freezing followed by the H-M splinters. Although the contribution from heterogeneous ice nucleation to the total crystal budget is relatively small, it is important, none-the-less.

5.4.1.3 Water Contents

Water contents of maritime clouds (Fig. 5.22a and 5.22b) were slightly less than those of continental clouds. Although in principle, these quantities are not expected to differ significantly for the same cloud type, the predicted differences, however, emerge mainly from the contrast of mean sizes of cloud droplets between continental and maritime clouds − continental clouds precipitate less efficiently compared to maritime clouds. Also, the greater prevalence of strong vertical velocities in CLASIC than in TWPICE is another possible cause[1].

As for the response to increases in solute aerosol loading, a similar response as

[1]This is primarily because, cloud water content is a strong function of vertical velocity - and it increases with increasing ascent velocity (Rogers and Yau, 1991). Hence, more cloud droplets were initiated in continental clouds and because of their small sizes their precipitation efficiency became low

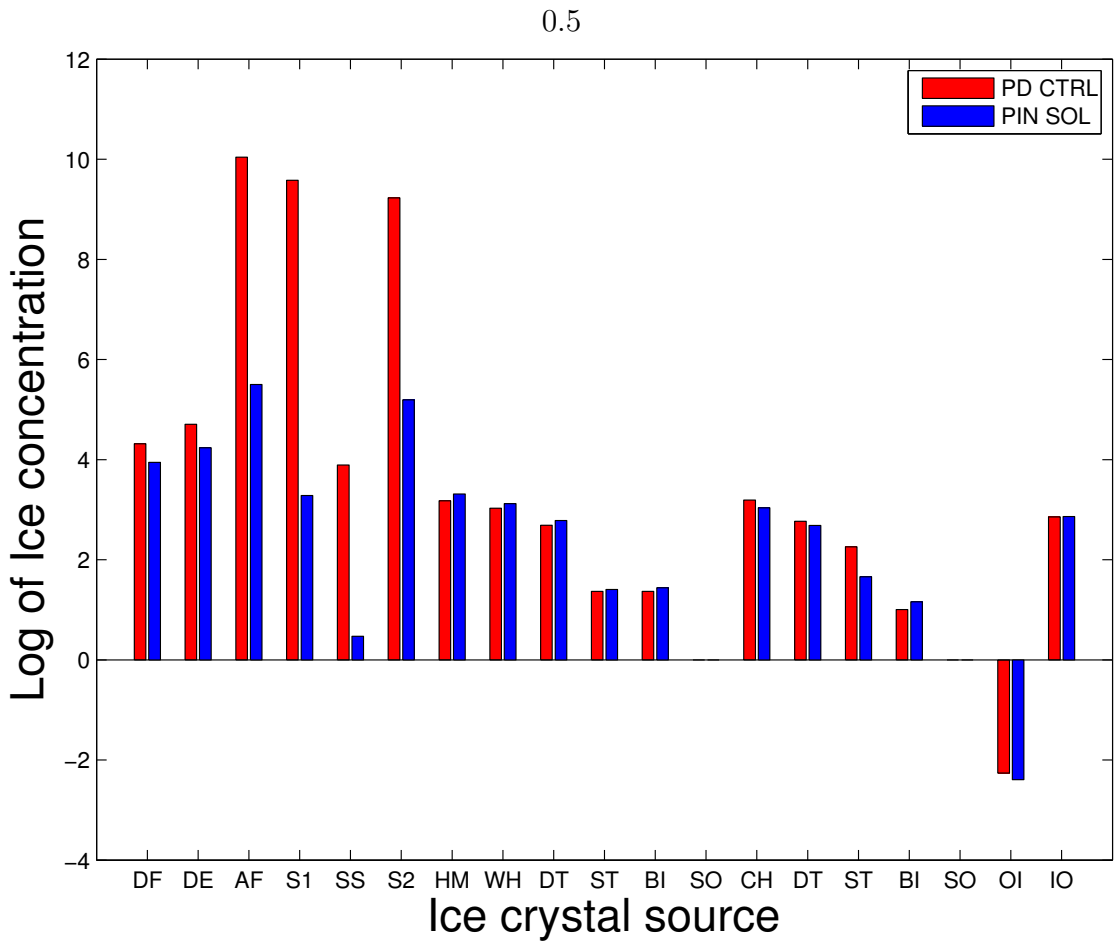

Figure 5.21: *Ice number budget in TWPICE. Meanings of abbreviations in (d) DF = droplets frozen homogeneously, DE = droplets evaporating during homogeneous freezing, AF = aerosols frozen homogeneous, (S1, SS, S2) droplets in 1^{st} mode of SO4, sea-salt, 2^{nd} mode of SO4 aerosols, respectively, that froze homogeneously. HM = H-M splinters, WH = total crystals from Warm Heterogeneous nucleation (Condensational, Depositional, and Immersion at temperatures > -30 °), (DT, ST, BO, SO) crystals by Warm Heterogeneous nucleation of dust, soot, biological organics and soluble organics, respectively. CH = total crystals from Cold Heterogeneous nucleation (Condensational, Depositional, and Immersion at temperatures < -30 °), (DT, ST, BO, SO) crystals by dry deposition from dust, soot, and biological organics and soluble Organics, respectively. Finally, OI and IO stand for total ice crystals from Outside-In and Inside-Out Contact freezing.*

in CLASIC is predicted for the water contents − there is a steady increase in LWC and a reduction of IWC in the upper troposphere, emerging mostly from regions of weak vertical velocities in TWPICE. The primary mechanism for this reduction in IWC aloft in TWPICE is the increase of snow production in deep convection and less detrainment of ice from the convective cores into cirrus.

Another secondary mechanism for this result is the weak response of cloud dynamics to changes in aerosol loading. If aerosol loading has not strengthened the

dynamics of the cloud, then no extra impetus (due to the aerosol induced thermodynamic effect) is created to force vertical advection of extra cloud droplets above freezing levels for homogeneous freezing to occur. The weak thermodynamic indirect effect can also somewhat indicate that homogeneous freezing of extra cloud droplets is less prolific in clean clouds than in polluted clouds. On the other hand, there is an increase of the liquid water contents in TWPICE, due to weakening of rain production within warm clouds (Fig. 5.23). With weak precipitation production, more liquid water remains in the cloud and this effect has a tendency of prolonging the lifetime of clouds.

5.4.1.4 Precipitation From the Warm Rain Process

About 75% of the rain mixing ratio in TWPICE is produced by liquid-only clouds as shown in Figs. 5.23a and 5.23b, while the remainder is from mixed-phase clouds, however, there was no appreciable change in the rain mixing ratio of these liquid-only clouds in response to the inclusion of aerosol pollution. Although considerable reduction in the efficiency of rain production in mixed-phase clouds was noted in the present conditions, the contribution of this reduction to the overall rain production was suppressed by the impassivity of rain production in liquid-only clouds. As a result, the increase in solute aerosol loading registered no change to the total rain production, indicating minimum perturbation to the collision-coalescence process in clean maritime clouds. This unperturbed precipitation production also explains why there was a weak response to aerosol loading by ice water contents aloft.

5.4.1.5 Precipitation from the Ice-Crystal Process

Intrinsic snow production in TWPICE was heavily suppressed by more aerosols, especially in ice-only clouds in regions of weak vertical velocities. Clouds in regions of weak vertical velocities dominated the ice-only cloud mass, hence, they control the net average microphysical properties of all ice-only clouds. This suppression of snow in ice-only clouds in regions of weak vertical velocities arises from the fact that, snow production in regions of strong vertical velocities was higher in the polluted case and the detrainment of ice into clouds within the regions of weak vertical velocities was limited. In addition, there was also a significant reduction of supersaturations in the regions of weak vertical velocities, which also reduces snow growth in those regions.

On the other hand, the unconditionally averaged snow mixing ratios were high in TWPICE as it was in CLASIC when aerosol loading was raised, mainly because

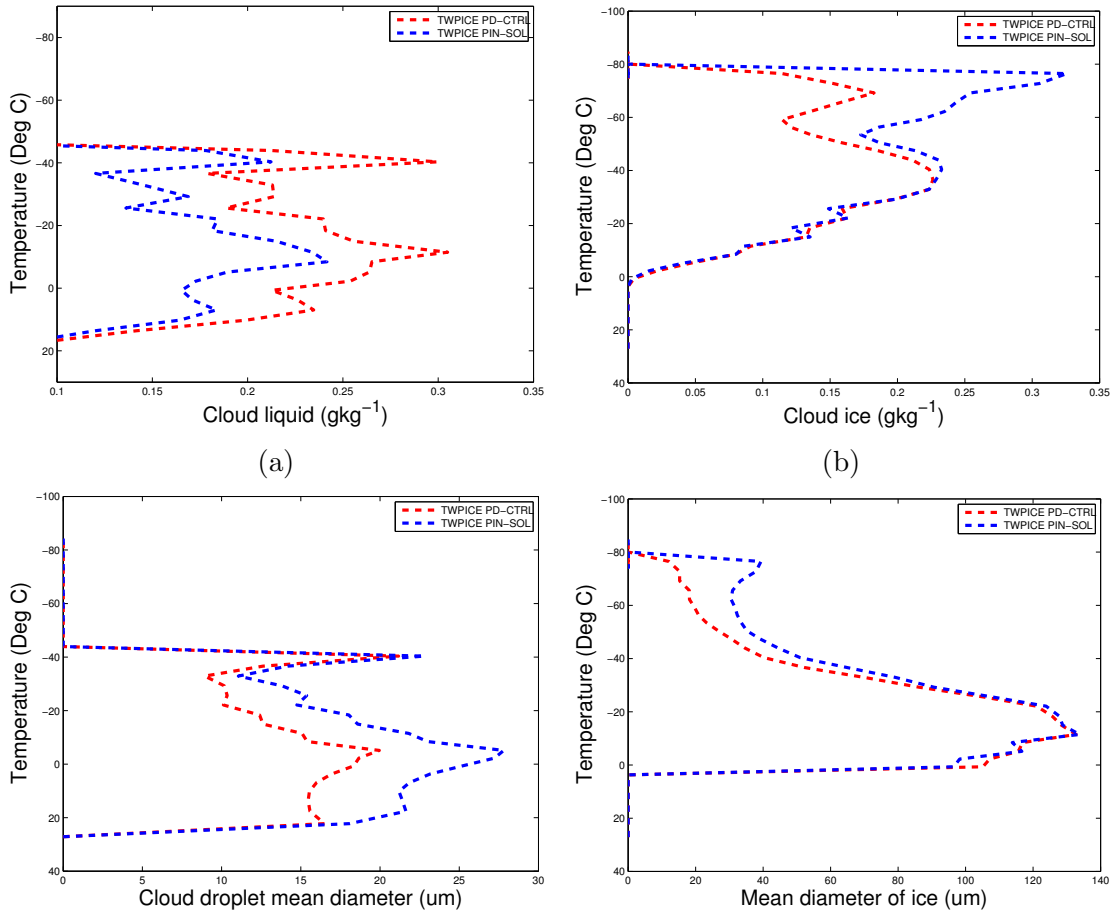

Figure 5.22: *Conditionally averaged (a) Liquid water content, (b) Ice water content, (c) Cloud droplets mean sizes and (d) Ice crystals mean sizes from the TWPICE case.*

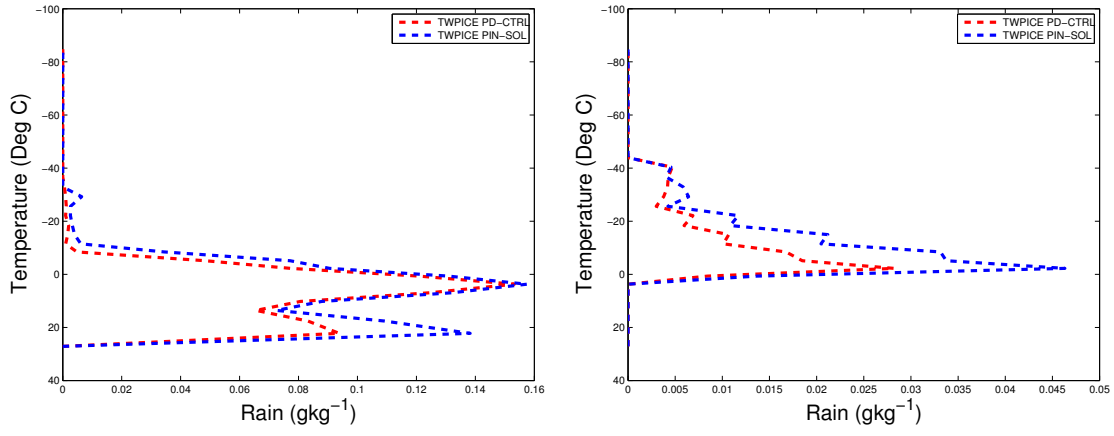

Figure 5.23: *Rain mass mixing ratios conditionally averaged over (a) liquid-only clouds and (b) mixed-phase clouds in TWPICE.*

of the net increase in cloud fraction with increasing aerosol. As for graupel, there was hardly any change noted in the production rates in all cloud types.

5.4.2 Response of Cloud Dynamical Properties to Increased Solute Aerosols

The dynamics of a cloud control the macro- and microphysics of the cloud. Macro physically, the dynamics determine the depth and spatial extent of the cloud. On the microphysics scale, the dynamics control (in some way) the collection efficiencies of cloud particles during collision-coalescence and aggregation processes. With this understanding, it was surprising to note that the response of cloud dynamics to more aerosols was minimal in TWPICE (Figs. 5.24a and 5.24b). This was the case because the greater efficiency of warm rain processes in eliminating cloud-liquid when aerosols are fewer over the oceans relative to land causes the freezing-related thermodynamic effect to be less important in TWPICE than in the continental case. Thus, no substantial homogeneous freezing of extra cloud droplets ensued in TWPICE due to aerosol pollution. The absence of substantial homogeneous freezing implied the absence of substantial latent heating to fuel the updrafts.

5.4.3 Response of Cloud Extent to Increased Solute Aerosols

In so far as the vertical profiles of horizontal cloud fraction are concerned, these simulations indicate that sensitivity occurs only in the lower- to middle troposphere for the maritime case (Fig. 5.24c). The increase in vertical profiles of cloud fraction in the lower to middle troposphere is primarily from mixed-phase and ice-only clouds mainly in regions of weak vertical velocities (Fig. 5.25). There is weak response emerging from liquid-only clouds. Although, no change in upper tropospheric cloudiness is reported (typically, ice-only clouds), there is strong evidence of glaciation in the mid troposphere − an increase in cloud fraction of ice-only and mixed-phase clouds.

As for the horizontal cloud fractions (Fig. 5.26a), a net increase in cloud fraction of 5% is predicted, alluding to the fact that overall, all cloud regimes became horizontally more extensive. Further investigation indicated that all cloud types became more extensive in the present-day, because volumetric cloud fraction showed an escalation of the number of cloudy grid-boxes for all cloud types, especially for mixed-phase clouds, followed by ice-only clouds (Fig. 5.26b).

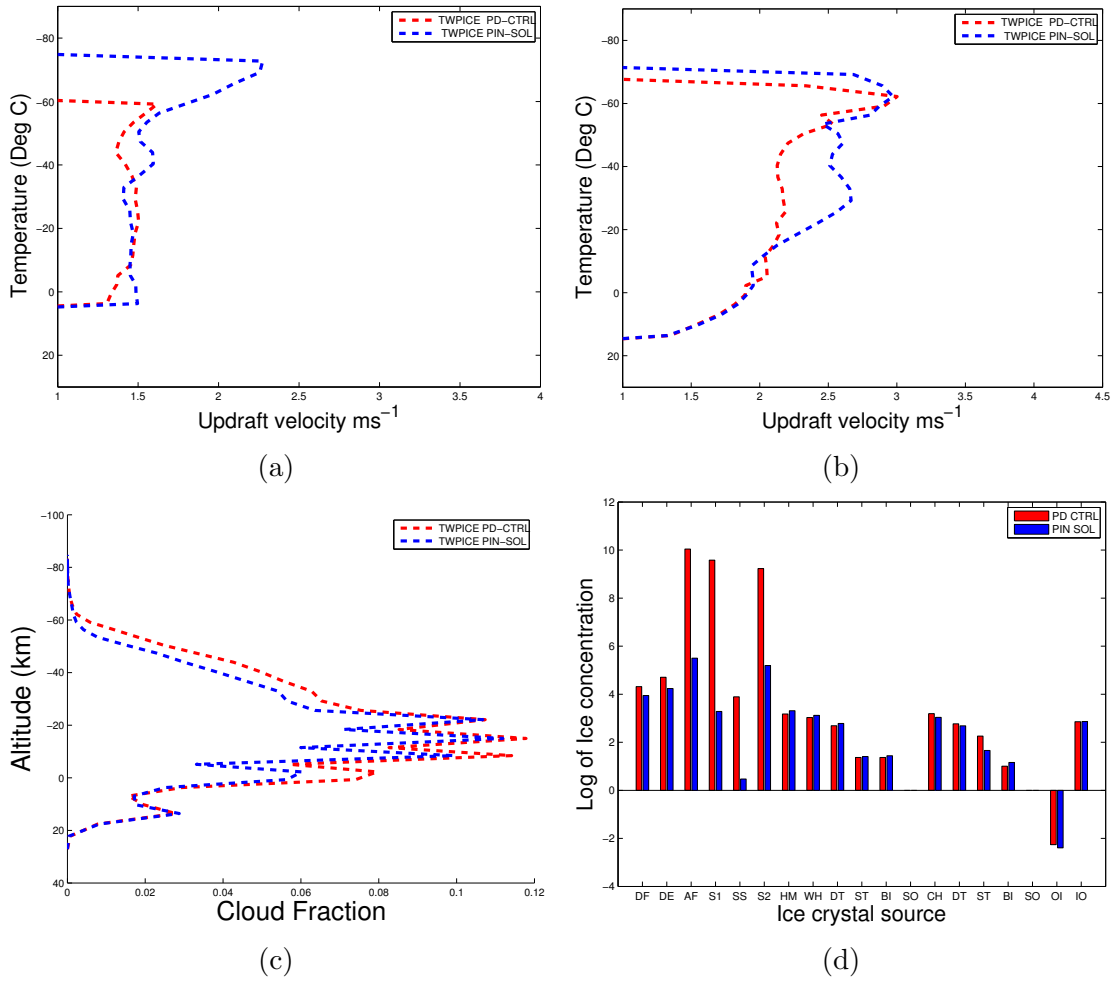

Figure 5.24: *Vertical velocity profiles conditionally averaged over clouds in TWPICE (a) weak vertical velocities and (b) strong vertical velocities. For weak vertical velocities, vertical velocity is less 1 m s^{-1} while it is greater than 1 m s^{-1} for strong vertical velocities. (c) Vertical profiles of cloud of cloud fraction (d) and ice number budget in TWPICE.*

5.4.4 Response of Cloud Optical Properties to Increased Solute Aerosols

Figure 5.27 presents both the intrinsic grid-point optical thicknesses of each individual cloud type (on the left) and for the domain averages (on the right). Figures 5.12 and 5.27 show contrasting characteristics between cloud optical properties of CLASIC and TWPICE, respectively. Apparently, maritime clouds are generally optically thinner than their corresponding continental counterparts, chiefly because continental clouds are characterized by smaller and numerous cloud droplets and also low precipitation efficiency due to less effective collision and coalescence, hence they are denser compared to maritime clouds (Fig. 5.4 and 5.22). Thus, continental clouds are thicker and darker; and their lifetime also, is relatively longer.

In terms of their response to more aerosols, TWPICE exhibits higher percentage

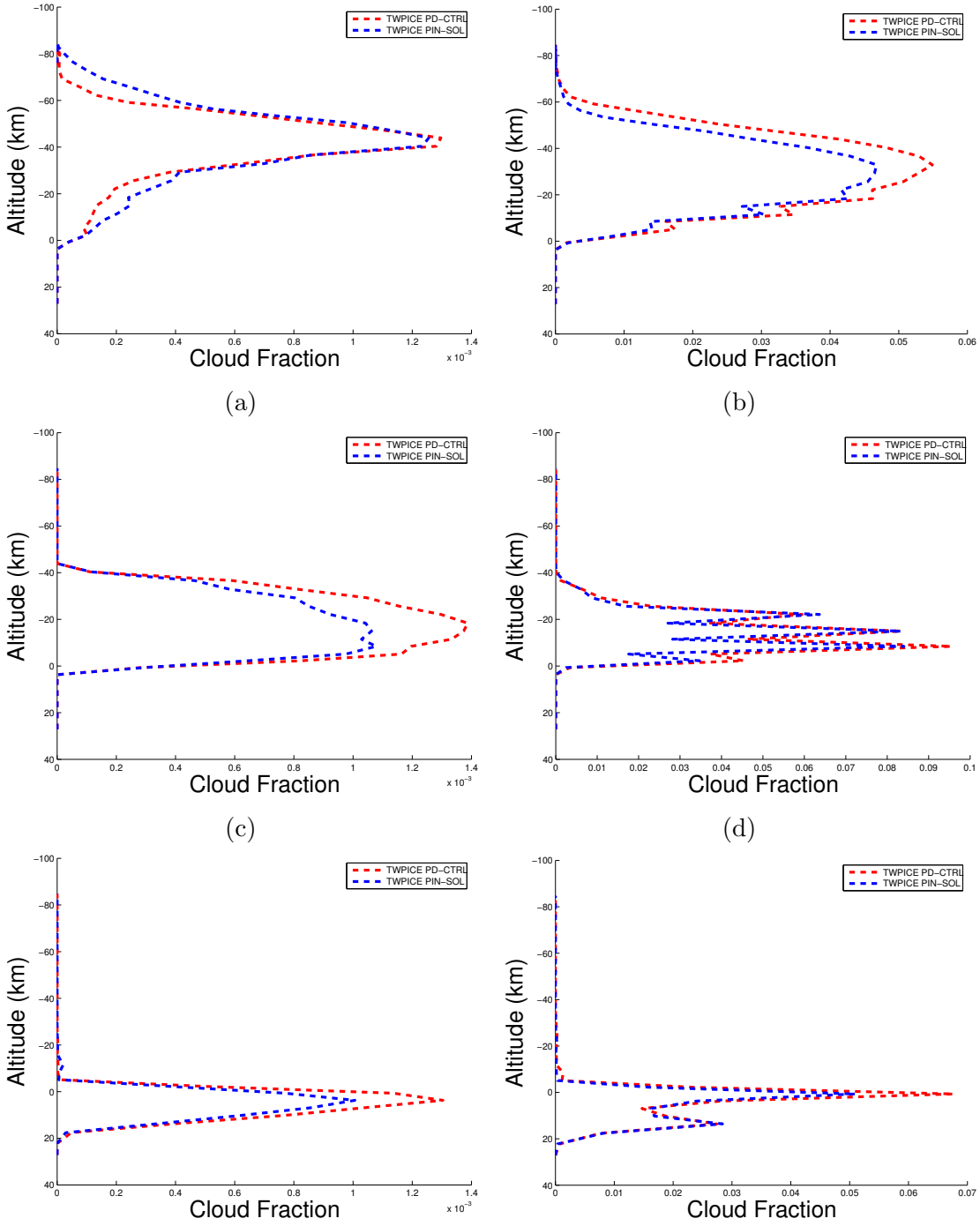

Figure 5.25: *Vertical profile of cloud fraction for all three types of phase of clouds, conditionally averaged over regions of strong vertical velocities (vertical velocity $\omega >= 1ms^{-1}$) (left) and weak vertical velocities (vertical velocity $\omega < 1ms^{-1}$) (right) in TWPICE. (a) and (b) are for ice-only clouds, (c) and (d) are for mixed-phase clouds, (e) and (f) are for liquid-only clouds.*

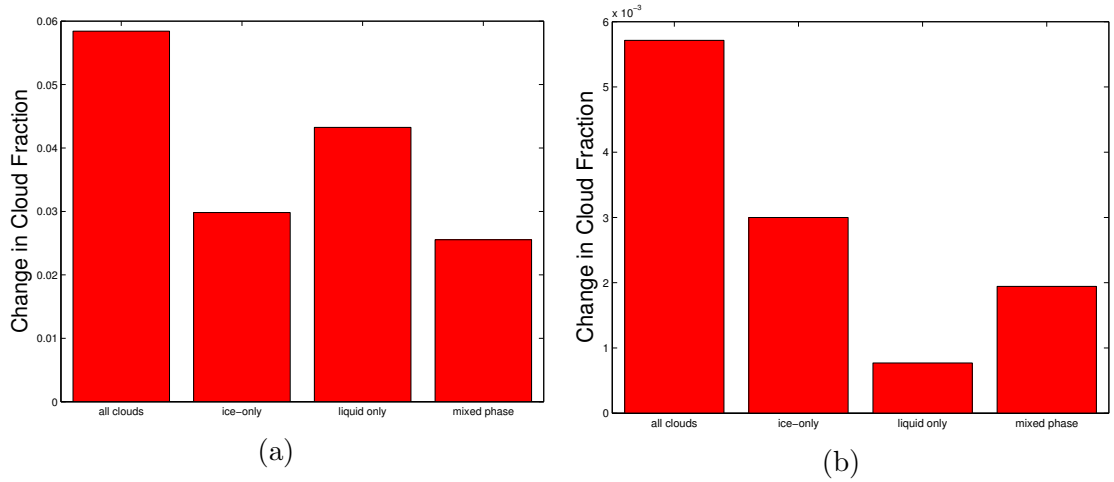

(a) (b)

Figure 5.26: *(a). The change in cloud fraction for all types of cloud species in TWPICE. (b). The change in volumetric cloud fraction for all types of cloud species in TWPICE.*

changes than CLASIC, because maritime clouds are still more sensitive to aerosol perturbation. Accordingly, their properties are more sensitive to aerosol changes than their continental counterparts, whose aerosol number concentrations have almost reached saturation. This huge change in optical properties of clouds implies that the reflectance of the cloud is also strongly affected. Fig. 5.28 clearly shows that the total optical thicknesses of all clouds and of each individual cloud type are much higher in the present-day than in the pre-industrial simulation for both the intrinsic and domain-wide averages.

5.4.5 Response of Radiative Fluxes and Cloud Radiative Properties to Increased Solute Aerosols

This section examines how modifications of microphysical properties of clouds affect the optical properties of clouds and the net radiation budget of the Earth. This was done by way of assessing TOA radiative flux changes (a similar approach applied to CLASIC).

5.4.5.1 All Clouds

Figure 5.29a presents radiative flux changes at the TOA due to changes in aerosol concentration from the pre-industrial to the present-day era. A strong negative radiative flux change at the TOA (-17.44 $\pm$6.1 Wm^{-2}) is registered in maritime clouds than in continental clouds (-9.46 $\pm$1.42 Wm^{-2}), due to low aerosol loadings in maritime atmospheres. Thus, maritime clouds are more responsive to anthropogenic changes in aerosol loadings compared to continental clouds, which may

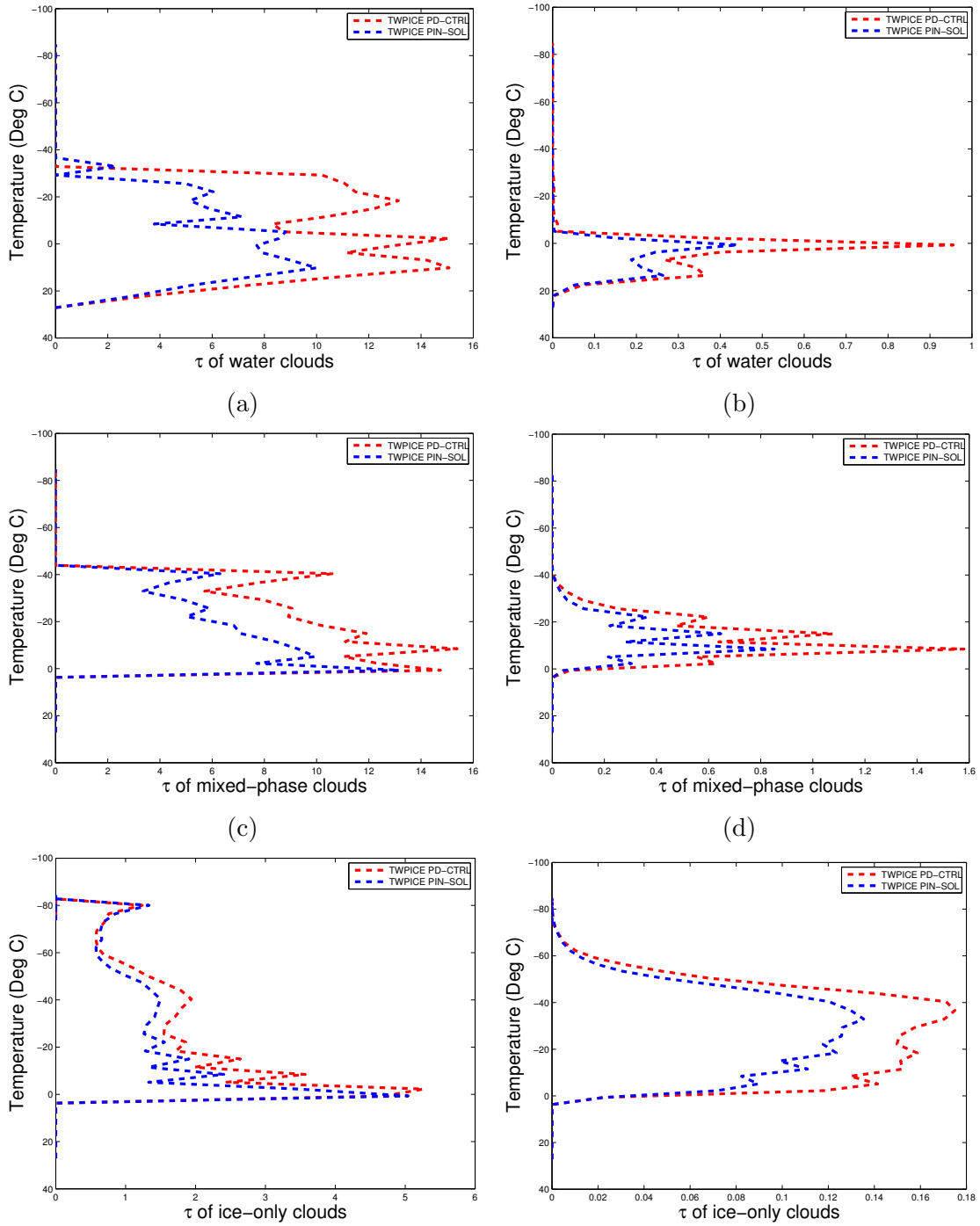

Figure 5.27: *Cloud optical thickness τ for different cloud phases conditionally averaged in cloudy regions (left) and domain averaged for targeted cloud phase (right). (a) and (b) are for liquid-only clouds, (c) and (d) are for mixed-phase clouds, (e) and (f) ice-only clouds in TWPICE.*

have reached a saturation point beyond which sensitivity to aerosol perturbations is minimal. This finding corroborates the explanation of Andreae et al. (2007) that,

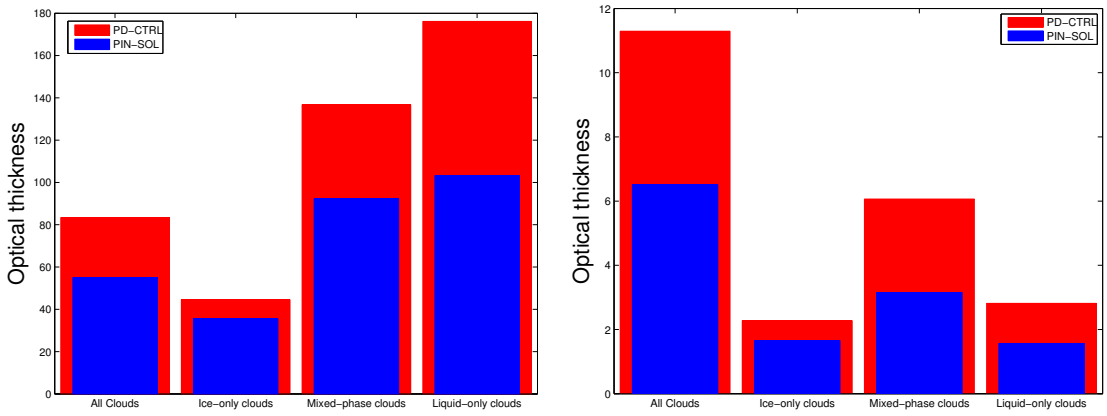

Figure 5.28: *Superimposed optical thicknesses predicted in the TWPICE simulation of mid-latitude continental clouds; (a) conditionally averaged over grid-boxes in which the mass mixing ratio of a targeted cloud type is greater than zero and (b) unconditionally averaged of the entire domain and duration of the simulation. Optical depth from each cloud-type is plotted by assuming that no other cloud-types are present.*

aerosol indirect effects are larger in clean clouds than in polluted ones. The primary contributions to this huge indirect effect are the massive increases of the droplet number concentrations by a factor of five and a doubling of the ice crystal number concentrations. In continental clouds, the droplet number concentrations just tripled where as the number concentrations of ice crystals increased by a factor of 1.5. Also the perturbation of microphysical properties of water clouds is quite strong in this maritime case than it is, in the continental one (e.g. Fig. 5.22a). Also, Fig. 5.28 clearly shows that present-day clouds are very thick, optically, compared to pre-industrial clouds.

Unlike in CLASIC where glaciated clouds exhibited a stronger AIE compared to water clouds, in this maritime case, both water-only (-9.08 $\pm$3.18 Wm^{-2}) and glaciated clouds (-8.36 $\pm$2.93 Wm^{-2}) were equally important in controlling the net AIE of clouds. This is chiefly due to the fact that microphysical properties of water clouds in this maritime case were more sensitive to aerosol loading, thus, because of their strong radiative signature especially in the shortwave, their contribution to the total AIE was strong. However, because of their existence above water clouds, glaciated clouds have the first interaction with solar radiation, thus, they are vital for AIEs.

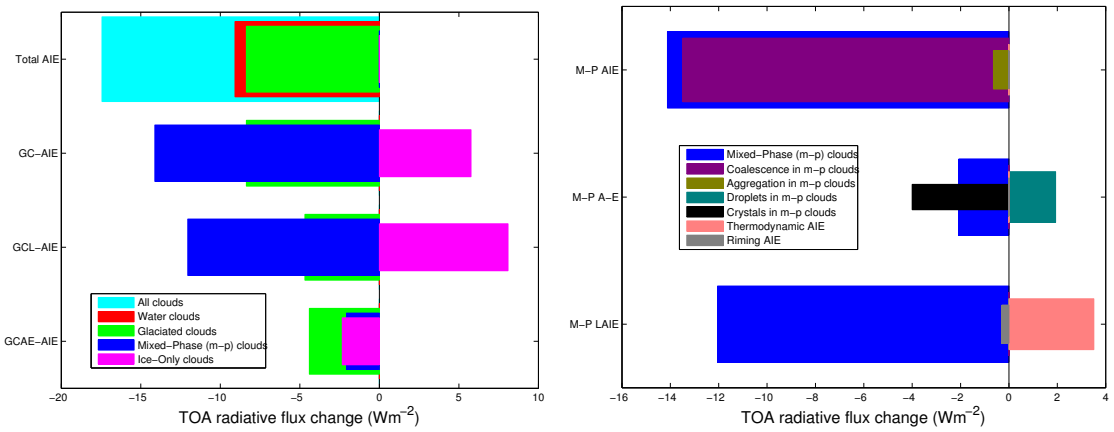

(a) (b)

Figure 5.29: *(a) The glaciated clouds aerosol indirect effects from solute aerosols (PD-CTRL - PINSOL) results are derived mainly from tests A and B through identifying salient microphysical processes that are responsible for modifying cloud radiative properties in TWPICE. Meaning of abbreviations: GC-AIE = Glaciated Clouds AIE, GCL-AIE = Glaciated Clouds Lifetime AIE, GCAE-AIE = Glaciated Clouds Albedo-Emissivity AIE. (b) The aerosol indirect effects for mixed-phase clouds. Meanings of abbreviations: M-P AIE = Mixed-phase clouds aerosol indirect effects, M-P A-E = Mixed-phase clouds albedo emissivity effects, M-P AIE = Mixed-phase clouds aerosol indirect effects.*

5.4.5.2 Glaciated Clouds

Unlike the continental case, in which ice-only clouds dominated the glaciated cloud quota, in TWPICE, the mixed-phase component (-14.12 ±4.94 Wm^{-2}) of glaciated clouds was predominant, whilst the ice-only clouds component (5.76 ±1.84 Wm^{-2}) actually exhibited a positive radiative flux change at the TOA. As explained earlier, homogeneous freezing was weak in clean marine clouds than in polluted continental clouds, hence, the properties of cirrus were less affected. This was primarily because of the weak perturbation of warm rain processes and the absence of strong updrafts that push extra cloud droplets aloft, hence the IWC aloft diminished quite strongly.

These damping processes are facilitated by the minimal reduction of cloud droplet sizes. Furthermore, mixed-phase clouds are horizontally more extensive than ice-only clouds (Figs. 5.25b and 5.25d). Also Fig. 5.22 shows that, in terms of cloud water contents, the upper tropospheric ice-water content diminished in the present-day while the liquid water content maintained an increase throughout the whole column of the atmosphere. The reduction in the water contents of ice-only clouds is caused by the strong increase in snow production aloft in all cloud types. The volumetric cloud fraction also reviews that, mixed-phase clouds contributed more to the overall change in volumetric fraction of glaciated clouds (Fig. 5.26b).

5.4.5.2.1 Mixed-Phase Clouds This section examines microphysical processes that are essential to aerosol indirect effects in mixed-phase clouds. The lifetime effects of mixed-phase and ice-only clouds are opposing. Mixed-phase clouds have a cooling effect (-12.05 $\pm$4.21 Wm^{-2}) due to the strong increase in their spatial extent and liquid water content chiefly due to the strong sensitivity of the warm rain process to aerosol pollution, while the response from ice-only clouds is a positive radiative flux change at the TOA (8.09 $\pm$2.83 Wm^{-2}).

Lifetime Effect

There are various processes that contributed to the lifetime indirect effect, most of which are presented in this section. The discussion under this subsection is based on the results shown in Fig. 5.29.

Coalescence Indirect Effect

Figure 5.29b shows that the coalescence indirect effect is strongly negative (-13.48 $\pm$4.72 Wm^{-2}) and dominates the indirect effect of mixed-phase clouds. This finding was expected because, rain production significantly declined in mixed-phase clouds (Fig. 5.23b) when aerosol concentrations were raised.

This implies that the efficiency of collision-coalescence processes also declined in mixed-phase clouds, primarily because of a reduction in the mean sizes of cloud droplets, which subsequently prolongs the lifetime of supercooled cloud droplets in present-day mixed-phase clouds. Thus, more insolation is reflected back to space, since warm clouds have a strong shortwave radiative signature because of their higher water contents and smaller cloud droplets. The magnitude of the coalescence effect contrasts with that noted above for CLASIC, which was even smaller than the aggregation effect.

Aggregation Indirect Effect

The aggregation indirect effect (-0.64 $\pm$0.22 Wm^{-2}) is quite insignificant compared to the coalescence indirect effect. This response indicates the insensitivity of the aggregation processes to changes in aerosol perturbation. The ice-phase cloud properties (ice-water content, effective radius of ice crystals and snow and graupel production) in mixed-phase clouds showed little changes due to aerosol increases, hence the small aerosol indirect effect.

Also, the predicted effective sizes of ice crystals within mixed-phase clouds was slightly larger in the present-day, hence, the collision efficiencies of the interacting ice particles can be enhanced, as reported by Keith and Saunders (1989) in their

laboratory investigation of sticking efficiencies of an interaction of larger solid hydrometeor (graupel) and ice crystals.

The Riming Aerosol Indirect Effect

The riming aerosol indirect effect caused a slight cooling (-0.29 $\pm$0.1 Wm^{-2}), chiefly because the mean size of rimers is smaller in the present-day and this diminishes the collection efficiency during riming. It is apparent that the contribution of coalescence is of higher importance than that of riming, because in mixed-phase clouds, the liquid component is proportionally higher than the ice component (Figs. 5.30a and 5.30b, respectively).

The liquid component of mixed-phase clouds is identifiably more responsive to more aerosols than the ice component, which in fact is insensitive. Consequently, it may be concluded that since coalescence exclusively involves the liquid phase, it thus yields a higher indirect effect than the riming process, which involves both the ice (graupel) and liquid components equally. Hence, the opposing responses in the properties of ice crystals and cloud droplets (e.g. crystal and droplet sizes in Figs. 5.30c and 5.30d, respectively) tend to buffer the riming effect.

The Thermodynamic Aerosol Indirect Effect

The thermodynamic effect showed a strong positive radiative flux change at the TOA (3.51 $\pm$1.22 Wm^{-2}), primarily because the general understanding of the thermodynamic effect enhances precipitation production through ice crystal processes (as noted earlier for snow), thereby reducing the lifetime of clouds. This was however not the case with continental clouds in which negative feedbacks manifested in the form of secondary effects arising from squall line development, which increases the cloud coverage and spatial extent of clouds, resulting in more solar radiation being reflected back to space.

Albedo-Emissivity Effect

The net albedo-emissivity effect of mixed-phase clouds had a cooling effect (-2.07 $\pm$0.72 Wm^{-2}), and was approximately a quarter of the lifetime effect. Paradoxically, the contribution from ice crystals (-4.00 $\pm$1.4 Wm^{-2}) within mixed-phase clouds is stronger than from water droplets (1.93 $\pm$0.68 Wm^{-2}), yet the change in mean sizes of cloud particles was minimal for ice crystals (Figs. 5.30c and 5.30d)

5.4.5.2.2 Ice-Only Clouds A similar assessment as described for the continental case was carried out in this maritime case to assess the respective importance of

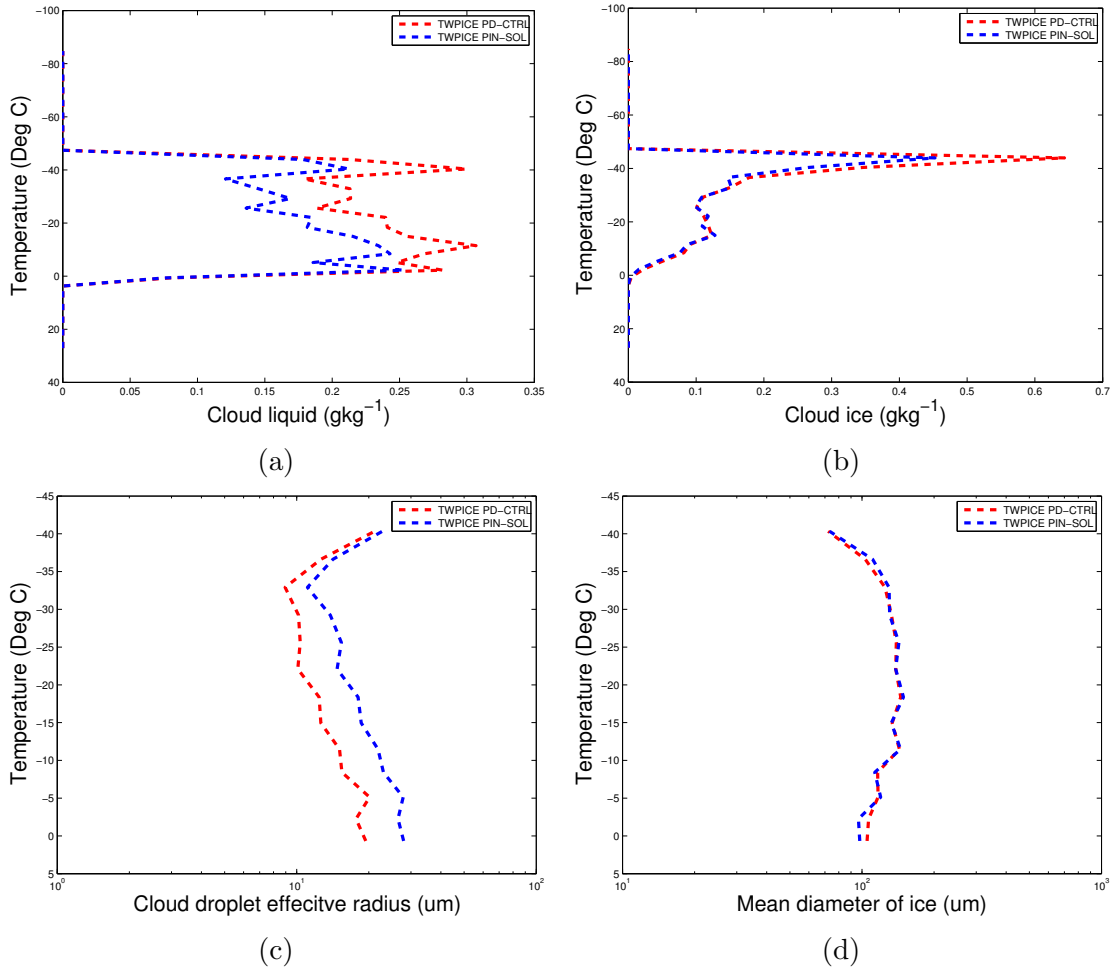

Figure 5.30: *(a) Cloud mixing ratio, (b) ice mass mixing ratio, (c) cloud droplet mean diameter and (d) ice crystal mean diameters, all are conditionally averaged over mixed-phase clouds in TWPICE.*

each microphysical process responsible for the radiative behavior of ice-only clouds. Surprisingly, unlike in the continental case, where the sum of the individual contributions of the responsible processes were very large compared to the overall indirect effect of ice-only clouds, here, the sum is smaller and also not astronomically incomparable. This was attributed to the fact that, although the mean size of cloud particles was reduced by the increase in solute aerosols, the sizes were still larger than those in the continental case; hence, the perturbations to these size dependent processes were less severe.

5.4.5.2.3 Albedo/Emissivity of Glaciated Clouds The albedo-emissivity effect for glaciated clouds caused a cooling effect (-4.4 $\pm$1.54 Wm^{-2}). The reduction in droplet sizes and increase in the number concentrations of cloud droplets make them more reflective, causing this cooling from the albedo-emissivity effect. Despite a slight re-

duction in crystal sizes and concentration aloft, the albedo-emissivity effect induced by ice crystals in ice-only clouds has a cooling effect (-2.33 $\pm$0.82 Wm^{-2}). This is attributed to the enhanced production of snow and graupel aloft, which reduces the number of effective ice crystals because it is theoretically understood that fewer cloud droplets are less reflective than numerous cloud particles.

5.4.6 Meteorological Factors Affecting AIEs

5.4.6.1 Effects of Wind Shear on AIEs

By reducing the horizontal wind shear, clouds generally became less reflective by as much as 5 Wm^{-2}, primarily because clouds under weak horizontal wind shear are less extensive (Fig. 5.31a). Most of the macro- and micro- physical properties of clouds were largely insensitive to the variation of the horizontal wind shear. However, updrafts in deep convective clouds were stronger under the WWS simulation (plot not shown) despite the fact that homogeneous freezing of both aerosols and water droplets was weak when the wind shear was low (Fig. 5.31b).

Furthermore, graupel production was actually insensitive to aerosol changes, hence, such a tiny riming indirect effect in this maritime case is justified.

These results agree well with those of Zeng et al. (2009), who noted an increase in the reflectance of clouds under a high wind shear scenario. Ultimately, the aerosol indirect effect under a weak wind shear scenario is quantitatively equal to the net aerosol indirect effect when the wind shear was not artificially perturbed, because the ensuing aerosol induced changes in microphysical processes and properties of clouds were microphysically similar under these two different horizontal wind shear scenarios. Hence, it can be concluded that the impact of strong wind shear is to increase the horizontal extent of the clouds.

5.4.6.2 Effects of Upper Tropospheric Relative Humidity on AIEs

Under a higher upper tropospheric relative humidity, clouds in this maritime case became more reflective, reflecting as much as 7 Wm^{-2} back to space. This result is a consequence of an increase in the cloud fraction, primarily of ice-only clouds (Fig. 5.32a). As in the continental case, there is a strong increase in the number concentrations of upper tropospheric humidity, arising primarily from enhanced aerosol freezing especially of sulphate aerosols (Fig. 5.32b). Updraft velocities in deep convection were less sensitive to aerosol loading, while those in stratiform regions were weakened significantly (Fig. 5.32c).

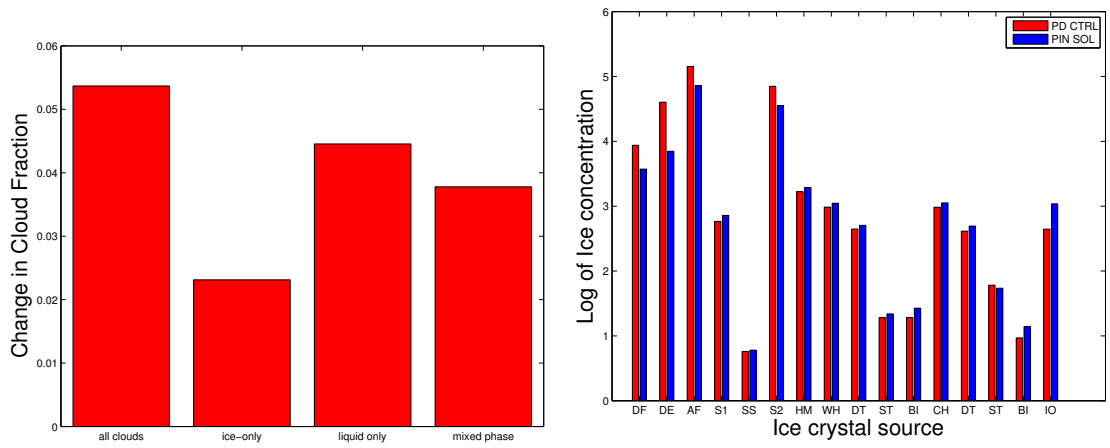

(a) (b)

Figure 5.31: *(a) Horizontal cloud fractions and (b) ice number budget under different wind shear scenarios for TWPICE. The red curve represents the strong wind scenario while the blue curve represents the weak wind shear scenario. Meanings of abbreviations in (d) DF = droplets frozen homogeneously, DE = droplets evaporating during homogeneous freezing, AF = aerosols frozen homogeneous, (S1, SS, S2) droplets in 1^{st} mode of SO4, sea-salt, 2^{nd} mode of SO4 aerosols, respectively, that froze homogeneously. HM = H-M splinters, WH = total crystals from Warm Heterogeneous nucleation (Condensational, Depositional, and Immersion at temperatures > -30 °), (DT, ST, BO, SO) crystals by Warm Heterogeneous nucleation of dust, soot, biological organics and soluble organics, respectively. CH = total crystals from Cold Heterogeneous nucleation (Condensational, Depositional, and Immersion at temperatures < -30 °), (DT, ST, BO, SO) crystals by dry deposition from dust, soot, and biological organics and soluble Organics, respectively. Finally, OI and IO stand for total ice crystals from Outside-In and Inside-Out Contact freezing.*

Most of the cloud fields remained largely unchanged, except for the ice water content which diminished quite substantially in the upper troposphere, mainly because of the strong increase in snow production in the upper troposphere, although the production of snow in the lower troposphere diminished quite substantially (Fig. 5.32d). Other forms of precipitation remained unchanged. Another emerging discovery is the increase in cloud-top height in the higher relative humidity scenario; this was predicted also for the continental case. The overall indirect effect of aerosols on all clouds (-16.32 $\pm$5.71 Wm^{-2}) under the high upper tropospheric humidity scenario is almost equal to that in the unperturbed humidity scenario.

In conclusion, upper tropospheric humidity has been found to have no unique role on aerosol indirect effect of clouds, but rather on the optical properties of clouds, mainly macro-physical properties (cloud fraction).

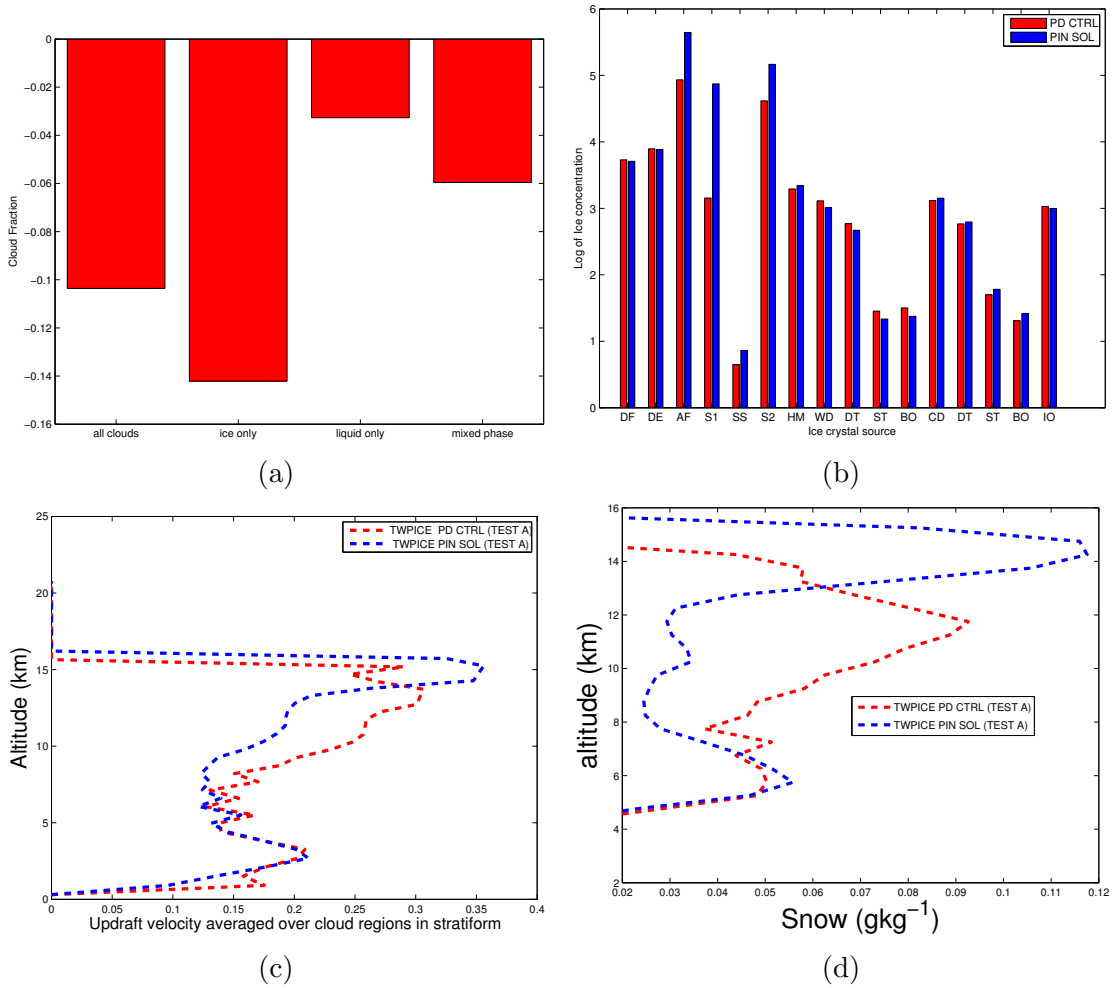

Figure 5.32: *(a) Cloud fraction, (b) ice number budgets, (c) updraft velocities in weak vertical velocities and (d) snow mixing ratio for different upper tropospheric relative humidity scenarios in TWPICE. The red curve represents the low humidity scenario while the blue curve represents the high humidity scenario.*

5.5 Summary

Cloud micro-/macro- physical and dynamical properties responded in various ways to increases in solute aerosol loadings from pre-industrial to present-day scenarios in both the mid-latitude continental case and the tropical maritime case.

The Mid-Latitude Continental Case - CLASIC

- Solute aerosol pollution amplified droplet concentrations by a factor of two, but the amplification factor was about half of the pollution factor. The extra cloud droplets competed for vapour, hence, diminished their mean sizes and warm rain processes. Also, crystal concentrations rose sharply above the -36°C level, owing to homogeneous freezing of cloud droplets and solute aerosols.

Significant increase in LWC was also predicted, while IWC diminished in the upper troposphere due to solute aerosol pollution.

- A weakening of strong convection was noted in the present-day free troposphere owing to increased gravitational burden rendered by increased condensate loading. However, a slight strengthening of cloud dynamics was noted for stratiform clouds, primarily because of the invigoration effect arising from the release of latent heat during homogeneous freezing of cloud droplets, evidenced by the warming of the upper troposphere by about 0.4 °C.

- On the macrophysical properties of the clouds, present-day clouds were more horizontally extensive, mainly mixed-phase clouds, primarily because riming and aggregation were less efficient in the polluted scenario. Another striking discovery was the proliferation of glaciated clouds in the present-day, especially mixed-phase clouds. Overall, the fraction and optical thickness of clouds were higher because of weak precipitation production in the polluted case.

- From the analysis of AIEs: (1), The AIE of glaciated clouds was about a factor of two higher than that of water-only clouds, owing to the fact that, they lie above water-only clouds, hence, they have the first interaction with radiation and also that they were more responsive to aerosol perturbation than water-only clouds. (2) The AIEs of ice-only clouds, is about a factor of two greater than that of mixed-phase clouds, primarily because of the same reasons explained above. (3) The albedo-emissivity effect of glaciated clouds is about a factor of five less than the lifetime effect of glaciated clouds. (4) In mixed-phase clouds, the aggregation AIE was a factor of two greater than the coalescence indirect effect, mainly because of enhanced glaciation in present-day clouds.

- Meteorology was found to play a very important role in the radiative properties of clouds: (1) Weakening of the wind shear caused a slight increase in the net fraction and optical thickness of clouds, hence, more SW radiation was reflected. (2) A humid upper troposphere increased the optical thickness of clouds, chiefly by boosting crystal concentrations but suppressing precipitation, hence, more SW radiation was reflected. (3) Finally, meteorology was found to have stronger influence on the properties of clouds than on aerosol-cloud interactions.

The Tropical Maritime Case - TWPICE

- A factor of four increase in droplet concentrations was predicted due to aerosol pollution, because in pristine environments, the droplet concentrations are controlled more by aerosol concentrations, than in a polluted case where they are driven more by updraft speeds. Water contents were lower than in the continental case, mainly because precipitation efficiency was higher in maritime clouds due to larger cloud particles. Overall, LWC increased steadily, while the IWC diminished quite significantly aloft.

- With solute aerosol pollution, the invigoration effect was weaker here than in CLASIC, owing to the weak homogeneous freezing of cloud droplets. This was evidenced by the weak response of vertical velocities to aerosol changes, because warm rain processes were not strongly perturbed in this case, therefore fewer extra cloud droplets were available for homogeneous freezing.

- Overall, there was an increase in vertical profile of cloud fraction chiefly through mixed-phase clouds and both horizontal fractions and optical thicknesses of clouds were higher in the present-day.

- As for radiative properties of clouds: (1) AIEs were higher than in continental clouds, i.e., a total AIE of -17.44 $\pm$6.1 Wm^{-2} was predicted in TWPICE, while only -9.46 $\pm$1.43 Wm^{-2} was predicted for CLASIC. (2) The contributions of both water-only and glaciated clouds to the net AIEs were equally important. (3) The ice-only clouds component of AIE had a positive radiative flux change at the TOA, while the mixed-phase component was negative and domineering the AIE of glaciated clouds. (4) The coalescence AIE was seen to dominate the aggregation indirect effect. (5) The thermodynamic AIE had a positive radiative flux change at the TOA, illustrating the absence of the formation of secondary cells of convection. (6) Finally, the albedo-emissivity effect was comparable to the lifetime AIE.

- On the role of meteorology on AIEs of glaciated clouds: (2) WWS reduced the horizontal coverage of clouds, thereby transmitting more SW radiation to the Earth's surface. (2) Higher upper tropospheric relative humidity caused a massive increase of the cloud fraction, hence, reflecting more solar radiation back to space. (3) As in the continental case, meteorology simply shifted systematically, the radiative properties of clouds and not significantly, the net AIEs.

Chapter 6

Influence of Solid Aerosols on Indirect Effects via Glaciated Clouds

Overall, the net impact of the solid aerosols in the present study was found to be relatively less pronounced compared to that of solute aerosols in both the continental and maritime cases. This mild behavior of the glaciation effect was chiefly due to the low number concentrations of solid aerosols compared to those of liquid ones and the relatively weaker anthropogenically induced increases of solid aerosols relative to solute aerosols. The microphysical processes leading to the glaciation effect are outlined in the following sections. The phrases, glaciation effect or glaciation indirect effect are used interchangeably in this section to refer to the response of microphysical and radiative properties of clouds to increases in number concentrations of solid aerosols.

6.1 Hypothesis

The overarching objective and hypothesis being tested in this chapter are to:

- Explore salient mechanisms of ice nucleation from extra ice nuclei and the hypothesized intensification of precipitation production via ice crystal processes, known as the *glaciation* effect.

  The hypotheses being tested here is that, solid aerosol pollution reduces the overall numbers of ice crystals in cirrus (cirrus clouds are being defined here as clouds existing above the homogeneous freezing level), by suppressing homogeneous freezing of cloud droplets. Also, that solid aerosol increases the ice crystal number concentrations in mixed-phase clouds by heterogeneous ice nucleation, thereby changing the phases (mainly from liquid to ice) and lifetimes of clouds in regions of clouds with weak vertical velocities (i.e. mixed-phase

regions typically).

6.2 Methodology

In order to investigate the glaciation indirect effect of solid aerosols, only the number and mass concentrations of solid aerosols from pre-industrial to present-day times were altered for the pre-industrial simulation, while the present-day simulation was the control simulation similar to the control simulation of the previous chapter. The same methodology applied for investigating the indirect effects of solute aerosols of adopting the results of Takemura (2012) to determine the pre-industrial aerosol loadings was used to estimate the pre-industrial loadings of solid aerosols as well (Table. 6.1). Tests A - D (Sect. 5.2) were repeated to isolate different aerosol indirect effects of solid aerosols on all clouds and on targeted cloud types. There was a challenge of eliminating the CCN activity of solid aerosols in the model without affecting the model microphysics. However, due to the low number concentrations of solid aerosol relative to solute aerosol, their effect on the warm clouds microphysics was assumed to be negligible. In order to prove this assumption, a further sensitivity test was carried out and is described in Sect. 6.5.

6.3 Results From The Mid-Latitude Continental Case (CLASIC)

As discussed earlier, anthropogenic emissions of solute aerosols had a strong contribution to the aerosol burden of continental atmospheres. Hence, strong modifications to the properties of continental clouds due to solute aerosol pollution were predicted. It is therefore necessary to investigate the importance of solid aerosols in altering the radiative properties of clouds. This section focuses on the glaciation effect in the CLASIC case; the TWPICE scenario is presented in the following section.

6.3.1 Response of Microphysical Properties to Increased Solid Aerosols

6.3.1.1 Initiation of Cloud Droplets

Cloud Droplet Concentrations

The intrinsic mean number concentration of cloud droplets was generally insensitive to anthropogenic increases in solid aerosols. The exception was in deep convection, where a slight increase in the number concentration of cloud droplets was predicted

Solid Aerosol material	Adjustment Factor
Dust/Metallic (DM)	0.89
Black carbon (Soot) (BC)	0.28
Non-Biological Organic (O)	0.67
Biological Aerosol (BIO)	0.67

Table 6.1: *Fractional changes of solid aerosol scenarios from pre-industrial (1850) to present-day (2000) for number and mass distributions (inferred from a global modelling study of the distribution of aerosols aerosol from pre-industrial to present-day scenarios Takemura (2012)).*

(Fig. 6.1a), in subzero temperatures when solid aerosol were increased. This weak increase in mean number concentration of cloud droplets was attributed to the internal mixing of solid aerosols with soluble components of CCNs, which is assumed in the microphysics scheme. Thus, extra solid aerosols initiate extra cloud droplets. However, the contribution of this slight increase of the number concentrations of cloud droplets in convective cores was too small to influence the overall count of cloud droplets owing the their low number concentration relative to solute aerosol. Even the unconditional averages of concentrations cloud droplets over the whole domain were insensitive to changes in loadings of solid aerosol changes.

Cloud Droplet Sizes

Cloud droplets showed a reduction in their mean sizes of up to 1 μm when solid aerosols were increased (Figs. 6.1c). This reduction in mean sizes occurred mostly in subzero temperatures, coinciding with the region where increases in droplet numbers in deep convection were noted. Since this reduction in the mean sizes of cloud droplets is more pronounced than the predicted increase in cloud droplet numbers, then another competing mechanism is responsible for the more pronounced reduction in cloud droplet sizes. Analysis of the ice crystal properties showed that, their number concentrations in the mixed-phase region was higher in the present-day, yet their mean sizes were unchanged. Therefore, the Bergeron-Findeisen processes might have contributed to this reduction in cloud droplet sizes.

6.3.1.2 Initiation of Cloud-Ice

Ice-Crystal Concentrations

Expectedly, the highest number concentration of ice crystals was predicted in convective cores due to the high supersaturations relative to stratiform clouds. However, because of the prevalence of glaciated clouds in weak vertical velocities relative to deep convection, the average concentrations of ice crystal in the whole domain are

controlled by glaciated clouds in vertical velocities that are weak. When the number concentration of solid aerosols was raised, a weak reduction in the number concentration of ice crystals was predicted aloft (Fig. 6.1b), mostly from clouds in regions of weak vertical velocities (updrafts speeds $< 1\text{m s}^{-1}$), supporting the hypothesis which was being tested that, solid aerosols reduce crystal concentrations aloft by suppressing homogeneous freezing of cloud droplets.

The ice crystal number budget (Fig. 6.2a) showed notable increases in heterogeneous nucleation of ice crystals mostly within the temperature range of mixed-phase clouds. The largest percentage increase in ice nucleation was predicted for soot; however, its contribution to the overall budget of ice crystals that were nucleated heterogeneously is about an order of magnitude less than that of dust. Although substantial increase in ice crystals that were heterogeneously nucleated was predicted, their influence on the overall microphysical properties of ice crystal was mild. The primary reason for this mild response of ice crystal number concentration to increases in solid aerosols is that, heterogeneous ice nucleation is not the dominant source of ice crystals; rather, homogeneous droplet and aerosol freezing prevail.

Ice-Crystal Sizes

There were no substantial changes to the mean sizes of ice crystals, although it was apparently shown that under conditions of increased solid aerosols, the overall sizes of ice crystals were relatively smaller (Fig. 6.1d) than those under pre-industrial solid aerosol conditions. This reduction in ice crystal sizes is obviously due to increased competition for available vapour by ice crystals, but the sparing reduction in the mean sizes of ice crystals indicate that other processes such as the Bergeron-Findeisen process help ice crystals to maintain their average sizes. Also, other ice multiplication processes such as the Hallett-Mossop mechanism and homogeneous freezing of solute aerosols and cloud droplets can buffer the microphysical effects of increased solid aerosols on ice properties. For instance, in this case study, Hallett-Mossop splinters were diminished by increased solid aerosols.

6.3.1.3 Water Contents

Figures 6.2c and 6.2d show the liquid and ice mixing ratios, respectively. No significant change in the mixing ratios of cloud liquid were predicted when solid aerosol concentrations were increased. However, a marked decrease in the mixing ratios of cloud ice under increased solid aerosol conditions was noted in the upper troposphere. This reduction in upper tropospheric ice mixing ratio was attributed to the weakening of deep convection when solid aerosol concentrations were raised,

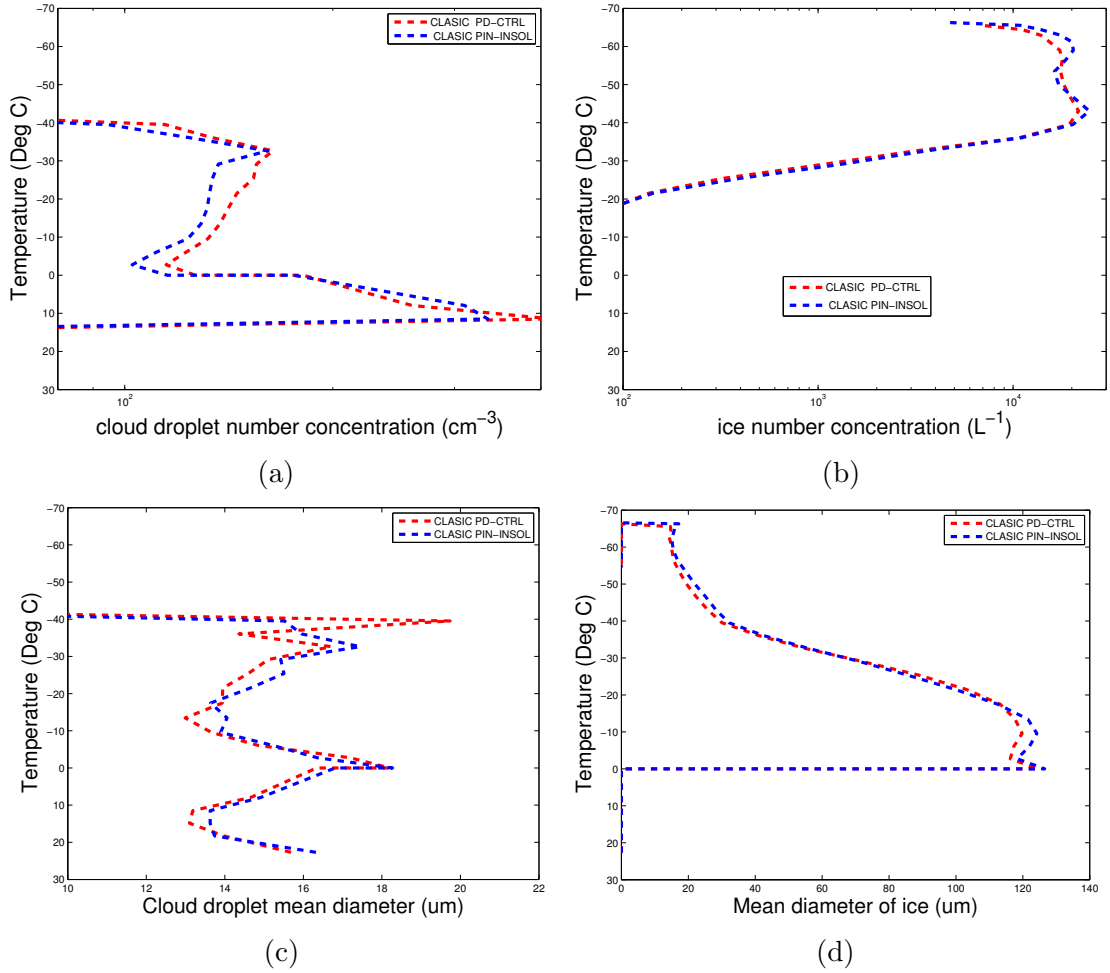

Figure 6.1: *The vertical profiles of (a) cloud droplet number concentrations, (b) ice crystal number concentrations (c) mean droplet sizes and (d) mean ice crystal sizes from the glaciation effect in CLASIC.*

because deep convective clouds can detrain moisture and ice into the upper troposphere. But in these simulations, it was shown that when solid aerosols were increased, the cloud-tops slightly shifted downwards, causing the reduction in ice mixing ratio aloft.

6.3.1.4 Precipitation Production

Contrary to the generally accepted idea that the glaciation effect increases precipitation production, it emerged from this research that, both snow and graupel production decreased significantly in the present-day simulation (Figs. 6.3a and 6.3b). This rather unexpected outcome emerged, despite the fact that no substantial changes to droplet and ice crystal sizes were predicted when solid aerosols were increased.

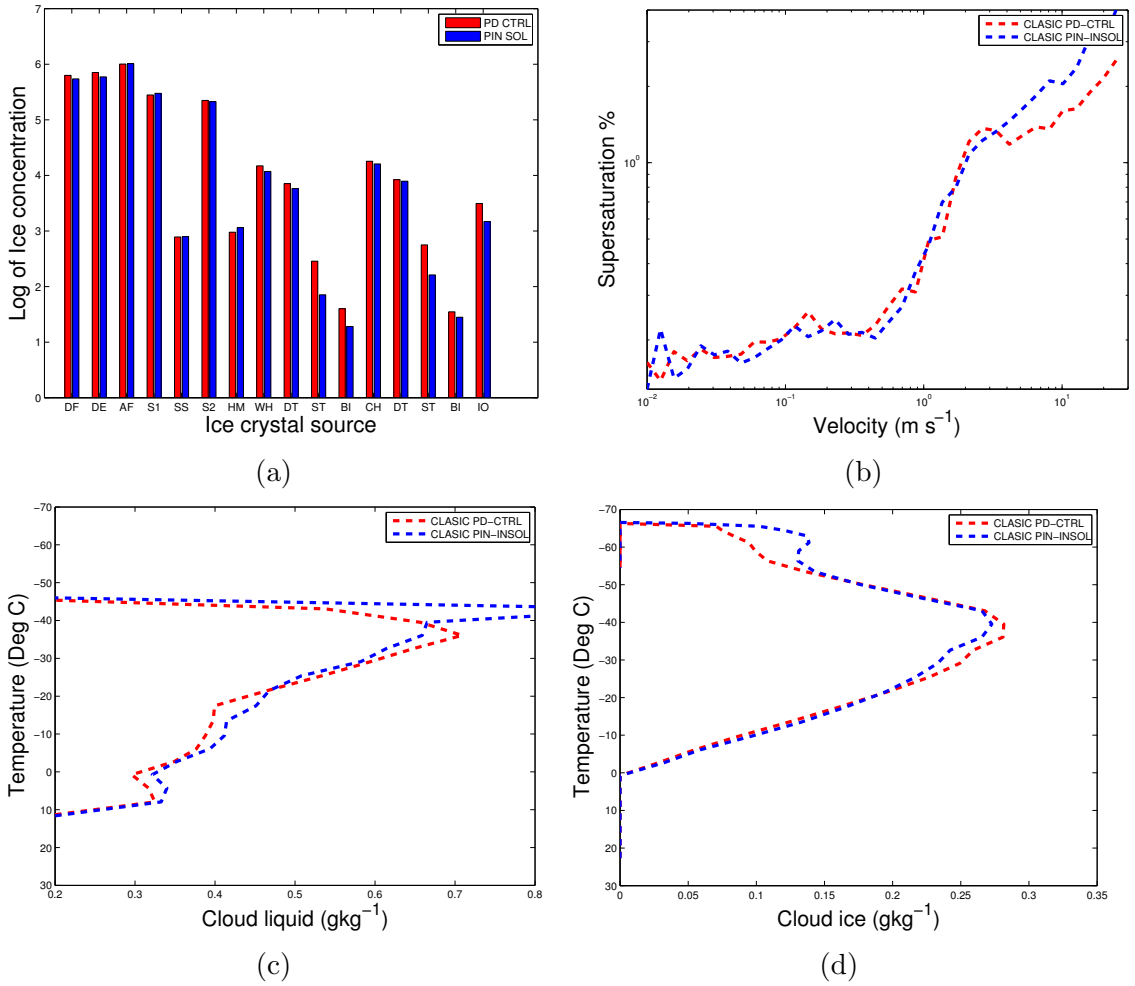

Figure 6.2: *(a) Ice number budget, (b) Water supersaturations as a function of vertical velocity conditionally averaged over the whole column, (c) cloud mass-mixing ratios and (d) ice mass mixing ratio unconditionally averaged in all clouds from CLASIC. Meanings of abbreviations in (d) DF = droplets frozen homogeneously, DE = droplets evaporating during homogeneous freezing, AF = aerosols frozen homogeneous, (S1, SS, S2) droplets in 1st mode of SO4, sea-salt, 2nd mode of SO4 aerosols, respectively, that froze homogeneously. HM = H-M splinters, WH = total crystals from Warm Heterogeneous nucleation (Condensational, Depositional, and Immersion at temperatures > -30 °), (DT, ST, BO, SO) crystals by Warm Heterogeneous nucleation of dust, soot, biological organics and soluble organics, respectively. CH = total crystals from Cold Heterogeneous nucleation (Condensational, Depositional, and Immersion at temperatures < -30 °), (DT, ST, BO, SO) crystals by dry deposition from dust, soot, and biological organics and soluble Organics, respectively. Finally, OI and IO stand for total ice crystals from Outside-In and Inside-Out Contact freezing.*

This is surprising, primarily because increased solid aerosols are expected to increase IN concentrations and hence, ice number concentrations. When ice number concentrations rise, precipitation production would be expected to rise as well, especially through the ice-phase in mixed-phase clouds (owing mostly to the Bergeron-

Findeisen process), this was however not the case in this mid-latitude continental case, rather all forms of precipitation were suppressed by increases in solid aerosols. This reduction in precipitation production was attributed to the reduction in the mean sizes of cloud particles, especially of cloud droplets. With smaller cloud particles, processes such as riming and aggregation, which produce precipitation become less effective. Warm rain production was largely unchanged, although a bias towards suppressed production was evident.

6.3.2 Response of Cloud Dynamical Properties to Increased Solid Aerosols

Figures 6.3c and 6.3d present the dynamical effects induced by the glaciation effect. Apparently, the increase in solid aerosol concentration significantly suppressed strong updrafts, although it had little effect on the intensity of weak vertical velocities. Ideally, it was expected that more solid aerosols would enhance condensational/depositional heating from condensational/depositional growth of ice crystals, which would then increase the strength of convective updrafts, but since the change in droplet number concentration was almost negligible, then the effectiveness of condensational heating was negligible. What was rather discovered was on one hand, the suppression of strong downdrafts (Fig. 6.3c), and on the other hand, the glaciation effect slightly strengthened slow updrafts (i.e. vertical velocity $< 1\text{m s}^{-1}$) mainly in the upper troposphere (Fig. 6.3d). The cause for this weak invigoration of slow updrafts in cirrus clouds was the release of latent heat during depositional growth of ice crystals. In addition, this important finding introduces new insights into the areas of influence of the glaciation effect.

6.3.3 Response of Cloud Coverage to Increased Solid Aerosols

6.3.3.1 Ascent dependent Vertical Profiles of Cloud Fraction

Fig. 6.4 shows the vertical profiles of cloud fractions for the three different types of cloud phases conditionally averaged in regions of both strong and weak vertical velocities. The fraction of deep convective ice-only clouds was higher for the increased solid aerosol simulation than for the pre-industrial simulation, while the opposite was true for the weak vertical velocities (Figs. 6.4a and 6.4b, respectively). This finding was attributed to the fact that both intrinsic snow and graupel production in deep convective clouds decreased with solid aerosol pollution, while no significant changes were noted in weak vertical velocities (plots not shown). The main mechanism for the reduction in cloudiness of ice-only clouds in weak vertical velocities is the weakening of strong vertical velocities, which reduces the amount of water that

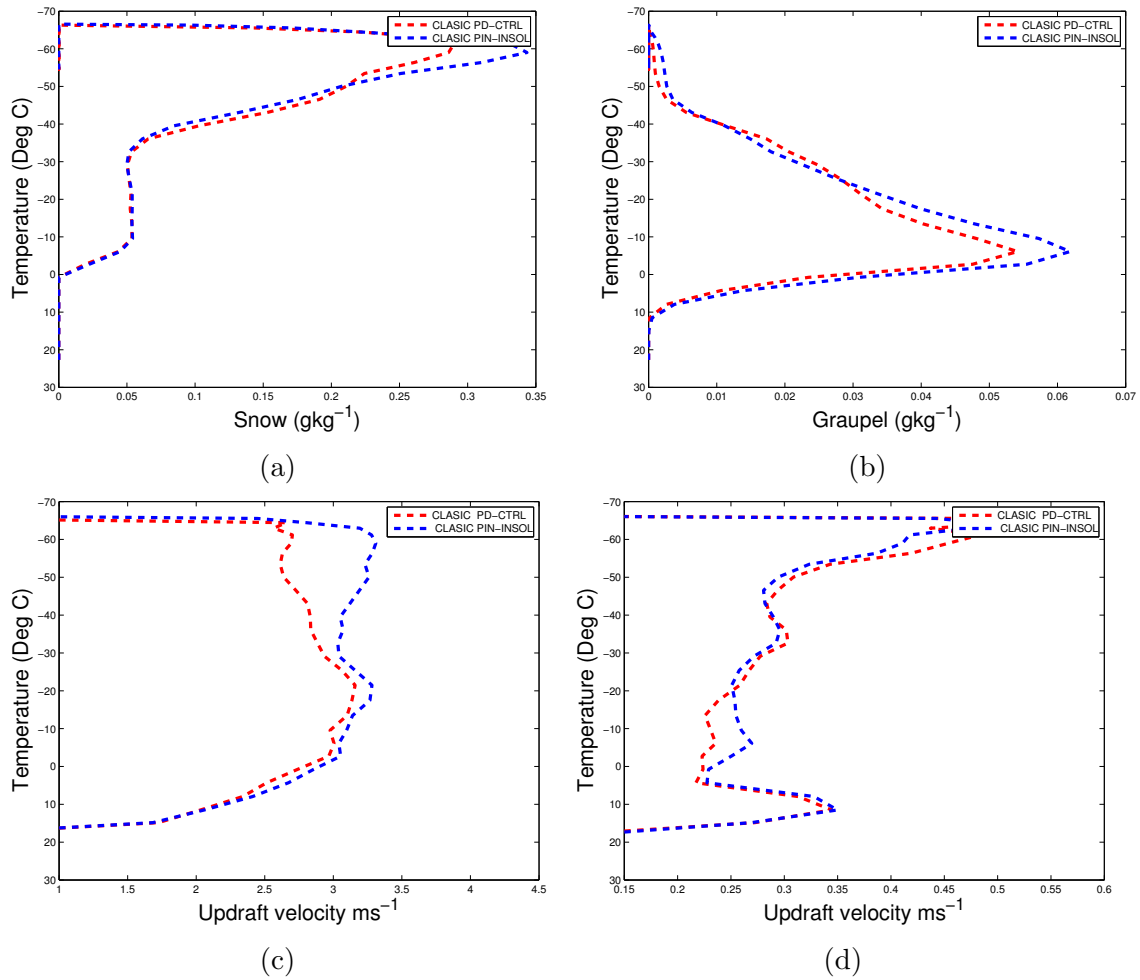

Figure 6.3: *Changes in (a) snow and (b) graupel average mixing ratios and positive (updrafts) ascent conditionally averaged over (c) deep convective clouds ($\omega > 1ms^{-1}$) and (d) clouds with weak vertical velocities ($\omega < 1ms^{-1}$) (bottom) in CLASIC, respectively.*

is detrained into the upper troposphere in the form anvil outflow into cirrus clouds as evidenced by the reduction in upper tropospheric IWC that was predicted by the control run.

As for mixed-phase clouds, an increase in vertical profiles of cloud fractions was predicted in both strong and weak vertical velocities, with the dominant increase being in stratiform clouds (Figs. 6.4c and 6.4d, respectively). This finding was strongly attributed to increases in IWC in mixed-phase clouds (caused by the increase in heterogeneous ice nucleation in mixed-phase clouds) and also to the trends of snow and graupel production in both strong and weak vertical velocities as described above. Interestingly, solid aerosol pollution showed no significant effect to the vertical profiles of fractions of water-only clouds.

6.3.3.2 Horizontal Cloud Fraction

Unexpectedly, the overall change in horizontal cloud fraction over the whole domain rose slightly due to solid aerosol pollution, although, different types of phases of clouds responded with different magnitudes of increases in cloud fractions (Fig. 6.5a). Mixed-phase clouds also exhibited the highest increase in horizontal cloud fraction, which is also in agreement with the findings of Fig 6.4. The main reason for this increase in the total horizontal fraction of clouds was the suppression of precipitation production, especially of snow and graupel.

The volumetric cloud fraction also exhibits similar trends as the horizontal cloud fraction, which simply means that there was an increase in the number of cloudy grid-boxes when the loading of solid aerosols was raised. It is noteworthy that the volumetric cloud fraction of ice-only clouds showed a significant decrease with solid aerosol pollution. This decrease is mainly attributed to the reduction in vertical profiles of cloud fraction of ice-only clouds in weak vertical velocities (Fig. 6.4b) and also a reduction in upper tropospheric IWC. This finding of an increase in horizontal cloud fractions exhibited by all clouds in this mid-latitude continental case is contrary to the widely accepted understanding that, the glaciation indirect effect favors the 'Bergeron-Findeisen' process, which in principle, should diminish the liquid-phase components of the clouds and increase precipitation via the ice-phase.

6.3.4 Response of Cloud Optical Properties to Increased Solid Aerosols

Figs. 6.5c and 6.5d show the intrinsic and domain-wide changes in the optical thicknesses between pre-industrial and present-day scenarios of solid aerosols. When solid aerosols were increased, the intrinsic optical thicknesses of clouds were generally lower except for those of liquid-only clouds, while unconditional averages of the optical thicknesses of clouds were higher in the control run. This behavior of the intrinsic optical thicknesses of clouds is attributed to the fact that, both the horizontal and volumetric cloud fractions and also the domain-wide optical thicknesses of clouds increased with increased solid aerosols. In other words, clouds became more extensive but optically thinner due to solid aerosol pollution.

6.3.5 Response of Radiative Fluxes and Cloud Radiative Properties to Increased Solid Aerosols

Generally, the common expectation of the glaciation effect is that it should enhance glaciation of the cloud, because at any given sub-zero temperature, the supersatu-

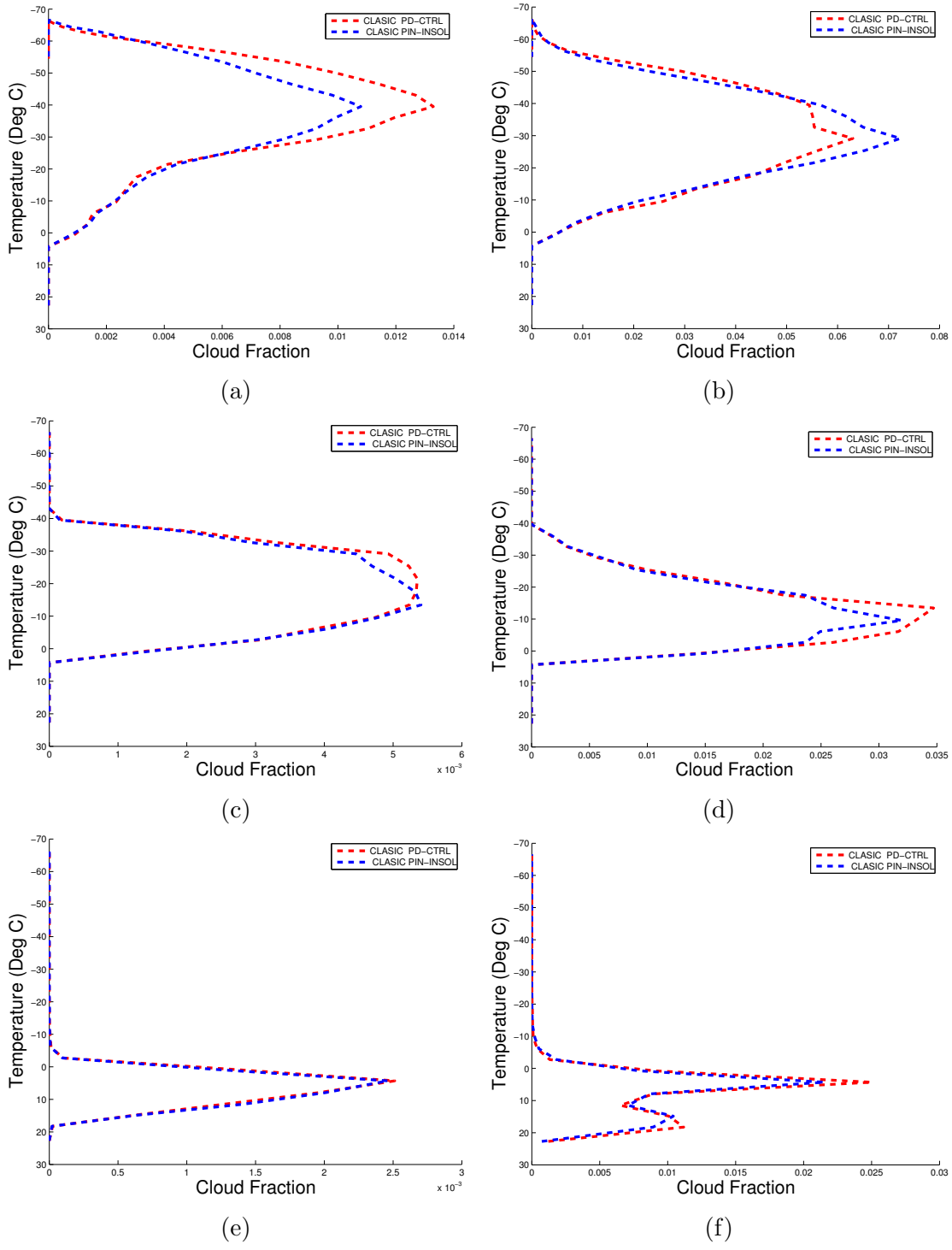

Figure 6.4: *Vertical profile of cloud fraction for all three types of phase of clouds, conditionally averaged over regions of strong vertical velocities (vertical velocity* $\omega >= 1ms^{-1}$*) (left) and weak vertical velocities (vertical velocity* $\omega < 1ms^{-1}$*) (right) in CLASIC. (a) and (b) are for ice-only clouds, (c) and (d) are for mixed-phase clouds, (e) and (f) are for liquid-only clouds, for CLASIC solid aerosol effects.*

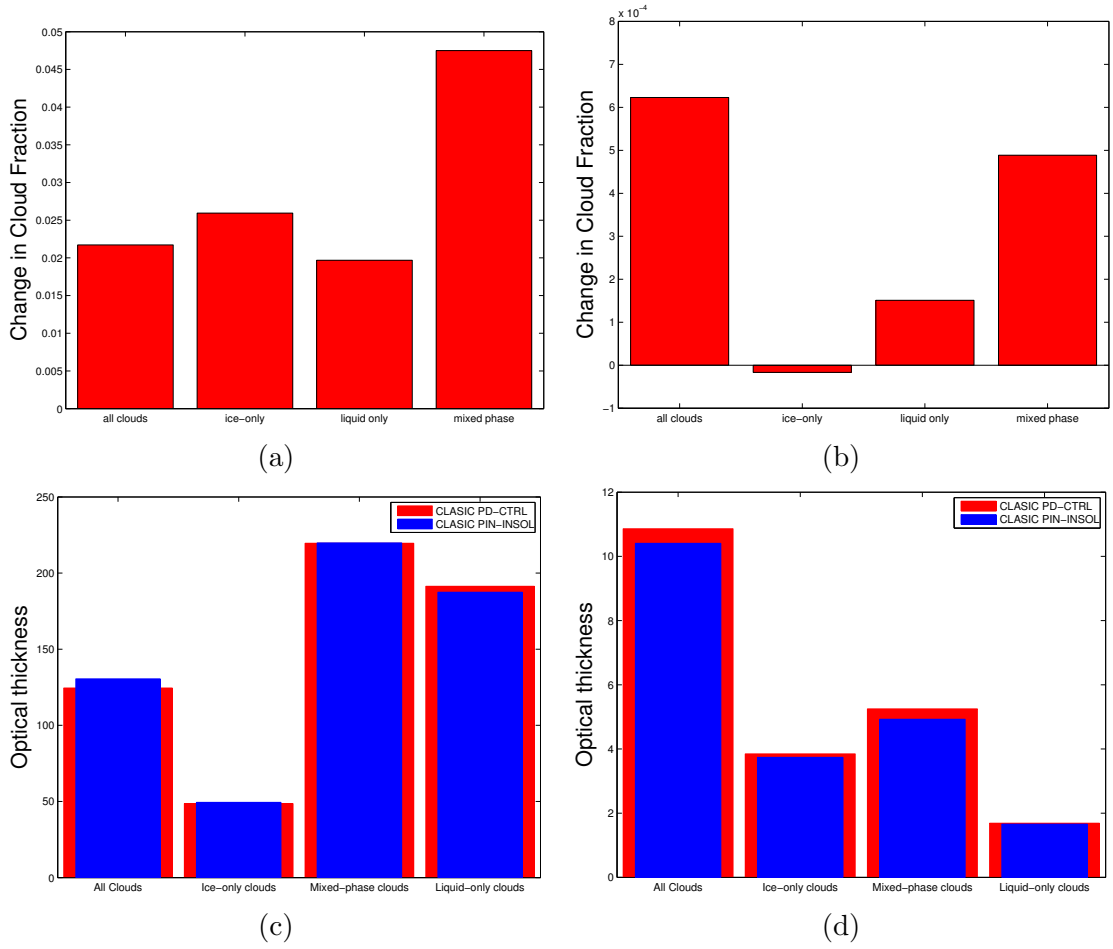

Figure 6.5: *Changes in horizontal cloud fractions and volumetric cloud frations are presented in (a) and (b), respectively and the intrinsic and unconditionally averaged optical thicknesses of clouds are presented in (c) and (d), for all the three types of phase of clouds in CLASIC.*

ration over an ice surface is lower than that over a water surface (Rogers and Yau, 1991), thus, the presence of ice crystals in a cloud tends to boost precipitation production via the ice phase. This increase in precipitation production is chiefly caused by the presence of ice in an environment that is almost always ice supersaturated. Since the latent heat of sublimation is higher compared to that of evaporation, water droplets tend to evaporate first when the environment becomes sub-saturated, keeping the environment close to water saturation and ice supersaturation. Thus, a mixed-phase cloud tends to stay supersaturated over an ice surface, causing rapid growth of ice crystals and ice-phase precipitation. Consequently, the lifetime of the cloud is bound to shorten under such a scenario.

This was however not the case in this study - all forms of precipitation diminished in the present-day simulations. Figure 6.6 shows the radiative flux changes arising

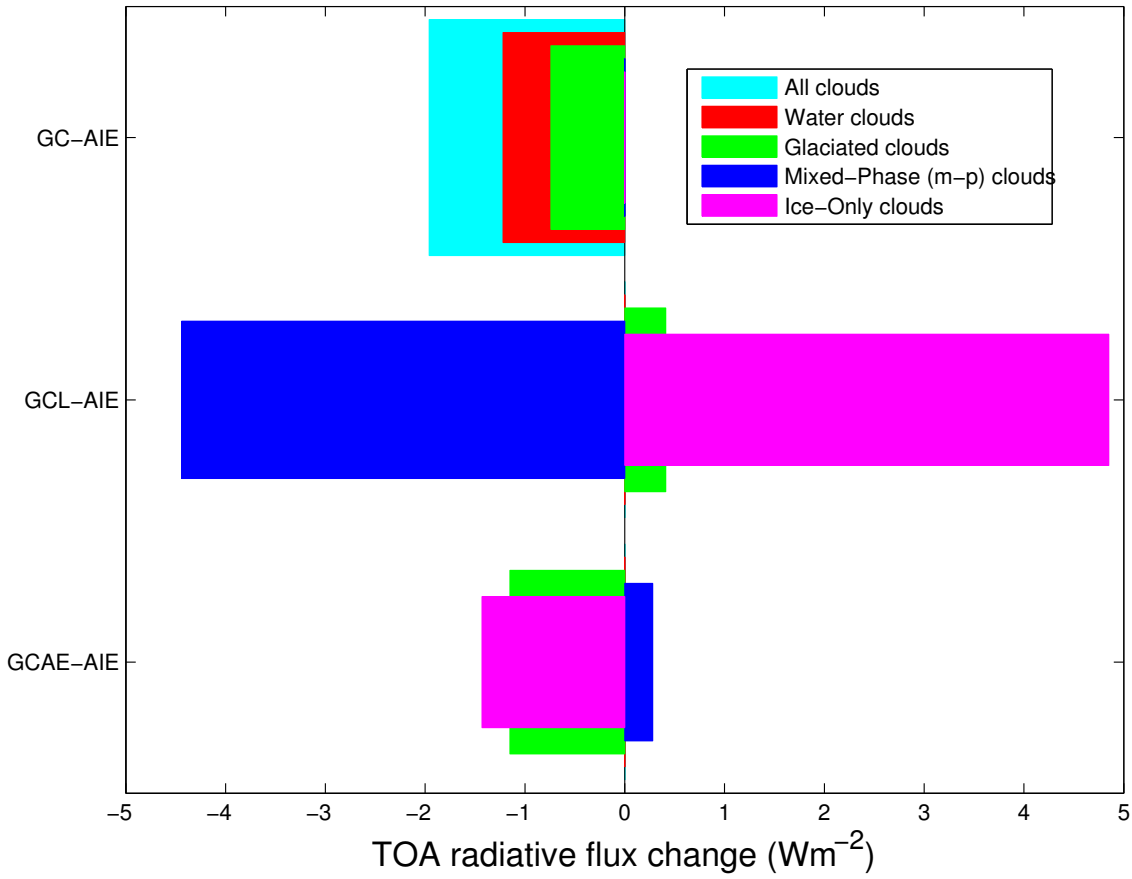

Figure 6.6: *The glaciation aerosol indirect effect, arising from increasing solid aerosol concentrations in CLASIC. Meanings of abbreviations: GC-AIE = Glaciated Clouds AIE, GCL-AIE = Glaciated Clouds Lifetime AIE, GCAE-AIE = Glaciated Clouds Albedo-Emissivity AIE.*

from boosting solid aerosol concentrations from pre-industrial times to present-day. It is noted that the glaciation indirect effect had a net cooling effect of about -1.96 $\pm$0.29 Wm^{-2} on the climate system. It can therefore be inferred that in our simulations, anthropogenic pollution of the atmosphere by solid aerosols in continental clouds has the same effect as the anthropogenic pollution of the atmosphere by solute aerosols. The only notable difference is that, solid aerosols modified the radiative properties of clouds less significantly compared to solute aerosols. This was primarily because solute aerosols were more abundant in terms of mass and number concentrations than solid aerosols. In this mid-latitude continental case, an increase in the fraction the unconditionally averaged optical thicknesses of all cloud types was predicted by the model when the number concentrations of solid aerosols were increased. This increase in the cloud fraction and the unconditionally averaged optical thicknesses increases the amount of solar radiation that is reflected back to

space.

Unlike in the case of increased solute aerosols, where the contribution to radiative flux changes from water-only clouds was smaller than that from glaciated clouds, the contribution from water-only clouds (-1.22 $\pm$0.18 Wm^{-2}) is higher than the contribution from glaciated clouds (-0.74 $\pm$0.11 Wm^{-2}) in the case of increased solid aerosols. This was the result despite an increase in the cloud fraction of glaciated clouds, Fig. 6.5c shows that the intrinsic optical thickness of glaciated clouds aloft has actually diminished. Thus, the presence of optically thin clouds at the top, causes transmission of more short-wave radiation to lower level clouds, hence, lower level clouds tend to take much control of the net radiative flux changes.

Despite the net increase in cloud fraction of ice-only clouds due to solid aerosol pollution, the net radiative flux change at the TOA of ice-only clouds is positive (3.42 $\pm$0.51 Wm^{-2}). This positive TOA flux change is attributed to the reduction in the optical thickness of ice-only clouds. It is not surprising to have a reduction of the optical thickness of ice-only clouds, because the ice mixing ratio diminished as well in the upper troposphere (Fig. 6.2d), while the liquid mixing ratio was largely insensitive to perturbations of solid aerosols. A slight reduction in mean sizes of cloud particles was noted (Figs. 6.1c and 6.1d) and as a result, a cooling effect from the albedo-emissivity effect (-0.74 $\pm$0.11 Wm^{-2}) that is commensurate with the magnitude of the decrease in the predicted particle sizes was predicted.

6.4 Results From The Tropical Maritime Case (TWPICE)

In order to examine the glaciation effect under a maritime scenario, the pre-industrial loading of solid aerosols was inferred from current aerosol loadings of TWPICE. As argued earlier, anthropogenic emissions of aerosols had little effect on the burden of remote maritime atmospheres; hence, only minimum modifications to cloud properties resulted. Nonetheless, it was remarkable to note that even with those minimal increases, solid aerosols indeed made a significant impact on the properties of maritime clouds. However, most fields (of cloud properties) remained unchanged despite increases in solid aerosol loadings. Thus, only those fields that responded to the perturbations of solid aerosols are presented here.

6.4.1 Response of Microphysical Properties to Increased Solid Aerosols

6.4.1.1 Initiation of Cloud Droplets

Cloud Droplet Concentrations

Both the conditional and unconditional averages of the number concentrations of cloud droplets were less sensitive to increases in the loading of solid aerosols, although a slight increase was noted especially in the lower troposphere (Fig. 6.7a). Just as in the continental case, this insensitivity is primarily due to the small number concentrations of solid aerosols relative to solute aerosols (Fig. 4.3), while the slight increases are attributed to the droplet nucleation by extra solid aerosols because of their internal mixing which is assumed in the model.

Cloud Droplet Sizes

As a result of the little changes to the number concentrations of cloud droplets noted above, the mean sizes of cloud droplets showed no significant response as well (Fig. 6.7c). This result is different from the continental case where a more pronounced reduction in the mean sizes of cloud droplets was noted, and was attributed to the Bergeron-Findeisen mechanism. In this maritime case, there is no evidence of that effect, hence, the predicted slight reduction in mean sizes of cloud droplets is strongly attributed only to the slight increase in droplet concentration.

6.4.1.2 Initiation of Cloud-Ice

Ice-Crystal Concentrations

Although the number concentrations of cloud droplets were less sensitive to increases in solid aerosols, there was a substantial increase in the number concentrations of ice crystals in the upper troposphere (Fig. 6.7b). The ice number budget shows an increase in the heterogeneous nucleation of ice crystals, especially by soot and biological organic aerosols (Fig. 6.8a). It is noteworthy that the heterogeneous ice nucleation only proliferated at temperatures greater than -30 °C, while it actually weakened at colder temperature. The reduction of the crystal concentrations at colder temperatures was attributed to the reduction in the IN activity of dust and primary biological aerosols at those temperatures when solid aerosol loading was raised. A slight increase in the number of droplets that froze homogeneously was also predicted.

The increase in the number concentrations of ice crystals in the upper troposphere is strongly attributed to homogeneous freezing of cloud droplets. Firstly, because it occurred above the homogeneous freezing level, and secondly, because the

heterogeneous nucleation of ice crystals at colder temperatures actually diminished in the present-day. The strengthening of cloud dynamics especially in the upper troposphere (Sect. 6.4.2) facilitated the homogeneous freezing of cloud droplets by vertically transporting supercooled cloud droplets above freezing levels, and also by vertically advecting ice crystals (nucleated in the lower troposphere) to upper levels of the troposphere.

Ice-Crystal Sizes

The mean sizes of ice crystals were unchanged below the homogeneous freezing level, however, in the upper troposphere, a reduction was predicted when solid aerosol concentrations were raised (Fig. 6.7d). This was attributed to increased competition for vapour, owing to increased concentrations of ice crystals within the same range of altitudes. Another conclusion to draw from Figs. 6.7d and 6.7b is the upward shift in the cirrus tops, which is attributed to the increase in the strength of cloud dynamics in the upper troposphere when solid aerosol concentrations were boosted (Sect. 6.4.2).

6.4.1.3 Water Contents

The liquid mixing ratio was barely sensitive to perturbations of solid aerosols (Fig. 6.8c), however, the mean mixing ratios of ice in the present-day showed a slight reduction and an upward shift of the cloud-top in the upper troposphere (Fig. 6.8d). Apparently, the upward shift in the cloud-top was more pronounced in stratiform clouds relative to deep convective clouds. The most significant reduction in upper tropospheric ice mixing ratio was in deep-convective clouds. The notable sink for this cloud ice was the enhanced snow production that was distinct in the upper troposphere when solid aerosol concentrations were raised (Sect. 6.4.1.4).

6.4.1.4 Precipitation Production

Unlike in the mid-latitude continental case where all types of precipitation were suppressed when solid aerosol concentrations were raised, in this tropical maritime case, there was a strong increase in snow mixing ratios (of both conditional and unconditional averages) when solid aerosol concentrations were raised (Fig. 6.9a). The increases in the production of snow were widespread, i.e., they were predicted equally in both stratiform and convective clouds, although, in terms of cloud types, the dominant increases were noted in ice-only clouds compared to mixed-phase clouds.

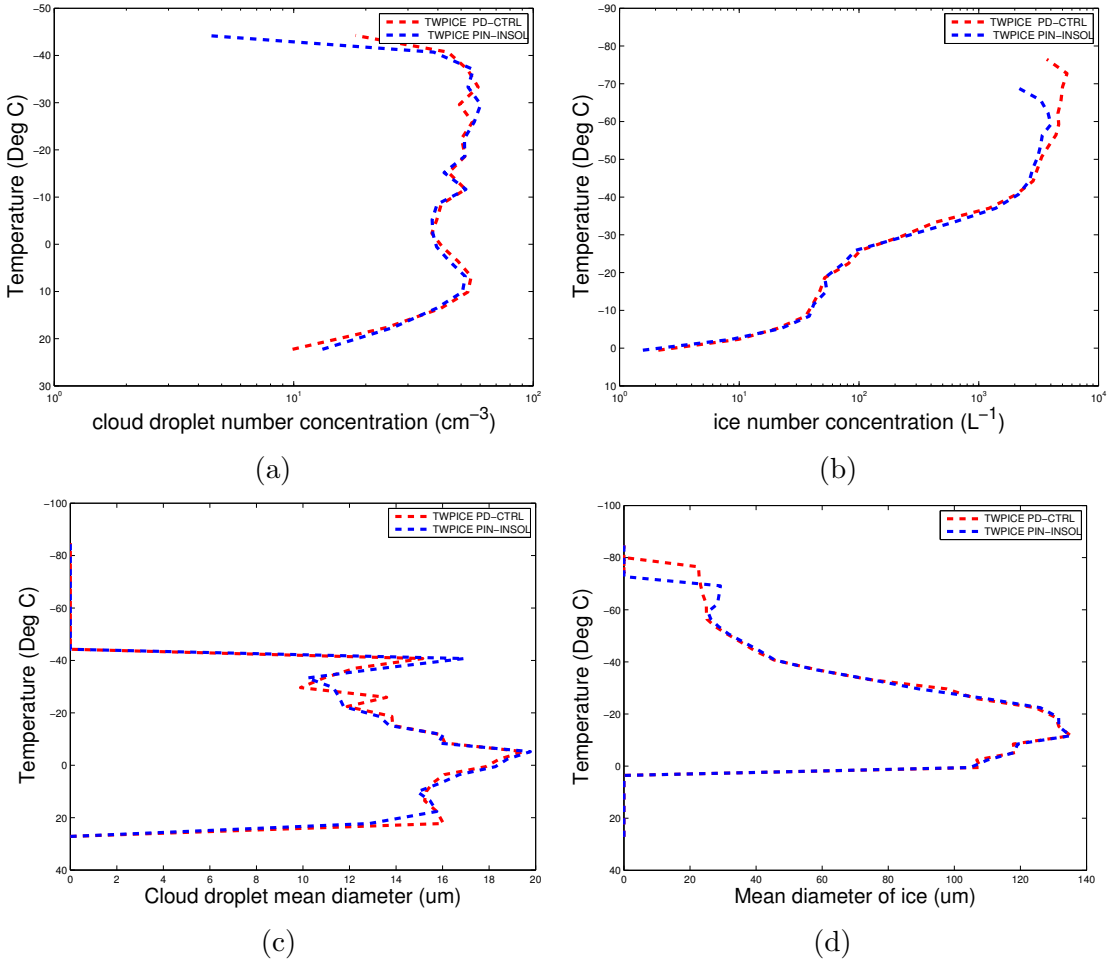

Figure 6.7: *The vertical profiles of (a) cloud droplet number concentrations, (b) ice crystal number concentrations (c) mean droplet sizes and (d) mean ice crystal sizes from the glaciation effect in TWPICE.*

The main mechanism through which high snow production was predicted in the increased solid aerosol case was the increase in upper tropospheric concentrations of ice crystals. Since the reduction in the mean sizes of ice crystals aloft was not commensurate with the increase in the number concentrations of ice crystals (i.e. the reduction of crystal sizes was mild relative to the increase in crystal concentrations), then aggregation was enhanced and snow production increased as a result. Also, the increase in the cloud-top height due to solid aerosol pollution deepened the depth within which ice crystals could grow and interact to form snow.

Graupel (Fig. 6.9b) and rain (plot not shown) mixing ratios remained largely un-altered, primarily because of their dependence on mean sizes of cloud particles, which have been less sensitive to solid aerosol pollution. Nonetheless, a bias towards low mixing ratios in solid aerosol pollution for both graupel (especially in convective clouds) and rain was noted.

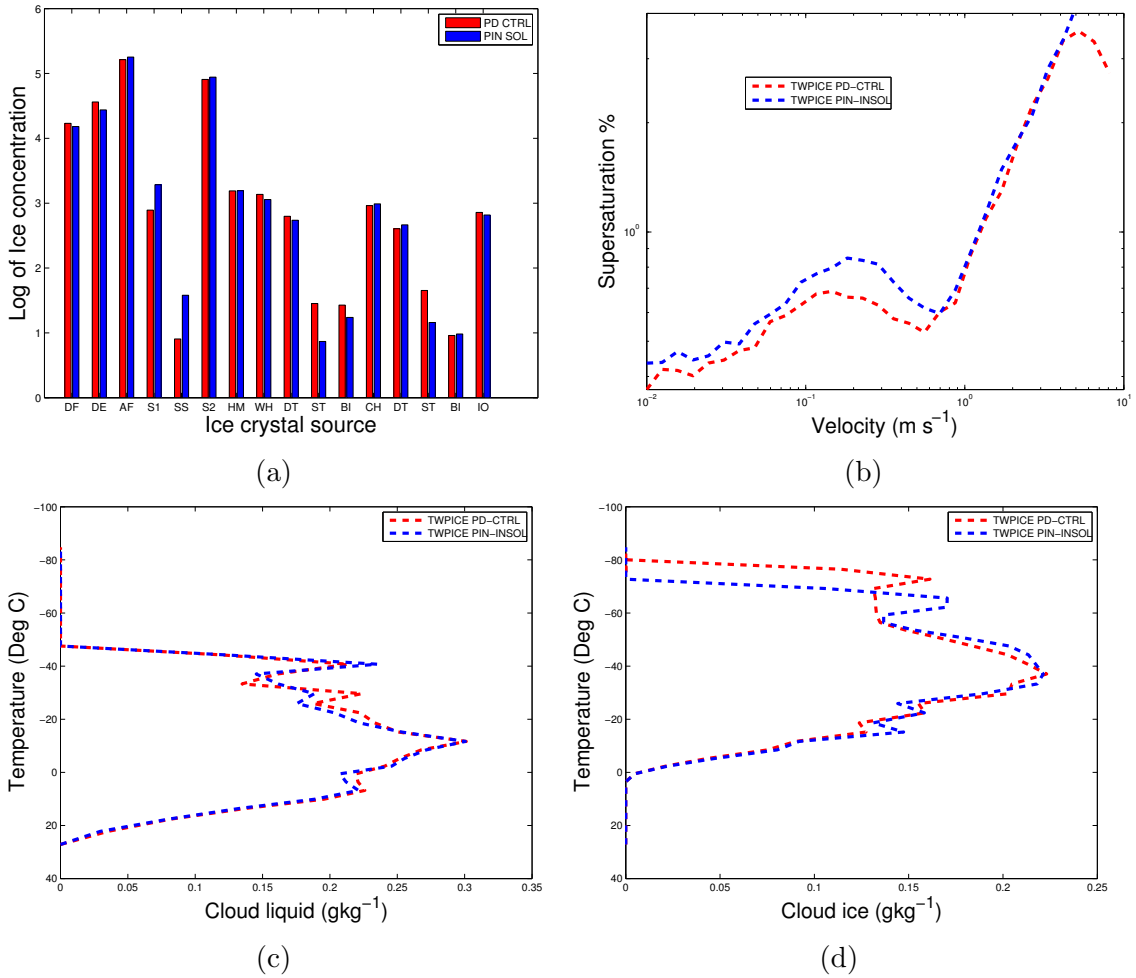

Figure 6.8: *(a) Ice number budget, (b) Water supersaturations as a function of vertical velocity conditionally averaged over the whole column, (c) cloud mass-mixing ratios and (d) ice mass mixing ratio unconditionally averaged in all clouds from TWPICE. Meanings of abbreviations in (a) DF = droplets frozen homogeneously, DE = droplets evaporating during homogeneous freezing, AF = aerosols frozen homogeneous, (S1, SS, S2) droplets in 1^{st} mode of SO4, sea-salt, 2^{nd} mode of SO4 aerosols, respectively, that froze homogeneously. HM = H-M splinters, WH = total crystals from Warm Heterogeneous nucleation (Condensational, Depositional, and Immersion at temperatures > -30 °), (DT, ST, BO, SO) crystals by Warm Heterogeneous nucleation of dust, soot, biological organics and soluble organics, respectively. CH = total crystals from Cold Heterogeneous nucleation (Condensational, Depositional, and Immersion at temperatures < -30 °), (DT, ST, BO, SO) crystals by dry deposition from dust, soot, and biological organics and soluble Organics, respectively. Finally, OI and IO stand for total ice crystals from Outside-In and Inside-Out Contact freezing.*

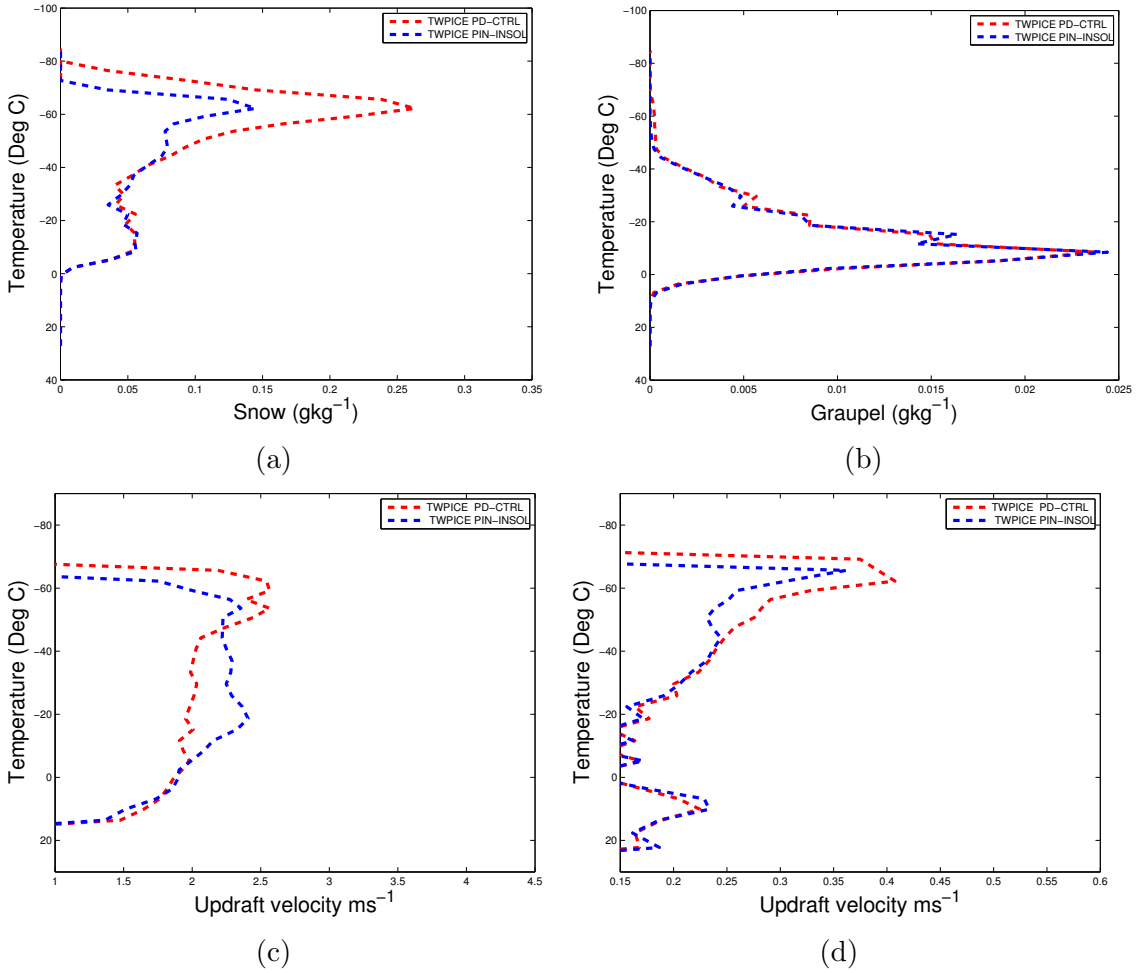

Figure 6.9: *Changes in (a) snow and (b) graupel average mixing ratios and positive (updrafts) ascent conditionally averaged over (c) deep convective clouds ($\omega > 1ms^{-1}$) and (d) clouds with weak vertical velocities ($\omega < 1ms^{-1}$) (bottom) in TWPICE, respectively.*

6.4.2 Response of Cloud Dynamical Properties to Increased Solid Aerosols

Overall, cloud dynamics was strengthened significantly in the upper troposphere in both weak and strong vertical velocities when the solid aerosol burden was increased (Figs. 6.9c and 6.9d, respectively). However, there was generally no change in the strength of slow updrafts in the lower troposphere. The source of energy for the strengthening of cloud dynamics aloft is the latent heating released during homogeneous freezing of cloud droplets and during depositional growth of ice crystals. As a result of the strengthened updrafts, cloud-tops were shifted upwards in the present-day, because strong updrafts have the potential to force air-parcels to overshoot cloud-tops due to their high momentum. The strength of strong updrafts in the middle troposphere was however weaker in the simulation with increased solid aerosol concentrations. This finding was attributed to increased gravitational

burden because of higher snow mixing ratios in the control simulation.

6.4.3 Response of Cloud Coverage to Increased Solid Aerosols

6.4.3.1 Ascent dependent Vertical Profiles of Cloud Fraction

Figure 6.10 shows the vertical profiles of cloud fraction for all the three phases of clouds for both convective and stratiform clouds. The main conclusion to draw from the figure is that there is very little response of clouds arising from solid aerosol perturbation. The exception is in glaciated clouds in deep convection, where slight increases in cloud fraction were predicted due to increased solid aerosols. This finding is attributed to the increase in ice crystal number concentrations arising from enhanced homogeneous freezing of cloud droplets due to solid aerosol pollution.

All other regimes of clouds shown in Fig. 6.10 have shown slight decreases in horizontal cloud fractions when concentrations of solid aerosols were increased. But as seen from the figure, the propotions of deep convective clouds to the total cloud fraction in the domain is about an order of magnitude less than that of stratiform clouds, hence, stratiform clouds control the domain-wide averages of cloudiness.

6.4.3.2 Horizontal Cloud Fraction

A net reduction in cloud fraction due to solid aerosol pollution was predicted (Fig. 6.11a) for all cloud types, with mixed-phase clouds recording the largest decrease in cloud coverage. This is in contrast with the continental case where an increase in solid aerosol number concentration resulted in an increase in the cloud fraction. The main mechanism for this reduction in the cloud coverage is the increase in snow production (Sect. 6.4.1.4) that was predicted when solid aerosol concentrations were raised. Precipitation production via the ice-phase is more efficient; hence, the cloud lifetime diminishes quickly under such a scenario. The volumetric cloud fraction also showed massive reductions in the number of cloudy grid-points, which shows that clouds have become less extensive with increases in solid aerosols. The net reduction in cloud fraction was however not very huge, it was less than 2%.

6.4.4 Response of Cloud Optical Properties to Increased Solid Aerosols

Despite the massive increases in snow production when solid aerosol concentrations were raised, the net intrinsic optical thickness of clouds was slightly higher under the increased solid aerosol scenario. Since snow production was higher in ice-only clouds and IWC actually diminished in the upper troposphere, then the mechanism that can explain the increase of the optical thickness of ice-only clouds is the increase

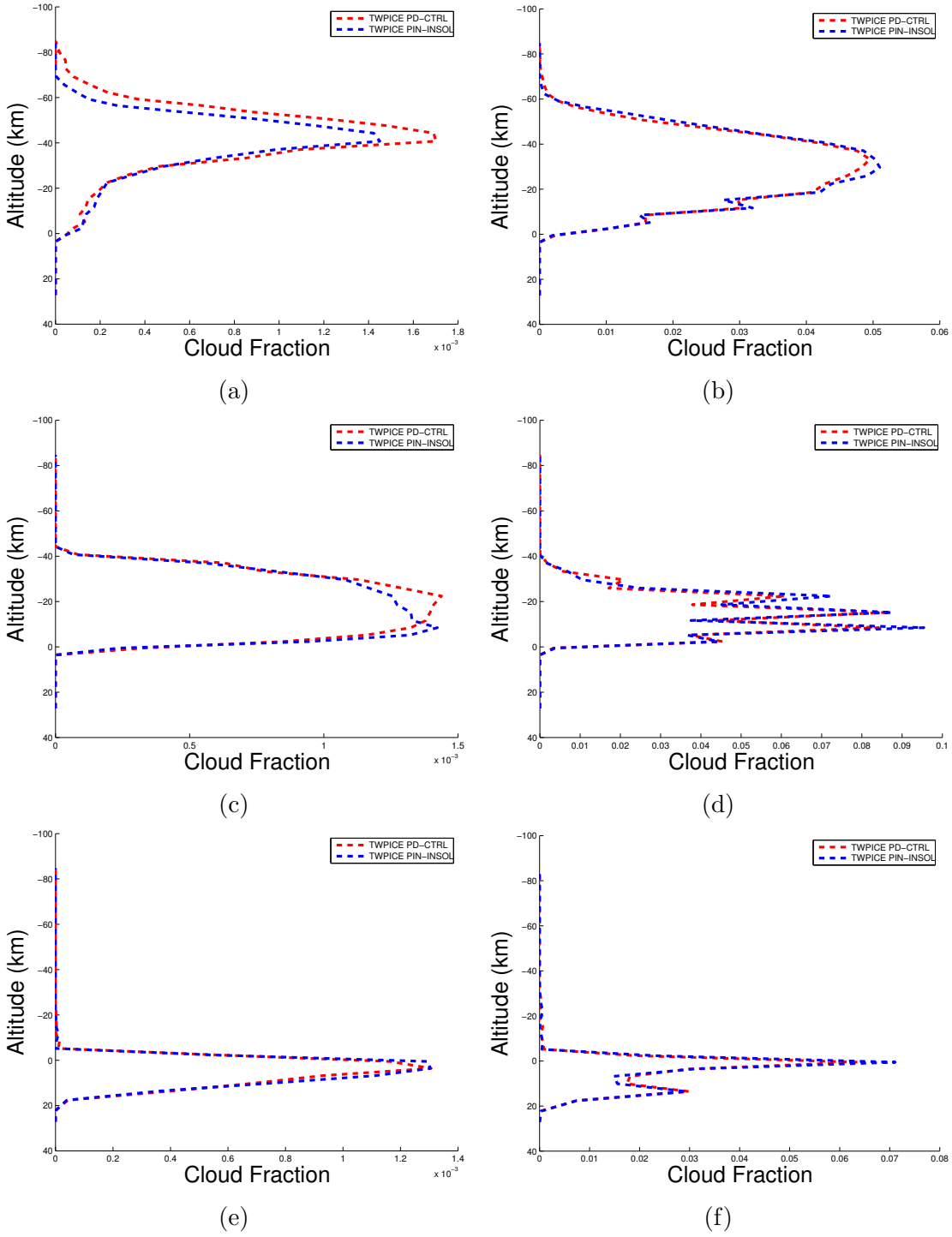

Figure 6.10: *Vertical profile of cloud fraction for all three types of phase of clouds, conditionally averaged over regions of strong vertical velocities (vertical velocity $\omega >= 1ms^{-1}$) (left) and weak vertical velocities (vertical velocity $\omega < 1ms^{-1}$) (right). (a) and (b) are for ice-only clouds, (c) and (d) are for mixed-phase clouds, (e) and (f) are for liquid-only clouds, for TWPICE solid aerosol effects.*

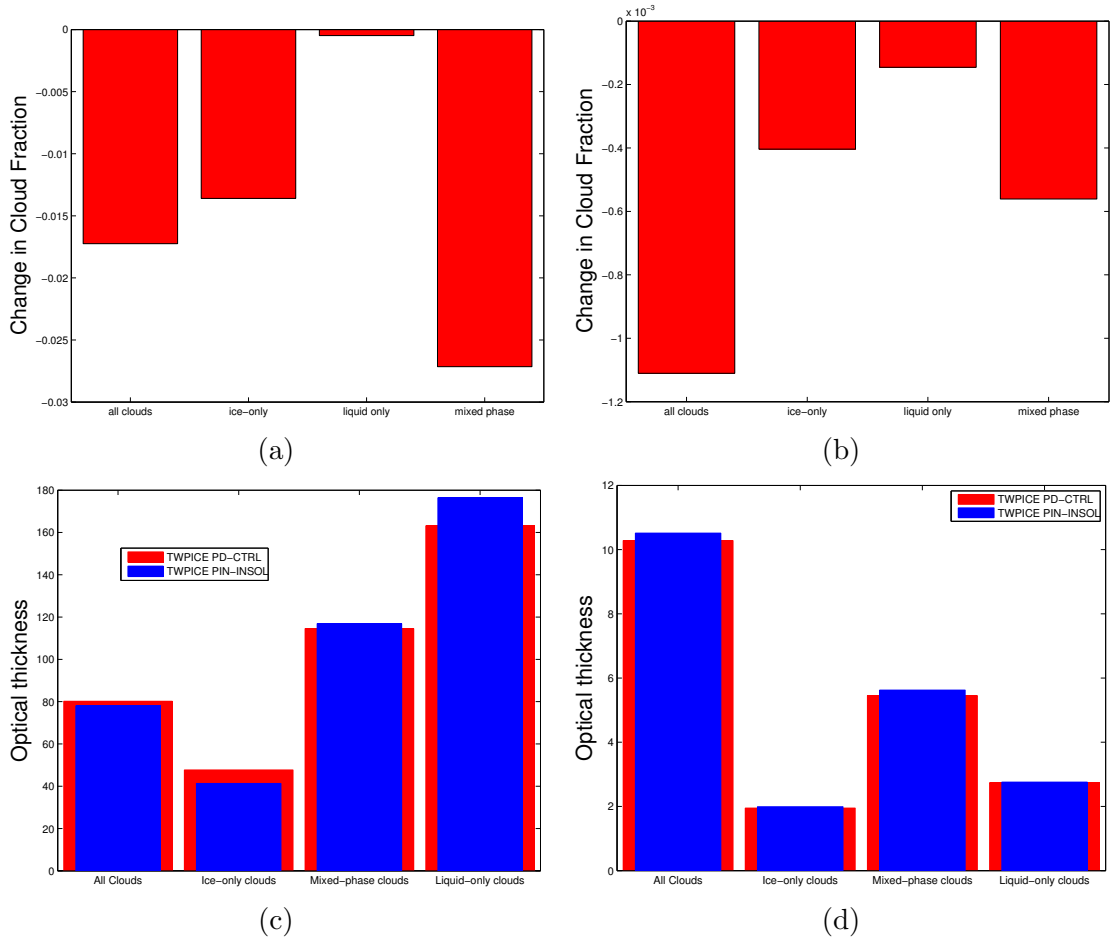

Figure 6.11: *Changes in horizontal cloud fractions and volumetric cloud frations are presented in (a) and (b), respectively and the intrinsic and unconditionally averaged optical thicknesses of clouds are presented in (c) and (d), for all the three types of phase of clouds in TWPICE.*

in the depth of clouds, which is reflected by the upward shift of cloud-tops in the control simulation. Other cloud phases became optically thinner mainly because of the reductions in the volumetric cloud fractions arising from the increase in snow production when solid aerosol concentrations were higher. The unconditional averages of the optical thicknesses of clouds were thinner in the present-day simulation mainly because of a reduction in the horizontal cloud fractions when solid aerosol concentrations were raised (Fig. 6.11d).

6.4.5 Response of Radiative Fluxes and Cloud Radiative Properties to Increased Solid Aerosols

It is shown in Fig. 6.12 that the glaciation indirect effect was relatively small (about 1 Wm^{-2}) compared to the total indirect effect (about -17.44 $\pm$6.1 Wm^{-2}) from solute

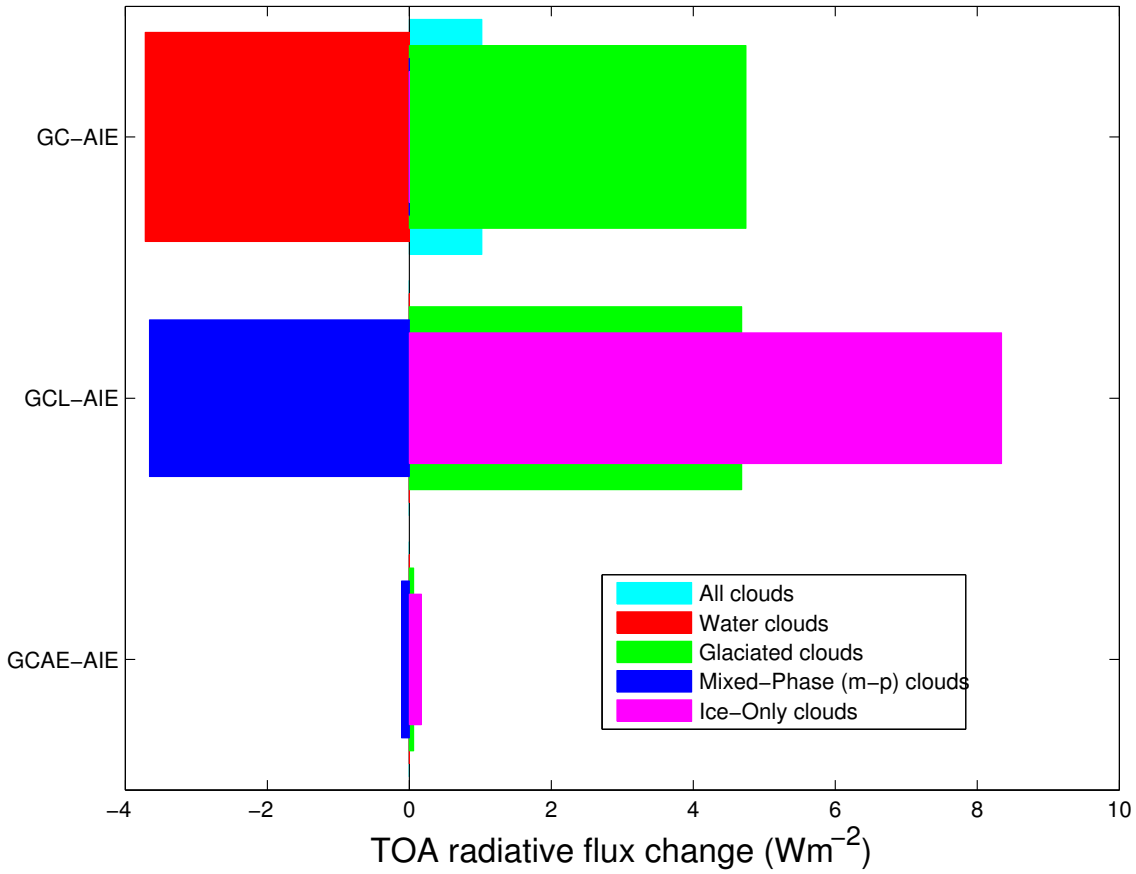

Figure 6.12: *The glaciation aerosol indirect effect, arising from increasing solid aerosol concentrations in TWPICE. Meanings of abbreviations: GC-AIE = Glaciated Clouds AIE, GCL-AIE = Glaciated Clouds Lifetime AIE, GCAE-AIE = Glaciated Clouds Albedo-Emissivity AIE.*

aerosol pollution. In addition to being relatively small, the glaciation indirect effect in fact, had a warming effect. This warming effect primarily resulted from the sharp reduction in fractions of all cloud types, caused by an increase in snow production particularly in ice-only clouds. Hence, the contribution to this warming effect by the glaciation indirect effect was dominated by glaciated clouds (4.74 $\pm$1.66 Wm^{-2}), since water-only clouds actually had a negative radiative flux change at the TOA (-3.72 $\pm$1.3 Wm^{-2}), although they hardly showed a change of the cloud fraction compared to other cloud types.

The net reduction in total cloud fraction from inclusion of solid aerosol pollution was also accompanied by a lower optical thickness of present-day clouds; thus, more solar fluxes were transmitted into the climate system by clouds. The small magnitude of the glaciation indirect effect is attributed to the low number concentrations of solid aerosols relative to those of solute aerosols. Additionally, Fig. 6.8a shows

that dust was the dominant source of heterogeneously nucleated ice crystals, and also, Table 6.1 shows that dust only changed by approximately 10% due to anthropogenic activities. Therefore, any changes in microphysical processes of clouds that resulted from other aerosol species were suppressed by the dominant contribution of dust to the ice number budget.

The largest contribution to the warming effect was from ice-only clouds (8.51 $\pm$2.98 Wm^{-2}), because mixed-phase clouds actually showed a negative radiative flux change at the TOA (-3.77 $\pm$1.3 Wm^{-2}). This is because the largest notable increase in snow mixing ratio was predicted in ice-only clouds, while no substantial changes were simulated in mixed-phase clouds. Finally, the mean size of cloud particles was largely unchanged by the increase in solid aerosols, hence, the resultant albedo-emissivity indirect effect was negligible in all cloud types.

6.5 IN Versus CCN Activity of Solid Aerosols

Since both the CCN and IN activities of solid aerosols are treated in the aerosol-cloud model, changes in solid aerosol loading from pre-industrial to present-day tend to affect both their CCN and IN activities. Therefore in order to isolate the aerosol indirect effect of the IN activity of solid aerosols from this complex relationship, a further sensitivity test was performed. In this test, the present-day simulation was repeated with the only modification being the IN activity of solid aerosols. This IN activity was raised by adjusting the baseline surface areas of solid aerosols using the same ratios that were applied to the concentrations of solid aerosols (Table 6.1) when their pre-industrial concentrations were estimated.

Results from the mid-latitude continental case showed that, by increasing the IN activity of solid aerosols, the number concentrations of ice crystals rises mostly from heterogeneous nucleation of ice at temperatures lower than -30 °C. This increase in ice crystal concentration suppresses homogeneous aerosol and cloud droplet freezing, because all forms of precipitation were higher in the control run, including warm rain. Consequently, the total cloud fraction under a high IN scenario is reduced quite significantly, mostly for glaciated clouds. Although water-only clouds have indicated an increase in their cloud fraction, their contribution to the total cloud fraction is small relative to other cloud types. Surprisingly, all cloud types have intrinsically become optically thicker with high IN activity. As a result of the increase in the optical thickness of clouds and the increase in the cloud fraction of water-only clouds, an increase in the reflectivity of solar radiation that gave rise to a negative radiative flux change at the TOA of -3.04 $\pm$0.46 Wm^{-2} was predicted. This result shows that

the negative radiative flux change at the TOA of -1.96 ±0.14 Wm^{-2} due to solid aerosol loading predicted above, is largely due to the increase of the IN activity of solid aerosols that arises from solid aerosol pollution.

As for the maritime case, there was an increase in the numbers of ice crystals aloft, mainly from heterogeneous nucleation under a high IN activity scenario. The mass mixing ratios of all forms of precipitation were suppressed in the high IN activity scenario, mainly because the mean sizes of ice crystals were smaller in the high IN activity case, hence, aggregation and riming were less efficient. However, the fraction of clouds was reduced slightly and they also became optically thinner under the high IN activity scenario, hence, clouds became less reflective in the present-day, yielding a warming effect of 5.48 ±1.91 Wm^{-2}. This result also shows that, it is indeed the IN activity of solid aerosol pollution that is responsible for the predicted radiative flux changes at the TOA.

6.6 IN Activity of Soluble Organic Aerosols

As described above (Sect. 3.2), a novel treatment of the IN activity of soluble organics (Murray et al., 2010) was included in the model. In this section, the effect of this treatment on the aerosol indirect effect of clouds was explored. Two pairs of model simulations were conducted; one with the IN activity of soluble organics switched off as in Chapter 5, and the other one was with this IN activity of soluble organics switched on. Each pair comprised of a control run, in which all aerosol loadings were set to their present-day scenarios, and the other with only soluble organic aerosols set to their pre-industrial conditions.

6.6.1 The Mid-Latitude Continental Case - CLASIC

Interestingly, the results from the mid-latitude continental case showed that the role of the IN activity of soluble organics on clouds is to increase the reflectivity of clouds. This increased reflectivity by clouds happened primarily via the increase in the optical thickness of clouds. The net optical thickness of clouds increased due to the IN activity of soluble organics, although the domain average of the optical thickness diminished. The fraction of the clouds was diminished with the IN activity of soluble aerosols mainly through the enhancement of snow production, especially in ice-only clouds. Since the IN activity of soluble organics is prevalent at very cold temperatures (lower than -65 °C), a significant increase in cloud-top height was predicted in the simulation with IN activity of soluble organics switched on. Also, a

slight increase in upper tropospheric ice crystal concentrations was noted, especially in the polluted case.

Finally, the radiative flux change at the TOA of 2.63 $\pm$0.39 Wm^{-2} was predicted from clouds due to the change in soluble organic aerosol loading from pre-industrial to present-day when their IN activity was switched off, while it was only 0.04 Wm^{-2} when soluble organics nucleated ice. This result is quite significant and very important because, if the IN activity of soluble organic aerosols is neglected in GCMs predictions, then, the predicted magnitudes of aerosol indirect effects may be overestimated. This cooling effect from the IN activity of soluble organics has the potential of buffering the predicted aerosol indirect effects on clouds, which are mostly predicted to have a cooling effect.

6.6.2 The Tropical Maritime Case - TWPICE

As for the maritime case, when aerosol pollution was included, the TOA radiative flux change was -4.18 $\pm$1.46 Wm^{-2} if organic IN were always absent, while it became only -2.88 $\pm$0.43 Wm^{-2} when soluble organic IN were always present. This finding shows that the effect of the IN activity of soluble organics is a warming of the climate system. This warming effect happens via a strong increase in ice crystals aloft, which then enhances snow production. Consequently, fractions and optical thicknesses of clouds are diminished; hence, more SW radiation is transmitted to the Earth's surface.

6.7 The AIE from all Aerosols

The effect of all aerosols (i.e. both solid and solute aerosols) on the microphysical and radiative properties of clouds was investigated. This was done by performing a pair of simulations, comprising the control run and a run with number and mass concentrations for all aerosol species set to their pre-industrial conditions; this test is denoted PIN-ALL.

6.7.1 The Mid-Latitude Continental Case - CLASIC

Microphysically, the responses of cloud properties in PIN-ALL were similar to those of soluble aerosols (Sect. 5.3, denoted PIN-SOL) for the mid-latitude continental case. Since both microphysical and radiative changes of clouds due to aerosol pollution in PIN-ALL simulation were dominated by the influences of solute aerosols (PIN-SOL), for analysis purposes, the results from PIN-ALL are therefore compared

with those of the PIN-SOL simulation (Chapter 5). The marked differences between PIN-SOL and PIN-ALL simulations are as follows.

The total change in horizontal cloud fraction of the PIN-ALL simulation is higher (by about 1%) than that of PIN-SOL, because in PIN-ALL, a smaller cloud fraction than in PIN-SOL was predicted. The reason for this massive loss of cloud mass was that the mass mixing ratios of all precipitation species were higher in PIN-ALL than in PIN-SOL. This finding implies that the presence of solid aerosols in the atmosphere is to raise precipitation production, mainly through snow. The reason why precipitation production was higher in PIN-ALL was that the mean sizes of cloud particles, especially of cloud droplets in PIN-ALL were larger than those in PIN-SOL. All other cloud fields remained largely unchanged. Both, conditionally and unconditionally averaged optical thicknesses of clouds were lower when all aerosols were set to their pre-industrial values, mainly because precipitation production was enhanced and cloud fraction was reduced in pre-industrial scenario relative to the control run.

The total indirect effect of aerosols on clouds from all aerosols was -7.56 $\pm$1.13 Wm^{-2}, which is significantly less than that from solute aerosols alone (-9.46 $\pm$1.41 Wm^{-2}) because the cloud fraction is lower in PIN-ALL and so was their optical thickness. This finding supports the idea that aerosol indirect effects from different sources and processes interact, compensate and buffer each other, such that the net effect when these various processes and sources are combined, may not be equal to the sum of the individual indirect effects.

6.7.2 The Tropical Maritime Case - TWPICE

There were no major differences between the aerosol indirect effects from PIN-ALL and from PIN-SOL for the tropical maritime case. Except that, snow production was higher when all aerosols were set to their pre-industrial times than when only solute aerosols were set. This finding again, brings us to the conclusion that solute aerosols control the aerosol indirect effects of clouds. Further investigation showed that this happens mainly through sulphate aerosols because of their high number concentration in the atmosphere relative to other aerosol species. Again, the net aerosol indirect effect from PIN-ALL was -14.03 $\pm$4.91 Wm^{-2}, which is less than that from solute aerosols alone in the maritime case of -17.44 $\pm$6.1 Wm^{-2} or from the sum of only liquid and only solid aerosol indirect effects (solid aerosols AIE = 1.02 $\pm$0.15 Wm^{-2}).

6.8 Summary

Increases of solid aerosols had less impact than increases of solute aerosols on clouds in both cases simulated (i.e. the responses of cloud properties due to increases in solid aerosol concentrations were minimal), mainly because of their lower number concentrations relative to solute aerosols.

The Mid-Latitude Continental Case - CLASIC

- The increase in droplet concentration due to increases in solid aerosols was negligible, while the ice crystal concentrations in the upper troposphere diminished, primarily because homogeneous freezing, especially of solute aerosols was unchanged. However, notable increases were predicted for heterogeneous nucleation of ice crystals, especially at temperatures greater than -30 °C (i.e. predominantly mixed-phase clouds).

- Updraft speeds especially in convective clouds decreased by as much as 1 m s^{-1} in the upper troposphere suppressing homogeneous freezing and supersaturations, hence, the upper tropospheric IWC was reduced in the present-day, while LWC was less sensitive to aerosol perturbation, this finding is contrary to the widely accepted hypothesis of the invigoration effect, however the new findings of Storer and van den Heever (2013) are in agreement with our results and we attribute this to increased condensate loading.

- Vertical profiles of cloud fractions of ice-only clouds in stratiform regions were diminished by solid aerosol pollution, while for mixed-phase clouds an increase with increasing pollution was predicted. The vertical profiles of cloud fractions reviewed a change of cloud phases, i.e. by a reduction in ice-only clouds and an increase in mixed-phase clouds with solid aerosol pollution.

- Precipitation production was less efficient in the present-day; the mass mixing ratios of all the species of precipitation were lower due to increases in solid aerosols, mainly because sizes of cloud particles became smaller with solid aerosol pollution. Consequently, the fractions and optical thicknesses of all continental clouds increased steadily due to solid aerosol pollution.

- A negative radiative flux change at the TOA (-1.96 $\pm$0.29 Wm^{-2}) resulted from boosting solid aerosol concentrations, primarily due to a decrease in ice

number concentrations, which caused a reduction in snow production and a slight increase of cloud fractions and lifetimes.

The Tropical Maritime Case - TWPICE

- As for the maritime case, the number concentration of cloud droplets were unchanged, but ice crystal concentrations aloft increased quite substantially due to increases in solid aerosols, mainly because homogeneous freezing of cloud droplets and heterogeneous nucleation of ice crystals at temperatures greater than -30 °C were boosted together with the cloud dynamics due to increases in solid aerosols. While on the other hand, homogeneous freezing of solute aerosols and heterogeneous nucleation of ice at temperatures lower than -30 °C were weakened in the present-day.
- The mass mixing ratios of snow were higher, mostly in ice-only clouds in the present-day than in the pre-industrial era. Graupel also exhibited a substantial increase, while there were no significant changes in rain mixing ratios.
- The net fraction and optical thicknesses of all clouds were diminished in the present-day primarily due to increased snow production.
- As a result of a reduction in the fraction and optical thicknesses of clouds due to higher production of snow in the polluted case, more SW radiation was transmitted into the climate system, causing a warming effect due to solid aerosol pollution.

Chapter 7

Conclusions

7.1 Major Results

It should be noted that the accuracy and consistency of these and related results are dependent on the nature of the models and the parameterizations used. Also, the nature of the large-scale forcing and the assumptions used in prescribing the aerosol profiles are important parameters in determining these results.

The total AIE of clouds from solute aerosols was two times higher in the oceanic than in the continental case. This is because the sensitivity of cloud properties to perturbations of aerosol concentration diminishes with the increasing of the background aerosol concentration. Also, the AIEs of glaciated clouds were found to be greater than those of water-only clouds by a factor of two in the continental case, while both cloud types were equally important in the maritime case. The radiative importance of glaciated clouds lied in their large collective spatial extent and their existence above water-only clouds. The glaciation AIE from solid aerosols had a cooling effect in continental clouds because of an increase in cloud fraction that was predicted. A warming effect was predicted in maritime clouds mainly because of a decrease in the cloud fraction when aerosol concentration was raised.

In addition to the traditional AIEs (glaciation, riming and thermodynamic), sedimentation, aggregation and coalescence were new AIEs identified, this finding is closely related to the recent work of Fan et al. (2013), who noted that microphysical processes are crucial in modifying the macrophysical properties of clouds. Importantly, it was discovered that these individual AIEs interact, compensate and buffer each other, hence, the relative importance of the contributions from responses of various processes vary during the climate change. Generally, the results show that the anthropogenic injection of aerosols into the atmosphere has the potential of offsetting the effects of CO_2-induced global warming. This is because the dominant effect

of anthropogenic aerosol pollution on clouds is to cool the Earth, which corroborates the findings of Gettelman et al. (2012); . Below, a summary of the most important pathways of aerosol indirect effects is presented. On average, the predicted AIEs had a standard deviation of around 15% associated with them in CLASIC and of about 30% in TWPICE.

7.2 Important Pathways of Aerosol Indirect Effects

The most important pathways identified in this study by which solute aerosols modify clouds and their indirect effects are summarized as follows.

- Solute aerosol pollution raised the number concentrations of cloud droplets (sulphate aerosols being the dominant source of cloud droplets), causing the diminishing of the mean sizes of cloud droplets and the inhibition of the warm rain processes and hence, promoting homogeneous freezing of cloud droplets.
- Subsequently, more ice crystals were detrained into the stratiform/cirrus and mixed-phase clouds from convective cores, hence the number concentrations of ice crystals aloft increased sharply, reducing their mean sizes. Consequently, the extent and optical thickness of clouds especially of glaciated clouds increased with anthropogenic aerosol pollution.
- Results showed that the negative net AIE from all clouds was dominantly a consequence of increases in spatial extent and optical thickness of clouds caused mainly by the reduction in mean sizes of cloud particles.
- Results also showed that homogeneous freezing of extra cloud droplets and aerosols and the subsequent detrainment of cloud ice into stratiform clouds are the dominant mechanisms of AIE of glaciated clouds. (These mechanisms are responsible for the higher sensitivity to aerosol changes of glaciated clouds compared to water-only clouds, because of this phenomenon, glaciated clouds emerged as more important in AIE of clouds compared to water-only clouds).

The most important pathway by which solid aerosols modify clouds and their indirect effects is as follows.

- Solid aerosol pollution boosted heterogeneous ice nucleation in the mixed-phase region of clouds, and strongly weakened fast updrafts. Subsequently, a reduction in the detrainment of ice crystals into cirrus was noted; hence, the upper-tropospheric crystal concentrations and IWC were reduced, while it increased in mixed-phase clouds.

- Consequently, the snow and graupel production were both suppressed by solid aerosol pollution, primarily because of the reduction in crystal numbers and IWC in cirrus. As a result, present-day clouds became more extensive (both horizontally and vertically, especially mixed-phase clouds), except for ice-only clouds whose volumetric fraction diminished.

- The optical thickness of glaciated clouds was actually thinner in the present-day because of the horizontal stretching of the clouds, but overall the optical thickness of the clouds was higher in the present-day, especially of mixed-phase clouds.

- As a result of an increase in the cloud fraction and optical thickness of present-day clouds, the AIE was a cooling of the climate system. Because present-day glaciated clouds were optically thinner intrinsically relative to warm clouds, warm clouds dominated the total AIE, while mixed-phase clouds controlled the glaciated cloud AIE.

The most important microphysical mechanisms for the process level aerosol indirect effects are as follows.

- The reduction in mean sizes of ice particles in cirrus clouds weakens both aggregation and sedimentation of cloud particles, however, aggregation was predicted to be more important than sedimentation in the negative AIE of ice-only clouds.

- On the riming AIE, the diminishing of the mean sizes of cloud droplets was more important as evidenced by the reduction of graupel production especially in mixed-phase clouds.

- Whereas for the freezing-related thermodynamic AIE, the strengthening of ascent velocity in striation clouds and of downdrafts, promoted the formation of secondary cells and hence the cloud cover and reflectance of radiation by clouds increased.

7.3 Summary of the Work Done

This study was carried out to investigate the salient features of aerosol indirect effects on glaciated clouds by using numerical simulations with a state-of-the-art aerosol-cloud model. In order to achieve this, three main objectives were set. The first objective was to modify and update the aerosol-cloud model. The second

objective was to compare the aerosol-cloud model results with observations from two field campaigns, one continental and another marine i.e. CLASIC and TWPICE campaigns, respectively. The observational datasets from these two cases were used to assess the performance of the aerosol-cloud model. The last main objective was to study the impacts of the variations of pre-industrial to present-day aerosol loadings on the macro- and microphysical properties of clouds and their indirect effects, with the main focus being on glaciated clouds.

In the first objective (the model development stage), the following modifications were applied to the model. The two size distribution modes of sulphate aerosols were separated and are now being treated separately as two independent aerosol groups, primarily to improve the accuracy of prediction of ice crystals in the upper troposphere. A double moment approach was applied for these two modes of sulphate aerosols, where both their mass and number mixing ratios are now being predicted. This treatment of sulphate aerosols enabled prediction of their mean sizes instead of prescribing them a priori.

Detailed/explicit microphysics is now being applied to most coagulation processes (aggregation, riming, and accretion). This improvement allows accretion processes to be predicted more accurately by resolving them explicitly in-lieu of the traditional bulk parameterization technique. Additionally, a γ-distribution was applied to all precipitating hydrometeors in place of the exponential one. Other changes involved treating different ice morphologies so as to accurately resolve collision and sticking efficiencies. Finally, recent improvements to the empirical parameterization of heterogeneous ice nucleation described in Phillips et al. (2013) have been incorporated into the aerosol-cloud model. After these modifications, the updated model was compared with its old performance published in Phillips et al. (2009). Significant improvements especially in the prediction of droplet and ice number concentration aloft were noted 3.2.

The second objective of this study was to simulate the two cases described above and to use these simulations and their corresponding observational data from the respective campaigns to validate the aerosol-cloud model. Rigorous comparison of the aerosol-cloud model with observations was performed for various cloud fields predicted by the model, such as; water contents, cloud fraction, precipitable water, cloud particle number concentrations and TOA radiative fluxes. The comparison between model predictions and observations was satisfactory; hence, the final objective of this PhD project could be carried out with good confidence. The remainder of this section is dedicated to highlighting the findings from the third objective of the research project.

7.4 Detailed Summary of Major Findings

This section summarizes the microphysical and dynamical responses of cloud properties to increased aerosols and also the responses of the radiative properties of clouds to more aerosols, with relation to changes in the TOA radiation fluxes. It also addresses different hypotheses that were tested in this research project.

7.4.1 Hypothesis I: Responses from Solute Aerosols

H1: *Solute aerosols modify glaciated clouds via the homogeneous freezing process of cloud droplets and of solute aerosols. Also, reduced sedimentation rates produce a lifetime effect, causing pollution by solute aerosols to modify cirrus clouds more than solid aerosols, owing to the much higher numbers of soluble aerosols relative to insoluble ones.*

7.4.1.1 Microphysical and Dynamical Responses

Cloud micro-/macro- physical and dynamical properties responded in various ways to changes in solute and solid aerosol loadings. Increasing the number concentration of solute aerosols from pre-industrial to present-day scenarios resulted in amplified droplet number concentrations. The amplification factor of cloud droplets was however smaller than that applied to solute aerosols. These extra cloud droplets triggered competition for water vapour causing diminished supersaturations and mean sizes of cloud droplets in both the tropical maritime and the mid-latitude continental cases. Because of pristine aerosol conditions in the maritime case relative to the continental one, both droplet and crystal sizes were larger for the maritime case than for the continental case predominantly because of low competition for vapour due to low cloud droplet count in maritime clouds. Even after solute aerosol pollution, the size of maritime cloud droplets was still larger than that in continental clouds in the pre-industrial conditions. This reduction in cloud particle sizes inhibited warm rain processes such as collision-coalescence, especially in the continental case.

Consequently, the number concentrations of ice crystals rose sharply at altitudes above -36°C level owing to homogeneous freezing of higher numbers of cloud droplets and solute aerosols. Remarkably, for the continental case, homogeneous freezing of cloud droplets and of aerosols were equally important sources of ice crystals, while for the maritime case on the other hand, homogeneous freezing of solute aerosols, especially sulphate aerosols, was by far the single largest mechanism by which ice crystals were nucleated because weak vertical velocities were more extensive in the maritime case. Accordingly, the ice crystal sizes at altitudes above -36°C level

decreased substantially when aerosol pollution was included for both the maritime and the continental cases, but, the fractional reduction of the sizes of ice crystals was higher for TWPICE (dropped from about 40 down to about 15 μm) than for CLASIC (dropped from about 21 down to about 16 μm).

A significant increase in liquid mixing ratios (in liquid and mixed-phase clouds) due to increases in solute aerosol loading was predicted, while ice mixing ratios decreased at altitudes above -36°C level in both TWPICE and CLASIC. In CLASIC, the reductions in ice mixing ratios aloft were attributed to the surge in the domain-wide average of snow mixing ratio and the increase in the spread of ice-only clouds when solute aerosol loading was increased. The domain-wide increase in snow mixing ratios in CLASIC was attributed to the increase in cloud fractions especially of ice-only clouds and also from the fact that the reduction in ice crystal sizes due to increases in aerosols was minimal. In TWPICE on the other hand, the intrinsic snow mixing ratio increased strongly in deep convective clouds, causing limited detrainment of cloud ice into stratiform regions. Also, the marked reduction in the sizes of ice crystals aloft contributed significantly to the reduction of snow mixing ratio in TWPICE, especially in stratiform clouds. As for rain and graupel, similar responses were noted in both cases, whereby their mixing ratios were lower in the present-day than in the pre-industrial era, mainly due to the reduction in the sizes of cloud particles predicted in both simulations.

On the macrophysical properties of the clouds, it was noted in both cases that present-day clouds are more horizontally extensive in both cases mainly through mixed-phase clouds in CLASIC, while in TWPICE, all cloud types were equally important. This was explained in terms of the riming and aggregation processes being less efficient especially in CLASIC where the mean sizes of cloud particles were smaller than those of TWPICE. Another most striking discovery was that present-day clouds are more glaciated (i.e having more ice) than pre-industrial clouds especially in the continental case because of the prevalence of homogeneous freezing of solute aerosols and cloud droplets but less efficient production of snow. A thermodynamic response was noted in both cases, with a warming of up to 0.5 °C mostly in the upper troposphere caused primarily by the release of latent heat during the condensation and freezing of extra cloud droplets for both cases.

Overall, the cloud fraction and optical thickness of present-day clouds were higher than those of pre-industrial clouds in both cases. Hence, present-day clouds have the potential to reflect more radiation back to space than pre-industrial clouds and also to offset some of the global-warming caused by greenhouse gases such as CO_2.

7.4.1.2 Impacts on Radiation and Aerosol Indirect Effects

From the analysis of aerosol indirect effects, it was found that the total aerosol indirect effects of clouds were about a factor of two higher over the oceans (-17.44 $\pm$6.1 Wm^{-2}) compared to continents (-9.46 $\pm$1.4 Wm^{-2}), primarily because other sensitivity tests with much higher aerosol concentrations than the ones presented herein, showed that as the atmosphere becomes highly polluted, the aerosol indirect effect of clouds becomes smaller and other cloud micro- and macro-physical properties become less sensitive to more aerosols. The other finding was that, in the continental case, the aerosol indirect effect of glaciated clouds (-6.33 $\pm$0.95 Wm^{-2}) from solute aerosol pollution was a factor of two greater than that of water-only clouds (-3.13 $\pm$0.41 Wm^{-2}).

This finding shows that in regions with mesoscale systems of vigorous deep convection over land, glaciated clouds may be higher importance in determining the total aerosol indirect effects. This result was explained by three main mechanisms. The first of which is that glaciated clouds lie above water-only clouds; therefore, they have the first interaction with radiation before it reaches water-only clouds below them. The other mechanism was that the cloud fractions of glaciated clouds were more responsive to changes in aerosol loading than those of liquid-only clouds. Finally, the collective vertical and lateral coverage of glaciated clouds was higher than that of water clouds alone. On the other hand, water-only clouds in the maritime case were as important as glaciated clouds in controlling the aerosol indirect effects (-9.08 $\pm$3.18 Wm^{-2} and -8.36 $\pm$2.93 Wm^{-2} were the radiative flux changes at the TOA for water-only and glaciated clouds, respectively). Focusing on glaciated clouds, the aerosol indirect effect of ice-only clouds (-4.14 $\pm$0.62 Wm^{-2}) for CLASIC was greater than that of mixed-phase clouds (-2.49 $\pm$0.37 Wm^{-2}). The explanation for this finding was similar to the one given above for the total indirect effect.

As for the tropical maritime case, the flux changes at the TOA for water-only (-9.08 $\pm$3.18 Wm^{-2}) and glaciated clouds (-8.36 $\pm$2.93 Wm^{-2}) were comparable, primarily because, water-only clouds were more extensive horizontally, than they were in the continental case. Also, the aerosol indirect effects of mixed-phase clouds (-14.12 $\pm$4.94 Wm^{-2}) dominated the glaciated clouds indirect effect, because the flux change of the indirect effect from ice-only clouds was actually positive (5.76 $\pm$2.06 Wm^{-2}) when soluble aerosol loading was increased. This finding was due to the limited perturbation of the ice water content that occurred as a result of weak homogeneous freezing of soluble aerosols and cloud droplets noted in TWPICE, as a result of the absence of strong updrafts in TWPICE compared to CLASIC.

The albedo-emissivity effect of glaciated clouds (-2.25 $\pm$0.34 Wm^{-2}) was about a half of the lifetime effect of glaciated clouds (-4.08 $\pm$0.61 Wm^{-2}) in CLASIC, while they were comparable in TWPICE, where the aerosol indirect effects of ice-only and mixed-phase clouds were opposing.

The tested hypothesis, H1, was strongly supported by the results in that; strong increases in the number concentrations of ice crystals aloft were predicted by the model when only solute aerosol pollution was considered. The competition for available vapour resulted in reduced particle sizes, and hence, reduced sedimentation of cloud particles and reduced efficiencies of rain and graupel production, leading to increased cloud fractions. Consequently, negative flux changes (solar cooling) for indirect lifetime and albedo/emissivity effects due to increased solute aerosols were predicted in both the maritime and continental cases. However, the lifetime effect from sedimentation being slower for smaller but more numerous ice crystals was found to be less important than the other mechanism of aerosol indirect effects such as aggregation, autoconversion and sedimentation (Fig. 5.15).

7.4.2 Hypothesis II: Responses from Solid Aerosols

H2: *Solid aerosol pollution reduce the overall numbers of ice crystals in cirrus, by suppressing homogeneous aerosol freezing. Also, solid aerosols increase ice crystal numbers in mixed-phase clouds by heterogeneous ice nucleation, thereby changing the phases and lifetimes of clouds in regions of weak vertical velocities (i.e. mixed-phase regions typically).*

7.4.2.1 Microphysical and Dynamical Responses

The effect of increasing solid aerosols on clouds was less than that of increasing solute aerosols in both cases simulated (i.e. the responses of cloud properties due to increase in solid aerosols was minimal), mainly because of their lower number concentrations relative to solute aerosols, at least in the regions studied and with the assumed aerosol and meteorological data. In the mid-latitude continental case, the increase in droplet number concentration due to increases in solid aerosols was negligible, while the number concentrations of ice crystals in the upper troposphere were diminished primarily because homogeneous freezing especially of solute aerosols was unchanged, while an increase in homogeneous freezing of cloud droplets was substantial. However, notable increases were predicted for heterogeneous nucleation of ice crystals, especially at temperatures greater than -30 °C (predominantly mixed-phase clouds). Also, updraft speeds especially in convective clouds decreased by as

much as 1 m s^{-1} in the upper troposphere, causing supersaturations to drop, hence, the upper tropospheric IWC was lower in the present-day.

Vertical profiles of cloud fraction have shown an increase of cloudiness in ice-only clouds in deep convection, and a reduction of cloudiness of ice-only clouds in present-day stratiform clouds. On the other hand, an increase in cloud fraction of mixed-phase clouds was predicted in regions of both strong and weak vertical velocities. Considering unconditional averages of cloudiness, the vertical profiles of cloud fractions indicated a change of cloud phases, i.e. by a reduction in ice-only clouds and an increase in mixed-phase clouds with solid aerosol pollution mainly because of the heterogeneous nucleation of ice at temperatures greater than -30 °C, which was more effective relative to heterogeneous nucleation at temperatures lower than -30 °C. This happens by increased primary numbers of ice crystals in mixed-phase clouds, which caused an increased loss of vapour by diffusional growth of ice and increased subsaturation. Also, the total cloud fraction of all cloud types was higher in the present-day than in the pre-industrial era, with the largest increase being in mixed-phase clouds.

Precipitation production was less efficient in the present-day; the mass mixing ratios of all the species of precipitation were lower due to increases in solid aerosols in this mid-latitude continental case, mainly because sizes of cloud particles were smaller with solid aerosol pollution included. Consequently, the cloud fractions of all continental clouds increased steadily due to solid aerosol pollution. Also, the domain-wide averages of optical thicknesses of clouds were higher when solid aerosols were increased for the continental case.

As for the maritime case, the concentrations of cloud droplets were unchanged, but ice crystal concentrations aloft increased quite substantially due to increases in solid aerosols, mainly because homogeneous freezing of cloud droplets and heterogeneous nucleation of ice crystals at temperatures greater than -30 °C were boosted due to increases in solid aerosols. On the other hand, homogeneous aerosol freezing and heterogeneous ice nucleation at temperatures lower than -30 °C were weakened in the present-day.

The mass mixing ratios of snow were higher, mostly in ice-only clouds in the present-day compared to the pre-industrial era. Graupel also exhibited a substantial increase, while there were no significant changes in rain mixing ratios. As a result, the net cloud fraction and also the cloud fractions of all cloud types diminished in the present-day. Also, present-day clouds were optically thinner due to increased snow production.

7.4.2.2 Aerosol Indirect Effects

In the mid-latitude continental case, the overall effects of boosting the number concentrations of solid aerosols were the same as those of boosting solute aerosols; therefore, a negative radiative flux change at the TOA resulted (i.e. a cooling effect of -1.96 $\pm$0.29 Wm^{-2}). This result was due to a decrease in ice number concentration from the glaciation effect, which caused a reduction in snow production. Consequently, a slight increase of the cloud fraction was predicted, which gave rise to a negative radiative flux change at the TOA from all clouds, which was smaller than that predicted from solute aerosols (-9.46 $\pm$1.42 Wm^{-2}).

This was however not the case with the tropical maritime case where a warming effect (1.02 $\pm$0.36 Wm^{-2}) was identified, mainly because increased solid aerosols raised the strength of updrafts aloft, raising cloud-tops and ice number concentrations in mixed-phase clouds. Subsequently, snow mixing ratios were heightened slightly, thereby reducing cloud fractions of all cloud types, hence, more solar radiation was transmitted into the climate system.

Further investigation to determine whether it is the IN activity or the CCN activity of solid aerosols that is responsible for the predicted changes in TOA radiative fluxes, showed that the increase of IN activity due to solid aerosol pollution is the most dominant process that causes the predicted radiative flux changes. Hence, the CCN activity of solid aerosols has a secondary contribution.

The tested hypothesis stated that solid aerosols may reduce the concentration of ice crystals in cirrus. This was found to be true for the mid-latitude continental case, in which ice crystal concentrations were reduced by solid aerosol pollution, because updrafts were weaker, hence the IWC aloft was reduced. While in the tropical maritime case, an increase in ice crystal number concentration was predicted aloft when solid aerosol concentrations were increased, primarily due to increases in homogeneous freezing of cloud droplets. Strengthened updrafts aloft also caused the upward shift of cloud-tops and hence causing increases in ice crystal concentrations. The ice crystal number budgets in both cases indicated that heterogeneous ice nucleation was more active in mixed-phase than in cirrus clouds. As for the lifetime of clouds, continental clouds lived longer with solid aerosol pollution due to suppressed precipitation production, while the opposite was true for continental clouds. Consequently, a cooling effect and a warming effect were predicted for the continental and maritime cases, respectively. In summary, the hypothesis, H2, was proved to be correct in both cases simulated except that there was no reduction of ice crystal number concentrations in maritime cirrus clouds primarily due to increases

in homogeneous freezing of cloud droplets.

7.4.3 Hypothesis III: Process Level Aerosol Indirect Effects

H3: *The thermodynamic, riming and glaciation indirect effects from soluble and insoluble aerosol are significant, but they do not dominate the total indirect effect on all clouds (warm and cold).*

In addition to the traditional aerosol indirect effects (glaciation, riming and thermodynamic indirect effects), new indirect effects were identified in this study. These AIEs were due to sedimentation, aggregation and coalescence and are schematically represented in Fig. 7.1. They are quantified in Chapter 5, and they all exhibited negative radiative flux change at the TOA for both the continental and maritime cases.

Fig. 7.1 presents a summary of the aerosol effects on climate. It shows that the injection of aerosols into the atmosphere results in two major types of aerosol effects on climate. The first of which is the direct effect (which was not considered in this study). The second aerosol effect is the indirect effect, which alters the radiation budget by modifying cloud properties, i.e. increasing the particle number concentration and reducing the mean sizes of cloud particles. The effect of increasing the aerosol number concentration and reducing the cloud particle sizes was to raise the reflectance of the cloud and giving rise to the albedo-emissivity effect.

The other pathway by which aerosols modify clouds is by redistributing the mass of condensate. This brings about the lifetime indirect effect. It can also be identified that more but smaller cloud droplets can also yield the lifetime indirect effect (Fig. 7.1). Increased aerosols modify various microphysical processes and their response is to either prolong or shorten the lifetime of clouds. The findings of this research show that these microphysical processes include the riming, thermodynamic, glaciation, coalescence, aggregation and sedimentation processes (7.1).

It was noted that some of these processes (e.g., the thermodynamic and riming effects) are intertwined, thus, their individual contributions may not add up to the predicted total indirect effect but rather, they interact, compensate and buffer each other in a cloud field. Noticeably, in mixed-phase clouds, both coalescence and aggregation indirect effects were substantial in CLASIC, but for TWPICE, the aggregation indirect effect was negligible because there were no significant changes in the mean sizes of ice particles in TWPICE due to solid aerosol pollution.

The analysis of the riming and thermodynamic aerosol indirect effects and the

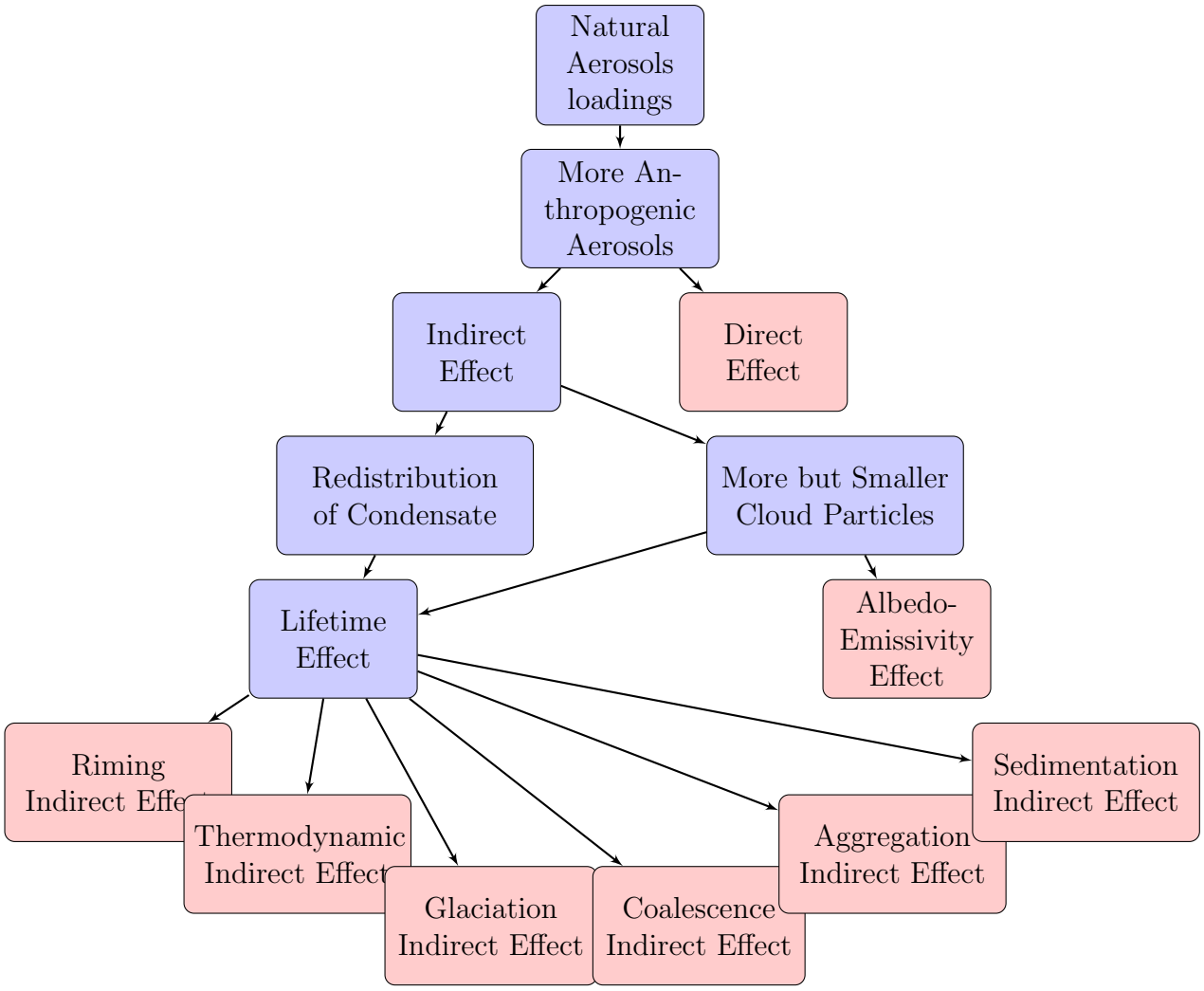

Figure 7.1: *A flow chart summarising the aerosol effects on the climate system, emphasising mainly on glaciated clouds. The different colours highlight intermediate and high level end of the chain of microphysical processes.*

other new indirect effects (e.g. sedimentation, aggregation and coalescence aerosol indirect effects) identified in this study showed that, when assessed in isolation, these process level indirect effects are much larger than when they are allowed to interact. This finding showed that these processes interact, compensate and buffer each other. Hence, the tested hypothesis, H3, was true when these effects are allowed to interact, however, when they are studied in isolation, these AIEs proved to be quite significant.

7.4.4 Hypothesis IV: Effects of Environmental Wind Shear on AIEs

H4: *Environmental wind shear modifies the glaciated-cloud indirect effect, by horizontally extending cirrus so as to increase its reflection of solar radiation and trap-*

ping of longwave radiation but also by modulating convective clouds' intensity, affecting their anvil outflow and generation of cirrus.

The role of meteorology on the cloud radiative properties and aerosol-cloud interactions was also investigated. In the continental case, weak wind shear unexpectedly increased the cloud fraction and also the reflectivity of clouds by about 4 Wm^{-2}, mainly because of a slight increase of the average cloud fraction. This increase in cloudiness was attributed to weak precipitation production especially of snow, despite conspicuous increases of the number concentrations of ice crystals aloft.

However, in the maritime case, under weak wind shear, clouds transmitted as much as 5 Wm^{-2} more solar radiation to the surface, primarily because they were less extensive primarily due to increased snow production, which resulted in the lifetime of clouds especially cirrus being shorter. Also, updrafts in deep convective clouds were stronger under the WWS simulation, despite the fact that homogeneous freezing of both aerosols and water droplets was suppressed by the weak wind shear. In summary, the hypothesis tested, H4, was true in as far as the microphysical and radiative properties of clouds were concerned, but not for the AIEs of clouds. The effect of wind shear on the AIEs of clouds was less significant.

7.4.5 Hypothesis V: Effects of Environmental Humidity on AIEs

H5: *Environmental humidity affects crystal numbers in cirrus by determining their rates of sublimation and ice precipitation during fall-out, which also controls the horizontal extent of cirrus and hence, modifying the glaciated-cloud indirect effect.*

In the mid-latitude continental case, cloud fractions were lower when upper tropospheric relative humidity was increased, owing to increased precipitation production. However, the optical thickness of clouds was actually boosted, hence, less solar energy was transmitted into the climate system, and as much as 17 Wm^{-2} of solar radiation was reflected back to space. The primary mechanisms for the increased optical thickness of clouds under a higher upper tropospheric relative humidity scenario were the increased ice crystal number concentration and cloud water contents. The high crystal number concentrations of ice clouds were attributed mainly to the enhanced homogeneous freezing of sulphate aerosols. Also, the invigoration of cloud dynamics was also noted under a higher humidity scenario.

While in the tropical maritime case, only about 7 Wm^{-2} were reflected back to space when the upper tropospheric humidity was raised primarily because of an increase in the cloud fraction especially of ice-only clouds. This increase in cloud

fraction in the maritime case was attributed mainly to enhanced aerosol freezing especially of sulphate aerosols, and lower snow mixing ratios when upper tropospheric relative humidity was increased. Updraft velocities in deep convection were less sensitive to aerosol loading, while those in stratiform clouds were weakened significantly. In summary, just as for the wind shear case the hypothesis tested, H5, was true in as far as the microphysical and radiative properties of clouds were concerned, but not for the AIEs of clouds. The effect of relative humidity on the AIEs of clouds was less significant.

Overall, the effect of meteorology (both wind shear and upper tropospheric relative humidity) on the net aerosol indirect effects of clouds was seen to be negligible, because the magnitudes of the indirect effects under the new artificially perturbed meteorological conditions were comparable to those predicted under their corresponding original meteorological conditions.

7.5 Future Work

The experience and knowledge gained in this work provided several ideas and techniques through which this work may be improved and advanced. More sensitivity tests would be carried out to further understand these microphysical mechanisms of aerosol indirect effects on clouds. For instance, the importance of certain microphysical processes (such as, in-cloud nucleation of cloud droplets, the Hallet-Mossop process and preferential evaporation of small cloud droplets during homogeneous freezing) on aerosol-cloud interactions need to be understood. The contribution of each individual aerosol group to the total aerosol indirect effect ought to be assessed as well. There is also need to extend the analysis of aggregation, sedimentation and coalescence indirect effects to solid aerosols and all aerosols combined. The effects of meteorology on solid aerosol indirect effects also need to be evaluated.

In the future, similar analysis carried out in Chapters 5 and 6 using Tests A to F shall be repeated, but with both solid and solute aerosols set to their pre-industrial number and mass concentrations. This analysis has already started, and the results for the total aerosol indirect effects from all aerosols are presented in Sect. 6.7. This analysis is crucial because the interactions of solid aerosols with clouds and of solute aerosols with clouds in the real atmosphere occur simultaneously.

In this project, tropical and mid-latitude cases were simulated and analyzed. It is however important to extend this study to a higher latitude case. Work on one such case has already started, where much higher spatial and temporal resolutions are being used in the simulations. The case that has been selected for this high

latitude study is the Indirect and Semi-Direct Aerosol Campaign (ISDAC) campaign (McFarquhar and Coauthors, 2011). This third case shall be aimed at broadening the scope of our investigation and findings. ISDAC is a unique scenario in that, apart from being a polar case, the surface of the domain was covered by sea-ice.

Another way of improving the methodology applied in this study is the use of tagging tracers instead of sensitivity tests to analyse aerosol-cloud interactions and aerosol indirect effects. This is because sensitivity tests tend to change the microphysics of clouds and hence, the results may be hypothetical. The other technique that will be employed in the future work is the use of ensemble runs for each test performed. Also, there is need to forecast the future trends of these aerosol indirect effects of glaciated clouds. Finally, the ultimate goal of the work is to develop informed parameterizations for aerosol indirect effects of glaciated clouds that can be applied in GCMs in order to accurately represent aerosol-cloud interactions with the aim of improving the prediction of our future climate.

Appendix A

Kohler Theory of Droplet Nucleation

As the RH rises, the water soluble component of the CCN deliquesces and undergoes diffusional growth following the Kelvin Eqn. A.1, which illustrates that at any given temperature, a saturation vapour pressure over the water droplet, $e_{s,w}(r)$ exists for every water droplet of radius r and is greater than the saturation vapour pressure the bulk water surface, $e_{s,w}(\infty)$:

$$e_{s,w}(r) = e_{s,w}(\infty) \exp^{(\frac{2\sigma_w}{R_v \rho_w T r})} \tag{A.1}$$

where, $R_v = R_v$ is the gas constant for water vapour and σ_w is the *surface tension* of water, which can be defined as the free energy per unit are of liquid water; $e_{s,w}(r)$ is defined as the equilibrium vapour pressure, which is the droplet vapour pressure when the rates of evaporation and condensation are exactly balanced between the droplet and its vapour. The Kelvin equation shows that the $e_{s,w}(r)$ increases with decreasing radius.

For a given vapour pressure e, cloud embryos whose $e_{s,w}(r) > e$ will decay whist those with $e_{s,w}(r) < e$ will grow and the growth rate will be proportional to (e $-$ $e_{s,w}(r)$). Diffusional growth of the droplet continues with the rising RH until a *critical radius* r_c is reached where $e_{s,w} = e_{s,w}(r_c)$. This critical radius, r_c is given by equation (A.2).

$$r_c = \frac{2\sigma_w}{R_v \rho_w T \ln(e/e_{s,w}(\infty))} = \frac{2\sigma_w}{R_v \rho_w T \ln S} \tag{A.2}$$

Just beyond r_c, the droplet is said to be *activated* and begins to grow freely and rapidly, still by diffusion into a macroscopic cloud particle, this is because further increase $r > r_c$ either by diffusing or by collision and coalescence makes it super-critical since $e_{s,w}(r)$ drops rapidly with increasing r. Droplets with larger r_c are nucleated first, hence, smaller CCN require large supersaturations for activation.

Water soluble substances reduce the surface tension of a pure water droplet by

replacing some of the water molecules on the droplet surface, this effect reduces drastically the equilibrium vapour pressure e' over a droplet of the solution so much that the solution may be supersaturated in a subsaturated ambient according to what is called the Raoult's law. This phenomenon is called the *solute effect* and is proportional to the concentration of the solvent in the solution and can be summarized numerically by equation (A.3) Rogers and Yau (1991).

$$\frac{e'}{e_s(\infty)} = 1 - \frac{b}{r^3} \tag{A.3}$$

Here b can be approximated by (A.4) and is referred to as the *solution term*:

$$b \approx \frac{4.3iM}{m_s} \tag{A.4}$$

where M is the solute mass, m_s is the molecular weight of the solute whilst i is the degree of ionic dissociation. Combining the Kelvin's equation (A.1) and the solution effect equation (A.4) leads to;

$$\frac{e'}{e_s(\infty)} = 1 + \frac{a}{r} - \frac{b}{r^3} \tag{A.5}$$

where a is given by (A.6) and is called the *curvature term*,

$$a = \frac{2\sigma_w}{R_v \rho_w T} \approx \frac{3.3 \times 10^{-5}}{T} \tag{A.6}$$

Eqn (A.5) shows that at smaller droplet sizes, the solution term dominates and the droplet grows with increasing humidity even at relative humidity below 100% (along this trajectory the droplet referred to as a hazy particle) until an inflexion point is reached where the curvature term takes over leading to spontaneous growth of the particle into a cloud droplet irrespective of the supersaturation trajectory. At the inflexion point, a *critical supersaturation*, S^{star} and a *critical radius*, r^{star} can be defined as follows:

$$S^{star} = 1 + \sqrt{\frac{4a^3}{27b}} \tag{A.7}$$

$$r^{star} = \sqrt{\frac{3b}{a}} \tag{A.8}$$

Appendix B

The Heterogeneous Ice Nucleation Scheme

This empirical heterogeneous ice nucleation scheme is derived from observations of ice nuclei made using the Cloud Flow Diffusion Chamber (CFDC) during the Ice Nuclei Spectroscopy Studies (INSPECT) field campaign. The scheme treats all the four known modes of ice nucleation (i.e. deposition, immersion, condensation and contact freezing).

B.1 The Reference Activity Spectrum

The reference activity spectrum is defined as the IN activity at water saturation that was observed during the INSPECT campaign. The reference activity spectrum that represents the IN activity below the water saturation at temperatures, T, lower than -35 $^{\circ}C$ is expressed as,

$$n_{IN,1,\star}(T,s) = c_1 \frac{exp^{12,96(s_i-1,1)0.3}}{\rho_c} \quad for \quad T \leq -35^{\circ}C \quad and \quad 1 \leq s_i \leq s_i^{hom} \tag{B.1}$$

where, $n_{IN,1,\star}$, is the number mixing ratio of active IN, s_i, is the saturation with respect to ice and $c_1 = 1000cm^{-3}$ is a constant that depends on the air-mass, while ρ_c is the air density. These measurements of the reference activity spectrum were taken at conditions that were below homogeneous aerosol freezing, hence, s_i^{hom}, is the saturation vapor pressure with respect to ice at homogeneous freezing of aerosols.

At humidity higher than those at homogeneous aerosol freezing, the reference activity spectrum is adjusted to,

$$n_{IN,1,\star} = n_{IN,1,\star}\gamma \quad for \quad T \leq -35^{\circ}C \quad and \quad 1 \leq s_i \leq s_i^{w} \tag{B.2}$$

where, $\gamma = 2$, is a constant that takes into account the rapid increases in IN activity

at water saturation that were observed during the campaign.

For temperatures warmer than -25 $°C$, $n_{IN,1,\star}$, is given by,

$$n_{IN,1,\star} = \psi c_1 exp^{12.96(s_i-1)-0.639} \tag{B.3}$$

which is a rescaling of the **?** formula by the use of the rescaling factor of $\psi = 0.058\gamma/\rho_c$. At temperatures between -35 and -25 $°C$, the reference activity spectrum is interpolated.

B.2 The Empirical Parameterization of the IN Activity

B.2.1 For the Deposition, Condensation and Immersion Freezing Modes

The number mixing ratio $n_{IN,x}$ of IN activated at a saturation ratio with respect to ice, s_i, is given by,

$$n_{IN,x} = \int_0^\infty (1 - exp^{(-\mu_x(D_x,S_i,T))}) \frac{dn_x}{dlogD_x} dlogD_x \tag{B.4}$$

where,

$$\mu_x = H_x(S_i,T)\xi(T)\frac{\alpha_x n_{IN,1,\star}}{\Omega_{x,1,\star}}\frac{d\Omega_x}{dn_x} \quad for \quad T \leq 0°C \quad and \quad 1 \leq s_i \leq s_i^w \tag{B.5}$$

x, in these expressions represents the chemical species of solid aerosols which are treated in the model (i.e. dust, soot and biological organic aerosols). The heterogeneous ice nucleation is treated explicitly by creating temporary grids (33 bins) of aerosol distributions, therefore, D_x is the mean diameter of aerosols within one particular size bin, and, dn_x, is the total number of aerosols with that size bin.

μ_x, is the average number of activated ice embryos per insoluble aerosol particle of size D_x. $H_x(S_i,T)$, is an empirical function that takes account of the fact that heterogeneous nucleation of ice is not prolific at sub-saturated conditions. $\xi(T)$, is a function that accounts for the temperature dependence of the onset of heterogeneous nucleation of ice by IN, and these onset temperatures are species specific. The α_x, term represents the fractional contribution of the x^{th} specie to, $n_{IN,1,\star}$, while, $\Omega_{x,1,\star}$, is the empirical baseline total surface area of aerosols with sizes between 0.1 - 1 μm, which were estimated in the CFDC and, Ω_x, is the total surface area of the available aerosols.

B.2.2 For the Contact Freezing Modes

As for contact freezing, the number mixing ratio of active IN is determined by assuming that each IN activates either in the condensation, immersion and deposition mode or in the contact freezing mode and the only difference is that, the onset temperatures of activation in the freezing mode are greater than those of the other modes. The differences between the onset temperatures of the other modes and those of contact freezing, ΔT, are species specific.

Therefore, the number mixing ratio of active contact IN is then related to that of the other modes as,

$$n_{x,CIN} = \alpha_x \xi(T - \Delta T_{onset}) \frac{n_{IN,1,\star}(T - \Delta T, S_i^w(T - \Delta T))}{\Omega_{x,1,\star}} \Omega_{x,int} \tag{B.6}$$

where, $\Omega_{x,int}$, is the total surface area of the interstitial IN (i.e. those that did not nucleate in the immersion mode).

Appendix C

Particle-Particle Interaction

From fluid dynamics concepts and observational studies, a good approximation of droplet terminal fall speeds for a droplet of radius r can be parameterized as in equation (C.1).

$$u(r) = kr, \qquad 40 < r < 0.6mm \tag{C.1}$$

where $k = 8{\times}10^3 s^{-1}$ is a constant. As a result of the size dependent terminal velocity spectrum, larger particles begin to overtake and collide with each other in a process known as *collision and coalescence*, the dominant precipitation forming mechanism in water clouds.

Considering a small droplet of radius r with terminal velocity $u(R)$ lying in the path of a larger droplet with radius R and falling with terminal velocity $u(R)$ $> u(R)$ and whose centres are geometrically separated by distance x called the *impact parameter*, the probability collision of the two droplets is called the *collision efficiency* E,

$$E = \frac{x_0^2}{(R+r)^2} \tag{C.2}$$

where, x_0 is the critical impact parameter, which measures the distance within which collision is certain otherwise no collision takes place due to aerodynamically and inertial forces. Not all colliding particle will coalesce or stick together some will rebound, the fraction of those that coalesce is given by coalescence/sticking efficiency, E_s, which depends on the geometrical, aerodynamical and thermodynamical properties of the droplets. The product of E_s and E gives the collection efficiency

$$E(R, r) = EEs. \tag{C.3}$$

During an interval of 1s, a droplet falling with terminal velocity $u(R)$ sweeps

smaller drops with terminal velocity $u(R)$ in a volume given by:

$$V = \pi(R+r)^2[u(R) - u(r)] \tag{C.4}$$

This leads to the average number, $dn(R,r)$ of droplets of radius r to $r+dr$ range collected by the large droplet,

$$dn(R,r) = \pi(R+r)^2[u(R) - u(r)]n(r)E(R,r)dr \tag{C.5}$$

Integrating equation (C.5) over the whole CDSD with respect to time leads to the rate of change of the droplet volume,

$$\frac{dR}{dt} = \frac{\pi}{3}\int_0^R \left(\frac{R+r}{R}\right)^2 [u(R) - u(r)]n(r)r^3E(R,r)dr \tag{C.6}$$

The rate of change of the droplet with altitude is the

$$\frac{dR}{dz} = \frac{dR}{dt}\frac{dt}{dz} = \frac{dR}{dt}\frac{dt}{dt \times speed} = \frac{dR}{dt}\frac{dt}{U - u(R)} \tag{C.7}$$

where U is the updraft velocity. If $r << R$ then $u(R) \approx 0.$ can be assumed and simplifies equation (C.7) to:

$$\frac{dR}{dt} = \frac{\bar{E}w_L}{4\rho_w}u(R) \tag{C.8}$$

Also equation (C.7) subsequently becomes:

$$\frac{dR}{dz} = \frac{\bar{E}w_L}{4\rho_w}\frac{u(R)}{U - u(R)} \tag{C.9}$$

where w_L is the LWC from equation (2.5) (Rogers and Yau, 1991). In the development of these droplets, cloud has been assumed to be a continuum, which is not true for real clouds, also, other factors such as turbulence and horizontal advection cannot be ignored.

Appendix D

Accretion Processes in the Model

Symbol	Meaning
$\mathrm{Ac}(\mathrm{q}_g;\, \mathrm{q}_w \mid q_g)$	Riming of cloud liquid by graupel
$\mathrm{Ac}(\mathrm{q}_g;\, \mathrm{q}_i \mid q_g)$	Accretion of cloud ice by graupel
$\mathrm{Ac}(\mathrm{q}_g;\, \mathrm{q}_s \mid q_g)$	Accretion of snow by graupel
$\mathrm{Ac}(\mathrm{q}_g;\, \mathrm{q}_r \mid q_g)$	Accretion of rain by graupel
$\mathrm{Ac}(\mathrm{q}_g;\, \mathrm{q}_r \mid q_i)$	Accretion of cloud ice by rain
$\mathrm{Ac}(\mathrm{q}_g/\mathrm{q}_s;\, \mathrm{q}_s \mid q_r)$	Accretion of snow by rain, forming graupel or snow
$\mathrm{Ac}(\mathrm{q}_g/\mathrm{q}_s;\, \mathrm{q}_r \mid q_s)$	Accretion of rain by snow, forming graupel or snow
$\mathrm{Ac}(\mathrm{q}_r;\, \mathrm{q}_w \mid q_r)$	Accretion of cloud liquid by rain
$\mathrm{Ac}(\mathrm{q}_s;\, \mathrm{q}_w \mid q_s)$	Riming of cloud liquid by snow
$\mathrm{Ac}(\mathrm{q}_s;\, \mathrm{q}_i \mid q_s)$	Accretion of cloud ice by snow
$\mathrm{Ac}(\mathrm{q}_s;\, \mathrm{q}_w \mid q_i)$	Snow from cloud ice by riming

Table D.1: *Microphysical conversion tendencies for mass mixing ratio (kg $kg^1 s^1$) (Sect. 3.2.2). The final species in each interaction is the first symbol within parentheses, while symbols after the semicolon denote the initial interacting species. NB: The table is modified version of the one in Phillips et al. (2007).*

Appendix E

Table of constants

parameter	value	units	reference
a_r	842.	$\mathrm{m}^{1-b_x}\mathrm{s}^{-1}$	
a_g	85.		
a_l	2.975×10^7		Rogers and Yau (1991)
a_i	559.		Phillips et al. (2009)
b_r	0.8	unitless	
b_g	0.5		
b_l	2.		Rogers and Yau (1991)
b_i	0.813		Phillips et al. (2009)
C_0	0.0044086		Heymsfield et al. (2007b)
C_1	7.03×10^{-5}		Heymsfield et al. (2007b)
C_2	0.207		Heymsfield et al. (2007b)
C_3	-0.006		Heymsfield et al. (2007b)
$D_{min,r}$	100	μm	
$D_{min,g}$	200		
$D_{min,s}$	200		
$D_{min,l}$	2		
$D_{min,i}$	2		

Table E.1: *Table of constants*

Appendix F

Sedimentation of Hydrometeors

F.1 Snow

The vertical velocity dimension relationship given in equation (F.1), extracted from Heymsfield et al. (2007a) is used to determine the terminal fall speeds at the surface, $V_{t,s}(D)$ for snow.

$$V_{t,s}(D) = a_s D^{b_s} \tag{F.1}$$

Here, b_s is a unitless parameter given by $b_s = C_2 + C_3 T$, T is in this case assumed to be -40.6. The coefficient $a_s = C_0 \exp^{C_1 T}$, while D is the maximum diameter of the particle. The values of the constants are given in Table E.1.

The mass dimension relationship given by Heymsfield et al. (2007b) is used:

$$m_s(D) = c_s D^{d_s} \tag{F.2}$$

Temperature dependence arises from $c_s = C_0 + C_1 T$ and $d_s = 1.75$, while C_0 and C_1 are 0.0044 and 7.03×10^{-5}. From the mass-dimension relation, the dimension dependent bulk density for snow $\rho_s(D)$ can then be derived simply from the mass-volume relationship.

$$\rho_s(D) = \left(\frac{6c_s}{\pi}\right) D^{d_s - 3.} \tag{F.3}$$

The particle size distribution (PSD) for snow follows a gamma distribution of the form shown in equation (F.4).

$$N_s(D) = N_{0,s} D^{\mu_s} \exp^{-\lambda_s D} \tag{F.4}$$

However, in the model we make the shape parameter $\mu_s = 0$ to get an exponential distribution. N_0 is the intercept parameter, while λ_s is the shape parameter. The ice water content IWC_s can be related to the intercept and shape parameter as

shown in equation (F.5) given by Heymsfield et al. (2007a).

$$IWC_s = c_s N_{0,s} \frac{\Gamma(d_s + \mu_s + 1)}{{\lambda_s}^{d_s+\mu_s+1}} \tag{F.5}$$

Heymsfield et al. (2002) relates the intercept parameter to the shape parameter as:

$$N_{0,s} = 3.61 \times 10^{-5} {\lambda_s}^{2.09} = \alpha {\lambda_s}^{\beta} \tag{F.6}$$

From equations (F.5) and (F.6), the intercept and slope parameters can be estimated:

$$N_{0,s} = \left[\frac{c_s \Gamma(d_s + 1)}{IWC_s \left(\frac{1}{\alpha}\right)^{(\frac{d_s+1}{\beta})}} \right]^{\frac{\beta}{d_s+1-\beta}} \tag{F.7}$$

$$\lambda_s = \left[c_s N_0 \frac{\Gamma(d_s + 1 + \mu_s)}{IWC_s} \right]^{\frac{1}{d_s+\mu_s+1}} \tag{F.8}$$

Finally, the mass-weighted fall speed, $V_{m,s}$ can be computed numerically from:

$$V_{m,s} \approx \frac{\sum_{D=1}^{N_t} N_s(D) m_s(D) V_{t,s}(D)}{\sum_{D=1}^{N_t} N_s(D) m_s(D)} \tag{F.9}$$

Here N_t is the total number of size bins for the dimensions of snow particles, which is currently 33 in the model.

F.2 Rain

The surface fall speeds for rain drops are determined from equation (F.1) with subscript r and the velocity-dimension constants shown in Table E.1. The mass and size spectra of rain drops are defined using equation (3.12). Rain drops follow an γ-distribution shown in equation (F.4) with a mass mixing ratio dependent intercept parameter $N_{0,r}$ taken from Thompson et al. (2004). The shape parameter λ_r and the mass-weighted fall speeds of rain follow Lin et al. (1983).

F.3 Graupel

The surface fall speeds for graupel are determined from equation (F.1) with subscript g and using the velocity-dimension constants shown in table (E.1). The mass and

size distribution of graupel are defined using equation (3.12). Graupel follows an exponential distribution shown in equation (F.4) for $\mu_g = 0$. The intercept parameter $N_{0,g} = 4. \times 10^{-4}$, shape parameter λ_g and mass-weighted fall speeds of graupel taken from Lin et al. (1983). The size-dependent shape H for graupel is given by:

$$H(j) = (1.0 - 10D(j))D(j) \tag{F.10}$$

while the size-dependent bulk density ρ_g of graupel is:

$$\rho_g(j) = 2.5\alpha_g D(j)^{\beta_g} \tag{F.11}$$

here $\alpha_g = 0.14128$ and $\beta_g = -0.3448$ are constants.

F.4 Cloud ice and Cloud Liquid

The surface fall speeds for cloud ice and cloud liquid are determined from equation (F.1) by replacing the subscript (s) with subscript (i) and l respectively with velocity-dimension constants shown in table (E.1). The mass and size distribution of cloud-liquid and cloud-ice are defined using equation (3.12). They both follow a gamma distribution shown in equation (F.4) with slope parameter $\mu_i = 1$ and $\mu_l = 3.5$. The intercept parameter $N_{0,x}$ and shape parameter λ_x are as described in Phillips et al. (2007). Different ice morphologies are now being treated in the model, Table 3.2 shows habits that presently considered in the emulated spectral microphysics.

Bibliography

, ????: .

Albrecht, B., 1989: Aerosols, cloud microphysics, and fractional cloudiness, science. *Science*, **245 (4923)**, 1227–1230.

Albrecht, B. A., C. W. Fairall, D. W. Thomson, A. B. White, J. B. Snider, and W. H. Schubert, 1990: Surface-based remote sensing of the observed and the adiabatic liquid water content of stratocumulus clouds. *Geophysical Research Letters*, **17 (1)**, 89–92.

Aleksic, N. M., R. Farley, and H. Orville, 1989: A numerical cloud model study of the hallett-mossop ice multiplication process in strong convection. *Atmospheric Research*, **23 (1)**, 1 – 30, doi:10.1016/0169-8095(89)90056-2, URL `http://www.sciencedirect.com/science/article/pii/0169809589900562`.

Allen, G., et al., 2008: Aerosol and trace-gas measurements in the darwin area during the wet season. *Journal of Geophysical Research*, **113**, D06 306, doi:10.1029/2007JD008706.

Anderson, R. J., R. C. Miller, J. L. Kassner Jr, and D. E. Hagen, 1980: A study of homogeneous condensation-freezing nucleation of small water droplets in an expansion cloud chamber. *Journal of the Atmospheric Sciences*, **37 (11)**, 2508–2520.

Andreae, M. O. and P. Merlet, 2001: Emission of trace gases and aerosols from biomass burning. *Global biogeochemical cycles*, **15 (4)**, 955–966.

Andreae, M. O., D. Rosenfeld, P. Artaxo, A. A. Costa, G. P. Frank, K. M. Longo, and M. A. F. Silva-Dias, 2004: Smoking rain clouds over the amazon. *Science*, **303 (5662)**, 1337–1342.

Andreae, M. O. et al., 2007: Aerosols before pollution. *Science(Washington)*, **315 (5808)**, 50–51.

Andronache, C., L. J. Donner, C. J. Seman, V. Ramaswamy, and R. S. Hemler, 1999: Atmospheric sulfur and deep convective clouds in tropical pacific: A model study. *J. Geophys. Res*, **104**, 4005–4024, doi:10.1029/1998JD200085.

Baker, M. B. and T. Peter, 2008: Small-scale cloud processes and climate. *Nature*, **451 (7176)**, 299–300.

Beard, K. V. and H. T. Ochs III, 1993: Warm-rain initiation: An overview of microphysical mechanisms. *Journal of Applied Meteorology*, **32 (4)**, 608–625.

Berg, L. K., C. M. Berkowitz, J. C. Barnard, G. Senum, and S. R. Springston, 2009: Overview of the cumulus humilis aerosol processing study. *B. Am.Meteorol. Soc.*, **90 (11)**, 1653, doi:10.1175/2009BAMS2760.1.

Bernholdt, D., et al., 2005: The earth system grid: Supporting the next generation of climate modeling research. *Proceedings of the IEEE*, **93 (3)**, 485–495.

Blyth, A. M. and J. Latham, 1990: Airborne studies of the altitudinal variability of the microphysical structure of small, ice-free, montanan cumulus clouds. *Q. J. R. Meteorol. Soc.*, **116**, 1405–1423.

Bony, S. and J.-L. Dufresne, 2005: Marine boundary layer clouds at the heart of tropical cloud feedback uncertainties in climate models. *Geophysical Research Letters*, **32 (20)**.

Borys, R. D., D. H. Lowenthal, S. A. Cohn, and W. O. J. Brown, 2003: Mountaintop and radar measurements of anthropogenic aerosol effects on snow growth and snowfall rate. *Geophysical Research Letters*, **30 (10)**, 1–4.

Boucher, O. and D. Randall, 2013: Climate change 2013: The physical science basis. contribution of working group i to the fifth assessment report of the intergovernmental panel on climate change, (ipcc). *Cambridge University Press, Cambridge, United Kingdom and New York, NY, USA.*, **5th**.

Breon, F., D. Tanre, and S. Generoso, 2002: Aerosol effect on cloud droplet size monitored from satellite. *Science*, **295 (5556)**, 834–8.

Brient, F. and S. Bony, 2012: How may low-cloud radiative properties simulated in the current climate influence low-cloud feedbacks under global warming-. *Geophysical Research Letters*, **39**, L20 807.

Briffa, K. R., 1999: The simulation of weather types in gcms: A regional approach to control-run validation. *Analysis of Climate Variability*, 121–138.

Buck, A. L., 1981: New equations for computing vapor pressure and enhancement factor. *Journal of Applied Meteorology*, **20 (12)**, 1527–1532.

Charlson, R., S. E. Schwartz, J. Hales, R. Cess, J. J. Coakley, H. JE., and H. DJ., 1992: Climate forcing by anthropogenic aerosols. *Science*, **255 (5043)**, 423–30.

Chen, W., C. P. Woods, J. F. Li, D. E. Waliser, J. Chern, W. Tao, J. H. Jiang, and A. M. Tompkins, 2011: Partitioning cloudsat ice water content for comparison with upper tropospheric ice in global atmospheric models. *J. Geophys. Res*, **116**, D19 206, doi:10.1029/2010JD015179.

Clark, T. L., 1974: A study of cloud phase parameterization using the gamma distribution. *J. Atmos. Sci*, **31**, 142–155.

Clark, T. L. and W. D. Hall, 1983: A cloud physical parameterization method using movable basic functions: Stochastic coalescence parcel calculations. *J. Atmos. Sci*, **40**, 1709–1728.

Clarke, A. D. and V. N. Kapustin, 2002: A pacific aerosol survey. part i: A decade of data on particle production, transport, evolution, and mixing in the troposphere. *Journal of the atmospheric sciences*, **59 (3)**, 363–382.

Clarke, A. D., S. R. Owens, , and J. Zhou, 2006: An ultrafine sea-salt flux from breaking waves: Implications for cloud condensation nuclei in the remote marine atmosphere,. *Journal of Geophys Research*, **111**, D06 202, doi: 10.1029/2005JD006565.

Clarke, A. D., et al., 2004: Size distributions and mixtures of dust and black carbon aerosol in asian outflow: Physiochemistry and optical properties. *Journal of Geophysical Research: Atmospheres*, **109**, D15S09.

Connolly, P. J., T. W. Choularton, M. W. Gallagher, K. N. Bower, M. J. Flynn, and J. A. Whiteway, 2006: Cloud-resolving simulations of intense tropical hector thunderstorms: Implications for aerosol-cloud interactions. *Q.J.R. Meteorol. Soc.*, **132**, 3079–3106, doi:10.1256/qj.05.86.

Corrigan, C. and T. Novakov, 1999: Cloud condensation nucleus activity of organic compounds: a laboratory study. *Atmospheric Environment*, **33 (17)**, 2661–2668.

Costantino, L. and F. M. Bréon, 2013: Aerosol indirect effect on warm clouds over south-east atlantic, from co-located modis and calipso observations. *Atmospheric Chemistry and Physics*, **13**, 69–88.

Cotton, W. R., R. R. M. Tripoli G. J., and M. E. A., 1986: Numerical simulation of the effects of varying ice crystal nucleation rates and aggregation processes on orographic snowfall. *Journal of Applied Meteorology*, **25 (11)**, 1658–1680.

Crawford, I., et al., 2011: Studies of propane flame soot acting as heterogeneous ice nuclei in conjunction with single particle soot photometer measurements. *Atmospheric Chemistry and Physics*, **11 (18)**, 9549–9561.

Cui, Z., K. S. Carslaw, Y. Yin, and S. Davies, 2006: A numerical study of aerosol effects on the dynamics and microphysics of a deep convective cloud in a continental environment. *J. Geophys. Res.*, **111 (D05)**, D05 201.

Cziczo, D. J., D. M. Murphy, P. K. Hudson, and D. S. Thomson, 2004: Single particle measurements of the chemical composition of cirrus ice residue during crystal-face. *J. Geophys. Res*, **109**, D04 201.

Dall'Oglio, G., S. Fonti, B. Melchiorri, F. Melchiorri, V. Natale, P. Lombardini, P. Trivero, and S. Sivertsen, 1976: Measurements of the cosmic background radiation through the 1.0-1.4-mm atmospheric window. *Physical Review D*, **13 (5)**, 1187.

DeMott, P. J., et al., 2011: Resurgence in ice nuclei measurement research. *Bull. Amer. Meteor. Soc*, **92**, 1623–1635.

Di Pierro, M., L. Jaeglé, E. W. Eloranta, and S. Sharma, 2013: Spatial and seasonal distribution of arctic aerosols observed by the caliop satellite instrument (2006–2012). *Atmospheric Chemistry and Physics*, **13 (14)**, 7075–7095, doi:10.5194/acp-13-7075-2013, URL `http://www.atmos-chem-phys.net/13/7075/2013/`.

Diehl, K., S. Matthias-Maser, R. Jaenicke, and S. Mitra, 2002: The ice nucleating ability of pollen:: Part ii. laboratory studies in immersion and contact freezing modes. *Atmospheric research*, **61 (2)**, 125–133.

Diehl, K., C. Quick, S. Matthias-Maser, S. Mitra, and R. Jaenicke, 2001: The ice nucleating ability of pollen: Part i: Laboratory studies in deposition and condensation freezing modes. *Atmospheric Research*, **58 (2)**, 75–87.

Dudhia, S.-Y. H., J. and K.-S. Lim, 2008: A new method for representing mixed-phase particle fall speeds in bulk microphysics parameterizations. *Journal of the Meteorological Society of Japan*, **86 (A)**, 33–44, doi:10.2151/jmsj.86A.33.

Dusek, U., et al., 2006: Size matters more than chemistry for cloud-nucleating ability of aerosol particles. *Science*, **312 (5778)**, 1375–1378.

Dymarska, M., B. J. Murray, L. Sun, M. L. Eastwood, D. A. Knopf, and A. K. Bertram, 2006: Deposition ice nucleation on soot at temperatures relevant for the lower troposphere. *Journal of Geophysical Research: Atmospheres (1984–2012)*, **111 (D4)**.

Eidhammer, T., P. J. DeMott, and S. M. Kreidenweis, 2009: A comparison of heterogeneous ice nucleation parameterizations using a parcel model framework. *Journal of Geophysical Research: Atmospheres (1984–2012)*, **114 (D6)**.

Eidhammer, T., et al., 2010: Ice initiation by aerosol particles: measured and predicted ice nuclei concentrations versus measured ice crystal concentrations in an orographic wave cloud. *J. Atmos. Sci*, **67**, 2417–2436, doi:http://dx.doi.org/10.1175/2010JAS3266.1.

Fan, J., L. R. L. Daniel Rosenfeld, Yanni Ding, and Z. Li, 2012: Potential aerosol indirect effects on atmospheric circulation and radiative forcing through deep convection. *Geophysical Research Letters*, **39 (9)**, L09 806.

Fan, J., L. R. Leung, D. Rosenfeld, Q. Chen, Z. Li, J. Zhang, and H. Yan, 2013: Microphysical effects determine macrophysical response for aerosol impacts on deep convective clouds. *Proceedings of the National Academy of Sciences*, **110 (48)**, E4581–E4590.

Fan, J., et al., 2009: Dominant role by vertical wind shear in regulating aerosol effects on deep convective clouds. *Journal of Geophysical Research. D. (Atmospheres)*, **114 (D22)**, D22 206.

Feingold, G., 2003: Modeling of the first indirect effect: Analysis of measurement requirements. *Geophysics*, **109**, doi:10.1029/2003GL017967.

Feingold, G., W. R. C. B. Stevens, and R. L. Walko, 1994: An explicit cloud microphysics/les model designed to simulate the twomey effect. *Atmos. Res.*, **33**, 207–233.

Ferek, R. J., D. A. Hegg, P. V. Hobbs, P. Durkee, and K. Nielsen, 2002: Measurements of ship-induced tracks in clouds off the washington coast. *Journal of geophysical research*, **103 (D18)**, 199–223, doi:10.1029/98JD02121.

Ferrier, B. S., 1994: A double-moment multiple-phase four-class bulk ice scheme. part i: Description. *J. Atmos. Sci.*, **51**, 249–280.

Field, P. R., A. J. Heymsfield, and A. Bansemer, 2006: Shattering and particle interarrival times measured by optical array probes in ice clouds. *J. Atmos. Oceanic Technol*, **23**, 1357–1371, doi:http://dx.doi.org/10.1175/JTECH1922.1.

Fitzgerald, J. W., 1973: Dependence of the supersaturation spectrum of ccn on aerosol size distribution and composition. *Journal of Atmospheric Sciences*, **30**, 628–634.

Fitzgerald, J. W., 1974: Effect of aerosol composition on cloud droplet size distribution: A numerical study. *Journal of Atmospheric Sciences*, **31**, 1358–1367.

Fred, G. and J. H. Seinfeld, 1980: Simulation of multicomponent aerosol dynamics. *Journal of Colloid and Interface Science*, **78 (2)**, 485 – 501, doi:http://dx.doi.org/10.1016/0021-9797(80)90587-1, URL `http://www.sciencedirect.com/science/article/pii/0021979780905871`.

Freidenreich, S. M. and V. Ramaswamy, 1999: A new multiple-band solar radiative parameterization for general circulation models. *J. Geophys. Res*, **104 (D24)**, 31 389–31 409.

Fridlind, A., A. Andrew, P. Jon, F. Paul, A. Hill, M. Greg, X. Shaocheng, and Z. Minghua, 2009: Arm/gcss/sparc twp-ice crm intercomparison study, tWP-ICE technical report.

Fridlind, A. M. and Co-authers, 2012: A comparison of twp-ice observational data with cloud-resolving model results. *J. Geophys. Res*, **117**, D05 204,, doi:10.1029/2011JD016595.

Fukuta, N., 1975: A study of the mechanism of contact ice nucleation. *Journal of the Atmospheric Sciences*, **32 (8)**, 1597–1603.

Gao, R., et al., 2004: Evidence that nitric acid increases relative humidity in low-temperature cirrus clouds. *Science*, **303 (5657)**, 516–520.

Garcia, E., C. J. Thomas, A. J. Hill, P. J. Prenni, G. D. DeMott, Franc, and S. M. Kreidenweis, 2012: Biogenic ice nuclei in boundary layer air over two u.s. high plains agricultural regions. *Journal of Geophysical research*, **117**, D18 209, doi: 10.1029/2012JD018343.

Gardiner, B. and J. Hallett, 1985: Degradation of in-cloud forward scattering spectrometer probe measurements in the presence of ice particles. *Journal of Atmospheric and Oceanic Technology*, **2 (2)**, 171–180.

Geresdi, I., 1998:: Idealized simulation of the colorado hailstormcase: Comparison of bulk and detailed microphysics. *Atmos. Res*, **45**, 237–252.

Gettelman, A., X. Liu, D. Barahona, D. Lohmann, and C. Chen, 2012: Climate impacts of ice nucleation. *Journal of Geophysical Research: Atmospheres*, **117 (D20)**, D20 201.

Greenwald, T. J., G. L. Stephens, T. H. Vonder Haar, and D. L. Jackson, 1993: A physical retrieval of cloud liquid water over the global oceans using special sensor microwave/imager (ssm/i) observations. *Journal of Geophysical Research: Atmospheres (1984–2012)*, **98 (D10)**, 18 471–18 488.

Gultepe, I., G. Isaac, and S. Cober, 2001: Ice crystal number concentration versus temperature for climate studies. *International journal of climatology*, **21 (10)**, 1281–1302.

Gunthe, S., et al., 2009: Cloud condensation nuclei in pristine tropical rainforest air of amazonia: size-resolved measurements and modeling of atmospheric aerosol composition and ccn activity. *Atmospheric Chemistry and Physics*, **9 (19)**, 7551–7575.

Hallett, J. and S. C. Mossop, 1974: Production of secondary ice particles during the riming process. *Nature*, **249**, 26 – 28.

Han, Q., W. B. Rossow, J. Chou, and R. M. Welch, 1998: Global survey of the relationships of cloud albedo and liquid water path with droplet size using isccp. *J. Climate*, **11**, 1516–1528.

Harrison, E. F., P. Minnis, B. R. Barkstrom, V. Ramanathan, R. D. Cess, and G. G. Gibson, 1990: Seasonal variation of cloud radiative forcing derived from the earth radiation budget experiment. *JOURNAL OF GEOPHYSICAL RESEARCH,*, **95 (D11)**, 18 687–18 703.

Haywood, J. and O. Boucher, 2000: Estimates of the direct and indirect radiative forcing due to tropospheric aerosols: A review. *Reviews of Geophysics*, **38 (4)**, 513–543.

Haywood, J., L. Donner, A. Jones, and J.-C. Golaz, 2009: *Global indirect radiative forcing caused by aerosols: IPCC (2007) and beyond In Clouds in the Perturbed Climate System*. MIT Press (In Clouds in the Perturbed Climate System), 451-467 pp.

Heisler, S. and S. Friedlander, 1977: Gas-to-particle conversion in photochemical smog: Aerosol growth laws and mechanisms for organics. *Atmospheric Environment*, **11 (2)**, 157–168.

Heymsfield, A., A. Bansemer, P. Field, S. Durden, J. Stith, J. Dye, W. Hall, and C. Grainger, 2002: Observations and parameterizations of particle size distributions in deep tropical cirrus and stratiform precipitating clouds: Results from in-situ observations in trmm field campaigns. *Journal of the Atmospheric Sciences*, **59**, 3457–3491.

Heymsfield, A., A. Bansemer, and C. Twohy, 2007a: Refinements to ice particle mass dimensional and terminal velocity relationships for ice clouds: Part 1: Temperature dependence. *Journal of the Atmospheric Sciences*, **64**, 1047–1067, doi: 10.1175/JAS3890.1.

Heymsfield, A., L. Miloshevich, C. Schmitt, A. Bansemer, C. Twohy, M. Peollot, A. Fridlind, and H. Gerber, 2005: Homogeneous ice nucleation in subtropical and tropical convection and its influence on cirrus anvil microphysics. *J. Atmos. Sci.*, **62**, 41–64, doi:10.1175/JAS-3360.1.

Heymsfield, A. J., 1977: Precipitation development in stratiform ice clouds: A microphysical and dynamical study. *Journal of the Atmospheric Sciences*, **34 (2)**, 367–381.

Heymsfield, A. J. and G. M. McFarquhar, 1996: High albedos of cirrus in the tropical pacific warm pool: microphysical interpretations from cepex and from kwajalein, marshall islands. *J. Atmos. Sci*, **53**, 2424–2451, doi:http://dx.doi.org/10.1175/1520-0469(1996)053⟨2424:HAOCIT⟩2.0.CO;2.

Heymsfield, A. J., G.-J. Van Zadelhoff, D. P. Donovan, F. Frederic, J. H. Robin, and J. I. Anthony, 2007b: Refinements to ice particle mass dimensional and terminal velocity relationships for ice clouds. part ii: evaluation and parameterizations of ensemble ice particle sedimentation velocities. *Journal of the atmospheric science*, **64**, 1068–1088., doi:http://dx.doi.org/10.1175/JAS3900.1.

Hill, A. A. and S. Dobbie, 2008: The impact of aerosols on non-precipitating marine stratocumulus. ii: The semi-direct effect. *Quarterly Journal of the Royal Meteorological Society*, **134**, 1155–1165, doi:10.1002/qj.277.

Hill, A. A., S. Dobbie, and Y. Yin, 2008: The impact of aerosols on non-precipitating marine stratocumulus. i: Model description and prediction of the indirect effect. *Q.J.R. Meteorol. Soc.*, **134**, 1143–1154.

Hirst, E., P. H. Kaye, R. Greenaway, P. Field, and D. Johnson, 2001: Discrimination of micrometre-sized ice and super-cooled droplets in mixed-phase cloud. *Atmospheric Environment*, **35 (1)**, 33–47.

Hobbs, P. V., 1969: Ice multiplication in clouds. *J. Atmos. Sci*, **26**, 315–318.

Hobbs, P. V., 1993: *Aerosol-cloud-climate interactions*. Academic Press Inc.

Hobbs, P. V., S. Chang, and J. D. Locatelli, 1974: The dimensions and aggregation of ice crystals in natural clouds. *Journal of Geophysical Research*, **79 (15)**, 2199–2206.

Hobbs, P. V. and L. Radke, 1969: Cloud condensation nuclei from a simulated forest fire. *Science*, **163 (3864)**, 279–280.

Hobbs, P. V. and A. L. Rangno, 1985: Ice particle concentrations in clouds. *Journal of the atmospheric sciences*, **42 (23)**, 2523–2549.

Hoeve, T. J. E., L. A. Remer, and M. Z. Jacobson, 2011: Microphysical and radiative effects of aerosols on warm clouds during the amazon biomass burning season as observed by modis: impacts of water vapor and land cover. *Atmos. Chem. Phys.*, **11**, 3021–3036.

Hoppel, W. A., G. M. Frick, and J. W. Fitzgerald, 2002: Surface source function for sea-salt aerosol and aerosol dry deposition to the ocean surface. *Journal of Geophysical Research: Atmospheres*, **107 (D19)**, AAC 7–1–AAC 7–17, doi:10.1029/2001JD002014, URL `http://dx.doi.org/10.1029/2001JD002014`.

Houghton, J. T., 1986: *The physics of Atmospheres*. Cambridge University Press.

Johnson, B., K. Shine, and P. Forster, 2004: The semi-direct aerosol effect: Impact of absorbing aerosols on marine stratocumulus. *Quarterly Journal of the Royal Meteorological Society*, **130 (599)**, 1407–1422.

Johnson, B. T., 2003: The semi-direct aerosol effect. Ph.D. thesis, The University of Reading.

Junge, C. and E. McLaren, 1971: Relationship of cloud nuclei spectra to aerosol size distribution and composition. *Journal of Atmospheric Sciences*, **28**, 382–390.

Kajikawa, M. and A. J. Heymsfield, 1989: Aggregation of ice crystals in cirrus. *J. Atmos. Sci.*, **46**, 3108–3121, doi:http://dx.doi.org/10.1175/1520-0469(1989)046⟨3108:AOICIC⟩2.0.CO;2.

Kaneyasu, N., P. V. Hobbs, Y. Ishizaka, and G. Qian, 2001: Aerosol properties around marine tropical cumulus clouds. *J. Geophys. Res.*, **106**, 14 435–14 445.

Kapustin, V. N., A. D. Clarke., S. G. Howell., C. S. McNaughton., V. L. Brekhovskikh., and J. Zhou, 2012: Evaluating primary marine aerosol production and atmospheric roll structures in hawaii's natural oceanic wind tunnel. *J. Atmos. Oceanic Technol*, **29**, 668–682, doi:http://dx.doi.org/10.1175/JTECH-D-11-00079.1.

Keith, W. T. and C. P. R. Saunders, 1989: The collection efficiency of a cylindrical target for ice crystals. *Atmospheric reseach*, **23**, 83 – 95.

Kessler, E., 1969: On the distribution and continuity of water substance in atmospheric circulations. *Meteor. Monogr.*, **32**.

Khain, A., D. Rosenfeld, and A. Pokrovsky, 2005: Aerosol impact on the dynamics and microphysics of deep convective clouds. *Quarterly Journal of the Royal Meteorological Society*, **131**, 2639–2663.

Khairoutdinov, M. and Y. Kogan, 2000: A new cloud physics parameterization in a large-eddy simulation model of marine stratocumulus. *American Meteorological Society*, **128**, 229–243.

King, M., 1993: *Aerosol-cloudclimate interactions - Radiative properties of clouds*. Academic Press.

Koch, D. and A. D. Genio, 2010: Black carbon semi-direct effects on cloud cover: review and synthesis. *Atmospheric Chemistry and Physics*, **10 (16)**, 7685–7696.

Koehler, K. A., et al., 2009: Cloud condensation nuclei and ice nucleation activity of hydrophobic and hydrophilic soot particles. *Phys Chem Chem Phys*, **11 (36)**, 7906–20, doi:10.1039/b905334b.

Kohler, H., 1936: The nucleus in and the growth of hygroscopic droplets. *Trans Farad Soc*, **32,**, 32,.

Kołaczkiewicz, J. and E. Bauer, 1985: Clausius-clapeyron equation analysis of two-dimensional vaporization. *Surface Science*, **155 (2)**, 700–714.

Korolev, A., 2007: Limitations of the wegener-bergeron-findeisen mechanism in the evolution of mixed-phase clouds. *J. Atmos. Sci*, **64**, 3372–3375, doi:http://dx.doi.org/10.1175/JAS4035.1.

Korolev, A. V. and P. I. Mazin, 2003: Supersaturation of water vapor in clouds. *American Meteorological Society*, **60**, 2957–2974.

La Mer, V. K. and R. Gruen, 1952: A direct test of kelvin's equation connecting vapour pressure and radius of curvature. *Transactions of the Faraday Society*, **48**, 410–415.

Lamb, D. and J. Verlinde, 2011: *Physics and Chemistry of Clouds*. Cambridge University Press.

Leaitch, W. R., G. A. Isaac, J. W. Strapp, C. M. Banic, and H. A. Wiebe, 1992: The relationship between cloud droplet number concentrations and anthropogenic pollution: Observations and climatic implications. *J. Geophys. Res.*, **97 ((D2)**, 2463–2474.

Lee, S. S., L. J. Donner, and V. Phillips, 2009: Sensitivity of aerosol and cloud effects on radiation to cloud types: comparison between deep convective clouds and warm stratiform clouds over one-day period. *Atmos Chem Phys*, **9**, 2555–2575.

Lee, S. S., L. J. Donner, and V. T. Phillips, 2009): Impacts of aerosol chemical composition on microphysics and precipitation in deep convection. *Atmospheric Research*, **94**, 220–237.

Lee, S. S., L. J. Donner, V. T. Phillips, and Y. Ming, 2008a: The dependence of aerosol effects on clouds and precipitation on cloud-system organization, shear and stability. *Journal of Geophysical Research*, **113 (D16202)**, D16 202,.

Lee, S. S., L. J. Donner, V. T. Phillips, and Y. Ming, 2008b: Examination of aerosol effects on precipitation in deep convective clouds during the 1997 arm summer experiment. *Q J ROY METEOR SOC*, **134**, 1201–1220.

Lee, S.-S., F. Graham, and P. Y. Chuang, 2012: Effect of aerosol on cloud-environment interactions in trade cumulus. *J. Atmos. Sci*, **69**, 3607–3632.

Lei, Y., Q. Zhang, K. He, and D. Streets, 2011: Primary anthropogenic aerosol emission trends for china, 1990–2005. *Atmospheric Chemistry and Physics*, **11 (3)**, 931–954.

Lesins, G., P. Chylek, and U. Lohmann, 2002: A study of internal and external mixing scenarios and its effect on aerosol optical properties and direct radiative forcing. *Journal of Geophysical Research: Atmospheres*, **107 (D10)**, 4094, doi: 10.1029/2001JD000973.

Liao, H. and J. H. Seinfeld, 1998: Effect of clouds on direct aerosol radiative forcing of climate. *Journal of Geophysical Research: Atmospheres (1984–2012)*, **103 (D4)**, 3781–3788.

Lim, K. S. S. and Y. S. Hong, 2010: Development of an effective double-moment cloud microphysics scheme with prognostic cloud condensation nuclei (ccn) for weather and climate models. *American Meteorological Society*, **138**, 1587–1612, doi:10.1175/2009MWR2968.1.

Lin, Y. L., R. D. Farley, and H. D. Orville, 1983: Bulk parameterization of the snow field in a cloud model. *Journal of climate applications: Meteorology*, **22**, 1065–1092.

Liou, K. N., 2002: *An introduction to atmospheric radiation*. Academic Press.

List, R. J., 1951: f& smithsonian meteorological tables.

Lohmann, U., 2002a: A glaciation indirect aerosol effect caused by soot aerosols. *Geophysical Research Letters*, **29**, doi:10.1029/2001GL014357.

Lohmann, U., 2004: Can anthropogenic aerosols decrease the snowfall rate-. *Journal of Atmospheric Sciences*, **61 (20)**, 2457–2468.

Lohmann, U. and J. Feichter, 2001: Can the direct and semi-direct aerosol effect compete with the indirect effect on a global scale? *Geophysical Research Letters*, **28 (1)**, 159–161.

Lohmann, U. and J. Feichter, 2005: Global indirect aerosol effects: a review. *Atmospheric Chemistry and Physics*, **5 (3)**, 715–737, doi:10.5194/acp-5-715-2005, URL `http://www.atmos-chem-phys.net/5/715/2005/`.

Lohmann, U., J. P. Johann Feichter, and R. Leaitch, 2000a: Indirect effect of sulfate and carbonaceous aerosols-a mechanistic treatment. *105*, **D10**, 12 193–12 206.

Lohmann, U., G. Tselioudis, and C. Tyler, 2000b: Why is the cloud albedo - particle size relationship different in optically thick and optically thin clouds-. *GEOPHYSICAL RESEARCH LETTERS*, **27 (8)**, 1099–1102.

Lohmann, U., et al., 2010: Total aerosol effect: radiative forcing or radiative flux perturbation-. *Atmospheric Chemistry and Physics*, **10 (7)**, 3235–3246, doi:10.5194/acp-10-3235-2010, URL `http://www.atmos-chem-phys.net/10/3235/2010/`.

Mahowald, N. M. and L. M. Kiehl, 2003: Mineral aerosol and cloud interactions. *Geophysical research letters*, **30 (9)**, 1475, doi:10.1029/2002GL016762.

Marcolli, C., S. Gedamke, T. Peter, and B. Zobrist, 2007: Efficiency of immersion mode ice nucleation on surrogates of mineral dust. *Atmospheric Chemistry and Physics*, **7 (19)**, 5081–5091.

Marshall, J. S. and W. M. K. Palmer, 1948: The distribution of raindrops with size. *Journal of meteorology*, **5 (4)**, 165–166.

Marsham, J. H. and R. J. Dobbie, S. Hogan, 2006: Evaluation of a large-eddy model simulation of a mixed-phase altocumulus cloud using microwave radiometer, lidar and doppler radar data. *Q. J. R. Meteorol. Soc.*, **132**, 1693–1715, doi:10.1256/qj.05.145.

Martin, G., D. Johnson, and A. Spice, 1994: The measurement and parameterization of effective radius of droplets in warm stratocumulus clouds. *Journal of the Atmospheric Sciences*, **51 (13)**, 1823–1842.

Matthias-Maser, S. and R. Jaenicke, 1995: The size distribution of primary biological aerosol particles with radii ¿ 0.2-m in an urban/rural influenced region. *Atmos. Res.*, **39 (4)**, 279–286.

May, P. T., J. H. Mather, V. Geraint, B. Keith N., J. Christian, M. Greg M., and M. Gerald G., 2008: The tropical warm pool international cloud experiment. *American Meteorological Society*, **89**, 629–645, doi:http://dx.doi.org/10.1175/BAMS-89-5-629.

McComiskey, A. and G. Feingold, 2012: The scale problem in quantifying aerosol indirect effects. *Atmospheric Chemistry and Physics*, **12 (2)**, 1031–1049.

McFarquhar, G. M. and Coauthors, 2011: Indirect and semi-direct aerosol campaign: The impact of arctic aerosols on clouds. *Bull. Amer. Meteor. Soc*, **92**, 183–201, doi:http://dx.doi.org/10.1175/2010BAMS2935.1.

McFarquhar, G. M., J. Um, M. Freer, D. Baumgardner, G. Kok, , and G. Mace, 2007: The importance of small ice crystals to cirrus properties: Observations from the tropical warm pool international cloud experiment (twp-ice). *Geophys. Res. Lett*, **34**, L13 803, doi:10.1029/2007GL029865.

Menon, S. and A. D. Del Genio, 2007: *Human-Induced Climate Change: An Interdisciplinary Assessment*. 32-48 pp.

Menon, S., A. D. Genio, D. Del Koch, and G. Tselioudis, 2002a: Gcm simulations of the aerosol indirect effect: Sensitivity to cloud parameterization and aerosol burden. *Journal of the Atmospheric Sciences*, **59 (3)**, 692 – 713, doi:10.1175/1520-0469(2002)059-0692:GSOTAI-2.0.CO;2.

Mercer, J. H., 1978: *West Antarctic ice sheet and CO2 greenhouse effect: a threat of disaster*. Ohio State University, Institute of Polar Studies.

Meyers, M. P., P. J. DeMott, and W. R. Cotton, 1992: New primary ice-nucleation parameterizations in an explicit cloud model. *Journal of Applied Meteorology*, **31 (7)**, 708–721.

Miles, N. L., J. Verlinde, and E. E. Clothiaux, 2000: Cloud droplet size distributions in low-level stratiform clouds. *Journal of the atmospheric sciences*, **57 (2)**, 295–311.

Miller, M. A., 2007: Sgp cloud and land surface interaction campaign (clasic): Science and implementation plan. *DOE/SC-ARM-0703*.

Ming, Y., V. Ramaswamy, L. J. Donner, and V. T. J. Phillips, 2006: A new parameterization of cloud droplet activation applicable to general circulation models. *Journal of the atmospheric sciences*, **63**, 1348–1356.

Mitchell, D. L., 1994: A model predicting the evolution of ice particle size spectra and radiative properties of cirrus clouds. part i: Microphysics. *Journal of Atmospheric Sciences*, **51 (6)**, 797–816.

Mitchell, D. L., 1996: Use of mass-and area-dimensional power laws for determining precipitation particle terminal velocities. *Journal of the atmospheric sciences*, **53 (12)**, 1710–1723.

Mitchell, D. L. and W. P. Arnott, 1994: A model predicting the evolution of ice particle size spectra and radiative properties of cirrus clouds. part ii: Dependence of absorption and extinction on ice crystal morphology. *J. Atmos. Sci.*, **51**, 817–832.

Morrison, H. and W. W. Grabowski, 2011: Cloud-system resolving model simulations of aerosol indirect effects on tropical deep convection and its thermodynamic environment. *atmospheric chemistry and physics*, **11**, 10 503–10 523, doi:10.5194/1cp-11-10503-2011.

Morrison, H. and J. O. Pinto, 2005: Mesoscale modeling of springtime arctic mixed-phase stratiform clouds using a new two-moment bulk microphysics scheme. *J. Atmos. Sci*, **62**, 3683–3704.

Murphy, D. and T. Koop, 2005: Review of the vapour pressures of ice and supercooled water for atmospheric applications. *Quarterly Journal of the Royal Meteorological Society*, **131 (608)**, 1539–1565.

Murray, B. J., et al., 2010: Heterogeneous nucleation of ice particles on glassy aerosols under cirrus conditions. *Nature Geosci*, **3**, 233–237, doi:10.1038/ngeo817.

Myhre, G., et al., 2009: Modelled radiative forcing of the direct aerosol effect with multi-observation evaluation. *Atmospheric Chemistry and Physics*, **9 (4)**, 1365–1392.

Nousiainen, T., H. Lindqvist, G. M. McFarquhar, and J. Um, 2011: Small irregular ice crystals in tropical cirrus. *J. Atmos. Sci*, **68**, 2614–2627, doi:http://dx.doi.org/10.1175/2011JAS3733.1.

O'Donnell, D., K. Tsigaridis, and J. Feichter, 2011: Estimating the direct and indirect effects of secondary organic aerosols using echam5-ham. *Atmos. Chem. Phys.*, **11**, 8635–8659.

Orr, B. W. and R. A. Kropfli, 1999: A method for estimating particle fall velocities from vertically pointing doppler radar. *Journal of Atmospheric and Oceanic Technology*, **16 (1)**, 29–37.

Pandithurai, G., et al., 2009: Aerosol effect on cloud droplet size as monitored from surface-based remote sensing over east china sea region. *Geophys. Res. Lett*, **36**, L13 805, doi:10.1029/2009GL038451.

Paterson, M. and K. T. Spillane, 1969: Surface films and the production of sea-salt aerosol. *Quart. J. R. Met. SOC*, **95**, 526–534.

Petters, M. D. and S. M. Kreidenweis, 2007: A single parameter representation of hygroscopic growth and cloud condensation nucleus activity. *Atmospheric Chemistry and Physics*, **7 (8)**, 1961–1971, doi:10.5194/acp-7-1961-2007, URL `http://www.atmos-chem-phys.net/7/1961/2007/`.

Phillips, V., et al., 2005: Anvil glaciation in a deep cumulus updraught over florida simulated with the explicit microphysics model. i: Impact of various nucleation processes. *Quarterly Journal of the Royal Meteorological Society*, **131**, 2019–2046, doi:10.1256/qj.04.85.

Phillips, V. T. J., C. Andronache, B. C. E. Morris, D. C. Sands, A. Bansemer, A. Lauer, C. McNaughton, and C. Seman, 2009: Potential impacts from biological aerosols on ensembles of continental clouds simulated numerically. *Biogeosciences*, **6**, 987–1014.

Phillips, V. T. J., A. M. Blyth, P. R. A. Brown, T. W. Choularton, and J. Latham, 2001: The glaciation of a cumulus cloud over new mexico. *J Roy Meteor Soc*, **127**, 1513–1534.

Phillips, V. T. J., T. Choularton, and A. M. Blyth, 2002: The influence of aerosol concentrations on the glaciation and precipitation of a cumulus cloud. *Quarterly Journal of Royal Meteorological Society*, **128**, 951–971.

Phillips, V. T. J., T. W. Choularton, R. J. llingworth, A. J. Hogan, and P. R. Field, 2003: Simulations of the glaciation of a frontal mixed-phase cloud with the explicit microphysics model. *Quarterly Journal of the Royal Meteorological Society*, **129 (590)**, 1351–1371, doi:10.1256/qj.02.100.

Phillips, V. T. J., P. J. DeMott, and C. Andronache, 2008: An empirical parameterization of heterogeneous ice nucleation for multiple chemical species of aerosol. *Journal of the atmospheric sciences*, **65**, 2757–2783, doi:10.1175/2007JAS2546.1.

Phillips, V. T. J., P. J. Demott, C. Andronache, K. A. Pratti, and C. Twohy, 2013: Improvements to an empirical parameterization of heterogeneous ice nucleation and its comparison with observations. *J. Atmos. Sci.*, **70**, 378–409.

Phillips, V. T. J., L. J. Donner, and S. T. Garner, 2007: Nucleation processes in deep convection simulated by a cloud-system-resolving model with double-moment bulk microphysics. *Journal of the Atmospheric Sciences*, **64**, 738–761, doi:http://dx.doi.org/10.1175/JAS3869.1.

Pratt, K. A. P., et al., 2009: In situ detection of biological particles in cloud ice-crystals. *Nat. Geosci*, **2**, 398–401, doi:10.1038/ngeo521.

Prenni, A. J., et al., 2009: Relative roles of biogenic emissions and saharan dust as ice nuclei in the amazon basin. *Nature Geoscience*, **2 (6)**, 402–405.

Pringle, K. J., H. Tost, A. Pozzer, U. Pöschl, and J. Lelieveld, 2010: Global distribution of the effective aerosol hygroscopicity parameter for ccn activation. *Atmospheric Chemistry and Physics*, **10**, 5241–5255, doi:10.5194/acp-10-5241-2010.

Pruppacher, H. R. and J. D. Klett, 1997: *Microphysics of clouds and precipitation.* Kluwer accademic publishers.

Quaas, J., O. Boucher, and F. M. Breon, 2004: Aerosol indirect effects in polder satellite data and the laboratoire de meteorologie dynamique zoom (lmdz) general circulation model. *Journal of Geophysical Research*, **109**, D08 205, doi:10.1029/2003JD004317.

Ramanathan, V., R. Cess, E. Harrison, P. Minnis, B. Barkstrom, E. Ahmad, and D. Hartmann, 1989: Cloud-radiative forcing and climate: Results from the earth radiation budget experiment. *Science*, **243 (4887)**, 57–63.

Ramanathan, V., et al., 2007: Atmospheric brown clouds: Hemispherical and regional variations in long-range transport, absorption, and radiative forcing. *Journal of Geophysical Research: Atmospheres (1984–2012)*, **112 (D22)**.

Ramaswamy, V., et al., 2001: Radiative forcing of climate change. *Third Assessment Report of the Intergovernmental Panel on Climate Change*, **3rd**, 349–416.

Rasmussen, R. M., I. Geresdi, G. Thompson, K. Manning, and E. Karplus, 2002: Freezing drizzle formation in stably stratified layer clouds: The role of radiative cooling of cloud droplets, cloud condensation nuclei, and ice initiation. *J. Atmos. Sci.*, **59.**, 837–860.

Reisner, J., R. M. Rasmussen, and R. T. Bruintjes, 1998: Explicit forecasting of supercooled liquid water in winter storms using the mm5 mesoscale model. *Quart. J. Roy. Meteor. Soc.*, **124**, 1071–1107.

Reponen, T., S. Grinshpun, S. Trakumas, D. Martuzevicius, Z. Wang, G. LeMasters, J. Lockey, and P. Biswas, 2003: Concentration gradient patterns of aerosol particles near interstate highways in the greater cincinnati airshed. *J Environ Monit.*, **5 (4)**, 557–62.

Roberts, P. and J. Hallett, 1968: A laboratory study of the ice nucleating properties of some mineral particulates. *Quarterly Journal of the Royal Meteorological Society*, **94 (399)**, 25–34.

Rogers, R. R. and M. K. Yau, 1991: *A short course in cloud physics*. 3d ed., Perganom.

Rosenfeld, D., W. L. Woodley, A. Lerner, G. Kelman, and D. T. Lindsey, 2008: Satellite detection of severe convective storms by their retrieved vertical profiles of cloud particle effective radius and thermodynamic phase. *Journal of Geophysical Research*, **113**, doi:10.1029/2007JD008600.

Rotstayn, L. D. and Y. Liu, 2003: Sensitivity of the first indirect aerosol effect to an increase of the cloud droplet spectral dispersion with droplet number concentration. *Journal of Climate*, **16 (21)**, 3476–3481, doi:10.1175/1520-0442(2003)016-3476:SOTFIA-2.0.CO;2.

Rotstayn, L. D. and J. E. Penner, 2001: Indirect aerosol forcing, quasi forcing, and climate response. *Journal of Climate*, **14 (13)**, 2960–2975, doi:10.1175/1520-0442(2001)014-2960:IAFQFA-2.0.CO;2.

Rozenberg, G., 1960: Light scattering in the earth's atmosphere (an essay on the 150th anniversary of the discovery by arago of the polarization of light in the daytime sky, and on the 100th anniversary of the discovery by govi of the polarization of light in scattering). *Physics-Uspekhi*, **3 (3)**, 346–371.

Salma, I. and W. Maenhaut, 2006: Changes in elemental composition and mass of atmospheric aerosol pollution between 1996 and 2002 in a central european city. *Environmental Pollution*, **143 (3)**, 479–488.

Satheesh, S. K., K. K. Moorthy, and B. V. K. Murthy, 1998: Spatial gradients in aerosol characteristics over the arabian sea and indian ocean. *J. Geophys. Res.*, **103 (D20)**, 26 183–26 192, doi:10.1029/98JD00803.

Seifert, A. and K. Beheng, 2006: A two-moment cloud microphysics parameterization for mixed-phase clouds, part ii: maritime versus continental deep convective storms, meteorol. *Meteorology and Atmospheric Physics*, **92**, 67–88, doi: 10.1007/s00703-005-0113-3.

Shaw, G., 1982: Perturbation to the atmospheric radiation field from carbonaceous aerosols. *Particulate Carbon*, Springer, 53–73.

Shaw, G. E., 1980: Transport of asian desert aerosol to the hawaiian islands. *J. Appl. Meteor*, **19**, 1254–1259, doi:http://dx.doi.org/10.1175/1520-0450(1980)019⟨1254:TOADAT⟩2.0.CO;2.

Shaw, R. A., A. J. Durant, and Y. Mi, 2005: Heterogeneous surface crystallization observed in undercooled water. *J. Phys. Chem. B*, **109 (20)**, 9865–9868.

Sheppard, B. and P. Joe, 1994: Comparison of raindrop size distribution measurements by a joss-waldvogel disdrometer, a pms 2dg spectrometer, and a poss doppler radar. *Journal of Atmospheric and Oceanic Technology*, **11 (4)**, 874–887.

Shukla, J., R. Hagedorn, M. Miller, T. Palmer, B. Hoskins, J. Kinter, J. Marotzke, and J. Slingo, 2009: Strategies: revolution in climate prediction is both necessary and possible: a declaration at the world modelling summit for climate prediction. *Bulletin of the American Meteorological Society*, **90 (2)**, 175–178.

Shukla, J., T. Palmer, R. Hagedorn, B. Hoskins, J. Kinter, J. Marotzke, M. Miller, and J. Slingo, 2010: Toward a new generation of world climate research and computing facilities. *Bulletin of the American Meteorological Society*, **91 (10)**, 1407–1412.

Siegel, R. and J. R. Howell, 1992: Thermal radiation heat transfer. *NASA STI/Recon Technical Report A*, **93**, 17 522.

Solomon, S., D. Qin, M. Manning, Z. Chen, M. Marquis, K. Averyt, M.Tignor, and H. M. (eds.), 2007: Climate change 2007: The physical science basis. contribution of working group i to the fourth assessment report of the intergovernmental panel on climate change, (ipcc). *Cambridge University Press, Cambridge, United Kingdom and New York, NY, USA.*, **4th**.

Stevens, B. and O. Boucher, 2012: The aerosol effect. *Nature*, **490 (a)**, 40–41.

Storer, R. L. and S. C. van den Heever, 2013: Microphysical processes evident in aerosol forcing of tropical deep convective clouds. *J. Atmos. Sci*, **70 (2)**, 430–446.

Streets, D. G., et al., 2003: An inventory of gaseous and primary aerosol emissions in asia in the year 2000,. *J. Geophys. Res*, **108 (8809)**, D21, doi: 10.1029/2002JD003093.

Sun, Y., et al., 2004: The air-borne particulate pollution in beijing-concentration, composition, distribution and sources. *Atmospheric Environment*, **38 (35)**, 5991–6004.

Svenningsson, B., et al., 2006: Hygroscopic growth and critical supersaturations for mixed aerosol particles of inorganic and organic compounds of atmospheric relevance. *Atmospheric Chemistry and Physics*, **6 (7)**, 1937–1952.

Swap, R., M. Garstang, S. Greco, R. Talbot, and P. Kalberg, 1992: Saharan dust in the amazon basin. *Tellus B*, **44 (2)**.

Takemura, T., 2012: Distributions and climate effects of atmospheric aerosols from the preindustrial era to 2100 along representative concentration pathways (rcps) simulated using the global aerosol model sprintars. *Atmos. Chem. Phys.*, **12**, 11 555–11 572.

Thompson, G., P. R. Field, R. M. Rasmussen, and D. H. William, 2008: Explicit forecasts of winter precipitation using an improved bulk microphysics scheme. part ii: Implementation of a new snow parameterization. *American Meteorological Society*, **136**, 5095–5115, doi:10.1175/2008MWR2387.1.

Thompson, G., R. M. Rasmussen, and K. Manning, 2004: Explicit forecasts of winter precipitation using an improved bulk microphysics scheme. part i: Description and sensitivity analysis. *American Meteorological Society*, **132**, 519–552.

Tompkins, A., 2000: The impact of dimensionality on long-term cloud-resolving model simulations. *Monthly Weather Review*, **128 (5)**.

Twomey, S., 1974: Pollution and the planetary albedo. *Atmospheric Environment*, **8**, 1251–1256.

Twomey, S. A., 1977: The influence of pollution on the shortwave albedo of clouds. *Journal of the Atmospheric Sciences*, **34 (7)**, 1149–1152.

Vaughan, G., C. Schiller, A. R. MacKenzie, K. N. Bower, T. Peter, H. Schlager, N. R. P. Harris, and P. T. May, 2008: Studies in a natural laboratory: High-altitude aircraft measurements around deep tropical convection. *Bull. Am. Meteorol. Soc*, 647.

Vonnegut, B., 1947: The nucleation of ice formation by silver iodide. *Journal of applied physics*, **18 (7)**, 593–595.

Walko, R. L., W. R. Cotton, M. P. Meyers, and J. Y. Harrington, 1995: New rams cloud microphysics parameterization. part i: The single-moment scheme. *Atmos. Res*, **38**, 29–62.

Wapler, K., T. P. Lane, P. T. May, C. Jakob, M. J. Manton, and S. T. Siems, 2010: Cloud-system-resolving model simulations of tropical cloud systems observed during the tropical warm pool-international cloud experiment. *Mon. Wea. Rev.*, **138**, 55–73, doi:http://dx.doi.org/10.1175/2009MWR2993.1.

Watson, R., H. Rodhe, H. Oeschger, and U. Siegenthaler, 1990: Greenhouse gases and aerosols. *Climate change: the IPCC scientific assessment*, **1**, 17.

Webster, P. J. and R. Lukas, 1992: Toga coare: The coupled ocean-atmosphere response experiment. *Bull. Amer. Meteor. Soc*, **73**, 1377–1416.

Williams, K. D., A. Jones, D. L. Roberts, C. A. Senior, and M. J. Woodage, 2001: The response of the climate system to the indirect effects of anthropogenic sulfate aerosol. *Climate Dynamics*, **17 (11)**, 845–856.

Yamamoto, M. K., et al., 2008: Observation of particle fall velocity in cirriform cloud by vhf and millimeter-wave doppler radars. *Journal of Geophysical Research*, **113 (D12)**, D12 210.

Yang, H., S. Dobbie, R. Herbert, P. Connolly, M. Gallagher, S. Ghosh, A.-J. SMRK., and C. J., 2012.: The effect of observed vertical structure, habits, and size distributions on the solar radiative properties and cloud evolution of cirrus clouds. *Q. J. R. Meteorol. Soc.*, **138**, 1221–1232.

Young, K. C., 1974a: A numerical simulation of wintertime, orographic precipitation. part i: Description of model microphysics and numerical techniques. *J. Atmos. Sci*, **31**, 1735–1748.

Young, K. C., 1974b: The role of contact nucleation in ice phase initiation in clouds. *Journal of the Atmospheric Sciences*, **31 (3)**, 768–776.

Zeng, X., et al., 2009: An indirect effect of ice nuclei on atmospheric radiation. *J. Atmos. Sci*, **66**, 41–61, doi:http://dx.doi.org/10.1175/2008JAS2778.1.

Glossary

advection	The transportation of matter by wind or air currents. 8
aerosol	A small particulate matter, suspended in the atmosphere, a fraction of which forms the nucleus of the cloud particles. 1
aerosol-cloud model	An atmospheric model, especially a cloud resolving model, which explicitly links the microphysics processes with the aerosol loading and chemistry. 40, 59, 62, 175, 176
aggregation	The process by which cloud ice collide and coalesce with each other to form snow flakes. 32, 34, 143
aggregation indirect effect	An aerosol indirect effect induced on the cloud through the aerosol effect on the aggregation process. 116, 137, 144
anthropogenic	Of or related to human as opposed to natural influence. 29
atmospheric window	These are bands of wavelengths in the atmosphere through which some corresponding longwave radiation can escape to space with minimal or zero attenuation, it is found within about 10 - 13μm wavelength range.. 25
bin-microphysics	A technique of explicitly integrating equations in a simulation. 39, 50
bulk-microphysics	A technique of utilising parametrisation to resolve a problem. 39, 44, 50
climate	The pattern of variation in meteorological variables in a given region over long periods of time. xx, 1–3, 113, 183, 184
cloud	A visible mass of water that has condensed or deposited on an aerosol particle. 1
cloud albedo	The ratio of radiation reflected to that of radiation incident on a cloud. 28
cloud base	The base of a cloud. 14, 32, 45
cloud droplets	Liquid droplets in the clouds with diameters of about 20μm or less. 21
cloud fraction	The fraction of the domain that is covered by clouds. 105
cloud ice	Ice crystals in the clouds with diameters of about 200μm or less. 21

cloud microphysics	The physics that governs cloud-scale processes. 16
cloud-top	The top of a cloud. 36
coalescence indirect effect	An aerosol indirect effect induced on the cloud through the aerosol effect on the collision and coalescence process. 116
collision-coalescence	The process by which cloud and rain droplets collide and coalesce with each other to form a rain drop. 99, 116, 177
cooling effect	Causes a net decrease in the temperature of the climate system. 30
emissivity	The fraction of the absorbed radiative energy that a body emissivity. xxvii, 23
glaciated clouds	Clouds comprising ice crystals, either mixed-phase clouds or ice-only clouds. 3, 84, 110, 143
glaciation indirect effect	An aerosol indirect effect induced on the cloud through the increase of IN and, hence, ice crystals. 37
graupel	Cloud ice that grow into precipitation mostly through riming. 21
hygroscopicity parameter	The measure of the aerosol's affinity for water. 10
ice phase clouds	Clouds comprising ice crystals only. 33
internal mixing	Is one in which the homogeneous structure of a particle reflects the chemical and physical average of different contributing aerosol components. 147
longwave radiation	The radiative energy that is emitted mostly by a terrestrial body. 1
mixed-phase clouds	Clouds comprising both water droplets and ice crystals only. 33, 36, 116, 137, 143
model run	A model simulation. 33, 93
multicomponent aerosol	An internally mixed aerosol particle. 8
optical thickness	A cloud with optical thickness τ, is one that transmits the fraction $e^{-\tau}$ of radiation through it. 30

parameterization	Representation of physical processes by numerical algorithms. 2, 46, 47, 54, 176
pre-industrial	The era prior to industrial revolution, estimated in this study to be before 1850. 31
radiation	A mechanism by which solar energy reaches the Earth's system. 1, 23, 27, 30, 78, 133, 135
rain	Cloud droplets that are large enough to fall-out of a cloud as precipitation. 21
reflectance	The fraction of the incident radiative fluxes that a body reflects. 31
sedimentation	The processes by which suspended atmospheric particles fall under the influence of gravity. 32
shortwave radiation	The radiative energy that is mostly received from the sun. 1
simulations	An attempt to imitate or reproduce a real state of the atmosphere using numerical means. 3, 35, 57, 71, 81, 175
snow	Cloud ice that grows into precipitation mainly through aggregation. 21
solid aerosols	Solid aerosol particles that do not dissolve in water. 3
solute aerosols	Aerosol particles that dissolve in water. 4
supersaturation	Is when the equilibrium vapour pressure over a cloud droplet surface is higher than over a plane surface of water. 10–12, 47
surface precipitation	Precipitation that reaches the ground. 80, 99
volumetric cloud fraction	The fraction of cloudy grid-boxes within the whole domain and the entire simulation period to the total grid-boxes in the whole domain and the entire simulation period.. 104
warming effect	Causes a net increase in the temperature of the climate system. 30
water-only clouds	Clouds comprising pure water droplets only. 99, 143, 179